

DOMINANT FREQUENCY ESTIMATION FOR ATRIAL
FIBRILLATION STUDIES

Thesis submitted for the degree
Doctor of Philosophy
to the University of Leicester

by

Anita Ahmad MEng
Department of Engineering
University of Leicester

May 2011

Statement of Originality and Authorship:

This work is original and unless otherwise acknowledged in the text or by references, has been performed by myself. Parts of this work have been published during the development of the research.

This work was performed in the Department of Engineering at the University of Leicester, during the period between November 2007 and May 2011 (supported by Ministry of Higher Education and Universiti Teknologi Malaysia).

None of this work has been submitted for another degree in this, or any other university.

Signed,

Anita Ahmad

Date:

DOMINANT FREQUENCY ESTIMATION FOR ATRIAL FIBRILLATION STUDIES

Anita Ahmad

This research work explores the feasibility of using frequency domain analysis in the study of arrhythmias. The research involves the application of spectrum analysis to obtain the dominant frequency (DF) of atrial electrograms (AE) at different sites in the atria. It is an alternative way of interpreting the chaotic electrical activity seen during AF and reveals critical sites to guide ablation.

As longer ablation procedure time implies higher risk to the patient, DF estimation needs to be obtained as quickly as possible. Four techniques (FFT, Blackman-Tukey, Autoregressive and Multiple Signal Classification) were used to compare the computation times taken for spectrum estimation analysis. The FFT technique produces an accurate DF result with the shortest time.

DF analysis was first used for ventricular fibrillation with data from the surface of the left ventricle (in animal studies). It was found that spectrograms show the DF drifting along time and with significant changes in power. This approach was then applied for bipolar AF signals (in human studies). The changes of the frequency along time were observed when the stimulation was given, either using high frequency stimulation or drug infusion.

We have developed a novel technique for the removal of ventricular signals from virtual AE. The surface ECG is used to identify ventricular activity. A band pass filter (8 Hz to 20 Hz) followed by rectification and then a low pass filter (6 Hz) are used for QRS detection. QRST subtraction was performed using three different approaches: flat, linear and spline interpolation. QRST subtraction affects the power of the signals but not the DF.

We also developed an adaptive power threshold tool to observe the distribution of the DFs with an adjustable power threshold setting. Using this tool the 3D maps can display the evolution of the DFs within a chosen threshold power bracket.

Acknowledgement

I lift up my praise and gratitude to Allah (swt), the Most Gracious, the Most Merciful, for everything in my life is under His consent and control, including studying PhD at the University of Leicester. I thank Him for sending me to Leicester, helping me in time of difficulties, giving me abundant wisdom and opening the doors widely for completing this thesis.

This thesis would not have been possible without the help and assistance from many people. I am deeply indebted to my supervisor Dr Fernando Soares Schlindwein and my co-supervisor Dr G. André Ng whose help, stimulating suggestions and encouragement have exceptionally helped me in all the time of research for and writing of this thesis.

I would also like to express my thankfulness to the Department of Engineering, University of Leicester for giving me a chance to do the research work.

I would also like to convey my appreciation to my Scholarship sponsors from the Malaysian Ministry of Higher Education and the Malaysian University of Technology (*Universiti Teknologi Malaysia*) for financing my study.

I am grateful to my colleagues from the Bioengineering Group for supported me in my research work. I want to thank them for all their help, support, interest and valuable hints. I dedicate my special thanks to João Loures Salinet Jr, Federico Cardona Rocha, Taher Biala and Cath Taylor. I also want to thank the Cardiovascular Research Group from Glenfield Hospital especially to Dr. Pete Brown, Dr. Peter Stafford and Dr. Jiun Tuan for all assistance on data collection and clinical interpretation.

I owe my deepest gratitude and my endless love to my husband, Ghazali Haji Abu. He deserves utmost special mention for his remarkable and inseparable support, love and prayers throughout this journey. He is always there cheering me up and standing by me during good and bad times. Last but not least, I extend my gratitude to my beloved sons and daughters, Muhammad ‘Ariff, Nur ‘Aliah, Nur Izzah, Nur Iffah and Muhammad Afdhal for their endless love, support and prayers.

This thesis is dedicated to my parents,
Haji Ahmad bin Haji Daud and Hajjah Manih bin Haji Chat,
who have always supported and encouraged me.

Table of Contents

page

Statement of Originality and Authorship	ii
Abstract	iii
Acknowledgement	iv
Dedication	v
1 INTRODUCTION	1
1.1 Scope of the studies	1
1.2 Organisation of thesis	3
2 PHYSIOLOGY OF THE HEART	6
2.1 Introduction	6
2.2 Cardiac cycle	8
2.3 Heart rate control mechanisms	9
2.3.1 Neurologic	9
2.3.2 Humoral	11
2.3.3 Intrinsic	12
2.4 Cardiac output	12
2.5 Normal cardiac electrical propagation	12
2.5.1 Depolarisation	14
2.5.2 Repolarisation	14
2.5.3 Automaticity	15
2.6 Action potential	15
2.7 ECG leads	19
2.7.1 Bipolar leads	19
2.7.2 Unipolar leads	19
2.8 Normal electrocardiogram	20
2.9 Nervous System	25

3	ARRHYTHMIAS	31
3.1	Introduction.....	31
3.2	Fibrillation	32
3.3	Ventricular Fibrillation.....	33
3.3.1	VF Mechanism.....	35
3.3.2	VF symptoms.....	35
3.3.3	VF treatment.....	35
3.4	Atrial Fibrillation	37
3.4.1	AF Mechanism.....	39
3.4.2	AF Symptoms.....	43
3.4.3	AF treatment.....	44
3.5	Ablation procedure.....	46
3.5.1	Contact mapping catheter.....	49
3.5.2	Non-contact mapping catheter.....	50
3.6	Targets for ablation	52
3.6.1	Pulmonary vein isolation.....	52
3.6.2	Ablation at mitral isthmus.....	54
3.6.3	Ablation at left atrial roof.....	55
3.6.4	Ablation at coronary sinus.....	55
3.6.5	Ablation at atrial septum.....	56
3.7	Bipolar and Unipolar recordings.....	56
3.7.1	Bipolar recordings.....	57
3.7.2	Unipolar recordings.....	58
4	COMPARISON OF COMPUTATION TIME FOR ESTIMATION OF DOMINANT FREQUENCY OF ATRIAL ELECTROGRAMS: FAST FOURIER TRANSFORM, BLACKMAN TUKEY, AUTOREGRESSIVE AND MULTIPLE SIGNAL CLASSIFICATION	62
4.1	Introduction.....	62
4.2	Frequency Domain Analysis.....	63
4.2.1	Fast Fourier Transform (FFT) Technique.....	63
4.2.2	Blackman-Tukey (BT) Technique.....	66
4.2.3	Autoregressive (AR) Technique.....	68
4.2.4	Pisarenko Harmonic Decomposition (PHD).....	69

4.2.5	Multiple Signal Classification (MUSIC).....	75
4.3	Method.....	76
4.4	Results	77
4.5	Conclusion	80
5	DOMINANT FREQUENCY ESTIMATION FOR VENTRICULAR FIBRILLATION FROM ANIMAL STUDIES.....	82
5.1	Introduction.....	82
5.2	Dominant Frequency Estimation for Ventricular Fibrillation in Animal Studies	88
5.2.1	Introduction.....	88
5.2.2	Method.....	88
5.2.3	Results.....	92
5.2.4	Discussion.....	94
5.2.5	Conclusion.....	96
6	DOMINANT FREQUENCY ESTIMATION OF ATRIAL FIBRILLATION FROM HUMAN STUDIES	98
6.1	Introduction.....	98
6.2	Hypothesis 1: High frequency stimulation (HFS) produces changes in frequency.....	98
6.2.1	Discussion.....	100
6.2.2	Conclusions.....	107
6.3	Hypothesis 2: Examining the effect of isoprenaline and atropine on frequency changes	108
6.3.1	Results and Discussion.....	109
6.3.2	Conclusions.....	114
7	QRST SUBTRACTION FOR ATRIAL ELECTROGRAMS	115
7.1	Introduction.....	115
7.2	Methods	116
7.2.1	QRS Detection.....	119
7.2.2	Flat interpolation.....	120
7.2.3	Linear interpolation.....	120
7.2.4	Spline interpolation.....	121
7.3	Results	122

7.4 Discussion.....	127
7.5 Conclusions.....	137
8 NON CONTACT MAPPING OF ATRIAL FIBRILLATION	138
8.1 Introduction.....	138
8.2 Validation of non contact mapping	138
8.3 Three Dimensional (3D) DF geometry	140
8.4 Adaptive power threshold for dominant frequency estimation in atrial fibrillation	141
8.4.1 Methods.....	142
8.4.2 Pruning DF with Regularity Index (RI).....	144
8.4.3 Pruning DF with Adaptive Power Threshold (APT).....	144
8.4.4 Calculating DF Occurrence.....	145
8.5 Results	147
8.6 Discussion.....	152
8.7 Conclusions.....	155
9 CONCLUSIONS AND FUTURE WORK.....	157
9.1 Introduction.....	157
9.1.1 Reducing ablation procedure time by choosing a fast computational method....	157
9.1.2 Removing ventricular influences from atrial electrograms.....	158
9.1.3 Observing the behaviour of contact mapping VF signals (from animal studies) and AF signals (from human studies).....	158
9.1.4 Observing 3D DF maps for noncontact mapping AF signals.....	159
9.2 Future work.....	161
9.2.1 Improving the frequency resolution.....	161
9.2.2 The optimization of the QRST subtraction method.....	161
9.2.3 AF signal complexity (Time domain analysis).....	161
9.2.4 Assessing the efficacy the DF and CFAE sites.....	162
9.2.5 Comparing approaches for estimating DF.....	162
References	163

List of figures

Figure 2.1 - Anatomy and function of the heart	7
Figure 2.2 - Systemic and pulmonary circulations	7
Figure 2.3 - Systole and diastole	9
Figure 2.4 - Heart rate is regulated by Baroreceptor Reflex; (a) atrial blood pressure inversely changes in heart rate (b) changes in carotid sinus pressure on the sympathetic and parasympathetic activity.	10
Figure 2.5 - Conduction system of the heart [<i>From Tortora and Derrickson, Principles of Anatomy and Physiology, 2009, John Wiley & Sons, Inc, with permission</i>]	13
Figure 2.6 - Ions influx and efflux during resting and depolarisation.	15
Figure 2.7 - Action potential	16
Figure 2.8 - Action potentials: fast response (left) and slow response (right).	18
Figure 2.9 - Bipolar and unipolar leads	20
Figure 2.10 - Components of a surface ECG.	21
Figure 2.11 - Normal ECG	24
Figure 2.12 - Organization of the nervous system	25
Figure 2.13 - PNS and CNS relationship.	26
Figure 2.14 - Motor neuron pathway in the ANS.....	28
Figure 2.15 - Sympathetic and parasympathetic actions	29
Figure 2.16 - Structure of sympathetic and parasympathetic divisions.	30
Figure 3.1 - Rapid and long impulse (modified from Mines, 1913).....	33
Figure 3.2 - Slow and short impulse (modified from Mines, 1913).....	33
Figure 3.3 - Monophasic action potential (MAP) signal for ventricle fibrillation (sampling frequency 1 kHz)	34
Figure 3.4 - Relation of time interval from collapse to CPR and defibrillation to survival [<i>From Valenzuela TD et al., Estimating effectiveness of cardiac arrest interventions: a logistic regression survival model, Circulation 1997; 96:3308-3313, with permission</i>].....	36
Figure 3.5 - Typical surface ECG of a patient in AF.....	38
Figure 3.6 - Structure and possible mechanism of AF; (A) autonomic ganglion and axon (yellow), (B) wavelet and mother wavelet (red), (C) PV triggered (red) and non PV triggered (green), (D) all autonomic and arrhythmic mechanism [<i>From Nathan and Eliakim., The Junction Between the Left Atrium and the Pulmonary Veins: An Anatomic Study of Human Hearts, Circulation 1996;34:412-422,with permission</i>].	40
Figure 3.7 - AF mechanism [<i>From Stanley Nattel et al., Mechanisms of Atrial Fibrillation: Lessons From Animal Models, Cardiovascular Diseases, 2005; 48(1):9-28, with permission</i>]. ..	41
Figure 3.8 - Risk for stroke in AF, re-drawn from [Wolf et al., 1991].....	43
Figure 3.9 - Therapeutic strategies and goals in AF patients [<i>Vias Markides et al., “Atrial Fibrillation: Classification, pathophysiology, mechanisms and drug treatment, Heart 2003; 89:939-943</i>].	44

Figure 3.10 - Catheter ablation insertion.	46
Figure 3.11 - Schematic drawing of the equipment in the electrophysiological laboratory.	47
Figure 3.12 - Schematic drawing of the radiofrequency catheter positioned on the endocardium.	48
Figure 3.13 - Types of catheter.	50
Figure 3.14 - EnSite catheter, (a) before deployment, (b) after deployment and (c) Display Workstation (courtesy of St. Jude Medical, used with permission).....	51
Figure 3.15 - PV isolation. The red blobs represent ablation.....	54
Figure 3.16 - Ablation at mitral isthmus.....	54
Figure 3.17 - Ablation at the left atrium roof.....	55
Figure 3.18 - Ablation at the left atrium septum.	56
Figure 3.19 - Bipolar recordings. [From Stevenson <i>et al.</i> , <i>Recording Techniques for Clinical Electrophysiology</i> , <i>J Cardiovasc Electrophysiol</i> , Vol. 16, pp. 1017-1022, September 2005, with permission].....	57
Figure 3.20 - Unipolar recordings. [From Stevenson <i>et al.</i> , <i>Recording Techniques for Clinical Electrophysiology</i> , <i>J Cardiovasc Electrophysiol</i> , Vol. 16, pp. 1017-1022, September 2005, used with permission].....	58
Figure 4.1 - Segmenting of the data for overlap processing	65
Figure 4.2 - Comparison of Fast Fourier Transform, Blackman-Tukey, Autoregressive and Multiple Signal Classification spectral estimates.	77
Figure 4.3 - Error versus SNR.....	79
5.1- (a) DF of pure sinusoid signal (left) and spectrum (right). (b) DF of the ECG signal (left) and spectrum (right).	84
Figure 5.2 - (a) length of the signal equal to an integer multiple of the period of the signal(s). (b) length of the signal not equal to an integer multiple of the period of the signal(s). (c) zero-padding effect.	86
Figure 5.3 - Raw signal (top), rectified signal (middle) and low pass filtered signal (bottom).	88
Figure 5.4 - Cardiac electrical recording and pacing [From Ng <i>et al.</i> , Effects of direct sympathetic and vagus nerve stimulation on the physiology of the whole heart ó a novel model of isolated Langendorff perfused rabbit heart with intact dual autonomic innervation, 2001, Experimental Physiology, used with permission].....	90
Figure 5.5 - VF signal (sample 31700).....	92
Figure 5.6 - Spectrum and spectrogram.....	93
Figure 6.1 - Catheter at coronary sinus (red circle).	99
Figure 6.2 - Spectrum and spectrogram for P1-VB.....	101
Figure 6.3 - Spectrum and spectrogram for P2-CL	104
Figure 6.5 - Spectrum and spectrogram for patient with isoprenaline infusion, (a) before infusion, (b) after infusion	110
Figure 6.6 - Effect of isoprenaline infusion	111
Figure 6.7 - Spectrum and spectrogram for patient with atropine infusion, (a) before infusion, (b) after infusion	112
Figure 6.8 - Effect of atropine infusion.	113

Figure 7.1 - (a) Surface ECG from patient in AF and (b) Intra-cardiac atrial electrogram from the same patient.....	117
Figure 7.2 - 3D representation of the atrium.....	118
Figure 7.3 - Linear interpolation between the points.....	121
Figure 7.4 - QRS detection (a) ECG after band pass filter, (b) Low pass filter and (c) Peaks of the signal.....	124
Figure 7.5 - The reference signal with QRS complex (blue dotted line) and atrial electrogram after QRS Subtraction (black line) using (a) flat interpolation (b) linear interpolation and (c) spline interpolation.	126
Figure 7.6 - Mean DF estimation of atrial electrogram using (a) flat interpolation (b) linear interpolation and (c) spline interpolation.....	128
Figure 7.7 - (a) Mean frequency before and after QRS subtraction using flat interpolation (blue dotted line: before subtraction, black line: after subtraction) for patient 1 to patient 5 and (b) Power spectrum, before and after QRS subtraction using flat interpolation.	131
Figure 7.8 - (a) Normal ECG versus QRS subtraction signal-(b) Normal ECG versus QRST subtraction signal.....	133
Figure 7.9 - Spectrum : QRS versus QRST subtraction using flat interpolation of surface ECG for normal heart.....	133
Figure 7.10 - (a) Normal surface ECG signal versus QRS subtraction using spline interpolation and (b) Normal surface ECG signal versus QRST subtraction using spline interpolation ...	135
Figure 7.11 - Spectra : QRS versus QRST subtraction using spline interpolation.....	135
Figure 7.12 - Spectrum from surface ECG of AF signal	136
Figure 7.13 - Spectrum for unipolar atrial electrogram	136
Figure 8.1 - The description of the exported file with the electrograms used in this research.....	139
Figure 8.2 - The reconstruction of 3 Dimensional mapping for 2048 points using (a) EnSite 3000 and (b) our representation in MATLAB (the colours have different meanings).....	140
Figure 8.3 - The reconstruction of 3 Dimensional mapping for 256 points using MATLAB.....	140
Figure 8.4 - 3D DF mapping.	141
Figure 8.5 - Multiple power thresholds.	145
Figure 8.6 - DF Occurrence calculation.....	146
Figure 8.7 - DF and power distribution.	147
Figure 8.8 - (a) power differences between before (red line) and after (blue line) QRS subtraction, (b) 3D DF before QRST subtraction, and (c) 3D DF after QRST Subtraction with the evident reduction of the area of interest.	149
Figure 8.9 - Mean frequency before and after QRST Subtraction	149
Figure 8.10 - Distribution of DF for Baseline.	150
Figure 8.11 - Distribution of DF for Post Ablation with APT20%	151
Figure 8.12 - Number of DF points versus occurrence using RI and APT20% for baseline.	152
Figure 8.13 - Comparison of DF occurrence over 16 seconds between DFRI, DFAPT10% and DFAPT20%.....	153
Figure 9.1 - Spectrum and spectrogram.	159

List of Tables

Table 2.1 - Electrodes location.....	19
Table 2.2 - ECG waves and intervals	22
Table 2.3 - Sequence of excitation of the heart and its respective heart's electrical signal (ECG).....	23
Table 4.1 - DF value comparison for all technique against the base Frequency	78
Table 4.2 - Calculation of error for FFT, Blackman-Tukey, Autoregressive and Multiple Signal Classification spectral estimates.	78
Table 4.3 - Cut off SNR for each technique	79
Table 4.4 - Computation time for 3000 signals.....	80
Table 5.1 - Dominant Frequency during Ventricular Fibrillation	94
Table 6.1 - Dominant frequency for P1-VB	102
Table 6.2 - Dominant frequency for P2-CL	104
Table 6.3 - Dominant frequency for P3-TJ	106
Table 6.4 - Centre of gravity for P2-CL	107
Table 6.5 - Frequency pre and post isoprenaline infusion	111
Table 6.6 - Frequency pre and post atropine infusion	113
Table 7.1 - DF and power for each interpolation	129
Table 8.1 - Average DF for DF-RI and DF-APT20%	151

List of Appendices

Appendix 1 - Monophasic action potential signals	175
Appendix 2 - Spectrum and spectrogram for VF studies	176
Appendix 2 a - Sample 031700 (a) baseline (b) right vagus nerve stimulation (c) left vagus nerve stimulation (d) sympathetic nerve stimulation	176
Appendix 2 b - Sample 042800 (a) baseline before sympathetic stimulation (b) baseline before vagus stimulation (c) left vagus nerve stimulation (d) right vagus nerve stimulation (e) sympathetic nerve stimulation	177
Appendix 2 c - Sample 050500 (a) baseline before sympathetic stimulation (b) baseline before vagus stimulation (c) right vagus nerve stimulation (d) sympathetic nerve stimulation	178
Appendix 2 d - Sample 050800 (a) baseline before sympathetic stimulation (b) baseline before vagus stimulation (b) right vagus nerve stimulation (c) left vagus nerve stimulation (d) sympathetic nerve stimulation	179
Appendix 2 e - Sample 051500 (a) baseline (b) right vagus nerve stimulation (c) left vagus nerve stimulation (d) sympathetic nerve stimulation.	180
Appendix 2 f - Sample 063000 (a) baseline (b) right vagus nerve stimulation.....	181
Appendix 2 g - Sample 071700 (a) baseline (b) right vagus nerve stimulation.....	182
Appendix 2 h - Sample 081400 (a) baseline (b) right vagus nerve stimulation (c) left vagus nerve stimulation (d) sympathetic nerve stimulation	183

List of abbreviations

AE	Atrial electrograms
AF	Atrial fibrillation
AFCL	Atrial fibrillation cycle length
ANS	Autonomic nervous system
APT	Adaptive power threshold
APD	Action potential duration
AR	Autoregressive
ARMA	Autoregressive moving average
ARP	Absolute refractory period
AV	Atrioventricular
BL	Baseline
BT	Blackman-Tukey
CFAEs	Complex fractionated atrial electrograms
CNS	Central nervous system
CO	Cardiac output
CS	Coronary sinus
CV	Cardiovascular
DF	Dominant frequency
ECG	Electrocardiogram
FFT	Fast Fourier transform
HFS	High frequency stimulation
HR	Heart rate
IVC	Inferior Vena Cava
LA	Left atrium
LIPV	Left inferior pulmonary vein

LV	Left ventricle
LVS	Left vagus stimulation
MAP	Monophasic action potential
MEA	Multi-electrode array
MUSIC	Multiple signal classification
OI	Organization index
PA	Pulmonary Artery
PNS	Peripheral nervous system
PSD	Power spectral density
PVI	Pulmonary vein isolation
PVs	Pulmonary veins
RA	Right atrium
RF	Radiofrequency
RI	Regularity index
RP	Refractory period
RRP	Relative refractory period
RSPV	Right superior pulmonary vein
RV	Right ventricle
RVS	Right vagus stimulation
SA	Sinoatrial
SNS	Sympathetic nerve stimulation
SV	Stroke volume
SVC	Superior vena cava
VF	Ventricular fibrillation

1 INTRODUCTION

1.1 Scope of the studies

Dominant frequency (DF) of electrophysiological data is an effective approach to estimate the activation rate during Atrial Fibrillation (AF) and it is important to understand the pathophysiology of AF and to help select candidate sites for ablation. Frequency analysis is used to find and track DF. It is important to identify the evolution of the frequency composition of the signal with time. The first part of the work looks specifically at the DF evolution for ventricular fibrillation from the surface of the left ventricle (animal studies). The evolution can be represented by spectrograms using short segment data analysis (Welch Technique).

The second part of the work looks specifically at different techniques that can be used for DF estimation of AF data. Fast Fourier Transform (FFT) approaches of modified periodogram and Blackman-Tukey (BT) technique are categorised as non-parametric (classical) methods, the Autoregressive (AR) approach is categorised as a parametric method and Multiple Signal Classification (MUSIC) is categorised as subspace method. It is important to minimise the catheter insertion time in the atria as it contributes to the risk for the patient. This is due to the possible complications during the procedure such as cardiac tamponade (dramatic fall in blood pressure), blood stream infection, pulmonary vein stenosis, *etc.* As longer ablation procedure time implies higher risk to the patient, DF estimation needs to be obtained as quickly as possible. A comparison of computation times taken for spectrum estimation analysis is presented in this study. Fast Fourier Transform (FFT), Blackman-Tukey (BT),

Autoregressive (AR) and Multiple Signal Classification (MUSIC) methods are used to obtain the frequency spectrum of the arterial electrograms. The time to produce DF was measured for each method. The method which takes the shortest time for analysis without jeopardising the accuracy of result is selected for real time application purpose.

Unipolar electrograms using non-contact mapping is a technique that measures the electrical activity in the atrium. The signals consist of atrial electrograms contaminated with the influence of the ventricular activity in the heart. To get accurate data analysis in the atrium, the ventricular activity influence should be removed beforehand. In the process of obtaining clean atrium data, the next part of the work was to develop a technique for the removal of ventricular contamination on virtual atrial electrograms. The surface ECG is used as a guide to identify the ventricular activity of the signals. QRS detection was based on the application of a band pass filter between 8 Hz and 20 Hz and low pass filtering the rectified signal. The cut-off of frequency of the low pass filter is determined by the lowest RR interval (RR interval is the interval from the peak of one QRS complex to the peak of the next QRS complex) of the ECG signals (354 beats per minute) and was chosen as 6 Hz. We aimed to evaluate the effects of cancellation on unipolar signals with minimal far field ventricular depolarization using three different approaches (flat, linear and spline interpolation).

The next part of the work looked specifically at the behaviour of atrial fibrillation (AF) signals. In time domain analysis, AF signal is known to be rapid with irregularity in timing and morphology. Dominant frequency is used to analyse the AF signal for the observation of signal behaviour in frequency and DF evolution along time. High frequency stimulation (HFS) and drugs infusion (isoprenaline and atropine) are used to stimulate the autonomic cardiac ganglia since these nerves are recognised as one of the mechanisms that contribute to

AF. The effect of the stimulations is recorded and analysed. The behaviour of the signal before, during and after stimulation is observed for high frequency stimulation while for drugs infusion only signals before and after infusion are analysed.

The final part of the work is to validate the 3D geometry between Matlab tools and St Jude equipment. Both tools can display voltage activity along time while Matlab tools have the capability to display frequency (DF) along time. Frequency evolution can be viewed in the form of a movie using MATLAB. The behaviour of 3D DF Mapping is observed before and after QRS subtraction. The 3D Mapping is then used to analyse the DF mechanism. Many literature reviews suggest that the mechanism of AF is still unknown while some studies suggest that AF mechanism may be due to re-entrant, focal source, autonomic nervous system and vortices of electrical waves (which led to the concepts of ‘rotors’). In line with the focal source idea we explore the possibility of DF occurrence to contribute to AF. From the point of view of rotors, DF ranking (high frequency density) approach is used to monitor the DF movement in the atrium. The dominant frequency sites are ‘pruned’ by the use of the regularity index and multiple level of adaptive power threshold approach. The implementation of an adaptive power threshold could help us concentrate attention to DFs within a certain power bracket.

1.2 Organisation of thesis

This thesis has nine chapters, including an introduction in Chapter 1. Chapter 2 describes the normal heart physiology. This chapter briefly explains the heart function, cardiac electrical propagation, the characteristic of the electrical signals and the part of the nervous system relevant to control of heart rate.

Chapter 3 presents an introduction to cardiac arrhythmias and the mechanisms that lead to fibrillation (both ventricular and atrial fibrillation). The treatments of these arrhythmias are also described.

In Chapter 4, we identify different methods to estimate the dominant frequency. The fastest method is used for the dominant frequency estimation of atrial electrograms. Chapter 5 describes the techniques used for dominant frequency estimation and the evolution of the frequency along time using signals from animal studies in ventricular fibrillation.

In Chapter 6, we use the technique that was described in Chapter 5 to analyse atrial fibrillation signals for the human studies. The changes in frequency were observed for high frequency stimulation and drugs infusion.

The technique used to remove the ventricular influences from atrial electrograms (QRST complex detection and the interpolation used for the QRST subtraction) is described in Chapter 7.

The validation of three dimensional (3D) representation of noncontact signals is described in Chapter 8. The dominant frequency (DF) estimation was performed for 2048 unipolar signals and the 3D DF maps were produced in this chapter. The comparisons of the DF maps before and after QRST subtraction, the application of adaptive power threshold on the DF estimation as a means to reduce the number of potential candidates for additional ablation after Pulmonary veins isolation (PVI) were also presented in this chapter.

Finally, Chapter 9 brings together the work covered in the thesis and gives some conclusions and suggestions for future work.

2 PHYSIOLOGY OF THE HEART

2.1 Introduction

The heart is the pump that circulates blood to the body [Tortora and Derrickson, 2009, Guyton and Hall, 1996]. Over a 75-year lifetime, the two ventricles combined pump 400 million litres of blood [Boron and Boulpaep, 2005]. The heart is divided into 4 chambers:

- a) Right atrium (RA)
- b) Right ventricle (RV)
- c) Left atrium (LA)
- d) Left ventricle (LV)

The flow of blood in and out of the heart is controlled by valves at the inlet and outlet of each ventricle. These are the tricuspid valve, pulmonary valve, mitral valve and aortic valve and they ensure that blood flows in one direction only.

The left side of the heart is comprised of the left atrium and the left ventricle. It takes in oxygenated blood from the lungs and pumps it out into the aorta from which it passes into smaller vessels to reach the cell tissues. The blood exchanges its oxygen and nutrients for the waste materials of the cells and is then returned to the right side of the heart (right atrium and right ventricle), which pumps it back to the lungs via the pulmonary artery. Once oxygenated, the blood returns to the left side of the heart through the pulmonary veins. The anatomy and functioning of the heart are pictured in Figure 2.1 and the systemic and pulmonary circulations are shown in Figure 2.2.

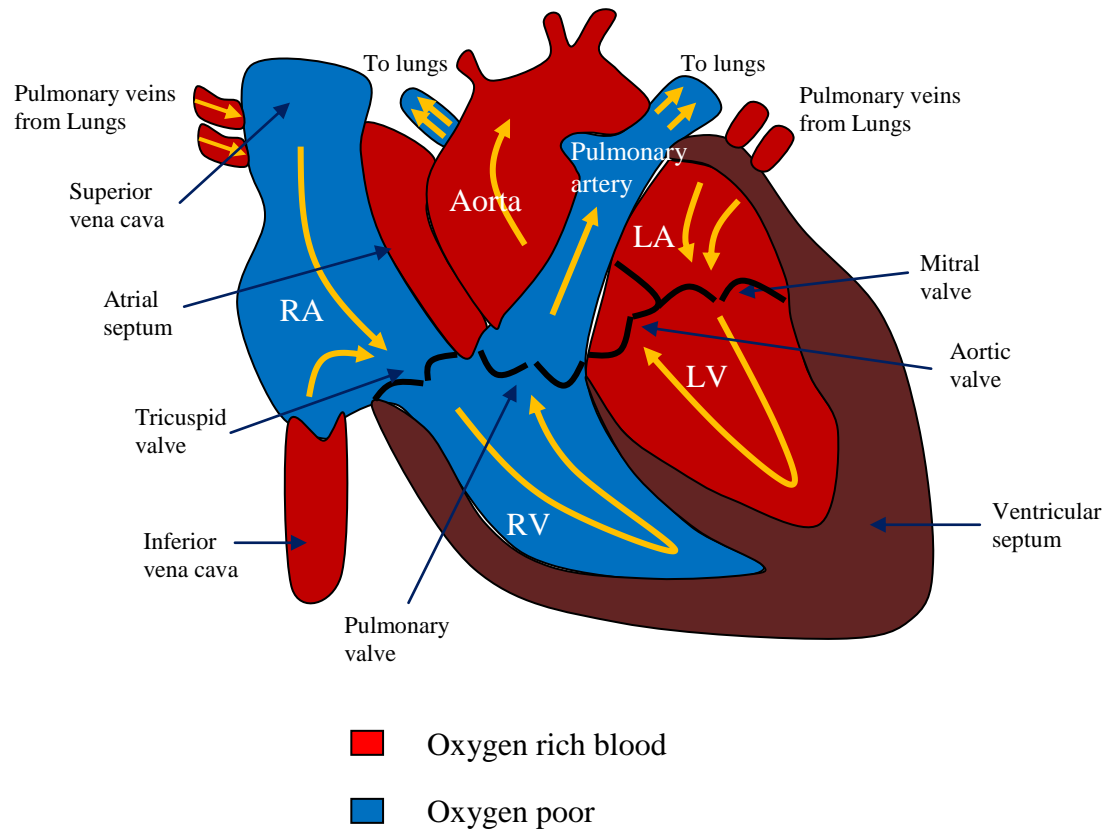


Figure 2.1 - Anatomy and function of the heart

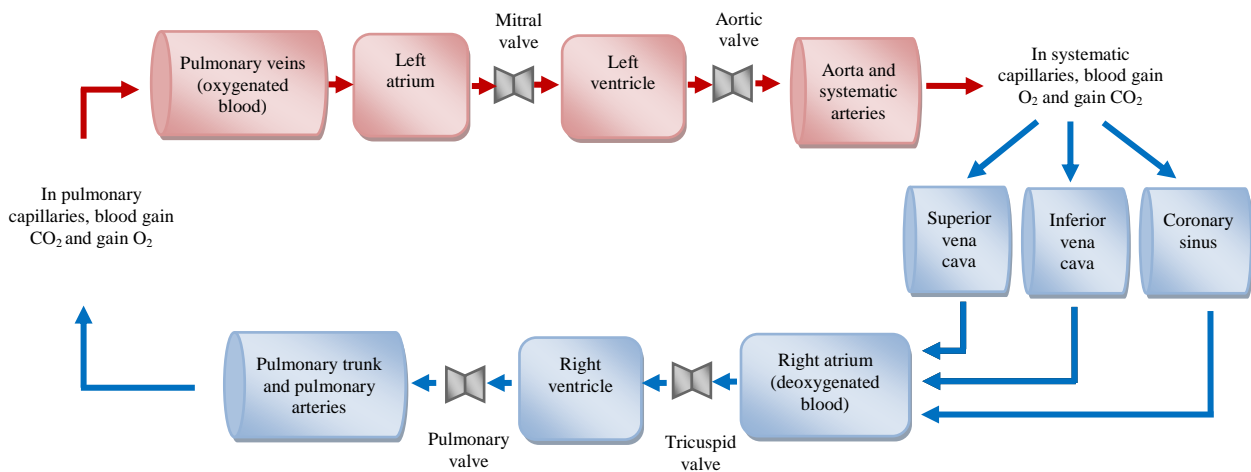


Figure 2.2 - Systemic and pulmonary circulations

2.2 Cardiac cycle

The heart performs these functions through regular rhythmic phases of contraction and relaxation known as the cardiac cycle. A single cardiac cycle includes all the events in the atria and ventricles associated with one heart beat. In one cardiac cycle, the atria and ventricles alternately contract and relax. This sequence generates the rhythmic pressure fluctuations that determine opening and closing of the heart valves and forcing blood from areas with high pressure to areas of lower pressure.

There are two phases in the cardiac cycle, systole (contraction) and diastole (relaxation). During systole, the right and left ventricles are contracting resulting in blood being pumped out to the lungs (via pulmonary artery) and to the rest of the body (via the aorta). No blood is entering the ventricles because both mitral and tricuspid valves are closed during systole. However, blood continues entering the atria through the vena cava and pulmonary veins.

Diastole is the period when the ventricles are relaxed. During this period, blood is passively flowing from the left atrium (LA) into the left ventricle (LV) and from the right atrium (RA) into the right ventricle (RV). The blood flows through the mitral valve and the tricuspid valve. At the end of diastole, both atria contract and propel an additional amount of blood into the ventricles. Figure 2.3 shows the systole and diastole phases and the respective flow of blood has been explained in the previous paragraph.

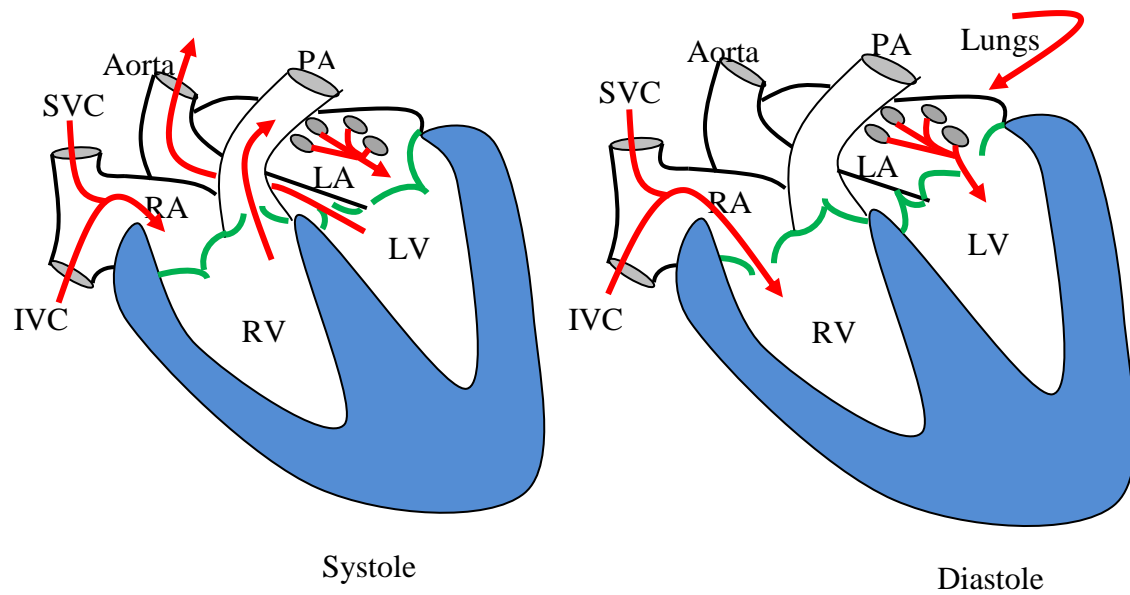


Figure 2.3 - Systole and diastole

The number of cardiac cycles per minute is defined as heart rate.

2.3 Heart rate control mechanisms

There are 3 mechanisms that control the heart rate: neurologic, humoral and intrinsic.

2.3.1 Neurologic

The heart rate is controlled mainly by the autonomic nervous system. Stimulation of the sympathetic system (with the release of its neurotransmitter noradrenaline) increases heart rate whereas stimulation of the parasympathetic system (whose neurotransmitter is acetylcholine) decreases heart rate [Levy and Pappano, 2007]. The parasympathetic system is predominant when the body is at rest. Inhibition of the parasympathetic by atropine increases the heart rate substantially, whereas inhibition of the sympathetic system by propranolol decreases the heart rate.

2.3.1.1 Baroreceptor reflex regulates the heart rate

Baroreceptors are stretch receptors located in the carotid sinuses and in the aortic arch. The changes in the atrial blood pressure cause inverse changes in heart rate as shown in Figure 2.4(a). The effects of changes in carotid sinus pressure on the sympathetic and parasympathetic activity are shown in Figure 2.4(b). The heart rate changes over the range of atrial pressure are mediated by sympathetic and parasympathetic activity.

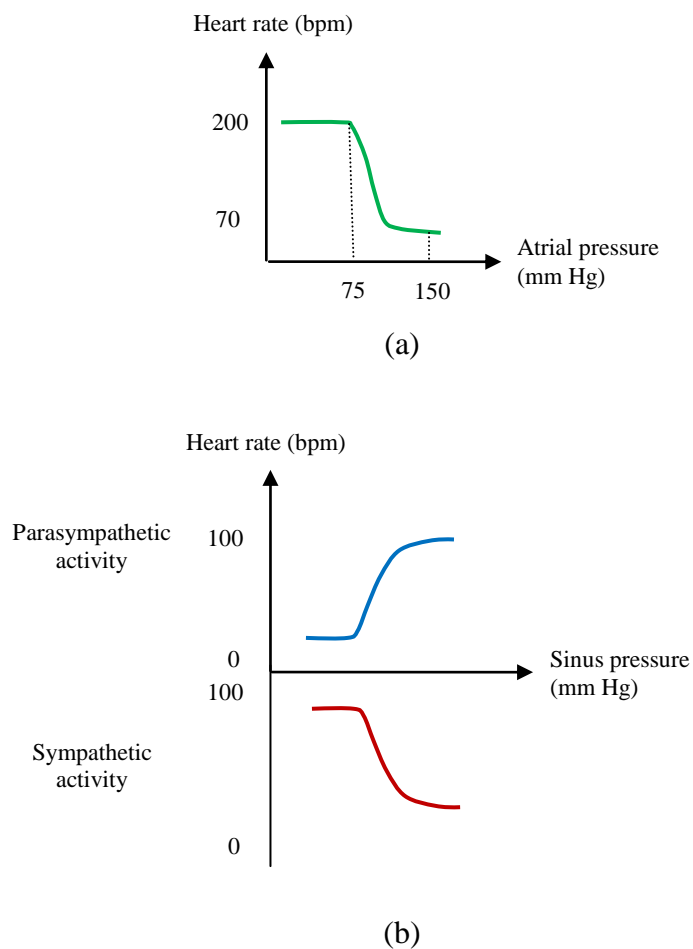


Figure 2.4 - Heart rate is regulated by Baroreceptor Reflex; (a) atrial blood pressure inversely changes in heart rate (b) changes in carotid sinus pressure on the sympathetic and parasympathetic activity.

When the blood pressure falls, the baroreceptors are stretched less, and this information is coded and sent to the cardiovascular (CV) centre. In response, the CV centre decreases

parasympathetic stimulation and increases sympathetic stimulation of the heart. Conversely, when the blood pressure increased, the baroreceptors send impulses at a faster rate to the CV centre. The CV centre responds by increasing parasympathetic stimulation and reducing sympathetic stimulation. Consequently, both the heart rate and force of contraction decrease.

One of the ways by which the heart keeps blood flowing properly is the Bainbridge Reflex.

2.3.1.2 Bainbridge reflex

The purpose of the bainbridge reflex is to make sure the amount of arterial blood being pumped out of the heart to the body equals the amount of venous returning to the heart from the body. When the inflow of venous blood increases, it will distend the right atrium more. An increasing in right atrial stretching (increased venous return) leading to increased heart rate (increased atrial output) is called the Bainbridge Reflex. Infusions of blood or saline solution increase atrial pressure and consequently accelerate the heart rate [Bainbridge, 1915].

2.3.2 Humoral

The principal humoral mechanisms were shown to be neurally mediated with a reduction in the secretion of vasopressin (antidiuretic hormone) by the pituitary gland [Levy and Pappano, 2007]. If vasopressin increases, urine volume decreases reducing blood volume and that will increase heart rate. However, if vasopressin decreases, urine volume increases decreasing blood volume which therefore slows down the heart rate.

2.3.3 Intrinsic

The intrinsic ability of the heart to change inotropically as a response to changes in the volume of inflowing blood is called Frank-Starling mechanism [Levy and Pappano, 2007]. The mechanism means that when the extra amount of blood flows into the heart (atria), the cardiac muscle itself is pre-stretched before systole. This in turn causes the muscle to contract with increased force increasing stroke volume.

2.4 Cardiac output

Cardiac output (CO) is the amount of blood ejected from the left ventricle into the aorta each minute [Tortora and Derrickson, 2009, Guyton and Hall, 1996]. The cardiac output varies with the level of activity of the body. Age, size of the body, exercising and metabolism are the factors that influence cardiac output. In human adults, the average cardiac output is about 5 litres per minute for man and 10 to 20% less for women.

Cardiac output (millilitres per minute) is a product of heart rate (beats per minute) and stroke volume (millilitres per beat). Stroke volume is the amount of blood ejected by the left ventricle with each contraction.

$$\begin{matrix} CO \\ (ml/min) \end{matrix} = \begin{matrix} SV \\ (ml/beat) \end{matrix} \times \begin{matrix} HR \\ (beats/min) \end{matrix}$$

2.5 Normal cardiac electrical propagation

Normal cardiac electrical propagation is illustrated in Figure 2.5.

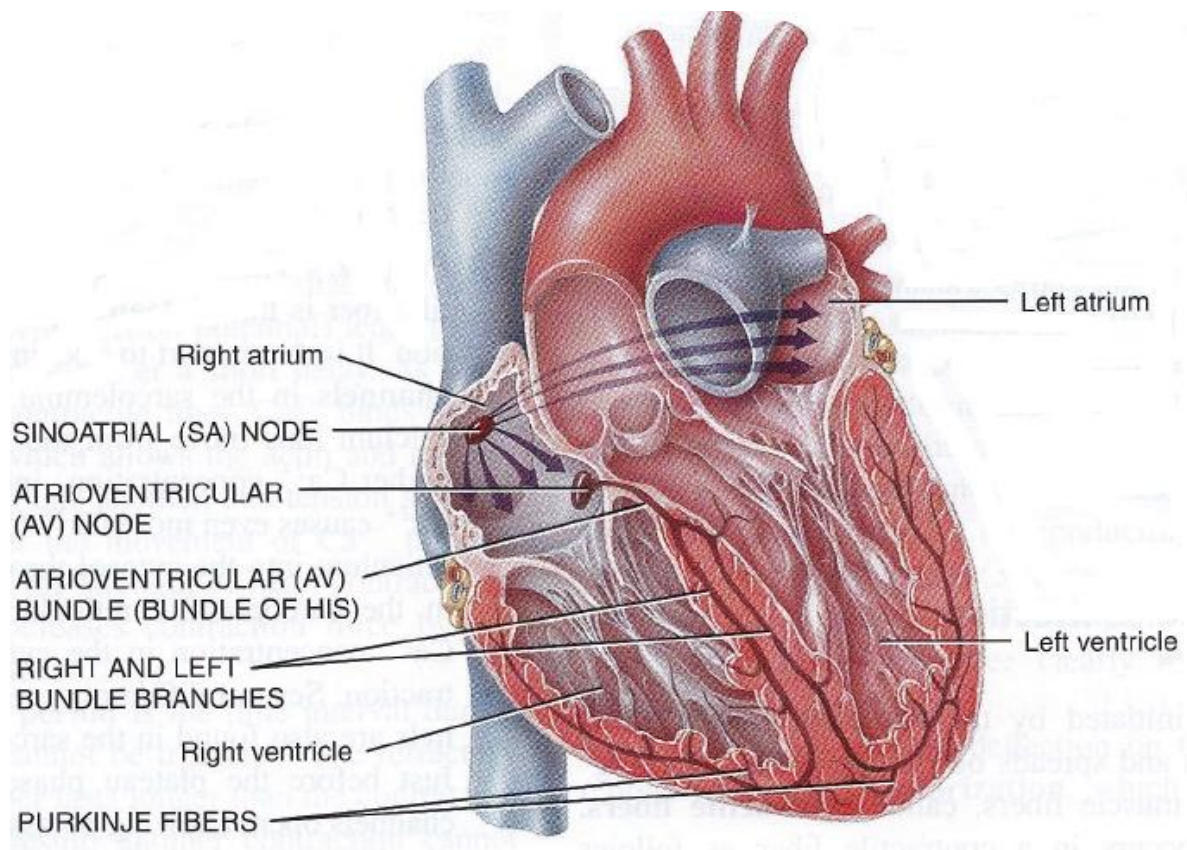


Figure 2.5 - Conduction system of the heart [From Tortora and Derrickson, *Principles of Anatomy and Physiology*, 2009, John Wiley & Sons, Inc, with permission]

The electrical conduction system is composed of the sinus node (pacemaker), the atrioventricular (AV) node with its anterior (fast) and posterior (slow) AV nodal fibres and the His-Purkinje system (His bundle, bundle branches and Purkinje fibres) [Conover, 1996].

The sinoatrial (or 'sinus') node, located high in the right atrium, near the superior vena cava, activates the atria via gap junctions at a rate consistent with the needs of the body. Atrial activation propagates from superior to inferior and from right to left. The impulse reaches the AV node, located in the septum between the two atria through the fast AV nodal pathway before atrial activation is completed. It is then conducted down the bundle of His (the only electrical connection between the atria and the ventricles) and into the ventricles through the

bundle branches (right and left) and the Purkinje fibres (first to the apex of the ventricular myocardium and then upward to the remainder of the ventricular myocardium).

The electrical cardiac cycle consists of three phases;

- a) Depolarisation
- b) Repolarisation
- c) Resting

The resting myocardial cell is negatively charged to about -90 mV. This negative charge is maintained until the cell is activated (depolarisation) or activates itself (automaticity).

2.5.1 Depolarisation

Depolarisation is the process by which a resting cell becomes more positive. Impulse from the sinus node activates a myocardial cell and it rapidly switches from its resting negative voltage of -90mV to a positive voltage [Lamb *et al.*, 1991, Marieb and Hoehn, 2007, Levy *et al.*, 2006] that momentarily reaches +30 mV. It is due to a large increase in permeability to sodium.

2.5.2 Repolarisation

Repolarisation is the process by which a depolarised cell is restored to its resting state. The process of repolarisation begins immediately after rapid depolarisation; a current flow maintains the membrane at a plateau of approximately 0 mV and then rapidly restores the membrane to its resting state of -90 mV. It is associated with an increase in potassium permeability and a return of the calcium permeability to normal. The plateau allows a refractory period to occur [Lamb *et al.*, 1991, Marieb and Hoehn, 2007], preventing the cell

from being activated again and ensures that each contraction is followed by enough time to allow the heart chamber to refill with blood before the next contraction.

2.5.3 Automaticity

Automaticity is the ability of a cell to depolarise itself (slow depolarisation). It reaches threshold potential, and produces an action potential. The cells of the conduction system differ from those of the rest of the heart as they are capable of spontaneous depolarisation (have the property of automaticity). Atrial and ventricular myocardial cells normally do not depolarise spontaneously [Conover, 1996]. Normally healthy cells will await a stimulus from the sinus node or another pacing source to activate them.

2.6 Action potential

Action potentials occur as the membrane suddenly depolarises and then repolarises back to its resting stage [Klabunde, 2005]. The action potential is due to the sequence of permeability changes to sodium and potassium [Levy *et al.*, 2006]. Figure 2.6 shows the ion channel changes during resting and depolarisation.

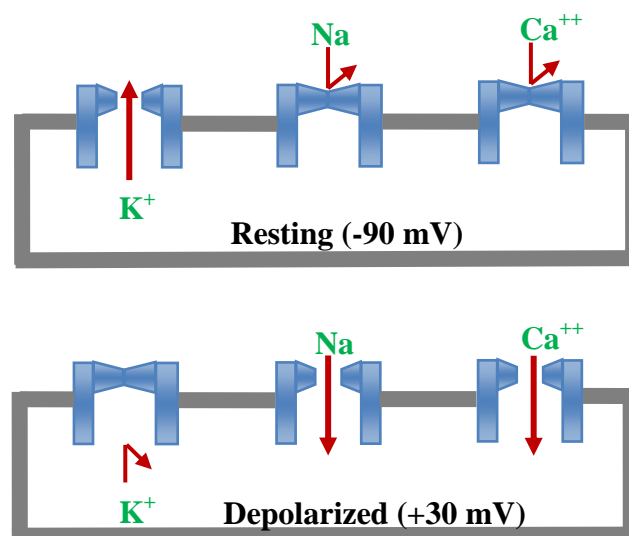


Figure 2.6 - Ions influx and efflux during resting and depolarisation.

The different phases of the action potential (Figure 2.7) represent:

1. rapid depolarisation (phase 0)
2. initial depolarisation (phase 1)
3. the plateau (phase 2)
4. rapid repolarisation (phase 3)
5. resting (phase 4)

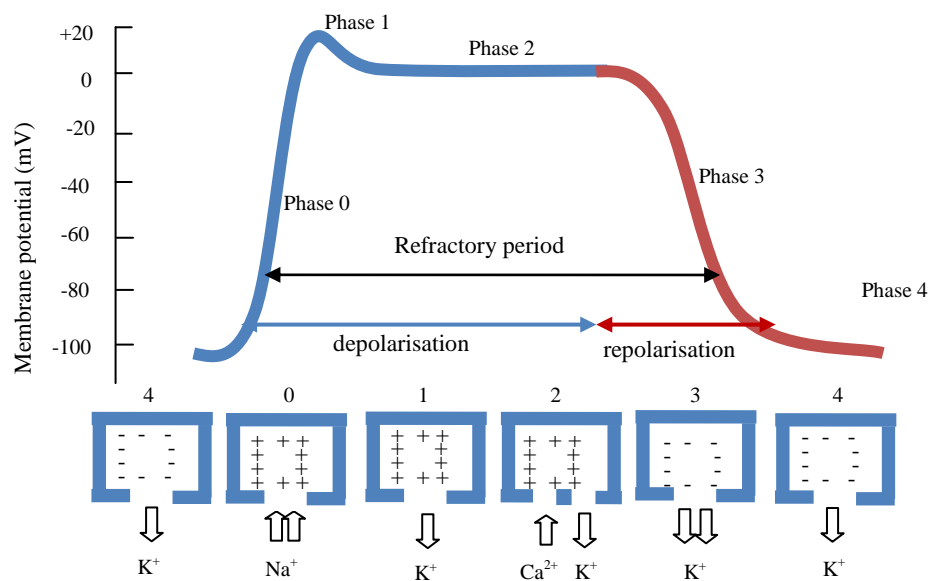


Figure 2.7 - Action potential

Phase 0

The rapid depolarisation in phase 0 is related to the influx of ion sodium (Na^+) into the myocyte. This initiates a positive feedback cycle that causes the increasing phase of the action potential (the membrane potential reverses from -90 mV to nearly +30 mV) [Marieb and Hoehn, 2007].

Phase 1

Phase 1 begins as the sodium ion channels begin to inactivate. The influx of sodium ion is slow, for the meantime the cell continues to lose potassium and chloride ions. The upstroke of the potential is followed immediately by early repolarisation [Levy *et al.*, 2006]. Repolarisation is brief and caused by the activation of a transient outward ionic current which consists mainly of K^+ .

Phase 2

Phase 2 is the plateau phase of the cardiac action potential. In this phase of the action potential Ca^{2+} enters the myocardial cell, which travels much more slowly than do the fast Na^+ ions. The influx of positive charge carried by Ca^{2+} is counterbalanced by the efflux of positive charge carried by K^+ . The permeability of K^+ is decreased which prolongs the plateau and prevents rapid repolarisation.

Phase 3

Phase 3 is the rapid repolarisation of the cardiac action potential. After a delay, the voltage-gated channel K^+ is open; this increases the membrane permeability to potassium. Consequently K^+ diffuses out more rapidly due to the concentration difference. At the same time the calcium channel is closed. When more K^+ ions leave the cell and fewer Ca^{2+} ions enter, the negative resting membrane potential is restored.

Phase 4

At phase 4 the cell has returned to resting membrane potential. This is the state in which the cell remains until it is again stimulated by an external electrical stimulus. This phase of the action potential is associated with diastole of the chamber of the heart.

There are two types of cardiac action potential; fast response and slow response [Levy *et al.*, 2006]. The fast response occurs in normal atrial and ventricular myocytes and in the specialized conducting fibres (Purkinje fibres) of the heart. The slow response occurs in the sinoatrial (SA) and atrioventricular (AV) nodes and the response depends on how rapidly they depolarise. Figure 2.8 shows a comparison of the action potentials of fast response and slow response cardiac cells.

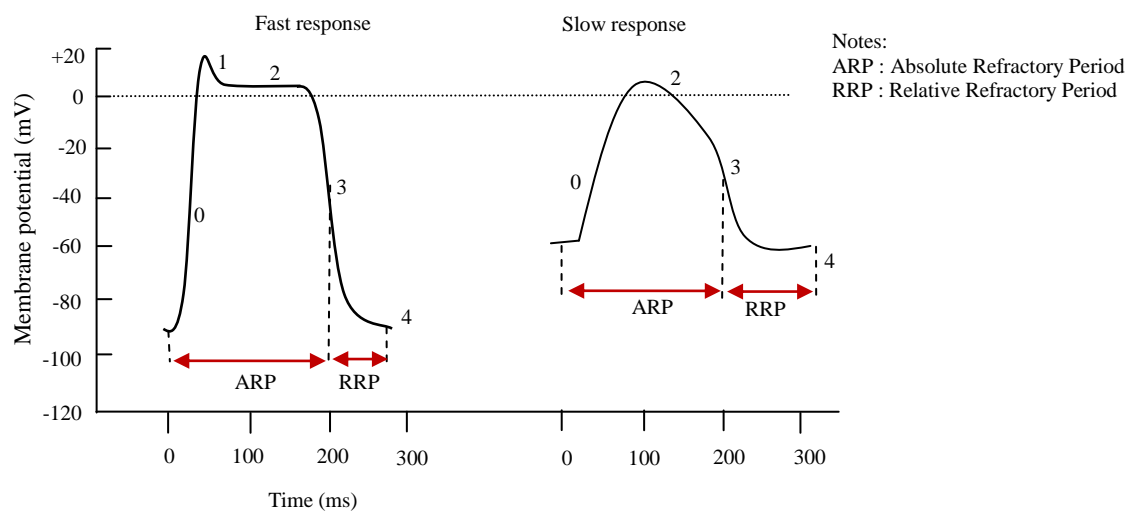


Figure 2.8 - Action potentials: fast response (left) and slow response (right).

Refractory period in cardiac muscle

In muscles, an Absolute Refractory Period (ARP) is the time interval during which a second contraction cannot be triggered [Tortora and Derrickson, 2009]. This means that no matter how strongly the cell is stimulated, it is unable to undergo a second action potential [Levy *et al.*, 2006]. The duration of the absolute refractory period in the ventricle is approximately 250 ms to 300 ms [Marieb and Hoehn, 2007, Guyton and Hall, 1996]. During Relative Refractory Period (RRP), the cell is able to be stimulated for a second action potential, but it requires a

stronger than normal stimulus. The RRP duration is about 50 ms. The ARP for atrial muscle is shorter than that for ventricular muscle (about 150 ms) and the RRP is another 30 ms.

2.7 ECG leads

There are 2 types of the ECG leads; bipolar leads and unipolar leads.

2.7.1 Bipolar leads

The bipolar leads consist of 2 or 3 limb electrodes placed on different regions of the body and the electrical activity is recorded between the electrodes. Table 2.1 shows the classical location of positive and negative electrodes.

Table 2.1 - Electrodes location

	Negative electrode	Positive electrode
Lead I	Right arm	Left arm
Lead II	Right arm	Left leg
Lead III	Left arm	Left leg

2.7.2 Unipolar leads

Unipolar leads use a single exploring electrode to record electrical cardiac activity. The second electrode is maintained at 'zero' potential (by connecting all the limb leads together at central common terminal, so that electrical activity is cancelled out). Unipolar leads record electrical activity from six chest positions (called V1, V2, V3, V4, V5 and V6). Augmented

unipolar leads are also taken from electrodes on the right arm (aVR), left arm (aVL) and left leg (aVF).

Figure 2.9 shows the standard positions for bipolar leads and unipolar leads.

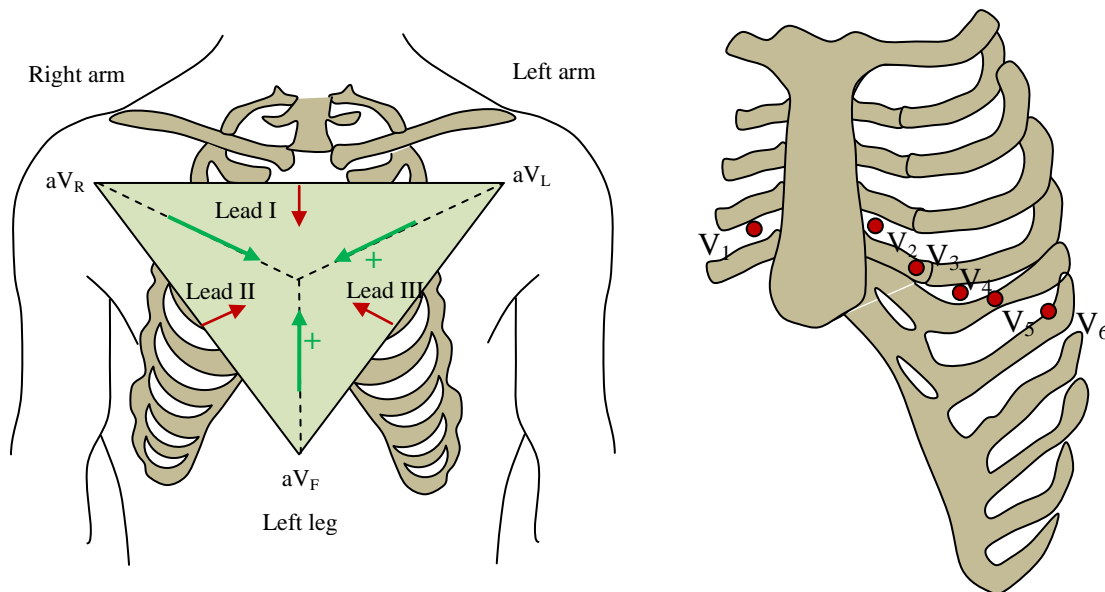


Figure 2.9 - Bipolar and unipolar leads

2.8 Normal electrocardiogram

Action potential propagation through the heart generates electrical voltages that can be measured at the surface of the body [Tortora and Derrickson, 2009]. The record of the electrical activity of the heart is called an electrocardiogram (ECG). The ECG is a composite of all the action potentials produced by all the heart muscle fibres during each heart beat.

Figure 2.10 shows the components of the surface ECG.

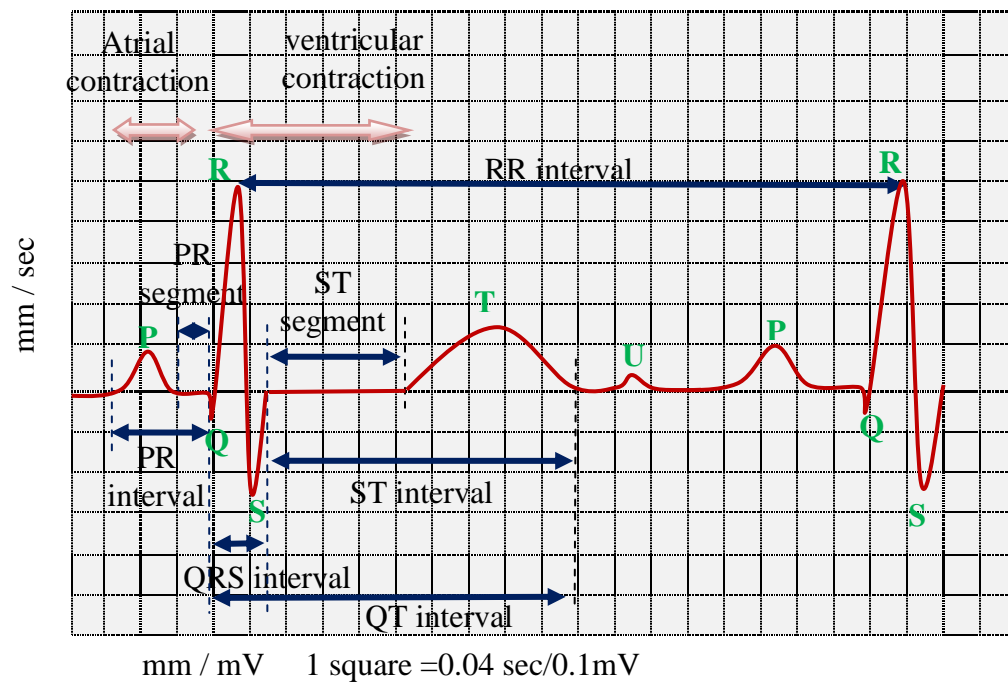


Figure 2.10 - Components of a surface ECG.

Table 2.2 shows the description and the duration of ECG waves and the intervals [Clifford *et al.*, 2006].

Table 2.2- ECG waves and intervals

Component	Description	Duration
P wave	SA node fires, sending the electrical impulse outward to stimulate both atria.	0.11 s Amplitude no more than 0.3 mV
QRS interval	Impulse from the Bundle of His throughout the ventricular muscles.	0.08 - 0.12 s
T Wave	Ventricular repolarisation, meaning no associated activity of the ventricular muscle.	Amplitude no more than 0.5 mV
PR interval	Time in which impulse travels from the SA node to the atria and downward to the ventricles.	0.12 – 0.20 s
QT interval	Duration of ventricular depolarisation and repolarisation.	less than 0.40 s
ST interval	From the QRS complex finishing point to the end of the T wave.	0.32 s
RR interval	Duration of ventricular cardiac cycle.	0.6 - 1.2s
PP interval	Duration of atrial cycle.	Depends of heart rate

Table 2.3 shows the sequence of excitation of the heart and its respective heart's electrical signal (ECG).

Table 2.3 - Sequence of excitation of the heart and its respective heart's electrical signal (ECG)

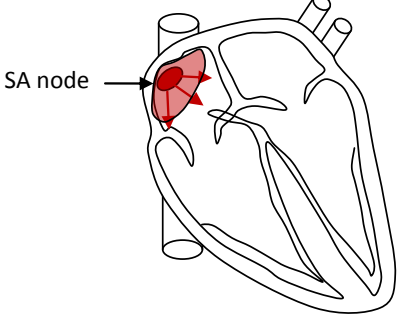
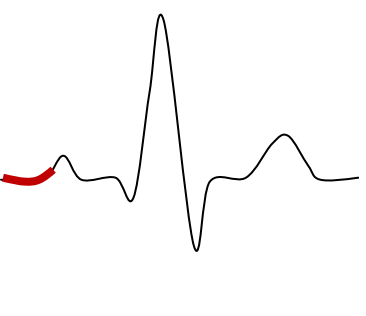
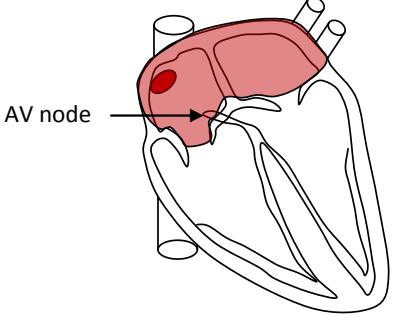
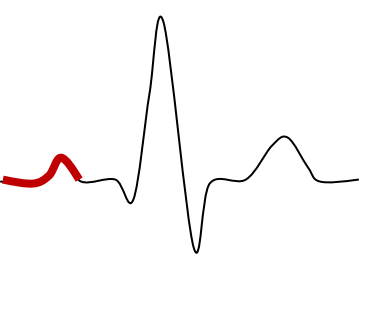
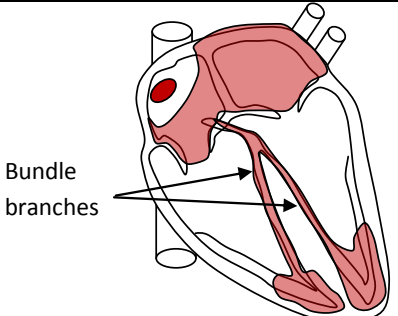
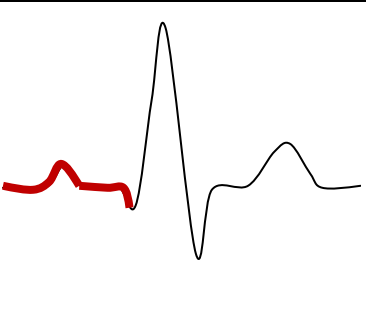
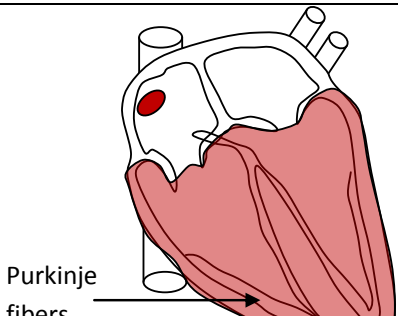
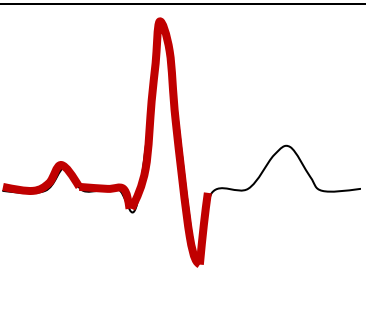
Sequence	Excitation of the heart	Deflection of ECG tracing
Atrial excitation begins: <i>Impulse generated by SA node</i>		
<i>Impulse delayed at AV node</i>		
Ventricular excitation begins: <i>Impulse passes to heart apex</i>		
<i>Ventricular excitation complete</i>		

Figure 2.11 shows the ECG tracing from a healthy normal heart.

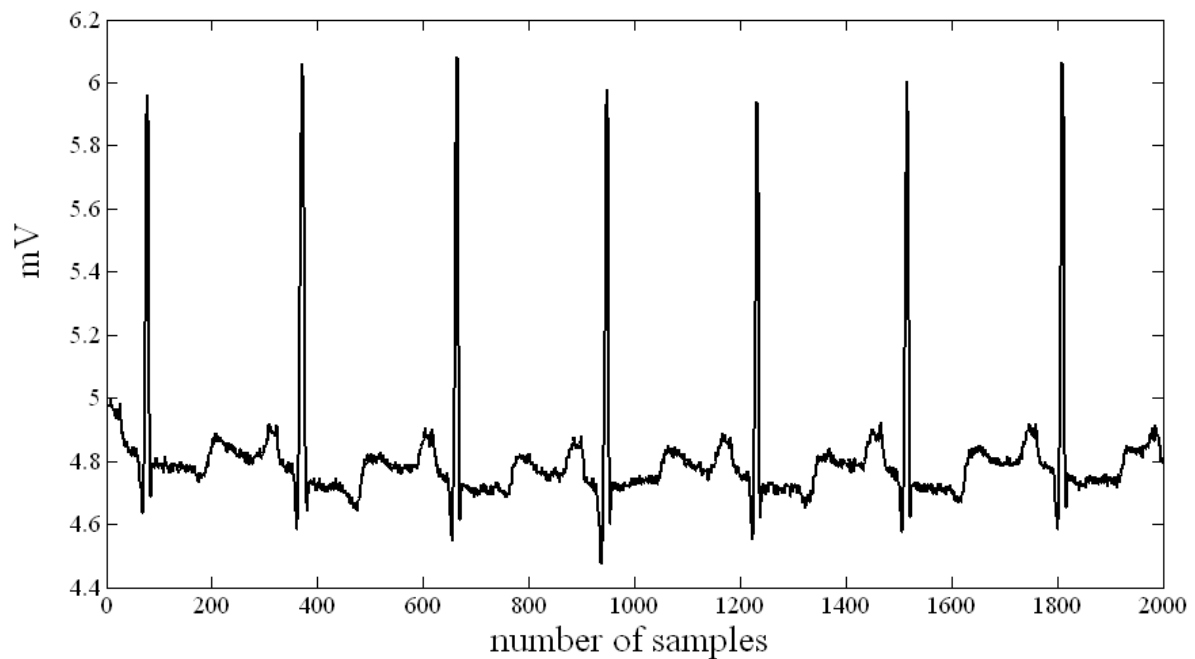


Figure 2.11 - Normal ECG

Use of the ECG in diagnosis

There are forms of description are needed before interpretation the ECG. The description should be specified in the same sequence [Hampton, 2008]:

- Rhythm
- Conduction interval
- Cardiac axis
- A description of QRS complex
- A description of a ST segments and T waves

The ECG changes in many conditions but only in some instances these changes are of diagnostic value. In many cases the changes are non-specific.

2.9 Nervous System

The nervous system is divided into two anatomical branches [Finkel *et al.*, 2006, Wolf *et al.*, 1991]

1. the central nervous system (CNS) which composed of the brain and spinal cord;
2. the peripheral nervous system (PNS) which includes neuron located outside the brain and spinal cord.

Figure 2.12 shows the organization of the nervous system.

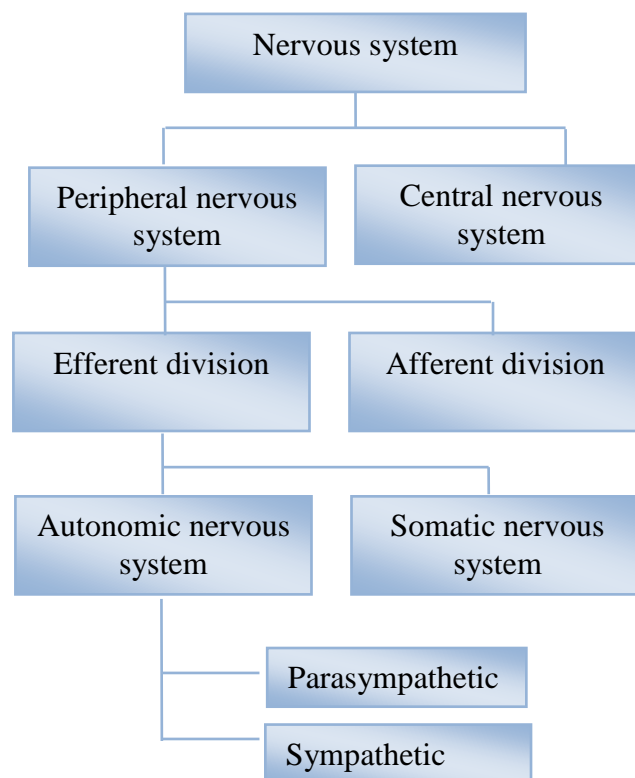


Figure 2.12 - Organization of the nervous system

The peripheral nervous system (PNS) is subdivided into:

1. the efferent division (the neurons of which carry signals away from the brain and spinal cord to the peripheral tissues);
2. the afferent division (the neurons that bring information from the periphery to the CNS).

Figure 2.13 shows the relationship between PNS and CNS.

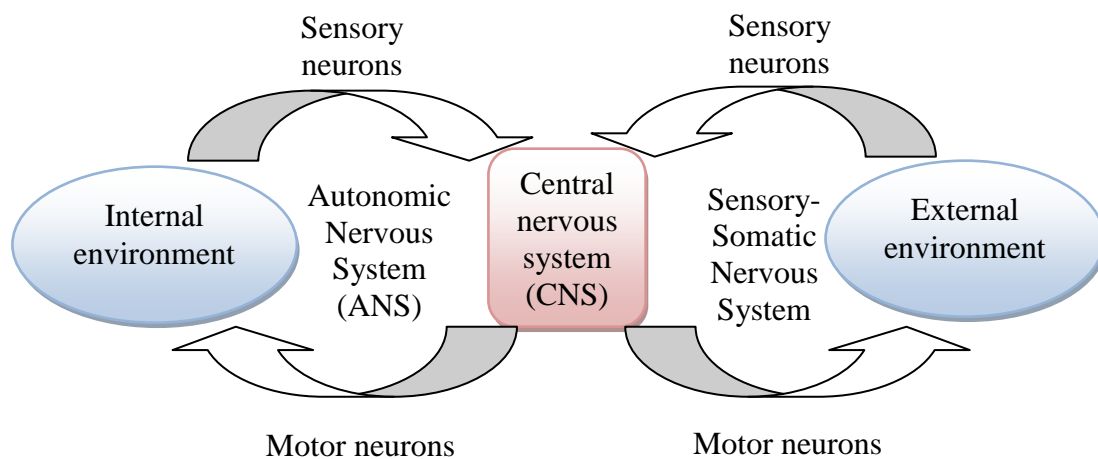


Figure 2.13 - PNS and CNS relationship.

The efferent division is subdivided into:

1. Autonomic nervous system (ANS)

The ANS is predominantly an efferent system transmitting impulses from the Central Nervous System (CNS) to peripheral organ systems. The ANS carries commands to smooth muscles, glands, and the heart. This will help maintain blood pressure, water and salt balance, dissolved gas concentration, etc.

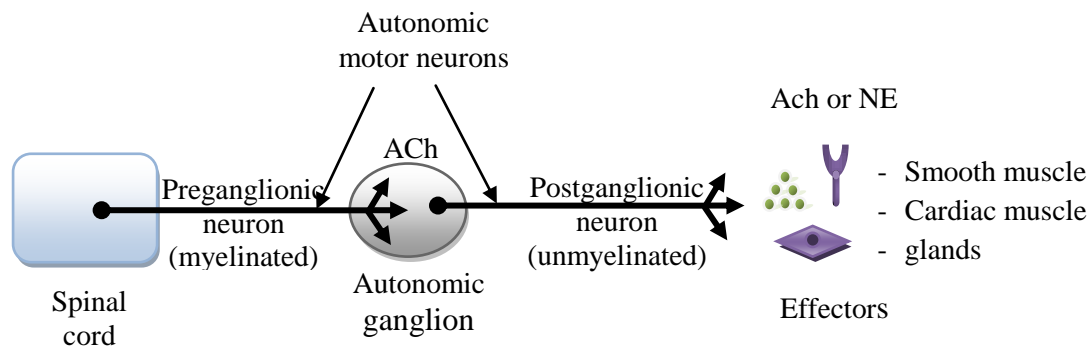
The ANS makes use of pairs of motor neurons. The body of the first motor neuron lies in the CNS, and the body of the second motor neuron lies in an autonomic ganglion (*i.e.*, the sympathetic trunk ganglia).

The ANS includes the sympathetic and parasympathetic division. The two divisions often innervate the same effectors, but they have opposing effects. As an example, the sympathetic division increases blood pressure, and the parasympathetic division decreases it.

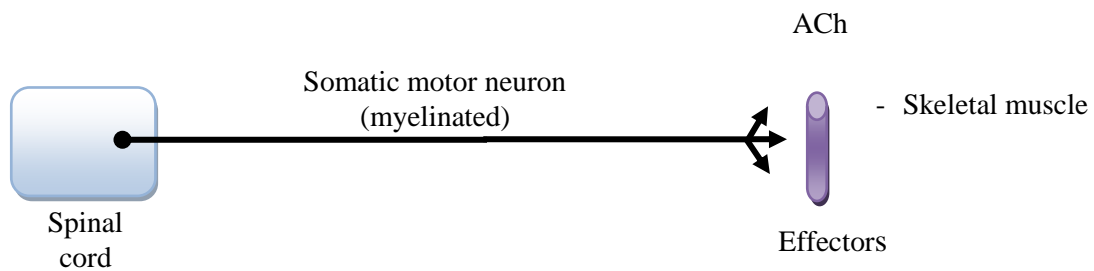
2. Somatic nervous system

This system is said to be voluntary because the responses can be controlled consciously. The somatic nervous system enervates all sensory organs, including the tongue, ears, eyes, and skin, as well as all the skeletal muscles, and the muscles attached to the bone and used for voluntary movement.

Figure 2.14 shows the motor neuron pathway in the ANS [Tortora and Derrickson, 2009]. There are 2 motor neurons in series. The first neuron has its cell body in the CNS; its myelinated axon extends from the CNS to an autonomic ganglion. The cell body of the second neuron is also in that autonomic ganglion; its unmyelinated axon extends directly from the ganglion to the effectors (smooth muscle, cardiac muscle or glands). In contrast, in somatic nervous system a single myelinated axon extend from CNS to the effector (skeletal muscle).



(a) Autonomic nervous system



(b) Somatic nervous system

Figure 2.14 – Motor neuron pathway in the ANS

Sympathetic division

The changes experienced by the body during emergencies have been referred to ‘fight or flight’ response. This response was first described by Walter Cannon in the 1920s [Cannon, 1920] as a theory that animals react to threats with a general discharge of the sympathetic nervous system. These reactions are triggered both by direct sympathetic activation of the effector organs and by stimulation of the adrenal medulla to release adrenaline and lesser

amounts of noradrenaline [Finkel *et al.*, 2006]. A major action of these hormones is to initiate rapid heart beating, heavy breathing and/or increase blood flow.

Parasympathetic division

In contrast to ‘fight or flight’ activities in sympathetic division, the parasympathetic enhances ‘rest and digest’ activities [Tortora and Derrickson, 2009]. Parasympathetic response support body function to restore more energy during time in rest and relaxing. Figure 2.15 shows the sympathetic and parasympathetic actions are elicited by different stimuli.

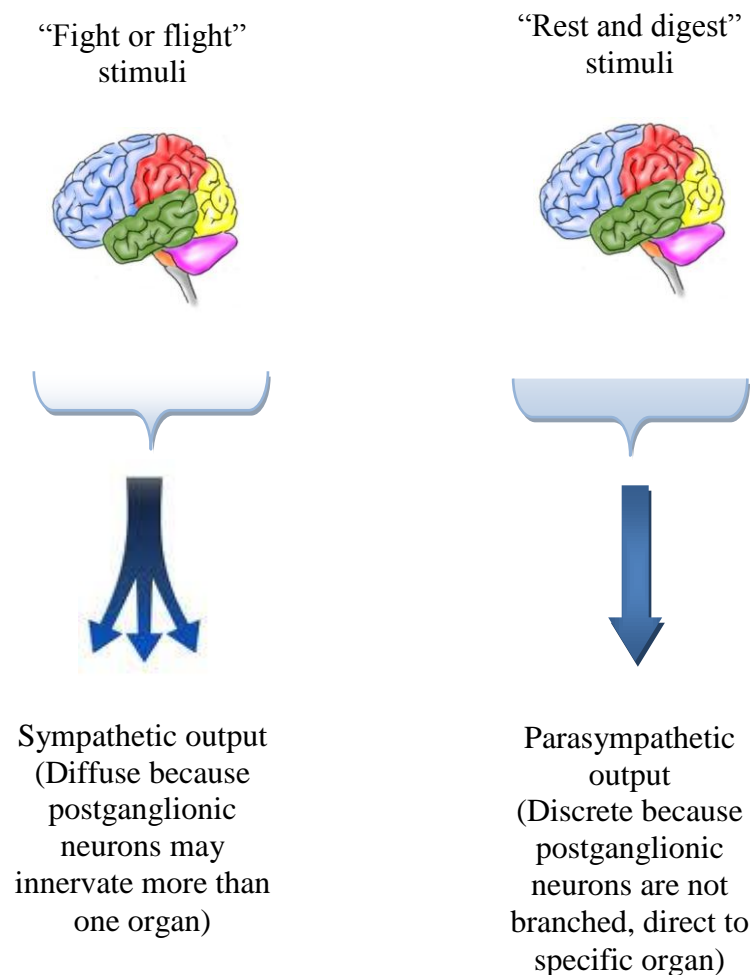


Figure 2.15 - Sympathetic and parasympathetic actions

Sympathetic and parasympathetic stimulation have opposite effects on organs that receive dual innervation. Figure 2.16 shows the structure of sympathetic and parasympathetic divisions.

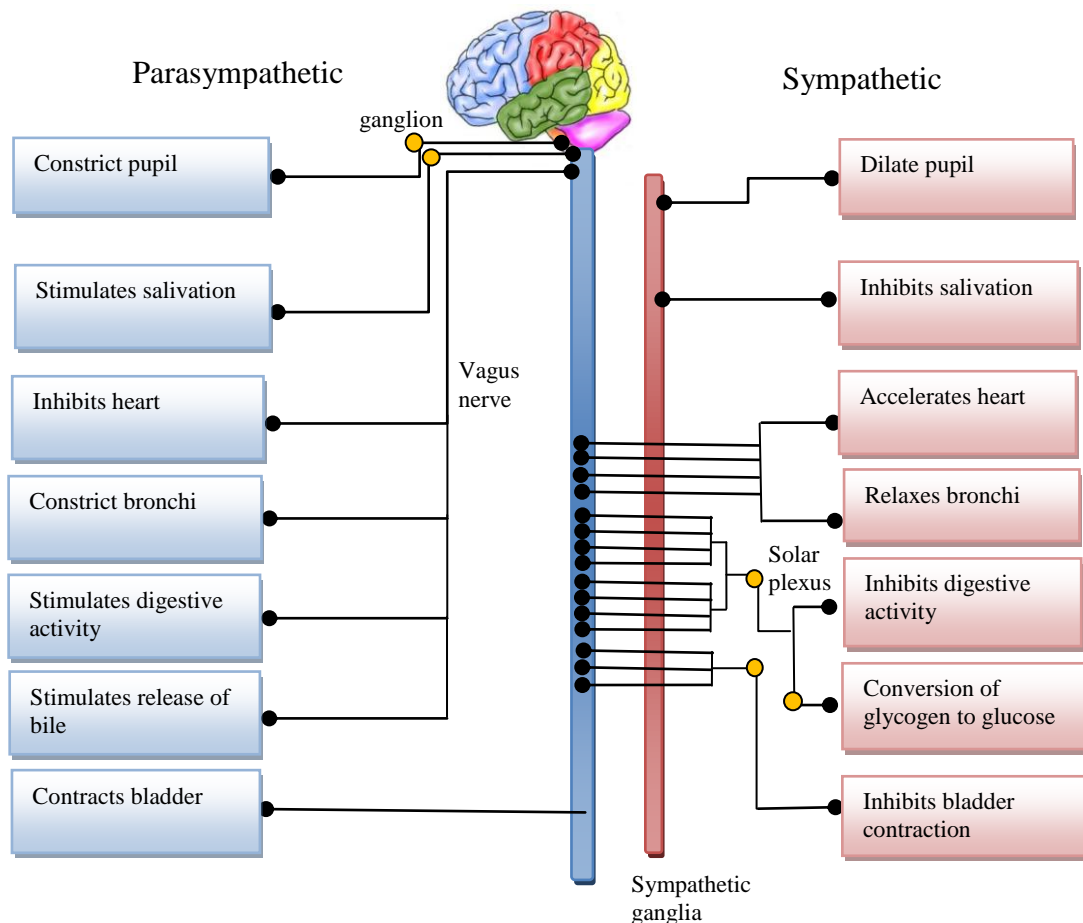


Figure 2.16 - Structure of sympathetic and parasympathetic divisions.

In ANS, the function of the ganglia is to provide relay points and intermediary connections between different neurological structures in the body, such as the peripheral and central nervous systems.

As a summary, in this chapter we are discussing about the normal physiology of the heart. In the next chapter, we will discuss about the abnormal physiology of the heart known as arrhythmias.

3 ARRHYTHMIAS

3.1 Introduction

An arrhythmia is an abnormality in the regularity of the heart beat [Youngson, 1992] and it will have an effect on heart pumping [Guyton and Hall, 1996]. Based on a figure of 300 000 sudden cardiac deaths per annum in the United States, the population incidence was just over 1/1000/year. An European study [Vreede-Swagemakers *et al.*, 1997] on victims between 20 and 75 years of age reported an overall yearly incidence of SCD of 1 per 1000. Cardiac arrhythmias occur when there is a malfunction in the electrical impulses within the heart, causing the heart to beat rapidly, slowly, or irregularly [Bennett, 2002]. The causes of cardiac arrhythmias are usually one or a combination of the following abnormalities of the heart [Guyton and Hall, 1996]:

1. Abnormal rhythmicity of the pacemaker;
2. Shift of the pacemaker from the sinus node to other parts of the heart;
3. Abnormal pathways of impulse transmission through the heart;
4. Blocks at different points in the transmission of the impulse through the heart;
5. Spontaneous generation of abnormal impulses in almost any part of the heart.

Cardiac arrhythmias can occur in either the atria (atrial fibrillation, supraventricular tachycardia, atrial tachycardia, Wolf-Parkinson-White syndrome) or the ventricles (ventricular tachycardia, ventricular fibrillation) [Bennett, 2002].

3.2 Fibrillation

Porter 1894 [Garrey, 1714] made this following statement about fibrillation regarding the nature of fibrillary process; *“Fibrillar contractions of the heart may be due to an interruption of the contraction wave. The contraction wave would thus be prevented from running its usual course, and the normal co-ordinated action of the ventricular cells would give place to the confusion conspicuous in fibrillary contractions.”*

Mines proposed a theoretical basis for the occurrence of re-entrant arrhythmias [Mines, 1913]. Supposing a rapid impulse travels in only one direction circuit, if the originally stimulated muscle fibres are still in refractory state, the impulse will die out because the refractory muscle cannot transmit a second impulse. The ability of circulating excitation to occur or persist depends on the relationship between conduction velocity, path length and the refractory period [Mayer, 1908]. There are three conditions that allow the impulse to travel around a path;

1. If the pathway around the circle is long, by the time the impulse returns to its point of origin, the originally stimulated muscle will no longer be refractory and the impulse can continue around the path.
2. If the velocity of the conduction becomes slow enough, an increased interval of time will elapse before the impulse returns to its point of origin. By this time, the originally stimulated muscle might be out of the refractory state and the impulse can continue around the path.
3. The refractory period of the muscle might become greatly shortened. In this case the impulse could also continue around the path.

Figure 3.1 shows the rapid impulse propagation causing the re-entry [Mines, 1913].



Figure 3.1 - Rapid and long impulse (modified from Mines, 1913).

However, if the impulse is slower and/or the refractory period is shorter, the excited state will have passed off at the region where the excitation started before the wave of excitation reaches this point again on the path at the completion of its revolution (Figure 3.2).



Figure 3.2 - Slow and short impulse (modified from Mines, 1913).

3.3 Ventricular Fibrillation

Ventricular Fibrillation (VF), first described by Erichsen in 1842, is the most serious cardiac arrhythmia [Erichsen, 1842]. It is described as the uncoordinated electrical activity of the heart [McWilliam, 1889]. The World Health Organization identified that the recorded deflections of ECG continuously change in shape, duration, magnitude, and direction [Robles *et al.*, 1978]. VF is responsible for 75 - 85% of sudden cardiac deaths [Weiss *et al.*, 2005, Logan *et al.*, 1981, Fish, 2004]. In 1940, Wiggers and Wegria demonstrated that VF could be induced when a strong stimulus was applied during certain period of the cardiac cycle [Wiggers and Wegria, 1940]. This period is called ‘vulnerable period’ and it corresponds

roughly to the T-wave of the surface ECG. VF is almost invariably fatal if it is not treated very rapidly. During VF the electrical signals are firing in a rapid, uncontrolled manner within the ventricle. This will cause heart to quiver rather than pump blood efficiently. The rate of electrical activation of the heart is too high at more than 550 excitations per minute. Figure 3.3 shows the electrical activity (Monophasic Action Potential) for VF, showing completely aperiodic and irregular beat-to-beat changes in the ventricular electrical complexes [Jalife, 2000].

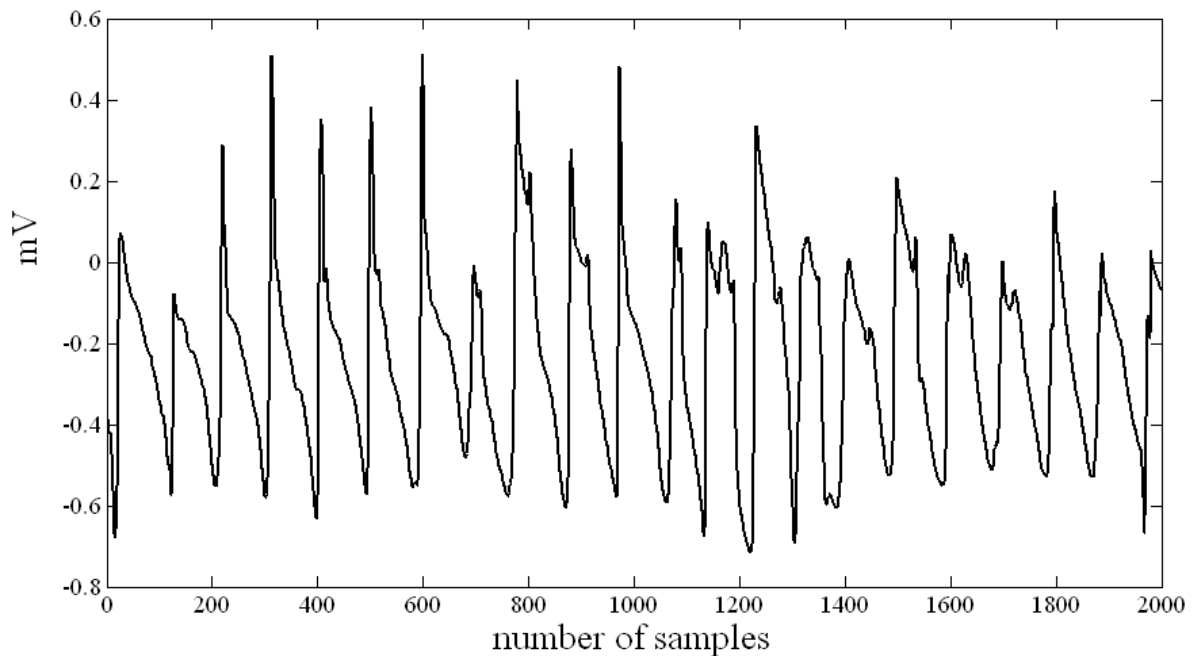


Figure 3.3 - Monophasic action potential (MAP) signal for ventricle fibrillation (sampling frequency 1 kHz)

From the Monophasic Action Potential we have an idea that the signal is extremely heterogeneous and complex during VF [Wiggers, 1940].

3.3.1 VF Mechanism

The mechanism of ventricular fibrillation has been under intense investigation but it remains unclear. Current debates discuss if the mechanism of VF is either based on the re-entrant idea [Han and Moe, 1964, Mines, 1913] or focal pattern [Sano and Tohru Sawanobori, 1970]. The mechanisms of conduction block have been one the focus in VF studies because conduction block is inherently involved in the initiation and maintenance of VF [Qin *et al.*, 2005].

3.3.2 VF symptoms

When a patient has VF, circulation stops and the patient collapses unconscious because the brain and muscles do not receive blood from the heart. There is no heart beat, blood pressure or respiration. The skin becomes cyanotic, cold and clammy; the patient becomes totally unresponsive in a short time with the pupils fixed and dilated [Joseph, 2002].

3.3.3 VF treatment

Immediate and effective treatment of ventricular fibrillation is important to avoid cardiac arrest. A number of studies indicate that cardiopulmonary resuscitation (CPR) must be started as soon as possible before advanced cardiac life support such as defibrillation, medications and endotracheal intubation (procedure by which a tube is inserted through the mouth down into the trachea) [Mickey *et al.*, 1984, Weaver *et al.*, 1986].

The treatment must be followed by defibrillation (an electrical shock delivered to the chest). A number of clinical studies show that the earlier electrical defibrillation is given, the greater the chances that the shock will be successful [Mark *et al.*, 1989, Weaver *et al.*, 1986]. The success of defibrillation to revert VF [Niemann *et al.*, 1992] is defined as:

1. termination of ventricular fibrillation;
2. termination of ventricular fibrillation followed by a spontaneous return to cardiac rhythm.

Valenzuela and his collaborators demonstrated the importance of early defibrillation and CPR to increase number of survival [Valenzuela *et al.*, 1997]. The curves corresponding to incremental delays from collapse are shown in Figure 3.4.

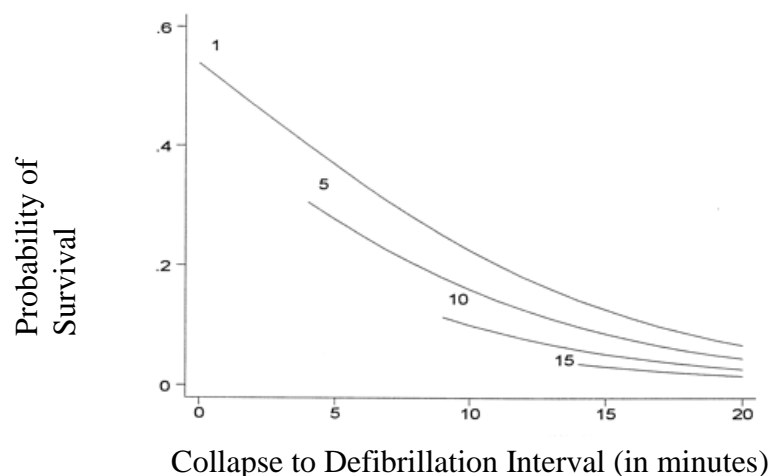


Figure 3.4 - Relation of time interval from collapse to CPR and defibrillation to survival [From Valenzuela TD *et al.*, *Estimating effectiveness of cardiac arrest interventions: a logistic regression survival model*, *Circulation* 1997; 96:3308-3313, with permission].

Weaver *et al.*, 1982 compared the effects of initial electrical shocks using 175 J and 320 J in patients with ventricular fibrillation [Weaver *et al.*, 1982]. They found that the survival is not related to the energy level for defibrillation. According to current guidelines, when using monophasic waveforms, the initial shock strength should be 200 J, followed by 300 J and 360 J until successful defibrillation [Kloeck *et al.*, 1997].

Antiarrhythmic drugs may then be given to help maintain the normal heart rhythm. Amiodarone prolongs the repolarisation of the action potential, increasing the effective

refractory period by blocking the potassium channels. However this drug has side effects such as bradycardia, thyroid, liver function disturbances, *etc.* Probability of having these side effects is 15% in the first year, increasing up to 50% when the drug is taken in long term [Erven and Schalij, 2010].

When the medication and defibrillation fails, ablation is another approach that needs to be considered. Haïssaguerre and collaborators reported the premature ventricular contraction from the Purkinje fibre network acts as a trigger for ventricular fibrillation in humans [Haïssaguerre *et al.*, 2002]. The reason why Purkinje fibre network produces ectopic rhythms that cause sudden death is unknown. It is probably related to the genetic basis, especially when the patient has family history of this disorder. Other research on animal studies shows that beta blocker drugs convert multiple wavelets VF to focal source VF and this focal source is near the papillary muscle. Ablation at this focal source terminated VF after 25 seconds [Pak *et al.*, 2003].

3.4 Atrial Fibrillation

The commonest heart rhythm abnormality encountered in clinical practice is Atrial Fibrillation (AF). There are about 2.3 million people in United States and 4.5 million people in the European Union with AF [Go *et al.*, 2001]. AF is associated with significant mortality and morbidity, especially when the patients have thromboembolic stroke [Kannel *et al.*, 1998, Benjamin *et al.*, 1998]. The prevalence of AF strongly depends on the age, with approximately 70% of individuals afflicted being between 65 and 85 years old [Fuster *et al.*, 2006]. According to the ATRIA study, AF was more common in white than in black patients, with incidences of respectively 2.2% and 1.5% [Go *et al.*, 2001].

Fuster *et al.*, 2006 defined AF in ACC/AHA/ESC as “a supraventricular tachyarrhythmia characterized by uncoordinated atrial activation with consequent deterioration of mechanical function” [Fuster *et al.*, 2006]. The World Health Organization task force defined AF as “irregular, disorganized electrical activity in the atria” [Robles *et al.*, 1978]. P-waves are absent on the ECG and the baseline consists of irregular waveforms, which continuously change in shape, duration, amplitude and direction. When the atrial rate is irregular, ventricular response also is irregular [Markides and Schilling, 2003]. Figure 3.5 shows the typical ECG for AF.

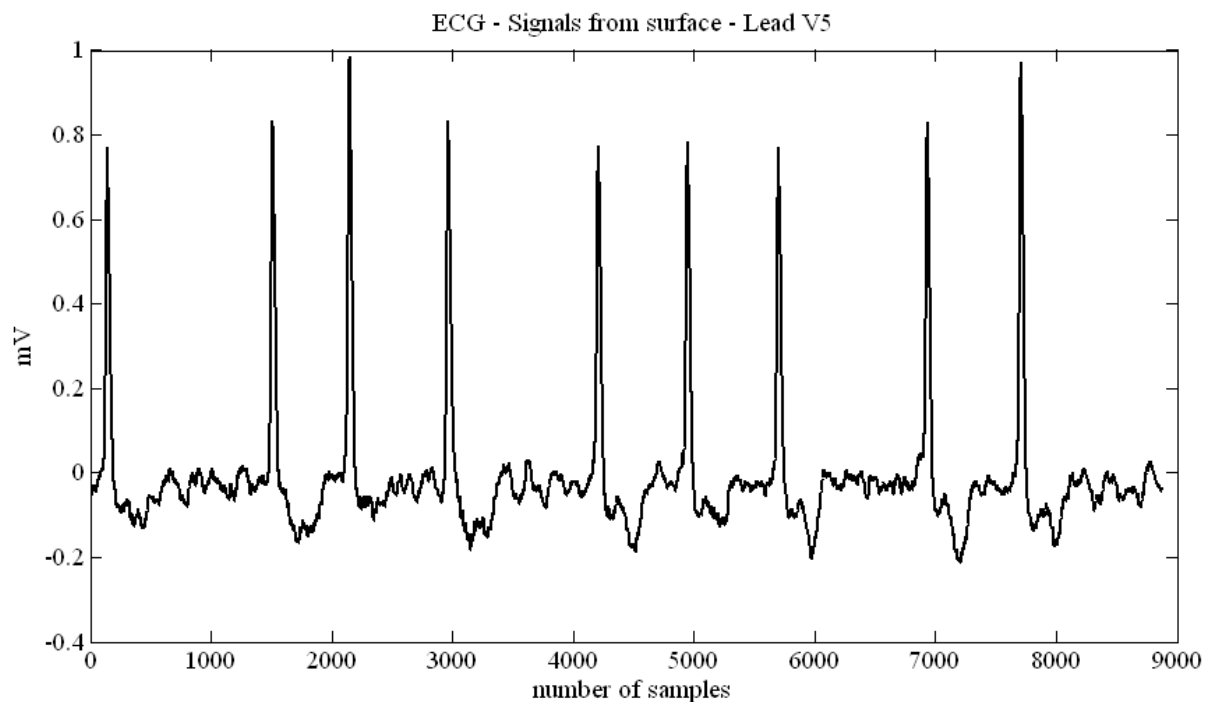


Figure 3.5 - Typical surface ECG of a patient in AF.

There are 3 clinical classifications of AF [Philip and Peter, 2001, Fuster *et al.*, 2006]:

1. Paroxysmal;
2. Persistent;
3. Permanent.

AF lasting less than 7 days is defined as paroxysmal. AF lasting more than 7 days and requiring electrical cardioversion to return to normal sinus rhythm is defined as Persistent. AF that continues indefinitely is classified as permanent. This classification is based on the regular trend of arrhythmia. It is useful to identify the cause and symptoms of arrhythmias. The majority of clinicians follow this classification in clinical practice. However an arrhythmia can change from paroxysmal to persistent or permanent.

During atrial fibrillation the atria fire at a rate of 350-600 per minute [Lemay *et al.*, 2004]. This creates small (or “fine”), irregular f (fibrillation) waves. Takahashi and co-workers investigated the relationship between the f wave’s amplitude and AF classification [Takahashi *et al.*, 1983]. They found that the f wave’s amplitude is smaller during paroxysmal AF than in persistent AF. The larger f waves in paroxysmal indicated a higher likelihood of progression to persistent AF.

3.4.1 AF Mechanism

The mechanism of AF is still not fully understood but is thought to involve either multiple wavelets [Moe *et al.*, 1959] propagating through the atria, focal high frequency re-entrant sources [Jalife J *et al.*, 1998] or autonomic nervous system also being implicated [Scherlag *et al.*, 2005]. The first drawings of structure and mechanism of arrhythmias (Figure 3.6) by Nathan and Eliakim bring attention to the presence of sleeves of cardiac tissue that extend onto the PVs [Nathan and Eliakim, 1966, Calkins *et al.*, 2007].

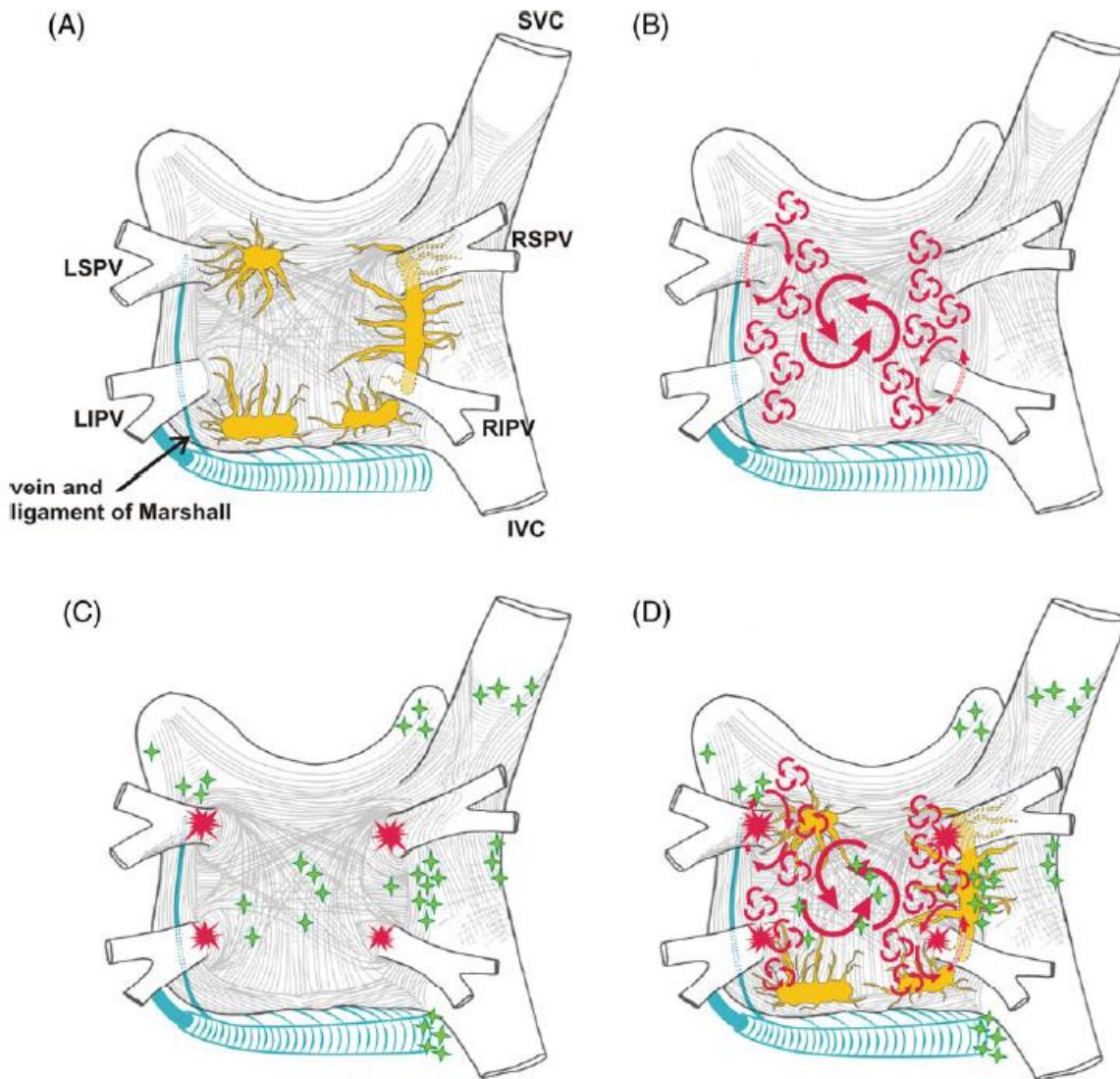


Figure 3.6 - Structure and possible mechanism of AF; (A) autonomic ganglion and axon (yellow), (B) wavelet and mother wavelet (red), (C) PV triggered (red) and non PV triggered (green), (D) all autonomic and arrhythmic mechanism [From Nathan and Eliakim., *The Junction Between the Left Atrium and the Pulmonary Veins: An Anatomic Study of Human Hearts*, *Circulation* 1996;34:412-422,with permission].

Figure 3.6 shows the electrophysiologic properties of the PVs and also the sleeves of myocardial tissue extend onto the superior and inferior vena cava. In animal studies, the investigators noted that AF was recorded from these thoracic veins [Zipes and Knopé, 1972]. It is also recognized that the muscular sleeves of the PVs are an important source of focal firing that may trigger or maintain AF.

In animal studies, the classic mechanisms of AF are from focal activity, single circuit or ‘mother wave’ re-entry and multiple re-entry [Nattel *et al.*, 2005]. Substantial effort on AF mechanisms in animal studies was performed in the late of 1800s and early 1900s. The ideas of AF mechanisms are highlighted in Figure 3.7.

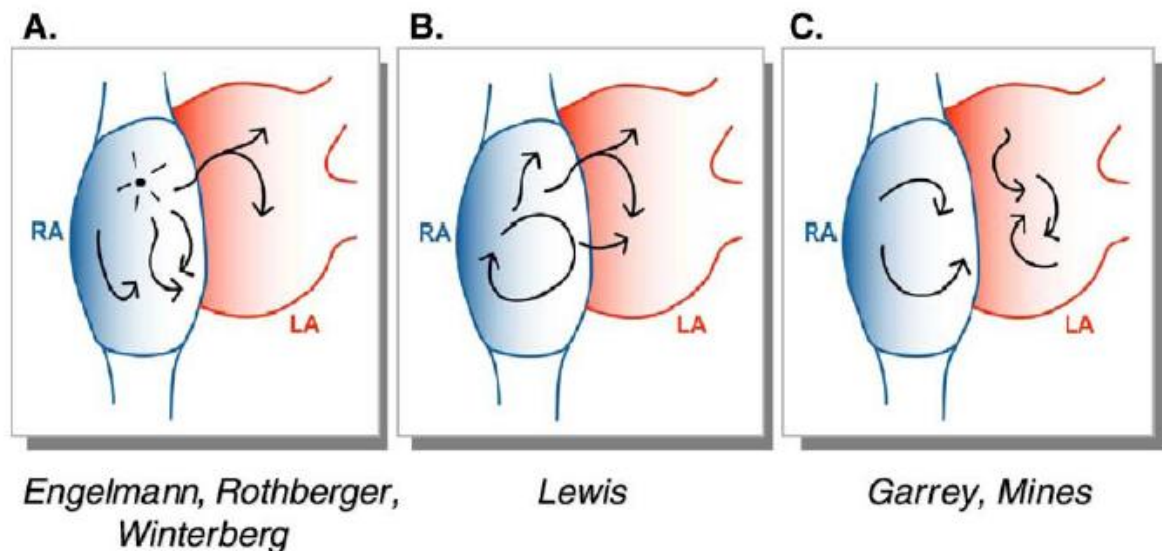


Figure 3.7 - AF mechanism [From Stanley Nattel *et al.*, *Mechanisms of Atrial Fibrillation: Lessons From Animal Models, Cardiovascular Diseases*, 2005; 48(1):9-28, with permission].

The significant spontaneous rhythmicity generated by heart fibres was first described by Engelmann in 1896 [Engelmann, 1896]. The characterization of AF via uncoordinated activity is produced by the activity of multiple ectopic foci by Winterberg and Rothberger *et al.* suggest that AF is underlined by a single rapid firing focus [Winterberg, 1906, Rothberger and Winterberg, 1915]. The idea of the AF mechanisms described by Engelmann, Winterberg and Rothberger was further discussed by Nattel *et al.* [Nattel *et al.*, 2005]. Lewis *et al.*, 1921 believed that single rapid re-entry circuit with fibrillatory conduction can cause AF while Mines [Mines, 1913] and Garrey [Garrey, 1924] mentioned that AF is due to a multiple functional re-entry circuit. The re-entrant circuit path first suggested by Mines had to be complex to account for the rapid chaotic atrial activation: As Garrey put it, “the impulse is

diverted into different paths, weaving and inter-weaving through the tissue mass, crossing and recrossing old paths again to course over them or to stop short as it impinges on some barrier of refractory tissue” [Garrey, 1924].

In order for the re-entry to be sustained, the circuit time has to be greater than the refractory period (RP) [Mines, 1913]. The minimum circuit time is equal to the refractory period, and the size of the smallest possible circuit is the distance travelled by the impulse in one refractory period is called the wavelength [Wiener and Rosenblueth, 1946]. When the wavelength is large (normal heart), the atria can only contain a small number of functional re-entrant waves and AF does not persist very long. However if the wavelength is reduced, for example, by reducing the refractory period, more waves can be accommodated and AF can persist. The same is true when the atria are enlarged. The classical view was that drugs can suppress AF by increasing the refractory period, for example, delaying repolarisation with a K^+ channel blocker [Nattel *et al.*, 2007].

The mechanism causes inefficient quivering of the atria instead of coordinated contraction. Consequently, the atria do not deliver blood into the ventricles effectively. This can result in stagnation of blood in the atria, giving rise to clot formation. A clot can travel into the arterial system and occlude circulation to the brain, resulting in an embolic stroke. One out of 6 strokes are attributable to AF and stroke rate in AF is about 4.5% per year, increasing with age [Wolf *et al.*, 1991].

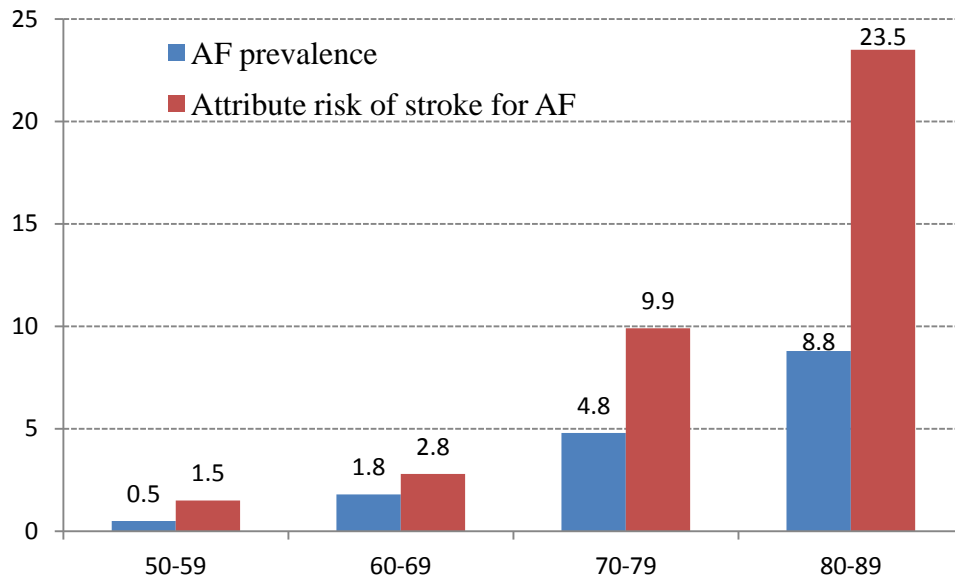


Figure 3.8 - Risk for stroke in AF, re-drawn from [Wolf *et al.*, 1991].

The risk of stroke increases with age as shown in Figure 3.8. The risk of stroke for AF patient aged 50 to 59 years and 80 to 89 years is respectively 1.5% and 23.5% [Wolf *et al.*, 1991]. It is associated with higher medical costs as well as increased risk of death and requires billions of dollars a year in health care expenditure [Benjamin *et al.*, 1998].

3.4.2 AF Symptoms

The initial stage of AF may be an embolic complication or suffered of heart failure, but most patients who are in AF complain of palpitation, chest pain, shortness of breath, tiredness, light headedness or fainting [Fuster *et al.*, 2006]. Such conditions greatly reduce quality of life for patients suffering AF.

3.4.3 AF treatment

The current available treatment of AF consists of medication, electrical cardioversion and ablation. In patients with paroxysmal AF, the treatment strategies generally focus on the control of the arrhythmia itself [Markides and Schilling, 2003]. However, in persistent AF, the clinician has to decide either to;

- a) restore and maintain sinus rhythm (rhythm control);
- b) accept the atrial arrhythmia and control ventricular rate (rate control).

Patient should be considered for anticoagulants if they have a risk factor of thromboembolism (Figure 3.9).

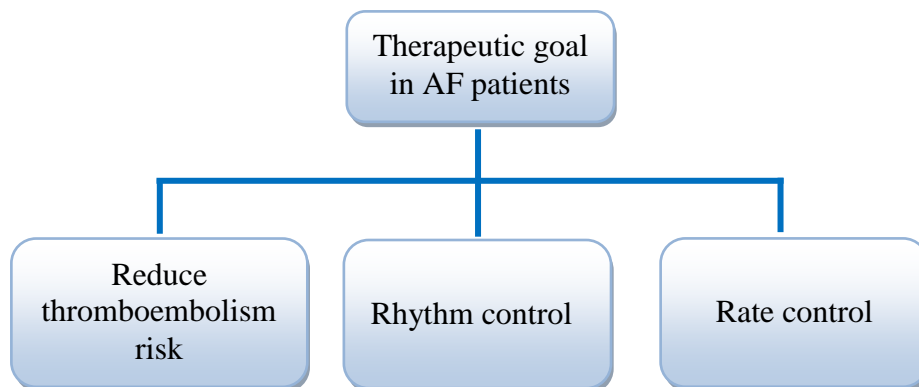


Figure 3.9 - Therapeutic strategies and goals in AF patients [Vias Markides *et al.*, “Atrial Fibrillation: Classification, pathophysiology, mechanisms and drug treatment, Heart 2003; 89:939-943].

Based on current guidelines, administration of an antiarrhythmic drug is the first treatment for patient with paroxysmal and persistent AF [Fuster *et al.*, 2006]. Typically, antiarrhythmic drugs such as amiodarone, propafenone and flecainide are used for sinus rhythm control [Pappone *et al.*, 2003]. Amiodarone is the most effective antiarrhythmic therapy and at one year it prevents the recurrences of AF in about 65% of treated patients [Fuster *et al.*, 2006, Naccarelli *et al.*, 2003]. However, antiarrhythmic drugs are not effective to prevent irregular

rhythms [Pappone and Santinelli, 2005]. The results of using medication for treatment of AF have been disappointing, leaving most patients in AF and failing to eliminate the risk of stroke [Navia *et al.*, 2009, Forleo and Tondo, 2009]. The common side effects of antiarrhythmic medications are dry mouth, difficult urination, vision problems, and dizziness [VanWormer *et al.*, 2008]. However, if the rhythm can be controlled successfully, the chance for people survival in year 1 and year 2 were 96% and 90% respectively [Pappone *et al.*, 2003].

If medication is not able to control the sinus rhythms, electrical cardioversion is considered [Jacquemet *et al.*, 2008]. The procedure is called defibrillation. It can be performed in 2 different ways: at the hospital (electrical cardioversion) or using an implantable cardioverter-defibrillator device (ICD).

When medication and electrical cardioversion control fail, ablation is usually the next step to be considered. Catheter-based radiofrequency ablation therapies offer a chance to cure AF. Recent studies show that AF patients undergoing catheter ablation are less prone to have recurrence AF in one year compared to those treated with antiarrhythmic medications [Nair GM *et al.*, 2009]. The chances for survival were 98% and 95% in year 1 and year 2 respectively [Pappone *et al.*, 2003]. The ablation performed in early paroxysmal AF has the highest chance for success compared to its use for persistent and permanent AF [Gonska *et al.*, 2009]. The success rate of 75% to 85% in paroxysmal AF after pulmonary vein (PV) isolation was reported by an experienced team [Oral *et al.*, 2006, Karch *et al.*, 2005, Pappone and Santinelli, 2005]. In persistent AF, the efficacy reported ranges from 22% to 45%, with most centres reporting an efficacy of 30% or less [Fuster *et al.*, 2006, Calkins *et al.*, 2007].

The ablation at dominant frequency sites results in significant prolongation of the atrial fibrillation cycle length (AFCL) compared to sites with non-dominant frequency [Skanes *et al.*, 1998, Mandapati *et al.*, 2000, Sanders *et al.*, 2006]. This result supports the use of DF mapping to identify suitable ablation targets.

3.5 Ablation procedure

There are several reasons for ablation procedures in the treatment of AF. These include decreased stroke risk, decreased heart failure risk, improved survival rate and the most important reason is to improve quality of life [Calkins *et al.*, 2007]. Ablation procedures attempt to isolate the foci that initiate and perpetuate AF. A sheath (9-10.5 Fr) placed in the femoral vein is used to induce the catheter through blood vessels until it is positioned in the heart under fluoroscopic guidance (Figure 3.10 and Figure 3.11).

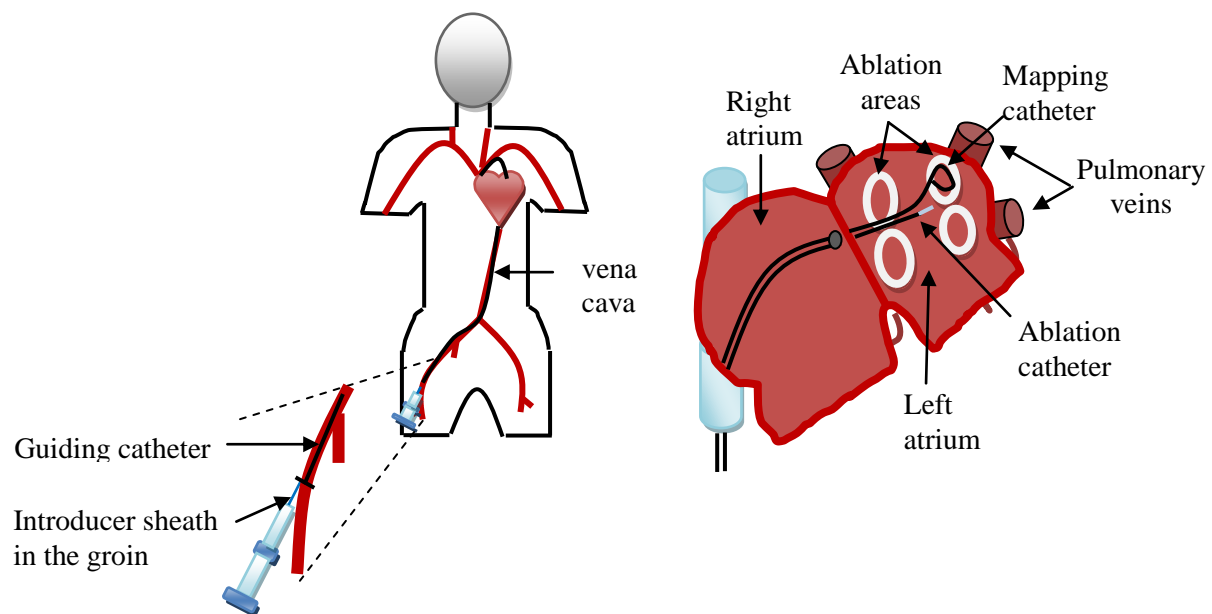


Figure 3.10 - Catheter ablation insertion.

Normally, the distal electrode is used for pacing and the proximal electrode is used to record electrograms from localized regions in the heart. Catheter-based radiofrequency ablation has become the most likely treatment option for patient with paroxysmal or persistent AF. The purpose of this technique is to apply RF energy directly to cardiac tissue to destroy or change conduction pathways in arrhythmias. In 1982, the first closed chest ablation developed by Gallagher and his collaborators was performed using high voltage direct current to treat supraventricular tachycardia for humans [Gallagher *et al.*, 1982]. Radiofrequency ablation (an alternative energy source) of supraventricular tachycardia in human was first used successfully in 1987 [Huang *et al.*, 1987]. The advantage of radiofrequency ablation compared to direct current is that the generation of lesions is without stimulation or sensory effects [Olaf, 2002]. The delivery of radiofrequency energy heats the tissue in direct contact with the electrode placed on the heart (Figure 3.11).

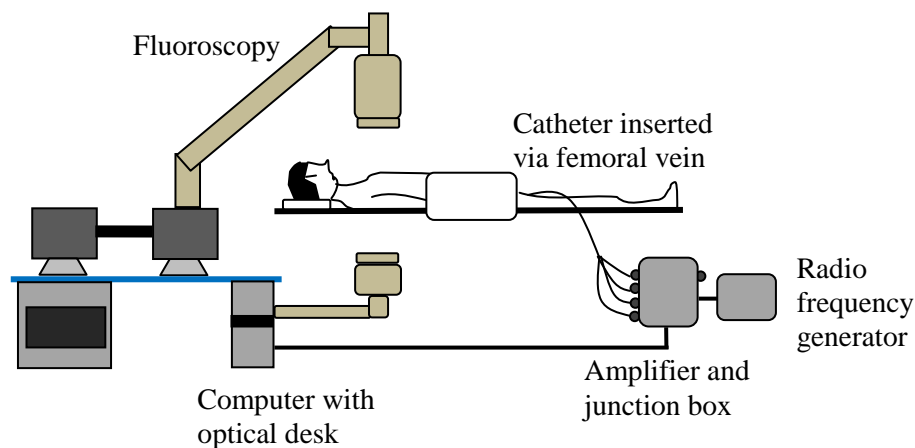


Figure 3.11 - Schematic drawing of the equipment in the electrophysiological laboratory.

The size of the area to be ‘burnt’ (ablated) depends on the size of the electrode as well as the balance between conduction of heat through the tissue and convective heat loss to the blood pool (Figure 3.12).

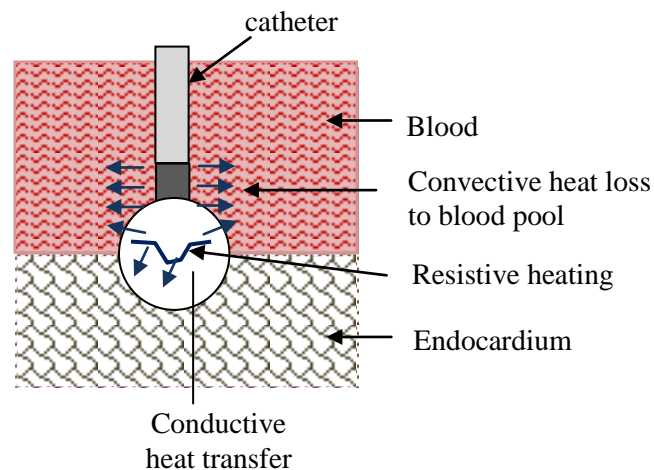


Figure 3.12 - Schematic drawing of the radiofrequency catheter positioned on the endocardium.

Radiofrequency energy is usually delivered for 30 to 60 seconds between the distal 4 mm tip of electrode catheter. The temperature at the tip of the electrode must be approximately 50°C or higher to destroy the tissue [Nath *et al.*, 1993, Calkins *et al.*, 2007]. A maximum power of 70 W should be used to deliver radiofrequency for circumferential pulmonary vein ablation [Oral *et al.*, 2006]. The electrophysiologists at Glenfield Hospital, Leicester use 50 W.

Freedom from AF was significantly higher for AF ablation compared to alternative medical treatment (antiarrhythmic drug therapy) that is respectively 78% and 37% [Pappone and Santinelli, 2008]. The definition of “success” is different among the studies. Different studies defined success as [Calkins *et al.*, 2007]:

1. freedom from symptomatic AF during follow-up;
2. freedom from symptomatic and asymptomatic episodes of AF;
3. greater than 90% reduction of AF burden;
4. proportion of patients free of AF each month of monitoring during follow-up.

3.5.1 Contact mapping catheter

The contact frequency mapping involves point-by-point acquisition of successive electrograms over time using a roving catheter. It may take up to 30 minutes to obtain a single map [Gojraty *et al.*, 2009]. There are several types of catheter positioned in the heart to record electrical activity or arrhythmogenic foci. Generally, the size of electrode catheter is 3 to 8 French [Josephson, 2008]. Small size catheter is used for children. For adults, the commonly used catheter size is 5 to 7. Once the catheter has reached the right atrium, it can be formed into a J-shape using its deflectable tip.

Typically a different type of catheter is placed in different areas of the atrium, such as:

- a) 10-pole catheter is positioned in the coronary sinus (CS);
- b) 20-pole catheter is placed in the right atrium to cover the area along the crista terminalis or superior vena cava (SVC);
- c) 10-pole or 20-pole circular catheters are positioned at the left superior pulmonary vein (LSPV) and left inferior pulmonary vein (LIPV);
- a) The roving catheter is initially located at the right superior pulmonary vein (RSPV).

Figure 3.13 shows some different types of catheter typically used for recording intra atrial electrical activity.

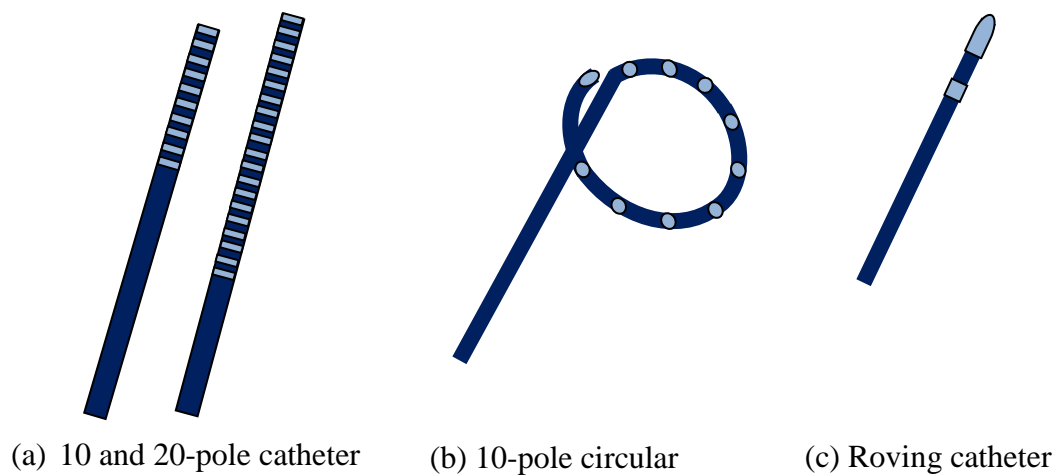


Figure 3.13 - Types of catheter.

The success of catheter ablation techniques depends on several steps:

- 1) Accurate localization of arrhythmogenic tissue;
- 2) The delivery of ablative electric field and heat to appropriate sites in the heart;
- 3) Depth of myocardium effect from ablative electric field.

These factors need better understanding for successful and accurate use of catheter ablation techniques.

3.5.2 Non-contact mapping catheter

The non-contact mapping system consists of the catheter with its multi-electrode array (MEA) and a custom designed amplifier connected to a Display Workstation (Figure 3.14).

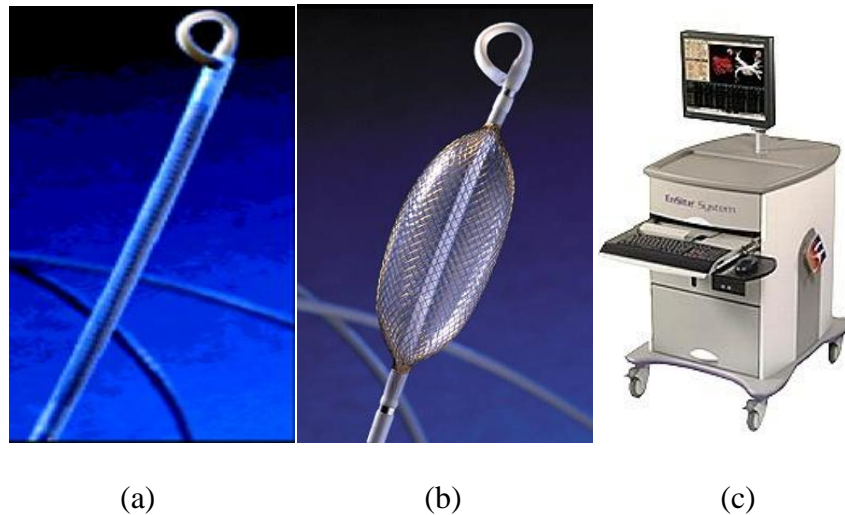


Figure 3.14 - EnSite catheter, (a) before deployment, (b) after deployment and (c) Display Workstation (courtesy of St. Jude Medical, used with permission).

The system simultaneously reconstructs more than 3000 unipolar electrograms, sampled at 1200 Hz with voltage sensitivity $10\ \mu\text{V}$, can display the data as standard ECG traces or translate them into a 3D graphical representation of the heart chamber in an isochronal or isopotential map [Schilling *et al.*, 2000]. The isopotential maps with the colour range represent the voltage amplitude as tools for the interpretation of wavefront propagation [Calkins *et al.*, 2008]. The multi-electrode array catheter consists of a 7.5 ml balloon mounted on a 9F catheter around which a braid of 64 deployed 0.003 inch diameter wires is woven. Each wire has one 0.025 inch break in deployment producing 64 non-contact unipolar electrodes. The system uses an inverse solution formulation for each sample to yield endocardial potentials. The system is applied in three steps:

1. Establish chamber geometry

- To trace the endocardial surface and reconstruct chamber geometry;

- This allows reconstruction of electrograms at endocardial sites in virtual electrograms (absence of physical electrode contact), allowing recording of cardiac electrical activity from thousands of points simultaneously;
 - To display and log the position of catheter (i.e., His catheter, Coronary Sinus catheter, etc), mitral valve, left atrial appendage etc.;
2. Identify site(s) critical for maintenance of re-entrant circuit(s)
 3. Navigate conventional catheter to critical site(s)
 - to navigate the catheter to sites of interest identified from the isopotential colour maps.

3.6 Targets for ablation

In the majority of laboratories, the main target site is pulmonary veins isolation (PVI). Additional lesion lines such as mitral isthmus, roof lines, endocardial coronary sinus and septum are the next target sites if the sinus rhythms was not restored with PVI alone [Haïssaguerre *et al.*, 2005]. Catheter ablation eliminated paroxysmal AF in left atrial posterior free wall, coronary sinus ostium, and interatrial septum, respectively with success rates of 63%, 100%, and 0% [Lin *et al.*, 2003].

3.6.1 Pulmonary vein isolation

An important electrophysiological study showed that a main focal origin of AF is located around the PVs [Haïssaguerre *et al.*, 1998]. This important source of ectopic foci at the PVs is possibly caused by several mechanisms [Jacquemet *et al.*, 2008, Nattel, 2003].

1. Spontaneous firing in the PVs may relate to ion kinetics (automaticity, early/delay after depolarisation or Ca^{2+} release-related mechanisms, less negative resting potential);
2. Structure (abrupt variation in fibre orientation, fibrosis);
3. Higher vulnerability to re-entry (short action potential duration (APD), slow conduction).

This procedure provides low complication rates and high success for paroxysmal and chronic AF [Pappone *et al.*, 2003, Pappone and Santinelli, 2005]. Haïssaguerre *et al.* [Haïssaguerre *et al.*, 2004] reported that 75% of terminated AF patients after PV isolation prolonged the atrial fibrillation cycle length (AFCL). Using a technique of segmental pulmonary vein ablation, Haïssaguerre *et al.* [Haïssaguerre *et al.*, 2000] reported that only 56% of 70 treated patients remained free of arrhythmias after one procedure. Oral *et al.* reported that 83% of patients remained free from AF at 5 months of follow-up for both paroxysmal or persistent AF [Oral *et al.*, 2002]. While using circumferential pulmonary veins ablation, Pappone *et al.* [Pappone *et al.*, 2001] reported that 85% patients of paroxysmal or persistent AF and 68% patient of permanent remained free from arrhythmia during a 6 to 12 months follow-up. A recent study by Oral *et al.* found that circumferential pulmonary veins ablation is more effective than segmental pulmonary vein ablation for paroxysmal AF [Oral *et al.*, 2003]. The success rate is respectively 88% and 67% and the patients remain free from arrhythmias at 6 months follow-up. Figure 3.15 shows the PV isolation.

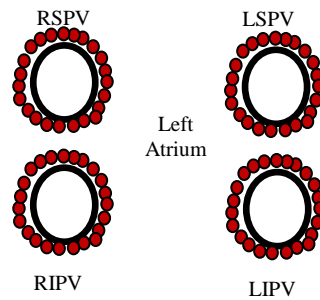


Figure 3.15 - PV isolation. The red blobs represent ablation.

3.6.2 Ablation at mitral isthmus

The mitral isthmus has been demonstrated to be a site of intra-atrial conduction block during the RF ablation of accessory pathways [Luria *et al.*, 2001]. The propagation caused by the functional or anatomic conduction block is capable to facilitate re-entry and may have a role in maintaining AF. The linear ablation technique of the mitral isthmus, defined as extending from the lateral mitral annulus to the ostium of the left inferior PV (LIPV) is shown in Figure 3.16 [Jaïs *et al.*, 2004]. The technique and validation criteria for the evaluation of conduction block at the mitral isthmus can be achieved in 92% of patients in paroxysmal AF after PV isolation.

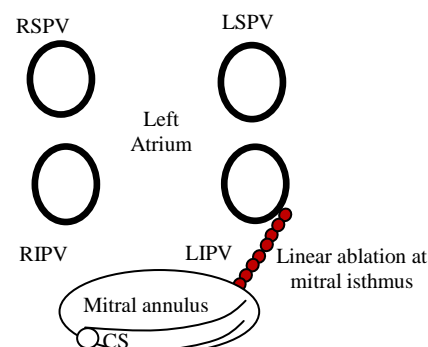


Figure 3.16 - Ablation at mitral isthmus.

3.6.3 Ablation at left atrial roof

Nademanee *et al.* reported that the LA roof is a region showing highly fragmented electrograms [Nademanee *et al.*, 2004]. This condition possibly sustained localized re-entry or focal activity that may maintain fibrillation. The ablation after pulmonary vein isolation along the roofline terminates AF in 47% of patients with paroxysmal AF [Hocini *et al.*, 2005]. Ablation of the LA roof was performed by making a contiguous line of ablation lesions joining the right superior pulmonary vein (RSPV) and left superior pulmonary vein (LSPV) as shown in Figure 3.17.

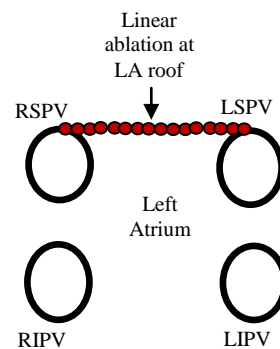


Figure 3.17 - Ablation at the left atrium roof

3.6.4 Ablation at coronary sinus

In recent years, the origin of AF has been reported from the coronary sinus (CS) musculature [Zhang *et al.*, 2009]. In 1907, Erlanger and Blackman had described the area near the orifice of the CS possesses a “degree of rhythmicity” in rabbit [Erlanger and Blackman, 1907]. CS fibres have automatic activity. With the presence of noradrenaline, they can be triggered into sustained and rapid rhythmic activity [Andrew and Paul, 1977]. Cumulative evidence from literature suggests that there are more anatomical parallels between the CS and the PVs, especially in terms of arrhythmogenicity. Thus, the CS is regarded as the “fifth pulmonary vein” [Zhang *et al.*, 2009, Rostock *et al.*, 2007].

3.6.5 Ablation at atrial septum

Linear ablation lines were generated on the left atrial septum, between the right inferior pulmonary vein (RIPV) and the mitral annulus [Scharf *et al.*, 2004] or from the right superior pulmonary vein (RSPV) to the foramen ovalis [Jaïs *et al.*, 1999] as shown in Figure 3.18.

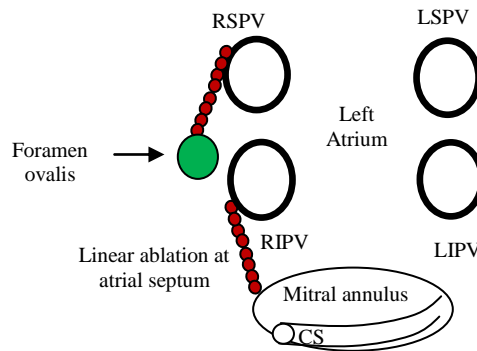


Figure 3.18 - Ablation at the left atrium septum.

The study observed that the atrial septum is the most common site for complex fractionated atrial electrograms (CFAEs) [Nademanee *et al.*, 2004]. The areas of CFAEs represent continuous re-entry of the fibrillation waves and were found mostly in the areas with slow conduction.

After pulmonary vein isolation, Knecht *et al.* recorded that 55% of patients terminate AF before performing roof and mitral lines, while 45% of patients still need these left atrial linear lines to terminate persistent AF [Knecht *et al.*, 2008].

3.7 Bipolar and Unipolar recordings

The electrodes located in the heart transform the depolarisation and repolarisation activities into an electrical signal that can be amplified, filtered and recorded. Cardiac electrograms are

generated by the potential differences between two recording electrodes during the cardiac cycle.

3.7.1 Bipolar recordings

Bipolar signals are produced in each position within the heart. Bipolar electrograms involve recording of the potential between two closely spaced electrodes. The recordings are obtained by connecting two electrodes that are identifying the area of interest to the recording amplifier [Stevenson and Soejima, 2005]. The bipolar electrode consists of the cathode (also called distal or tip pole) and the anode (proximal or ring pole) at the cardiac tissue being stimulated. Bipolar recordings are used to determine the focal source of arrhythmias by identifying the point of earliest activation in relation to a stable reference. The precision of finding the source of particular electrical signals depends on the distance between the recording electrodes. The basic idea of bipolar recordings is shown in Figure 3.19.

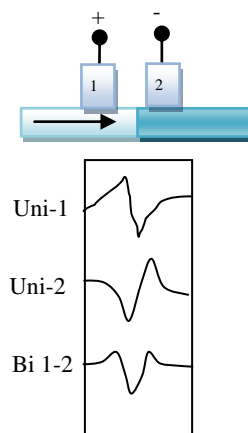


Figure 3.19 - Bipolar recordings. [From Stevenson et al., *Recording Techniques for Clinical Electrophysiology*, *J Cardiovasc Electrophysiol*, Vol. 16, pp. 1017-1022, September 2005, with permission].

Assume the horizontal bar (top) as a sheet of myocardium with depolarisation propagating from left to right. Electrode 1 is connected to the positive input of the amplifier and electrode 2 is connected to the negative input. The potentials generated from electrode 1 and 2 are shown in Figure 3.19 (labelled as Uni-1 and Uni-2 respectively). The signal from electrode 2 is slightly delayed compared to the signal from electrode 1 because the wavefront at electrode 2 reaches it later. The signal in electrode 2 is inverted because it is connected to the negative input of the recording amplifier. The bipolar signal is generated when these signals are added together (labelled as Bi 1-2). The amplitude of the bipolar signal is inversely proportional to the square of the distance from a point midway between the two electrodes and the signal source [Brody *et al.*, 1961].

3.7.2 Unipolar recordings

Unipolar signals are generated when one varying signal is compared with a constant signal reference placed outside the heart [DeCaprio *et al.*, 1977]. The unipolar electrodes have one pole (cathode or negative input) in close association with cardiac tissue and other (anode or positive input) outside of the heart. Figure 3.20 shows the basic concept of unipolar recording.

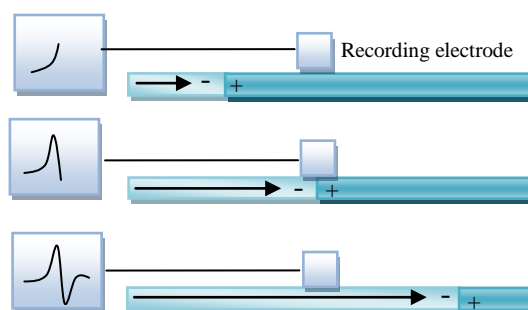


Figure 3.20 - Unipolar recordings. [From Stevenson *et al.*, *Recording Techniques for Clinical Electrophysiology*, *J Cardiovasc Electrophysiol*, Vol. 16, pp. 1017-1022, September 2005, used with permission].

The unipolar electrode will record the electrical propagation through the cardiac tissue with reference to an electrode located at some distance away from the heart. The unipolar signal amplitude is inversely proportional to the distance between the electrode and the signal source [Brody *et al.*, 1961]. The amplitude and shape of unipolar signals depends on the distance of the cardiac events.

The advantages of bipolar signals compared to unipolar signals is that they reduce far-field signals [Issa *et al.*, 2009, Nakagawa and Jackman, 1998] and they are less prone to electrical noise. Bipolar and unipolar signals have different characteristics. Bipolar signals often show a small spike that represents the electrical activity between the electrodes. Distant cardiac activity is usually cancelled out as it is a common-mode signal. For these reasons bipolar signals are useful to identify the focal source of arrhythmias or fractionated potentials. However, bipolar signals are sensitive to the orientation of the two electrodes and the direction of movement of the activation wavefront [Hoffman and Cranfield, 1960].

The advantage of using the unipolar electrogram is that the timing of the steepest negative slope of the unipolar potential most closely correlates with the local activation time [Nakagawa and Jackman, 1998]. There are several mechanisms that could explain the negative potential of unipolar signals;

1. The electrophysiological properties demonstrated that the atrial tissue disease (i.e. ventricular septal defects, pulmonary stenosis, atrial septal defects etc) corresponded to relatively decreased resting membrane potential [Hordof *et al.*, 1976].
2. The study demonstrated that the potential distribution is dependent on the cycle length and activation pattern in patients with atrial arrhythmia [Lin *et al.*, 2005]. Some studies show a slow response of action potential during short atrial pacing cycle

length. This probably caused by nonuniform atrial fibres in the diseased atrium that may affect the conduction velocity. As a result, atrial fibres will be activated asynchronously and present a lower unipolar voltage [Spach and Dolber, 1986].

Tada and his collaborators reported a quantitative analysis for bipolar and unipolar electrograms performance and identified factors related to successful and unsuccessful AF ablation after PVI [Tada *et al.*, 2002]:

1. The timing parameter recorded by the ablation catheter relative to the earliest pulmonary vein potential recorded by Lasso catheter will distinguish either successful or unsuccessful ostia ablation sites (using both unipolar and bipolar);
2. The amplitude for successful ablation sites is larger than amplitude for unsuccessful sites (using both unipolar and bipolar recordings);
3. A steeper intrinsic deflection was noticed for unipolar electrograms at successful than at unsuccessful ostia ablation sites;
4. The morphology recorded by the ablation catheter never matched the morphology recorded by Lasso catheter for bipolar electrograms;
5. The morphology recorded by ablation catheter usually matched the morphology recorded by Lasso catheter for unipolar electrograms.

As a conclusion, there are several types of arrhythmia that have an effect on quality of life has and these have been discussed in chapter 3. The treatment is dependent on the type and severity of the arrhythmia. Sometimes a combination of treatments is required. The treatment using radio frequency ablation may contribute to serious complications and this procedure needs a technique that can provide a very fast computation time for estimation of dominant frequency. Therefore, in the next chapter we will discuss about several techniques that can be used to estimate the DF accurately. The fastest techniques that can estimate accurate DF will be use for the next analysis.

4 COMPARISON OF COMPUTATION TIME FOR ESTIMATION OF DOMINANT FREQUENCY OF ATRIAL ELECTROGRAMS: FAST FOURIER TRANSFORM, BLACKMAN TUKEY, AUTOREGRESSIVE AND MULTIPLE SIGNAL CLASSIFICATION

4.1 Introduction

Catheter ablation of AF is a complex interventional electrophysiological procedure. There are about 20-40% cases of recurrences requiring repeat operation and this procedure may contribute to serious complications [Lévy, 2009]. Its risk is higher than that of ablation for other cardiac arrhythmias [Calkins *et al.*, 2007]. The worldwide survey of AF ablation reported that 6.0% complication were recorded (524/8745) [Cappato *et al.*, 2005]. This survey also reported about 1.2% incidence of cardiac tamponade. Cardiac tamponade presents either as sudden dramatic fall in blood pressure, or more insidiously, as a gradual decrease in blood pressure [Calkins *et al.*, 2007]. Univariate analysis shows that sex, age, insertion difficulty, length of the inserted catheter, type of catheter and, term of insertion were among contributors for catheter related blood stream infection [Prudente *et al.*, 2009]. The risks include requiring prolonged hospitalization, long-term disability or death [Calkins *et al.*, 2007].

Since the duration of the overall surgical procedure for ablation is one of the contributors to blood stream infection, computation time is critical for any technique that is to be used during this surgical procedure. Our aim in this study is to compare the computation time for four different spectrum analysis techniques and compare the different techniques in their ability for producing accurate results for identification of dominant frequency (DF).

With current technology the data collection capability for non-contact mapping systems consists of a catheter mounted multielectrode array allowing the recording up to 3360 points of virtual electrograms at 1200 Hz [Schilling *et al.*, 1998]. With this number of data points, it is important to identify an approach that can be used to produce accurate DF maps with minimum computation time.

This will in turn help the electrophysiologist to identify the dangerous frequencies as target ablation sites and to apply ablation effectively in an expeditious manner. The frequencies between 4-12 Hz are associated with AF and shall be given attention.

The main objective of this study is to reduce the risk during catheter procedure by selecting the technique for accurate estimation of DF with the shortest computation time.

4.2 Frequency Domain Analysis

4.2.1 Fast Fourier Transform (FFT) Technique

The application of the Fast Fourier Transform (FFT) is important in signal processing computations using specially in spectral analysis [Ifeachor and Jervis, 2002]. The discrete Fourier transform of $x(nT)$ is given by

$$X\left(\frac{k}{NT}\right) = \sum_{n=0}^{N-1} x(nT) e^{-j2\pi nk/N} \quad [4.1]$$

The FFT algorithm is the main choice for obtaining the Discrete Fourier Transform (DFT) because of its speed. Another reason is that Fourier analysis has been in existence since 1822 and has achieved a high degree of familiarity, respectability and development, as well as

varieties of applications. For the DFT the number of complex multiplications is N^2 . FFT is a fast algorithm to calculate the DFT. If N is an integer power of 2, and the FFT decomposition uses radix-2, there are $\log_2 N$ stages of FFT computation. Basically there are N complex multiplications per stage, giving a total of $N \log_2 N$ multiplications, [Cooley *et al.*, 1967, Cooley *et al.*, 1969]. Therefore the advantage of speed is expected to be approximately:

$$\frac{N^2}{N \log_2 N} = \frac{N}{\log_2 N}$$

The assumption for FFT analysis is that a frequency domain description is likely to expose important information which is not obvious in the time-domain signal [Lynn and Fuerst, 2000]. The FFT generates frequency domain data that is linearly-spaced as a function of frequency. The frequency step (distance between 2 consecutive FFT values) is the sampling frequency divided by the number of data points.

$$\text{frequency resolution (Hz)} = \frac{\text{sampling frequency (fs)}}{\text{number of points (nfft)}}$$

Longer FFT sizes provide resolution smaller frequency step but slower processing, while shorter FFT sizes provide larger frequency steps but faster time response. When distributing the linearly-spaced FFT data on a logarithmic axis, it can be easily seen that short FFTs may provide inadequate frequency resolution, while long FFTs (larger length of the signal) can provide better frequency resolution.

The Welch technique, also based on FFT algorithm, is used to compute the periodogram. This technique uses signal segmentation and averaging to improve statistical properties of the spectral estimates [Welch, 1967]. The equation for computing the averaged periodogram is:

$$\hat{P}_w(f_k) = \frac{1}{M} \sum_{m=1}^M \hat{P}_m(f_k), \quad 0 \leq f_k \leq f_s/2 \quad [4.2]$$

where $\hat{P}_m(f_k)$ is the periodogram of the m^{th} segment of data.

The ends of the data sequence are tapered to zero when data is windowed. This technique contributes a loss of information and short duration events in the tapered area may be missed. In order to overcome this problem, one can partition the data sequence into overlapping segments. Each segment is windowed and transformed separately. Most features of the data will be included in the sequences if the overlap is about 50% to 75%. The estimation of the true spectrum is obtained when the resulting spectra are averaged. The segmenting of the data is shown in Figure 4.1.

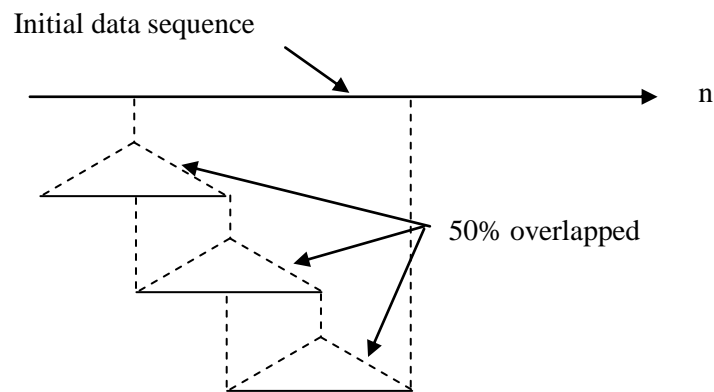


Figure 4.1 - Segmenting of the data for overlap processing

This method is called overlapping processing. Usually this 50% to 75% overlapping provides 90% of the performance improvement for most weighting functions [DeFatta and David, 1988]. DF was obtained from the Welch/FFT analysis. There are a few considerations to the use of DF analysis especially for the electrograms [Berenfeld, 2007]:

- a) The estimation of the power spectrum uses the FFT because this is an efficient and widely available method;
- b) The maximum frequency is inversely proportional to the sampling interval Δt as $\frac{1}{2\Delta t}$;
- c) The frequency resolution in the power spectrum is inversely proportional to the length of the signal $\Delta f \propto \frac{1}{T}$ where T is the length of the signal collected ($T = N\Delta t$). This has implications for the interpretation of the DF obtained.

4.2.2 Blackman-Tukey (BT) Technique

This method was proposed by Blackman and Tukey (1958) [Ifeachor and Jervis, 2002]. The estimator is based on the Wiener-Khinchin theorem, which states that power spectrum density is the Fourier Transform of the autocorrelation function of the series [Kay, 1988, Beauchamp and Yuen, 1979].

If fewer data points are used, the variance of the autocorrelation estimate increases and the estimate become less reliable [Ifeachor and Jervis, 2002]. The averaging associated with windowing a series decreases the spectral resolution of the methods, from the frequency intervals of $1/N$, to a windowed frequency interval of about $1/M$, where M is the length of the window. As a result, wider windows yield higher spectral resolution, and vice-versa. The drawbacks of Blackman-Tukey are suppression of weak signal main-lobe responses by strong side-lobes and frequency resolution is limited by the available data record duration.

This method involves 3 steps [Ifeachor and Jervis, 2002]:

1. The autocorrelation sequence of the data is estimated using the formula;

$$\hat{R}_{xx}(m) = \frac{1}{N} \sum_{n=0}^{N-1} x_n x_{n-m} \quad m=0,1,2,\dots,N-1 \quad [4.3]$$

where: x_n is the n -th value of the data series,

N is the total number of points in the data series

m is the autocorrelation lag

$\hat{}$ signifies estimated value.

2. Windowing the autocorrelation sequence.

The windowing of the autocorrelation sequence is normally carried out using a hamming window that has the following characteristics:

$$w(m) = 0.54 + 0.46 \cos\left(\frac{2\pi m}{M}\right), \quad -(M-1) \leq m \leq M-1$$

$$w(m) = 0, \quad \text{otherwise} \quad [4.4]$$

3. Finding the Fourier transform to yield the following PSD estimate [Kay, 1988]:

$$\hat{P}_{BT}(f) = \sum_{m=-(M-1)}^{M-1} \hat{R}_{xx}(m) w(m) e^{-j2\pi f m} \quad [4.5]$$

where: $w(m)$ is a window function of length

$2(M-1)-1$, which is zero for $|m| \geq M-1$

The PSD estimate is determined over the frequency range $-\frac{1}{2f_s} \leq f \leq \frac{1}{2f_s}$ where f_s is the sampling frequency.

4.2.3 Autoregressive (AR) Technique

Autoregressive technique involves selection of model order and the estimation of model parameters from the collected data. This technique is widely used because it produces frequency spectra with a high frequency resolution and the algorithm to estimate the AR parameters results in a system of linear equations, which are computationally fast to solve [Kay, 1988]. In this model, the data x_n are considered to be the output of a system with a random input u_n . The relation between input and output are described by the following difference equation which represents the auto-regressive moving average ARMA (pole-zero) model:

$$x_n = -\sum_{k=1}^p a_{pk} x_{n-k} + \sum_{k=0}^q b_{qk} u_{n-k} \quad [4.6]$$

where: p, q are model orders for the AR and the MA parts, respectively

a, b are model parameters (a_{pk} being the k^{th} parameter of the p^{th} -order model)

The autoregressive (AR) part of this general equation is given by:

$$x_n = -\sum_{k=1}^p a_{pk} x_{n-k} + u_n \quad [4.7]$$

Knowing p past values of the series we can estimate the next output as:

$$\hat{x}_n = -\sum_{k=1}^p a_{pk} \quad [4.8]$$

Equation [4.8] defines the AR with all-pole model. While, the MA model is given by:

$$\hat{x}_n = \sum_{k=0}^q b_{qk} u_{n-k} \quad [4.9]$$

The prediction error e_{pn} is defined as the difference between the actual sample value x_n and its predicted value \hat{x}_n .

$$e_{pn} = x_n - \hat{x}_n = x_n + \sum_{k=1}^p a_{pk} x_{n-k} \quad [4.10]$$

The power spectrum of an AR process is:

$$\hat{P}_{AR}(f) = \frac{\sigma_e^2 T}{|1 - \sum_{k=1}^p a_{pk} e^{-j2\pi f k}|^2} \quad [4.11]$$

where σ_e^2 is the variance of e_{pn} and T is the sampling period.

Autoregressive (AR) Spectrum Analysis is an alternative way to estimate the power spectral density (PSD) for a sampled process. There are several features of AR technique that make it attractive [Marple, 1980]:

- a) AR PSD estimates have a better frequency resolution than the conventional periodogram estimation for the same length of signal collected.
- b) AR spectral estimate does not have the distortion produced by side-lobe leakage effects.
- c) AR methods yield reasonable spectral estimation for short data records.

4.2.4 Pisarenko Harmonic Decomposition (PHD)

Pisarenko method is suitable to find the frequencies of sinusoids in noise. The technique makes use of a noise subspace eigenvector to estimate the frequencies of the sinusoids. This method is based on the eigendecomposition algorithm of the correlation matrix of the noise-corrupted signal [Proakis and Dimitris, 1996]. If we have a signal consisting of p sinusoidal components it satisfies the difference equation

$$x(n) = - \sum_{m=1}^{2p} a_m x(n - m) \quad [4.12]$$

and corresponds to the system with system function

$$H(z) = \frac{1}{1 + \sum_{m=1}^{2p} a_m z^{-m}} \quad [4.13]$$

The polynomial

$$A(z) = 1 + \sum_{m=1}^{2p} a_m z^{-m} \quad [4.14]$$

has 2 roots on the unit circle which correspond to the frequencies of the sinusoids. For the sinusoids with white noise, $w(n)$ we can observed that

$$y(n) = x(n) + w(n) \quad [4.15]$$

From equation [4.12] and [4.15] ,

$$\begin{aligned} y(n) - w(n) &= -\sum_{m=1}^{2p} y(n-m) = \sum_{m=0}^{2p} a_m w(n-m) \\ \sum_{m=0}^{2p} a_m y(n-m) &= \sum_{m=0}^{2p} a_m w(n-m) \end{aligned} \quad [4.16]$$

where $a_0 = 1$.

The difference equation for an ARMA (p, p) process in which both the AR and MA parameters are identical [Proakis and Dimitris, 1996]. This symmetry is a characteristic of the sinusoidal signals in white noise. The difference equation for ARMA can be expressed in matrix form as

$$Y^T a = W^T a \quad [4.17]$$

where $Y^T = [y(n) \ y(n-1) \ \dots \ y(n-2p)]$ = observed data vector of dimension $(2p+1)$

$W^T = [w(n) \ w(n-1) \ \dots \ w(n-2p)]$ = noise vector

$a = [1 \ a_1 \ \dots \ a_{2p}]$ = coefficient vector

If we pre-multiply equation [4.17] with Y , we obtain

$$\begin{aligned}
E(YY^T)a &= E(YW^T)a = E[(X + W)W^T]a \\
\Gamma_{yy}a &= \sigma_w^2 a
\end{aligned} \tag{4.18}$$

The equation [4.18] is in the form of eigenequation, that is

$$(\Gamma_{yy} - \sigma_w^2 I)a = 0 \tag{4.19}$$

where σ_w^2 = eigenvalue of the autocorrelation matrix Γ_{yy} .

Therefore the parameter vector a is an eigenvector associated with the eigenvalue σ_w^2 . The autocorrelation values for p sinusoids observed in additive white noise, are given by

$$\begin{aligned}
r_{yy}(0) &= \sigma_w^2 + \sum_{i=1}^p P_i \\
r_{yy}(k) &= \sum_{i=1}^p P_i \cos 2\pi f_i k, \quad k \neq 0
\end{aligned} \tag{4.20}$$

where $P_i = A_i^2/2$ is the average power in the i th sinusoid

A_i = corresponding amplitude.

Hence equation [4.20] can be written as

$$\begin{bmatrix} \cos 2\pi f_1 & \cos 2\pi f_2 & \dots & \dots & \dots & \cos 2\pi f_p \\ \cos 4\pi f_1 & \cos 4\pi f_2 & \dots & \dots & \dots & \cos 4\pi f_p \\ & & \vdots & & & \\ & & & \vdots & & \\ \cos 2\pi p f_1 & \cos 2\pi p f_2 & \dots & \dots & \dots & \cos 2\pi p f_p \end{bmatrix} \begin{bmatrix} P_1 \\ P_2 \\ \vdots \\ P_p \end{bmatrix} = \begin{bmatrix} r_{yy}(1) \\ r_{yy}(2) \\ \vdots \\ r_{yy}(p) \end{bmatrix} \tag{4.21}$$

If we know the frequencies $f_i, 1 \leq i \leq p$, the powers of the sinusoids can be determined

from [4.21]. Thus, the noise variance can be obtained from [4.20] as

$$\sigma_w^2 = r_{yy}(0) - \sum_{i=1}^p P_i \tag{4.22}$$

The problem that remains is to find the p frequencies $f_i, 1 \leq i \leq p$ that need knowledge of the eigenvector a corresponding to the eigenvalues σ_w^2 . Pisarenko observed that for an ARMA process consisting of p sinusoids in additive white noise, the variance σ_w^2 corresponds to the minimum eigenvalues of Γ_{yy} when the dimension of the autocorrelation matrix equals or exceeds $(2p + 1) \times (2p + 1)$ [Pisarenko, 1973]. The required ARMA coefficient vector corresponds to the eigenvector with the minimum eigenvalue. Hence, the frequencies $f_i, 1 \leq i \leq p$ are obtained from the roots of the polynomial

$$A(z) = 1 + \sum_{m=1}^{2p} a_m z^{-m} \quad [4.23]$$

where the coefficients are the elements of the eigenvector a , corresponding to the minimum eigenvalue σ_w^2 .

In summary, the methods of Pisarenko harmonic decomposition use the following steps:

1. estimate the autocorrelation matrix Γ_{yy} from the data;
2. find minimum eigenvalue and the corresponding minimum eigenvector;
3. find the roots that constitute the frequencies $\{f_i\}$. By using these frequencies, we can determine signal powers $\{P_i\}$ by substituting the estimates $r_{yy}(m)$.

We assumed that the sinusoidal signal consists of p real sinusoids in the previous discussion.

Now we shall assume that the signal consists of p complex sinusoids of the form

$$x(n) = \sum_{i=1}^p A_i e^{j(2\pi f_i n + \phi_i)} \quad [4.24]$$

where the amplitudes $\{A_i\}$ and the frequencies $\{f_i\}$ are unknown and the phases $\{\phi_i\}$ are independent random variables uniformly distributed on $(0, 2\pi)$. Then the random process $x(n)$ is wide-sense stationary with autocorrelation function

$$\gamma_{yy}(m) = \sum_{i=1}^p P_i e^{j(2\pi f_i m)} \quad [4.25]$$

where, $P_i = A_i^2$ = the power of the i^{th} sinusoid for complex sinusoids.

Since the sequence observed is $y(n) = x(n) + w(n)$, where $w(n)$ is a white noise sequence with spectral density σ_w^2 , the autocorrelation function for $y(n)$ is

$$\gamma_{yy}(m) = \gamma_{xx}(m) + \sigma_w^2 \delta(m), \quad m = 0, \pm 1, \dots, \pm(M-1) \quad [4.26]$$

Therefore the $M \times M$ autocorrelation matrix for $y(n)$ can be expressed as

$$\Gamma_{yy} = \Gamma_{xx} + \sigma_w^2 I \quad [4.27]$$

where Γ_{xx} = autocorrelation matrix for the signal $x(n)$

$\sigma_w^2 I$ = the autocorrelation matrix for the noise.

The signal matrix Γ_{xx} can be represented as

$$\Gamma_{xx} = \sum_{i=1}^p P_i S_i S_i^H \quad [4.28]$$

where H = conjugate transpose

$$S_i = [1, e^{j2\pi f_i}, e^{j4\pi f_i}, \dots, e^{j2\pi(M-1)f_i}] = \text{signal vector of dimension } M \quad [4.29]$$

Now, let us perform an eigen-decomposition of the matrix Γ_{xx} . Let the eigenvalues $\{\lambda_i\}$ be ordered in decreasing value with $\lambda_1 \geq \lambda_2 \geq \lambda_3 \geq \dots \lambda_M$ and let the corresponding eigenvectors be denoted as $\{v_i, i=1, \dots, M\}$. In the absence of noise the eigenvalues $\lambda_i, i = 1, 2, \dots, p$ are nonzero while $\lambda_{p+1} = \lambda_{p+2} = \dots = \lambda_M = 0$. Furthermore, it follows that the signal correlation matrix can be expressed as

$$\Gamma_{xx} = \sum_{i=1}^p \lambda_i v_i v_i^H \quad [4.30]$$

Thus, the eigenvectors $v_i, i=1,2,\dots,p$ span the signal subspace as do the signal vectors $s_i, i=1,2,\dots,p$. These p eigenvectors for the signal subspace are called the principal eigenvectors and the corresponding eigenvalues are called the principal eigenvalues.

In the presence of noise, the noise autocorrelation matrix in [4.27] can be represented as

$$\sigma_w^2 I = \sigma_w^2 \sum_{i=1}^M v_i v_i^H \quad [4.31]$$

By substituting [4.30] and [4.31] into [4.27], we obtain

$$\begin{aligned} \Gamma_{yy} &= \sum_{i=1}^p \lambda_i v_i v_i^H + \sum_{i=1}^M \sigma_w^2 v_i v_i^H \\ &= \sum_{i=1}^p (\lambda_i + \sigma_w^2) v_i v_i^H + \sum_{i=p+1}^M \sigma_w^2 v_i v_i^H \end{aligned} \quad [4.32]$$

This eigen-decomposition separates the eigenvectors into two sets.

- i) Set $\{v_i, i=1,2,\dots,p\}$ is a principal eigenvectors (signal subspace);
- ii) Set $\{v_i, i=p+1,\dots,M\}$ is a noise eigenvectors (noise subspace) which are orthogonal to the vectors in the noise subspace.

We see that the Pisarenko method is based on an estimation of the frequencies by using the orthogonality property between the signal vectors and the vectors in the noise subspace. For complex sinusoids, if we select $M = p + 1$, there is only a single eigenvector in the noise subspace (corresponding to the minimum eigenvalue) which must be orthogonal to the signal vectors. Thus we have

$$s_i^H v_{p+1} = \sum_{k=0}^p v_{p+1}(k+1) e^{-j2\pi f_i k} = 0 \quad i = 1, 2, \dots, p \quad [4.33]$$

But [4.33] implies that the frequencies $\{f_i\}$ can be determined by solving for the zeros of polynomial

$$V(z) = \sum_{n=0}^p v_{p+1}(k+1) z^{-k} \quad [4.34]$$

all of which lie on the unit circle. The angles of these roots are $2\pi f_i$, $i = 1, 2, \dots, p$.

4.2.5 Multiple Signal Classification (MUSIC)

The multiple signal classification is the improvement of Pisarenko harmonic decomposition [Schmidt, 1979]. This is an eigen-based subspace decomposition method and is best used to estimate the frequencies of complex sinusoids in additive white noise [Vaseghi, 2008].

Assume that $y(n)$ is a random process that consists of p complex exponentials in white noise,

$$y(n) = \sum_{i=1}^p A_i e^{-j(2\pi f_i n + \phi_i)} + n(n) \quad [4.35]$$

The autocorrelation matrix of a noisy signal can be written as:

$$R_{yy} = R_{xx} + R_{nn} \quad [4.36]$$

where : R_{xx} is the autocorrelation matrix of the signal;

R_{nn} is the autocorrelation matrix of the noise.

Eigen-analysis is used to partition the eigenvectors and the eigenvalues of the autocorrelation matrix of a noisy signal into 2 subspaces, signal subspace and noise subspace. The eigenvector can be divided by two groups, the p signal eigenvector corresponding to the p largest eigenvalues and $M - p$ noise eigenvector corresponding to the smallest eigenvalues [Hayes, 1996].

Ideally, p of these roots will lie in the unit circle on the frequencies of the complex exponentials. The smallest eigenvalue determines the noise variance and the corresponding eigenvector is the prediction polynomial for the clean signal [Pisarenko, 1973].

In MUSIC, the effects of spurious peaks are reduced by averaging. The power spectrum estimate is defined as

$$P_{xx}(f) = \sum_{i=p+1}^N |v_i^H e(f)|^2 \quad [4.37]$$

where N is the dimension of the eigenvectors

v_i is the i -th eigenvector of the correlation matrix;

p is the dimension of the signal subspace.

Since $P_{xx}(f)$ has its zeros at the frequencies of the sinusoids, hence the reciprocal of $P_{xx}(f)$ has its poles at these frequencies [Vaseghi, 2008]. Then, the MUSIC spectrum can be written as

$$P_{MUSIC}(f) = \frac{1}{\sum_{i=p+1}^N |v_i^H e(f)|^2} \quad [4.38]$$

4.3 Method

The spectrum estimation analysis was tested using sinusoid signals in noise to identify their DF using the 4 different approaches. In FFT analysis, Welch method estimates the frequency spectrum of 30000 data series. The Fourier transform was calculated separately for each of the segments, where one segment consists of 2048 points. The analysis was performed by taking the average of the segments using a 4096-point FFT and an overlap of 50% with a hamming window.

In Blackman-Tukey method, the autocorrelation was determined using 4096 points. This autocorrelation function was windowed with the same hamming window used for the FFT approach (4096 points). The autoregressive spectrum was determined based on the finite linear aggregate of the previous value of the process and the current value of white noise. The model order used was $p=8$. As for MUSIC, two complex exponentials with the same window are used to identify the spectrum. The characteristic of the spectrum is compared between nonparametric method (FFT & BT), parametric method (AR) and subspace method.

4.4 Results

The spectrum estimation was determined using several test frequencies: 8.0 Hz, 7.7 Hz, 7.0 Hz, 6.3 Hz, 5.5 Hz and 5.0 Hz. Figure 4.2 shows the graphical results of Fast Fourier Transform, Blackman-Tukey, Autoregressive and MUSIC in which tested using sinusoidal wave of 8 Hz. DF is being consistently estimated as 8 Hz.

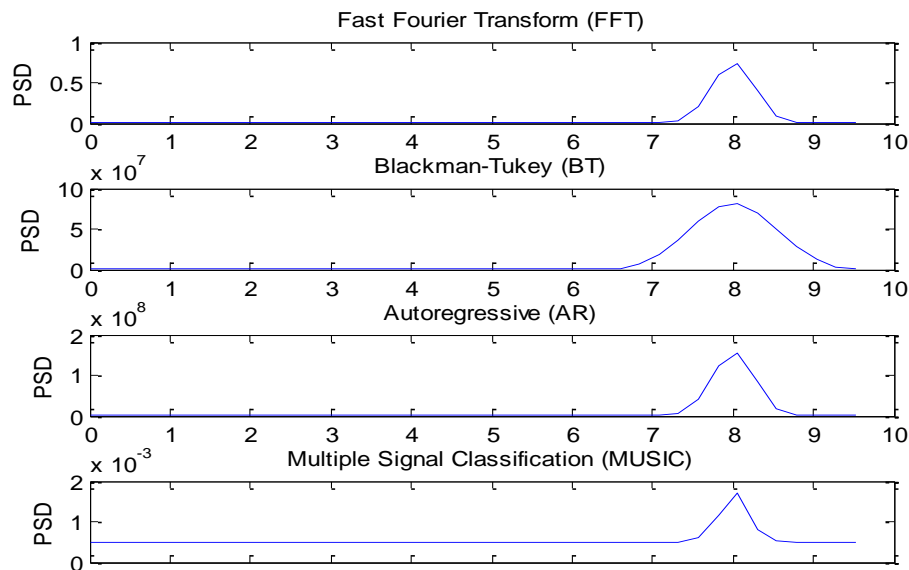


Figure 4.2 - Comparison of Fast Fourier Transform, Blackman-Tukey, Autoregressive and Multiple Signal Classification spectral estimates.

Table 4.1 shows the DF value comparison for all techniques against the base Frequency.

Table 4.1 - DF value comparison for all technique against the base Frequency

Base Frequency(Hz)	8	7.7	7	6.3	5.5	5
FFT	8.06	7.81	7.08	6.35	5.62	4.88
BT	8.06	7.81	7.08	6.35	5.62	4.88
AR	8.06	7.81	7.08	6.35	5.62	4.88
MUSIC	8.06	7.81	7.08	6.35	5.62	4.88

The results show consistent value of DF produced by all techniques. Table 4.2 shows that, the percentage of error is the same for all techniques tested. The percentage is ranging from 0.71 to 2.34% for frequency from 5 to 8 Hz.

Table 4.2 - Calculation of error for FFT, Blackman-Tukey, Autoregressive and Multiple Signal Classification spectral estimates.

Frequency	8	7.7	7	6.3	5.5	5
% error	0.71	1.47	1.14	0.76	2.09	2.34

The electrogram signal consists of signal and noise. We simulate signal to noise ratio to observe the error of the frequency. Figure 4.3 shows the error obtained for Signal-to-Noise Ratios (SNR) varying between 60 dB to -60 dB for all techniques. The range of SNR is chosen assuming the noise will not exceed 1000 times compare to the signal ($SNR = 20 \log \frac{v_s}{v_n}$ where, v_s is voltage signal and v_n is voltage noise).

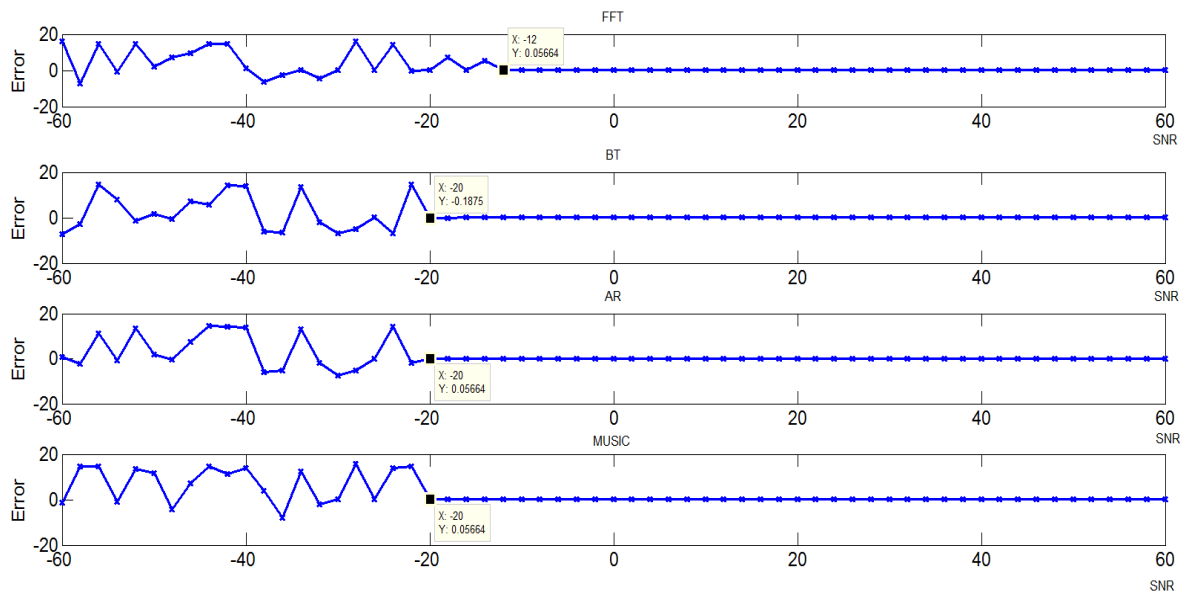


Figure 4.3 – Error versus SNR

The cut off for signal to noise ratio was summarised in Table 4.3. FFT is showing minimum error of frequency at -12 dB while the other techniques are at -20 dB. Typically, in electrogram signal, noise level does not supersede the signal level (SNR=0). Therefore, FFT capability of SNR -12 dB is sufficient to handle the noise in normal electrogram analysis. Other techniques are showing a better capability to handle the noise.

Table 4.3 – Cut off SNR for each technique

Techniques	Cut-off Signal to Noise Ratio
FFT	-12
BT	-20
AR	-20
MUSIC	-20

The total computation time was calculated using 30000 data series. There are about 3360 points of virtual electrogram and this is the state-of-art for mapping atrial activation [Schilling *et al.*, 1998].

Table 4.4 shows a significant difference in processing time between the 4 techniques tested. In summary, FFT takes 22.8 seconds to process 3000 signals compared to 340.9 s for BT, 206.4 s for AR and 10851.8 s for MUSIC. As discussed before, all techniques produce the same estimation for DF. Therefore, the time taken to produce the estimation is the main factor for the choice of which technique should be used. The FFT is the fastest technique, as expected.

Table 4.4 - Computation time for 3000 signals

Frequency	Time calculated in seconds for 3000 signals			
	FFT	BT	AR	MUSIC
Average	22.8	340.9	206.4	10851.8

4.5 Conclusion

The study shows significant difference (FFT = 22.8 seconds versus BT=340 second, AR=206.4 seconds and MUSIC=10851.8 seconds) in computation time between the techniques while the estimated value for DF was the same for all four techniques (as stated in Table 4.1), with the difference being in the shape of the spectral estimates, which does not affect DF. Despite the differences in computation time, all techniques are capable to identify the main dominant frequency. The signal to noise ratio simulation shows FFT can handle

noise up to -12 dB while other techniques up to -20 dB. The choice of a particular technique contributes to the overall surgical procedure time. As discussed before the duration of catheter deployment is a factor that can contribute to blood stream infection. Therefore, the selection of the fastest technique will reduce the risk of the procedure.

As shown by the result of this study, FFT is the best technique as it produces accurate estimates of DF in a speed compatible for quasi real time analysis (it reduced the required number of complex multiplication). The other techniques were tested to verify the differences in spectral estimation (for instance, we know that for very short segments the spectral resolution of the FFT is poor).

In the next chapter, we will demonstrate FFT capability to estimate DF in animal studies. As a robust technique, FFT is widely used to analyse both Atrial Fibrillation as well as Ventricular Fibrillation signals.

5 DOMINANT FREQUENCY ESTIMATION FOR VENTRICULAR FIBRILLATION FROM ANIMAL STUDIES

5.1 Introduction

Time-domain methods have been successfully applied in the characterization of AF periods using ECG [Vaya and Rieta, 2007]. Anuradha and collaborators used time domain methods to classify cardiac signals [Anuradha *et al.*, 2008]. They used adaptive neuro fuzzy interface system (ANFIS) and compared their results with those obtained using the analytical method. As a result they concluded that ANFIS is the best of the two methods for ECG classification.

In the frequency domain, the analysis methods are based on the use of spectral procedures and generate various types of information such as dominant frequency of the spectrum. Berenfeld and his collaborators investigated the mechanism that underlies the arrhythmia and focussed on the analysis of human AF in the frequency domain [Berenfeld, 2007]. They reviewed the use of the Fourier power spectrum and its DF to determine the AF mechanism in patients. In a previous paper, they introduced the method of dominant frequency mapping to identify the excitation frequency distribution during AF [Berenfeld *et al.*, 2000]. This technique provides accurate sites of the activity and gives stable demonstration for AF maintenance in the isolated sheep heart. They have also shown that different parts of the atria have different frequency characteristics. Everett *et al.* introduced a new method for measuring AF organization and in this algorithm they refer to an Organization Index (OI) [Everett *et al.*, 2001] defined as:

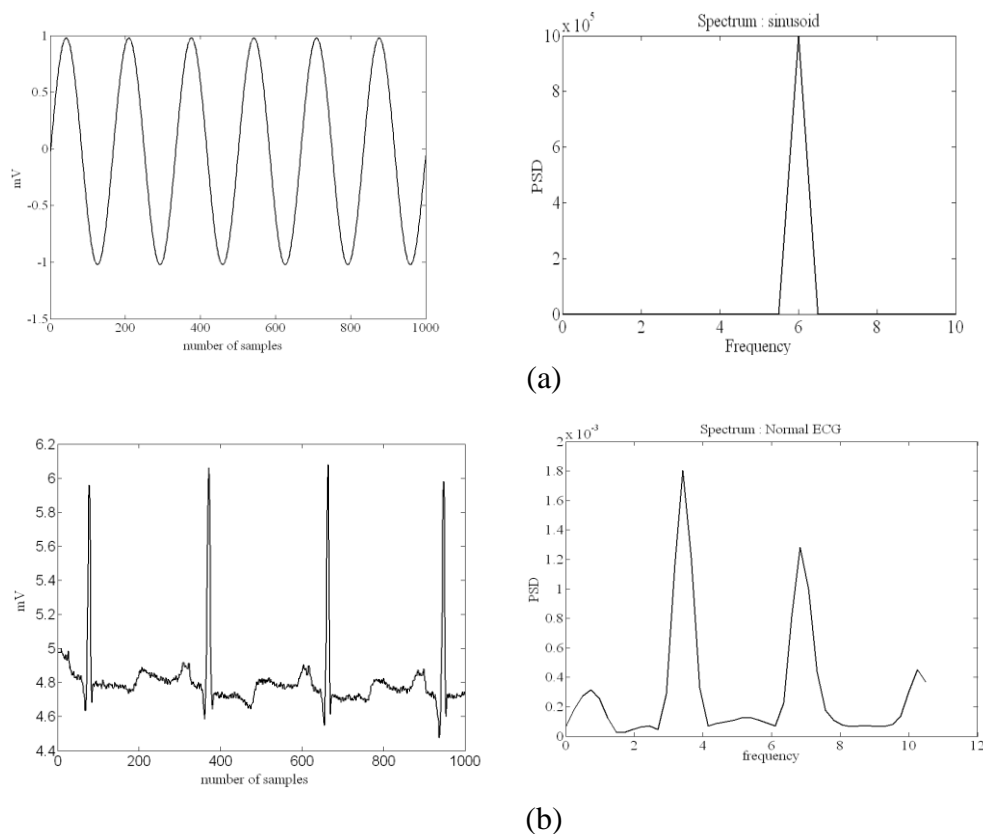
$$OI = \frac{\text{area under DF and three of its harmonics}}{\text{total area under the resulting magnitude spectrum up to (not including) 5th harmonic peak}}$$

They found that OI enables to determine if all of the different frequencies are contributing to the AF or if one area is a dominant contributor to the AF. A paper from Jerome Kalifa, 2006 reports that the value of the DFs in the left atrium are equal or higher than those in the right atrium [Kalifa *et al.*, 2006]. Daniela Husser *et al.* 2004 have reviewed the article about the usefulness of the frequency analysis for non-invasive assessment of electrical remodelling in AF and confirmed that it is helpful for guiding AF therapy [Husser *et al.*, 2004]. They are using filtering, subtraction of averaged QRST complexes and power spectral analysis to show large inter-individual variability. This measurement correlates well with intra-atrial cycle length, a parameter that is important in AF control and response to therapy.

Jin-Long Huang showed that the highest dominant frequency is normally located in the left atrium and pulmonary veins [Huang *et al.*, 2006]. The excitation of LA and PVs may drive part of the atria to manifest fibrillatory conduction. Sanders *et al.*, 2005 used FFT to determine the DF for patients who have both paroxysmal and permanent AF from left atrium (LA) to right atrium (RA) to CS [Sanders *et al.*, 2005]. They found that the frequency in the majority of atria and CS is slow (≤ 5 Hz). A faster rate (7-8 Hz) was observed at the posterior wall of the LA with DF sites at each of the pulmonary veins (PVs). Lazar found that the DFs at posterior RA are slowest, intermediate in the CS and highest at the PV/LA junction [Lazar *et al.*, 2004]. These findings are consistent with observations made in animal models that suggest that the posterior LA may serve an important role in maintaining AF for paroxysmal AF.

Dominant Frequency (DF) is defined as the frequency of the signal at which the power spectrum has the maximum value. The general application of DF analysis is to estimate the

atrial activation rates [Ng and Goldberger, 2007]. Researchers who apply spectral techniques show that AF has significant periodic elements with different degrees of regularity. It has also been shown that certain areas of the atria can have higher activation frequencies than other areas. Those may be drivers that preserve AF and could be targets of ablation therapy [Skanes *et al.*, 1998, Mansour *et al.*, 2001, Lazar *et al.*, 2004, Sahadevan *et al.*, 2004, Sanders *et al.*, 2005, Huang *et al.*, 2006, Pachon *et al.*, 2004]. The ability of DF analysis to reflect the atrial activation rate is dependent on how well the electrogram signal can be approximated by a single sinusoidal function with a frequency equal to the activation rate. Figure 5.1 shows the comparison of DF estimation for pure sinusoid signal with one frequency and the ECG signals (which have more than one frequency peak).

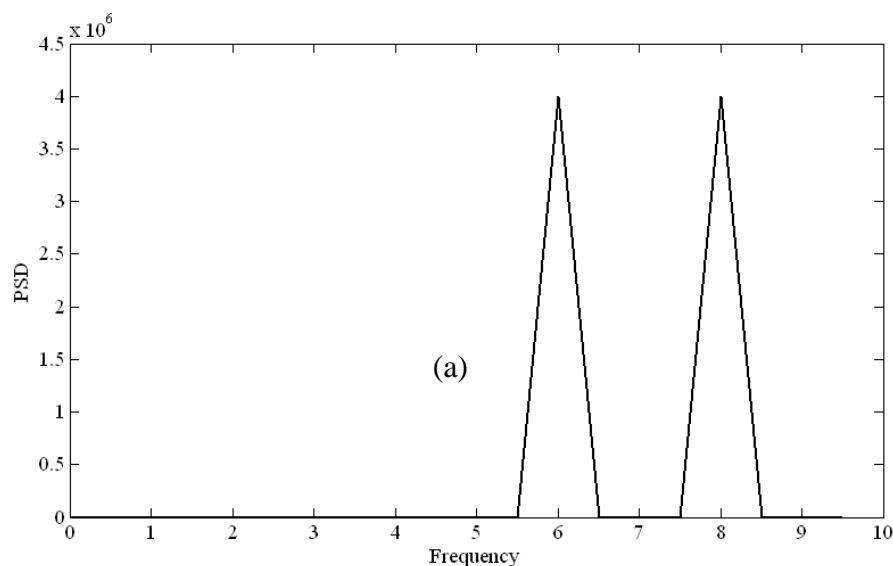


5.1- (a) DF of pure sinusoid signal (left) and spectrum (right). (b) DF of the ECG signal (left) and spectrum (right).

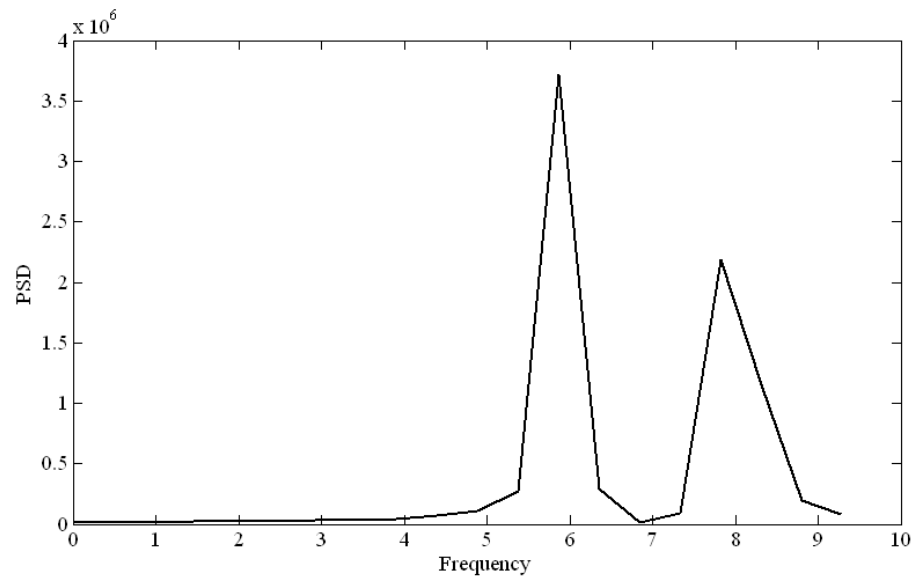
The magnitude spectrum for a pure sinusoidal waveform centres on a single frequency point.

To compute the spectrum of a signal the values of this signal for all time are required. In practice the signal is acquired for a finite duration only, consequently one can only estimate the spectrum from the finite data record measured.

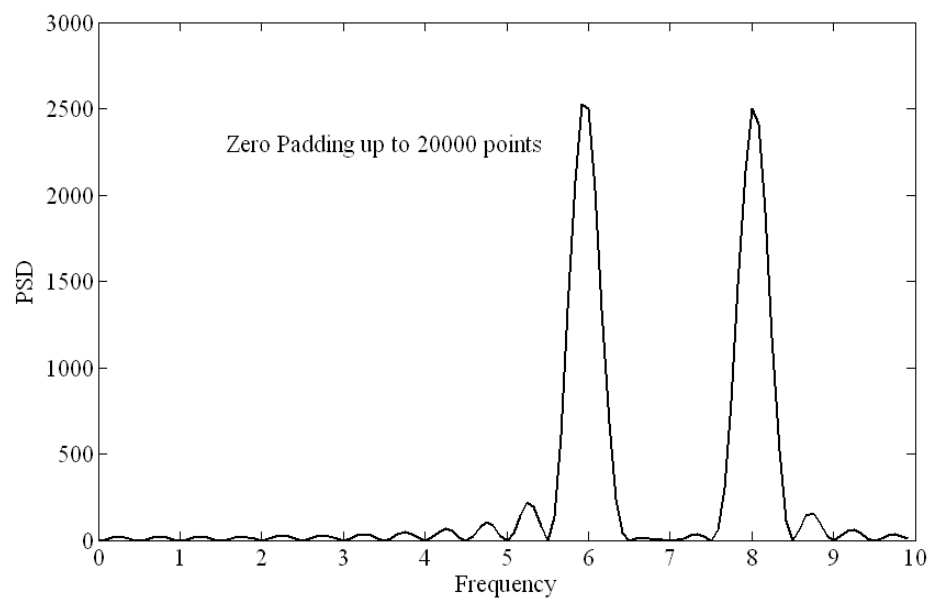
Let's say we have a signal with two known frequencies (6 Hz and 8 Hz), using $N=2000$ number of samples (with sampling frequency $f_s=1000$ Hz); the spectrum generated by FFT was obtained and it is shown in Figure 5.2(a). This is a very particular case in which the FFT spectrum gives sharp results in the frequency domain at the frequencies contained in the signal. It is a particular case because the length of the signal analysed corresponded exactly to an integer multiple of the period of the signal(s). Figure 5.2 (b) shows the Fourier spectrum for the case when the frame analysed does not correspond to an integer multiple of the period of the signal(s). It introduced a smearing in the frequency domain called "leakage effect".



(a)



(b)



(c)

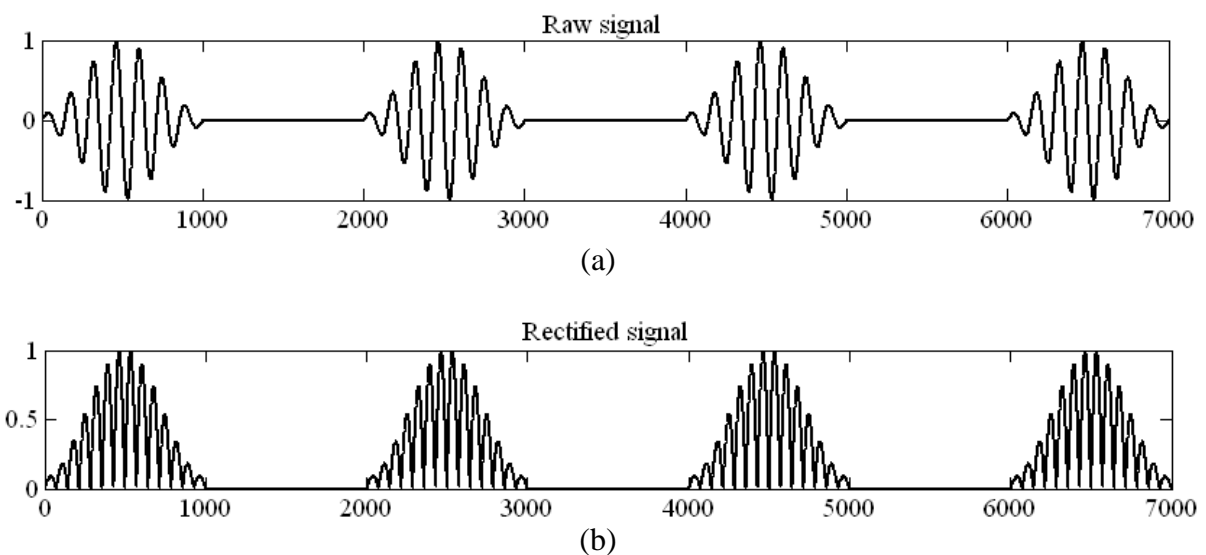
Figure 5.2 - (a) length of the signal equal to an integer multiple of the period of the signal(s). (b) length of the signal not equal to an integer multiple of the period of the signal(s). (c) zero-padding effect.

Leakage can be improved by using zero-padding and performing the Fourier algorithm with a larger number of points. Figure 5.2 (c) shows the spectrum after applying zero-padding of 2048 points. Zero padding does not improve the underlying resolution of the transform, but

provides an interpolated transform with a smoother appearance [Marple, 1987]. The accurate estimation of the spectral peaks is also enhanced with zero-padding.

Rectification and filtering

The correlation between the DF and the mechanical activation is still debated. There are 2 approaches for identifying the DF. Most of the studies rectify the electrical signal (atrial electrogram) and implement low pass filtering before performing spectral analysis [Sanders *et al.*, 2005, Gojraty *et al.*, 2009, Shimizu *et al.*, 2007] as shown in Figure 5.3. This approach is useful to identify bursts or spindles of electrical activity. The second approach is performing the spectral analysis without rectifying and low pass filtering. The raw electrograms are used straight away to identify the DF. In this study, we used the latter approach because we are interested in identifying the frequency for the electrical activity and not to identify the (slower) frequency for bursts of electrical activity.



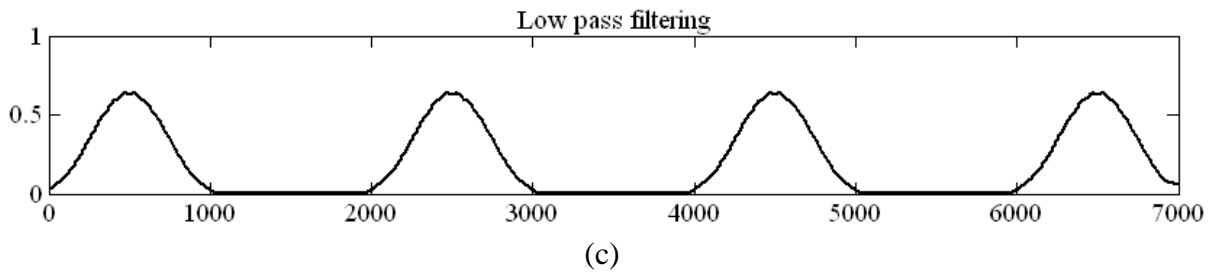


Figure 5.3- Raw signal (top), rectified signal (middle) and low pass filtered signal (bottom).

5.2 Dominant Frequency Estimation for Ventricular Fibrillation in Animal Studies

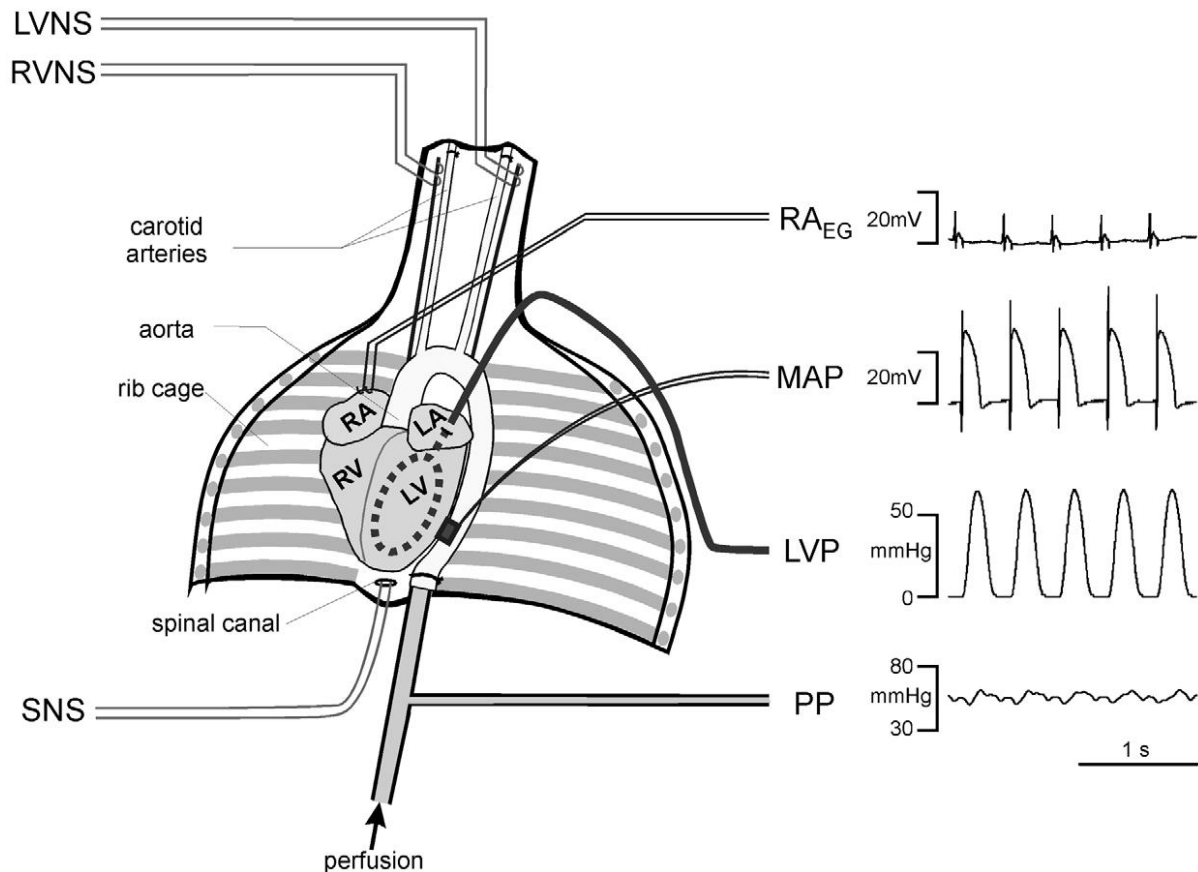
5.2.1 Introduction

In contact mapping studies, there are 2 types of arrhythmia that have been used to analyse the frequency spectrum; ventricular fibrillation (animal studies) and atrial fibrillation (human studies). Both of these signals show a different dominant frequency and characteristics. The objective of this chapter is to estimate the DF for ventricular fibrillation in animal studies.

5.2.2 Method

The data was taken from the sections of Ventricular Fibrillation (VF). Adult New Zealand White rabbits were premedicated with Hypnorm and anaesthesia induced 15 min later by Hypnoval given via an ear vein [Ng *et al.*, 2001]. A midline cervical incision was made and the trachea was identified and intubated with a 5 mm diameter plastic tube that was secured with silk sutures. Thereafter, general anaesthesia was maintained with pentobarbitone sodium. The trachea was cannulated and ventilation was maintained with positive pressures via a small animal ventilator. The common carotid arteries were identified and isolated with silk sutures and the vagus nerves partially dissected free at the mid-cervical level. The

midline cervical incision was extended down the front of the chest wall to expose the ribcage. The pectoral muscles were dissected on both sides to expose subclavian vessels that were tied off with silk sutures. The rabbit was killed with an overdose of pentobarbitone sodium together with 500U heparin. The thoracic cavity was opened via incisions on both sides and the anterior portion of the ribcage was removed exposing the mediastinal contents. The pericardium was then cut and an ice-cold Tyrode solution applied to the surface of the beating heart to lower temperature and metabolic rate. The descending aorta was identified and cannulated with a flanged 5 mm diameter plastic tube through which ice-cold Tyrode solution was injected. The pulmonary artery was cut to allow flow of perfusate out of the right heart. The vertebral column was dissected at the level of the 12th thoracic vertebra and at the 1st cervical vertebra. The preparation extending from the neck to the thorax was then dissected from the rest of the surrounding tissues. The procedures were undertaken in accordance with the Animals (Scientific Procedures) Act 1986 and conformed with the Guide for the Care and Use of Laboratory Animals Published by the US National Institutes of Health (NIH Publication no. 85–23, revised 1985).



5.4 – Cardiac electrical recording and pacing [From Ng *et al.*, Effects of direct sympathetic and vagus nerve stimulation on the physiology of the whole heart – a novel model of isolated Langendorff perfused rabbit heart with intact dual autonomic innervation, 2001, *Experimental Physiology*, used with permission]

Cardiac electrical recording and pacing

Figure 5.4 shows a pair of platinum electrodes (Grass Instruments, Astro-Med Inc., USA) was inserted into the right atrial appendage for recording of atrial electrograms. In the experiments which examined the effects of autonomic modulation of atrioventricular conduction, these electrodes were also used for atrial pacing with a constant current stimulator (DS7A, Digitimer). A custom-made suction electrode was used to record monophasic action potentials (MAPs) from the epicardial surface of the left ventricular free wall using a DC-coupled high input impedance differential amplifier.

Autonomic nerve stimulation

I. Vagus nerves. The vagus nerves were separated from adjacent tissues and each nerve supported on a pair of platinum electrodes.

II. Sympathetic stimulation. For sympathetic stimulation, a method similar to that described by Gillespie & Muir (1967) was used. A custom-made insulated silver wire was inserted into the spinal canal at the 12th thoracic vertebra and the tip of the wire was advanced to the level of the 2nd thoracic vertebra to allow bipolar stimulation of both sides of the cardiac sympathetic outflow. The electrodes for stimulation of the sympathetic and vagus nerves were connected to a 2-channel constant voltage square pulse stimulator (S88, Grass Instruments) which allowed stimulation over a range of frequencies (1–20 Hz) and strengths (1–20 V) at 2 ms pulse width. One channel was used for sympathetic stimulation and the other for stimulation of the left or right vagus nerve.

The length of the samples provided up to 20 seconds. The data was recorded at 1 ms sampling interval. Data were recorded from the left ventricular free wall of the left ventricle of a rabbit. There are 4 conditions:

BL - baseline (VF without nerve stimulation);

SNS - VF in the presence of simultaneous sympathetic nerve stimulation;

LVS - VF in the presence of simultaneous left vagus nerve stimulation;

RVS - VF in the presence of simultaneous right vagus nerve stimulation.

Data represent VF signals immediately after induction of VF. Figure 5.5 shows the electrical signal of VF.

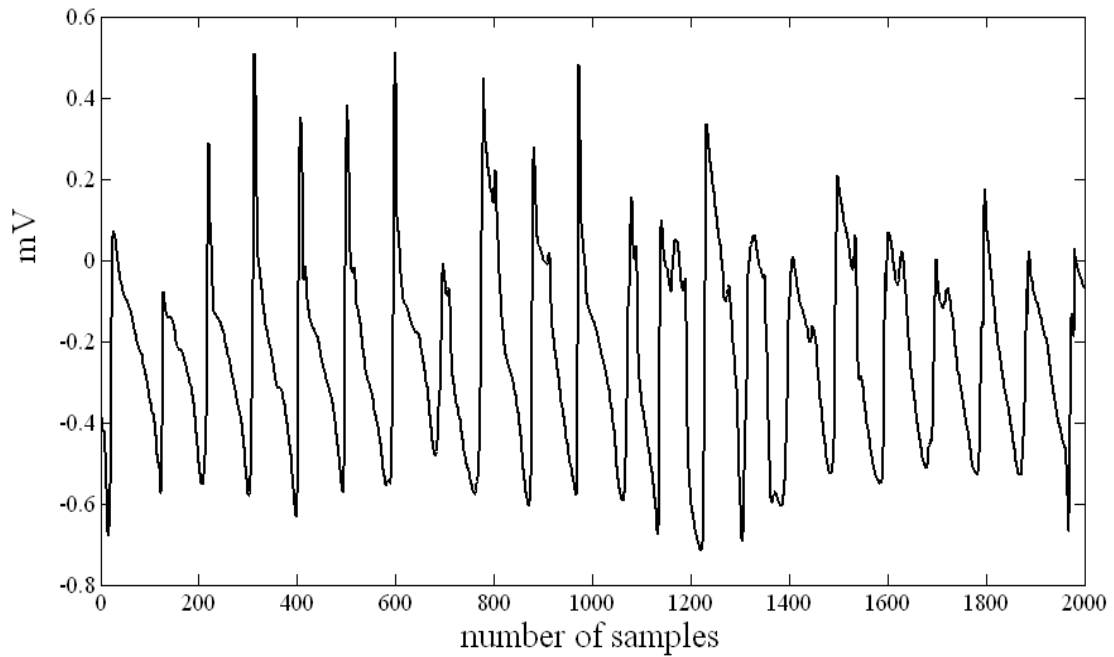


Figure 5.5 - VF signal (sample 31700)

VF was induced using 30 stimuli at 30 ms cycle length between each stimulus. This represents a burst of rapid pacing over the vulnerable period in the cardiac cycle to trigger VF. There are 8 experiments where data was recorded. All of them are recorded with the codes of 31700, 42800, 50500, 50800, 51500, 63000, 71700 and 81400. An example of VF data collected at baseline during one experiment is shown in Appendix 1. Welch technique [Welch, 1967] is used to calculate the power spectrum of the signals using 1000 samples window, 1 Hz frequency resolution, hamming window, with 50% overlap over 20s.

5.2.3 Results

Figure 5.6 shows the overall spectrum and the spectrogram obtained from one sample (subject coded 031700rv).

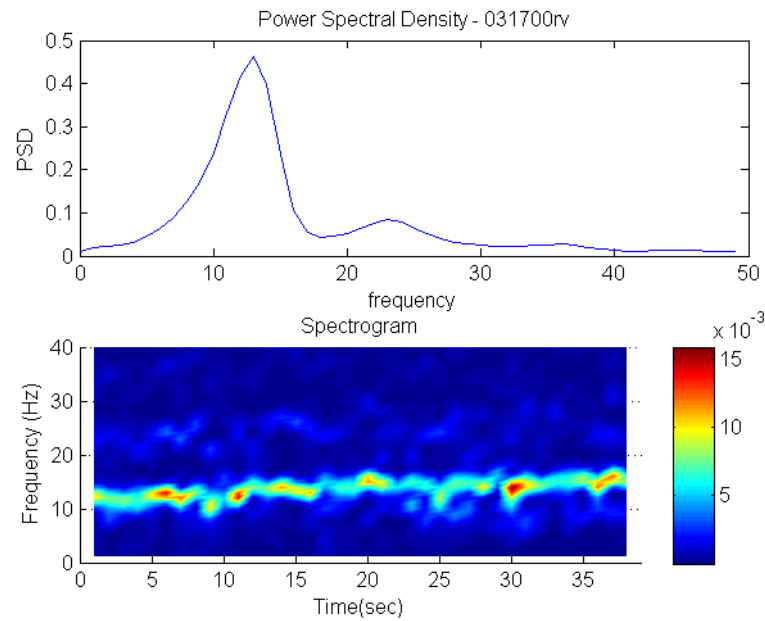


Figure 5.6 - Spectrum and spectrogram

In Figure 5.6, the top graph shows the power spectrum of the signal (power spectral density versus frequency) while the bottom graph represents the evolution of the frequency spectra along time. The spectrogram was plotted using the information of spectrum sequence of spectra as shown on the top graph. We observed the dominant frequency in this sample is 13 Hz, which represents the highest power in the signal. In the spectrograms, frequency with high power is indicated by red colour indicator while frequency with low power is represented by blue colour. This was plotted for each second until the end of recorded data.

The spectra and spectrograms obtained for each condition namely baseline (BL), right vagus nerve stimulation (RVS), left vagus nerve stimulation (LVS) and sympathetic nerve stimulation (SNS) are shown in Appendix 2. Table 5.1 shows DF values observed for all conditions.

Table 5.1 Dominant Frequency during Ventricular Fibrillation

Sample	DF (Hz)					
	BL	LVS	BL	RVS	BL	SNS
31700	12	13	12	13	12	13
42800	14	13	14	13	11	14
50500	-	-	12	14	11	12
50800*	12	9	12	10	11	12
51500	13	10	13	11	13	13
63000	-	-	11	9	11	11
71700	-	-	14	12	14	17
81400	13	12	13	12	13	14
Average	13.2	11.4	12.9	11.8	11.9	13.3
Max	14.0	13.0	14.0	14.0	14.0	17.0
Min	12.0	9.0	11.0	9.0	11.0	11.0

5.2.4 Discussion

Table 5.1 shows that 100% of the DF data (9 to 17 Hz) is within the range of 9 to 19.2 Hz as reported by Chen [Chen *et al.*, 2000]. Table 5.1 shows data extracted for LVS, RVS and SNS comparatively to their BL. On average, DF for LVS is lower than BL ($p=0.135$). All data shows the same trend. Similarly, average of RVS is lower than BL for 7 out of 8 samples ($p=0.155$). In contrast, average of SNS is higher than BL for 6 out of 8 samples ($p=0.070$). In addition, there are 2 samples for which DF for BL and SNS remain unchanged. There are several samples with incomplete data due to the measurement conditions considered too unreliable.

From the spectrogram, we observed that the majority of the samples show an increase in DF along time. The reason is that the sympathetic stimulation should normally shorten the refractory period, consequently, the DF increases.

Vagal stimulation shows an opposite effect to sympathetic stimulation [Levy and Zieske, 1969]. Based on the frequencies that we obtained from this analysis, we also found the same behaviour; SNS frequency (13.3 Hz) is higher than baseline (11.9 Hz) while VNS frequencies (11.8 Hz versus 12.9 Hz and 11.4 Hz versus 13.2 Hz) are lower than baseline. During vagal stimulation, the dynamic decrease in heart rate was observed [Ng *et al.*, 2001]. Differential effects exist between right and left vagal stimulation. Right vagus has a more potent effect on sinus rate and left vagus has more potent effect on AV conduction [Ng *et al.*, 2001]. Data in Table 5.1 confirmed the finding with average RVS frequency (11.8 Hz) is higher than LVS frequency (11.4 Hz).

In contrast, sympathetic stimulation exerts positive heart rate and heart conduction effects. Stimulation of sympathetic nerve endings releases noradrenaline [Hartzell HC, 1998] that will increase repolarisation in the ventricles. The conduction velocity is increased and this will cause the frequency to increase.

Relevance of autonomic stimulation (sympathetic / vagal) and its effects on fibrillation

The relevance of autonomic stimulation and VF is complicated. However in some cardiac disease states such as myocardial infarct and heart failure the autonomic nervous system is in disarray, which is coupled to a simultaneous increase in the heart's susceptibility to ventricular tachyarrhythmias (ventricular tachycardia and fibrillation). Often the sympathetic

system is unregulated and sympathetic nerve activity is high whilst the parasympathetic nerve system is down regulated i.e. vagal activity is low.

As we have shown from rabbit studies, sympathetic stimulation increases the susceptibility to VF whilst vagal stimulation protects the heart against VF. So it is understandable and logical to suggest that the increased sympathetic activity and reduced vagal tone in these fatal conditions underlies the increased risk for VF.

We have shown that this might be mediated via an electrical restitution mechanism. The phenomenon of sympathetic stimulation (SS) and vagal stimulation manipulating the rhythm of VF itself, which is more difficult to explain. The analysis shows that SS increases the dominant frequency of VF and vagal stimulation reduces the DF of VF. However, an explanation as to what this means is difficult. Although reducing the DF may imply that VS alters the organisation of VF into a more stable rhythm. More stable rhythms may be easier to manage and prevent. On the reverse side, increasing the DF as seen in sympathetic stimulation may imply a more dangerous and difficult to manage rhythm that is highly self perpetuating.

5.2.5 Conclusion

The method of dominant frequency estimation and the frequency evolution along time were explained. Frequencies within 9 to 17 Hz were observed for ventricular fibrillation. These methods allow us to observe the frequency changes over a required period. In addition, we also can observe the power which corresponds to the frequency of the electric signals.

As mentioned previously, the signals were obtained during continued sympathetic (SNS) and left (LVS) or right vagal (RVS) stimulation. The result shows that with SNS increasing DF and both LVS and RVS decreasing DF. No significant difference between LVS versus RVS but this is yet to be confirmed statistically (it is beyond this study capability to conclude that).

In the next chapter, we will estimate the frequency of atrial fibrillation signal in human studies. This will involve high frequency stimulation and drug infusion procedure.

6 DOMINANT FREQUENCY ESTIMATION OF ATRIAL FIBRILLATION FROM HUMAN STUDIES

6.1 Introduction

Cardiac autonomic ganglia are nervous tissues which can be found on the surface of the heart. They are thought to play an important role in initiation and maintenance of AF [Benjamin J. Scherlag *et al.*, 2005]. In this study, we use two different hypotheses for these ganglia:

- 1) high frequency stimulation produces changes in frequency. The stimulation is used to activate cardiac ganglia on the epicardium of the atria;
- 2) isoprenaline and atropine have an effect on dominant frequency.

6.2 Hypothesis 1: High frequency stimulation (HFS) produces changes in frequency

For this study, we analysed intracardiac electrograms of 3 patients who were in AF during routine electrophysiology study. All signals were recorded from a decapolar catheter (consisting of 5 bipole electrode positions starting at CS1-2 and ending at CS9-10). The decapolar catheter was placed in the coronary sinus (Figure 6.1), which allows assessment of left atrial electrical activity. It is known that high frequency stimulation at selected endocardial sites can lead to stimulation of vagal tissue within autonomic ganglia [Scanavacca *et al.*, 2006]. The effect of vagal nerve stimulation can be seen as slowing of the ventricular rate, caused by atrioventricular conduction block. In this study, high frequency stimulation between 20 - 50 Hz at the proximal poles of the CS catheter (CS9-10 position) was delivered using a programmable cardiac stimulator used for electrophysiological studies. We defined a vagal response as production of atrioventricular block for at least 1s after applying high frequency stimulation over a 30 s period. Signals

recorded on the CS1-2 and CS3-4 position during this period where a vagal response is seen, are then analysed using FFT and compared before, during and after stimulation.

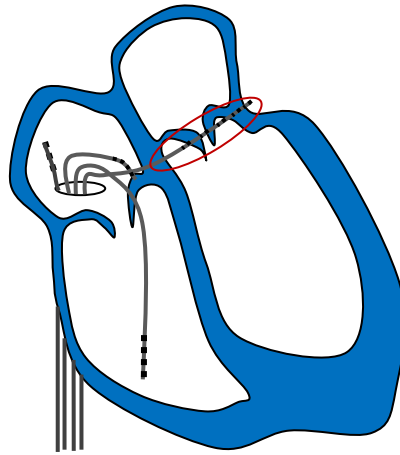


Figure 6.1 - Catheter at coronary sinus (red circle).

Yoshihide Takahashi, *et al.*, 2005 found that the optimal measurement site to get a repeated serial measurement is the coronary sinus (CS). The stability of the catheter during measurement is one of the reasons why the coronary sinus is a good place to record electrical activity in the left atrium.

The signals have been analysed using Fast Fourier Transform (FFT) analysis. After signal processing, an FFT was performed over 4096 points every one second from 30 second recordings. The maximum peak in the magnitude spectrum was defined as the dominant frequency (DF). The red colour shows the frequencies with high power while the blue colour corresponds to low power. The advantage of using a spectrogram is it allows us to see how the frequency changes along time.

The data have been taken from 3 patients. They are:

- 1) P1-VB (stimulation at 50ms);
- 2) P2-CL (stimulation at 20ms);
- 3) P3-TJ (stimulation at 40ms).

The data have been analysed and spectra were produced for all the patients.

6.2.1 Discussion

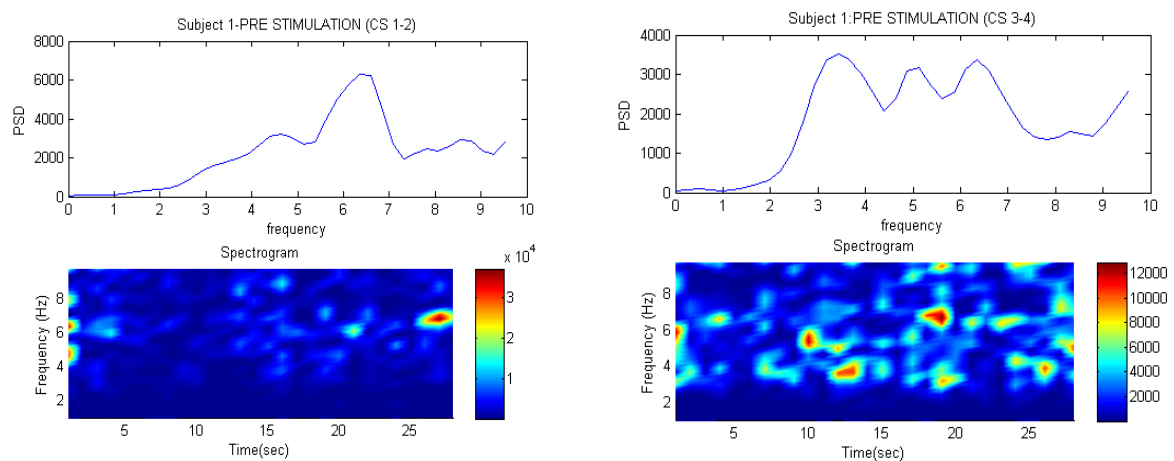
Patient 1 (P1-VB)

The position for each bipolar (channel) labelled as:

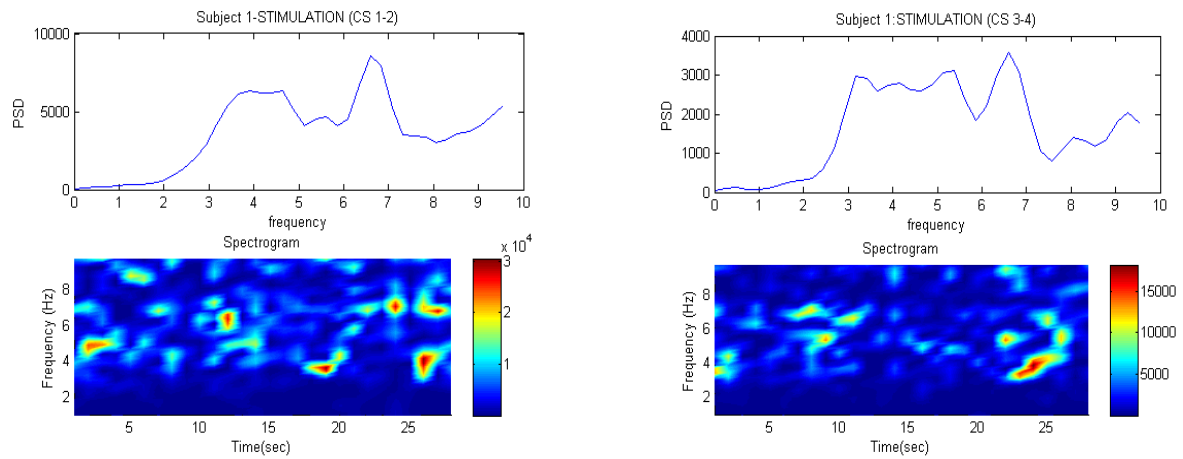
- Channel 9 : CS 1-2
- Channel 10 : CS 3-4

The spectral plots for channel 9 and channel 10 are shown in Figure 6.2.

P1-VB-PRE STIMULATION



P1-VB- STIMULATION



P1-VB- POST STIMULATION

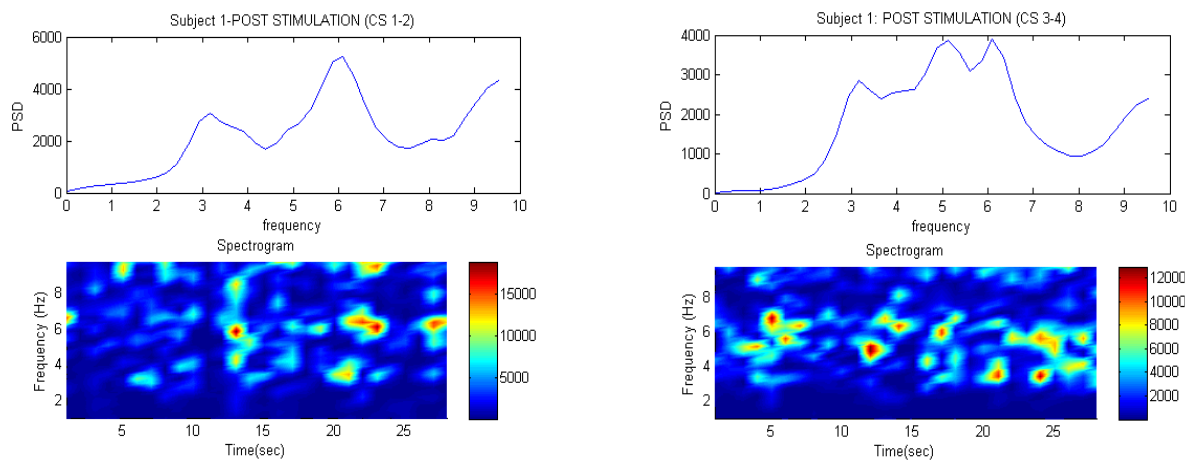


Figure 6.2 - Spectrum and spectrogram for P1-VB

The DF has been recorded for each of the channels during pre-stimulation, stimulation and post-stimulation conditions. The frequencies for atrial electrograms for CS 1-2 and CS 3-4 for P1-VB are shown in Table 6.1.

Table 6.1 - Dominant frequency for P1-VB

Channel Condition	9 (CS 1-2) (Hz)	10 (CS 3-4) (Hz)
Pre-stimulation	6.35	3.42 / 6.35
stimulation	6.59	6.59
Post-stimulation	6.10	6.10

Pre-Stimulation observation

According to P1-VB data, the DF during pre-stimulation is 6.35 Hz for channel 9 and 10. Besides, it is observed that channel 10 has dual spectrum peaks at 3.42 Hz and 6.35 Hz. The spectrograms also confirmed the situation based on the colour spectrum observed. The highest peak is observed at 6.35 Hz, but stating only the DF might be an oversimplification of the more complex activity here.

During Stimulation observation

There are increasing trends of DF during stimulation stage observed comparatively to Pre-stimulation. The stimulation produces an increase in the dominant frequency, which is an indication of stimulation of nearby autonomic ganglia.

Post Stimulation observation

In short, all DF for Post stimulation are lower than pre-stimulation DF.

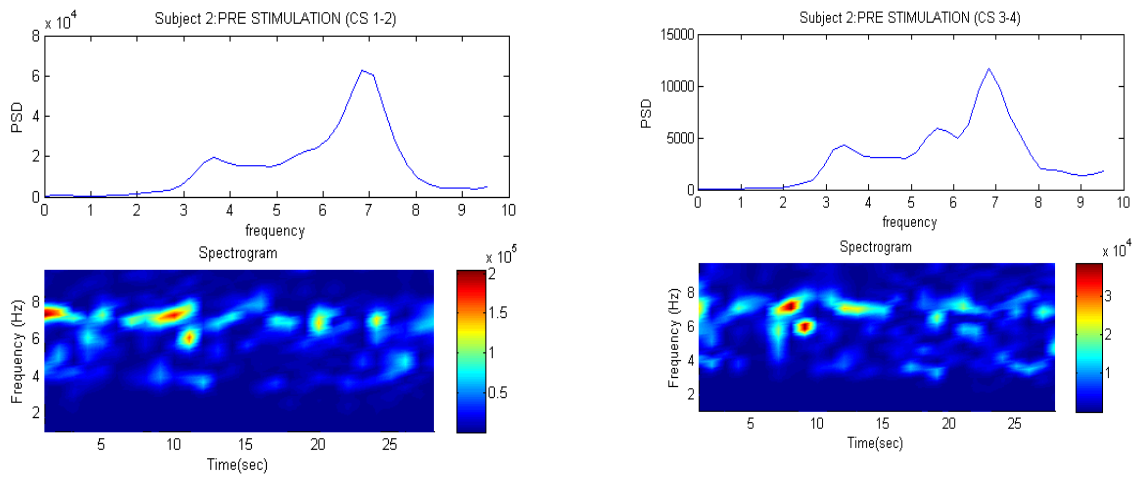
Patient 2 (P2-CL)

For patient P2-CL, the position for each bipolar (channel) recorded are labelled as:

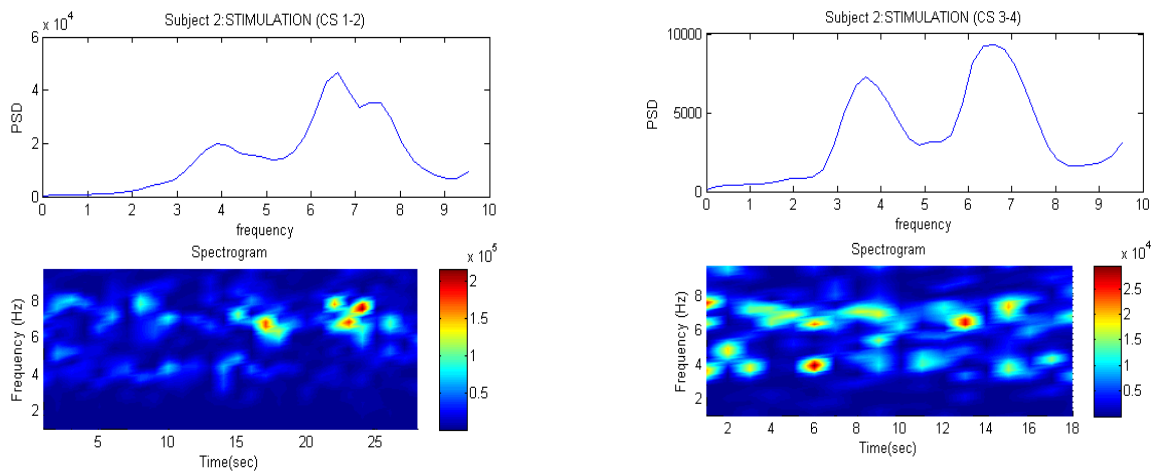
- Channel 6 :Coronary sinus 1-2;
- Channel 7 :Coronary sinus 3-4;

The spectra for P2-CL are shown in Figure 6.3 and their dominant frequencies in Table 6.2.

P2-CL-PRE STIMULATION



P2-CL- STIMULATION



P2-CL- POST STIMULATION

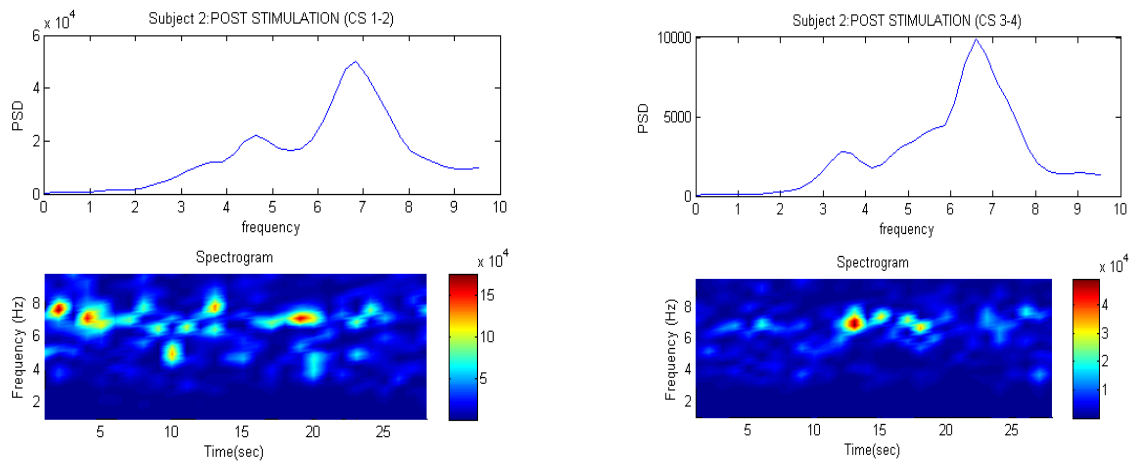


Figure 6.3 - Spectrum and spectrogram for P2-CL

Table 6.2 - Dominant frequency for P2-CL

Channel \ Condition	6 (CS 1-2)	7 (CS 3-4)
	(Hz)	(Hz)
Pre-stimulation	6.84	6.84
stimulation	6.59	6.35
Post-stimulation	6.84	6.59

Pre-Stimulation observation

The DF at pre-stimulation is 6.84 Hz.

During Stimulation observation

There is a declining trend of DF during stimulation period observed for all channels. There is 6.59 Hz for channel 6 and 6.35 Hz for channel 7.

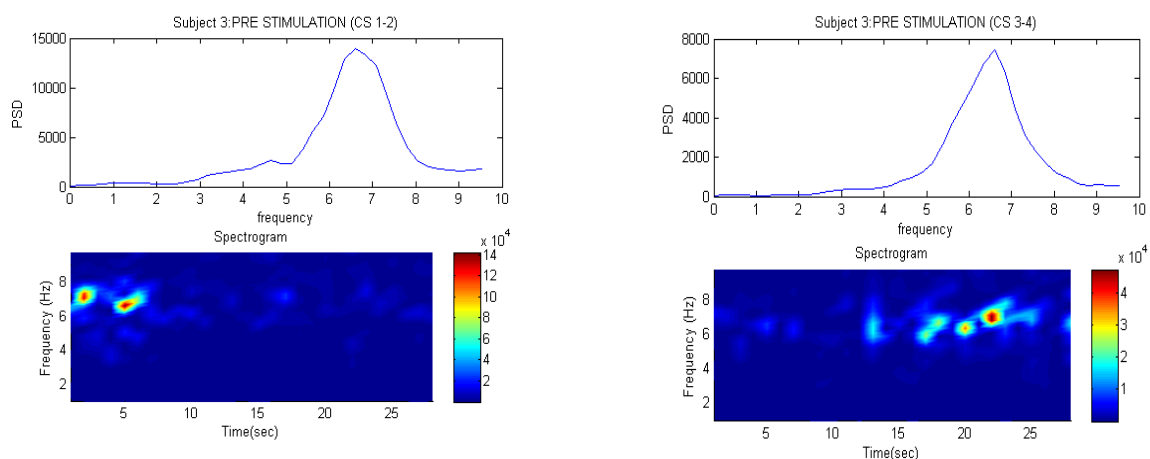
Post Stimulation observation

In brief, all data show an increase of DF from the state of stimulation to the state of post stimulation (6.59 to 6.84 Hz and 6.35 to 6.59 Hz) on channels 6 and 7.

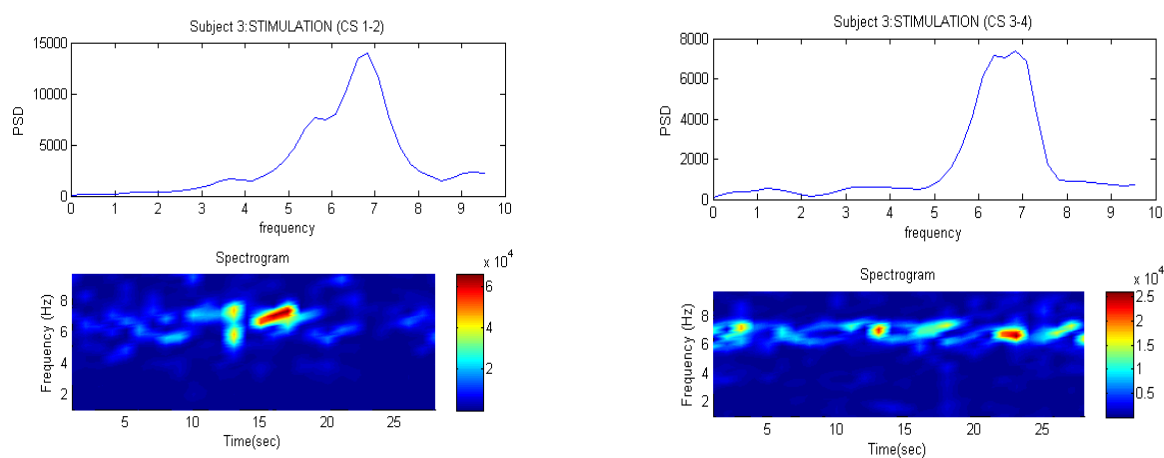
Patient 3 (P3-TJ)

The position for each bipolar (channel) labelled is the same as P2-CL. The spectra for P3-TJ are shown in Figure 6.4 and their frequency in Table 6.3.

P3-TJ-PRE STIMULATION



P3-TJ-STIMULATION



P3-TJ-POST STIMULATION

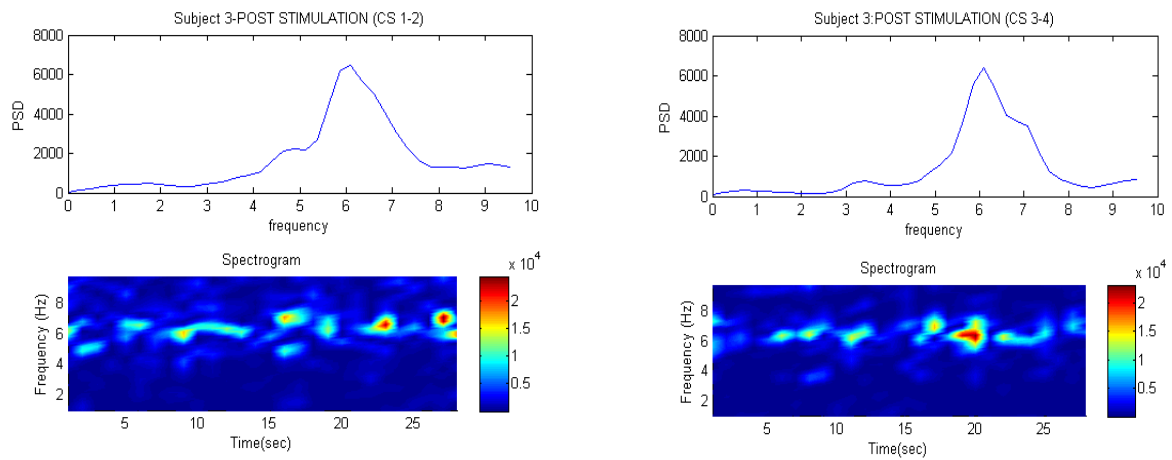


Figure 6.4 - Spectrum and spectrogram for P2-CL

Table 6.3 - Dominant frequency for P3-TJ

Channel \ Condition	6 (CS 1-2) (Hz)	7 (CS 3-4) (Hz)
Pre-stimulation	6.59	6.59
stimulation	6.84	6.84
Post-stimulation	6.10	6.10

Pre-Stimulation observation

For P3-TJ, the DF during pre-stimulation is 6.59 Hz for channels 6 and 7.

During Stimulation observation

There are increasing trends of DF during stimulation period observed for channel 6 and 7.

Post Stimulation observation

DF for Post stimulation is lower than DF for pre-stimulation.

6.2.2 Conclusions

From most human studies, the dominant frequency in AF is ranging between 4 Hz to 10 Hz [Ropella *et al.*, 1988, Sanders *et al.*, 2005]. It is more commonly around 6 Hz to 7 Hz. In physiological studies, we should see a general frequency increase during stimulation. That means the frequency at pre-stimulation should be lower than during stimulation and this should return to pre-stimulation state after stimulation stops. The reason is that stimulation of the ganglia is supposed to promote atrial conduction in AF. The initiation and maintenance of AF is significantly enhanced by simultaneous parasympathetic stimulation (shortening the refractory period of the atria) [Nakagawa *et al.*, 2008, O'Donnell *et al.*, 2002].

There is an expected behaviour of DF value obtained for patients P1-VB and P3-TJ. However, in patient P2-CL, the DF during stimulation is less than pre-stimulation and post-stimulation. This is not the expected behaviour. However, we observed the spectrum during stimulation is wide and shifting to the right. If we use 'centre of gravity' approach for this spectrum, the DF estimation is obtained as shown in Table 6.4.

Table 6.4 - Centre of gravity for P2-CL

Channel Condition	6 (CS 1-2) (Hz)	7 (CS 3-4) (Hz)
Pre-stimulation	6.84	6.84
stimulation	6.96	6.59
Post-stimulation	6.84	6.71

The centre of gravity is the centre value for a range of data. For this study, this approach is used to identify the centre frequency of the spectrum. However, during stimulation, only channel 6 shows the DF (6.96 Hz) higher than pre stimulation (6.84 Hz) and post stimulation (6.84 Hz). Overall, the result for patient P2-CL does not conform to the theory.

6.3 Hypothesis 2: Examining the effect of isoprenaline and atropine on frequency changes

In this study, we analysed the signals for 10 patients who had persistent AF during electrophysiological study. The signals were recorded by decapolar catheter. Five of the patients received intravenous isoprenaline infusion (2 microgram/min). The signals from coronary sinus electrograms were recorded when heart rate gives a response (heart rate increased) and is stable. After stopping isoprenaline and allowing heart rate to return to baseline, atropine (1 mg) was given. The remaining 5 patients received atropine until the heart rate responded and was stable. Then, the signals were recorded again over 30s. The signals were analysed using Fast Fourier Transform (FFT) before and after giving each drug.

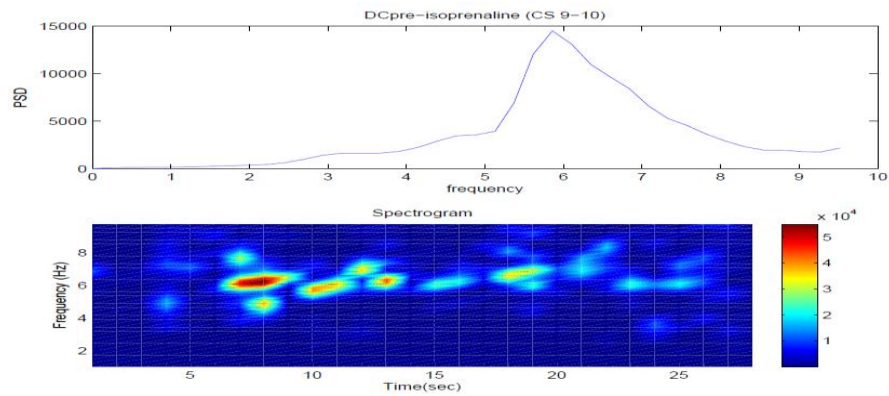
There was approval from the Local Ethics Committee for mapping and ablation studies for patients undergoing AF ablation which include blood sampling and collection of electrical data during the procedures. Data collected for this study relate to patients who had consented to the above. The drugs isoprenaline and atropine were given to the patients at the discretion of the clinicians during the procedures according to clinical protocol.

The discrete Fourier transform was calculated separately for each of the segments. The analysis was performed by taking the average of the segments, each with 2048 points sampled at 1000Hz, using a 4096-point FFT and an overlap of 50% with a Hamming window.

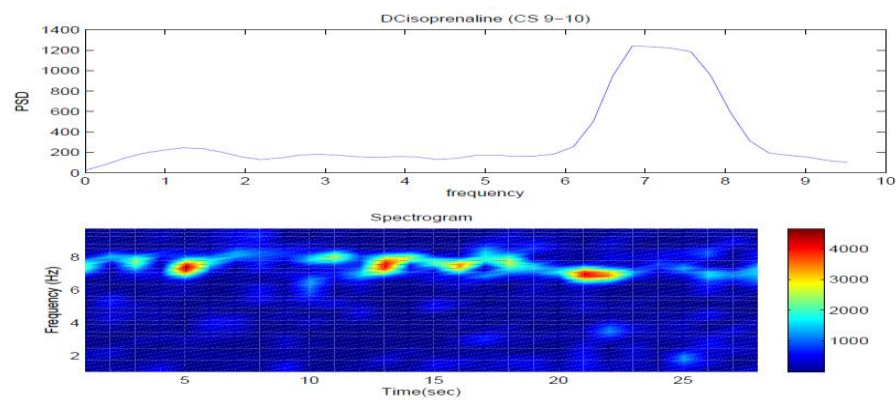
6.3.1 Results and Discussion

All signals were recorded from a decapolar catheter. The decapolar catheter was placed in the coronary sinus for assessment of left atrial electrical activity. Intravenous isoprenaline infusion is given and FFT analysis was used to identify the dominant frequency for each coronary sinus. Channel CS9-10 was selected for analysis due to its position that is the farthest from the ventricle.

Figure 6.5 shows the DF and spectrogram for patient before and after isoprenaline infusion. As we can see the DF before isoprenaline infusion (subject DC) is 5.86 Hz and after infusion is 6.84 Hz. The average of the DF was compared using the Student's t-test, at the 5% significance level ($p=0.06$). An increase in frequency after isoprenaline infusion is significant at 5% level.



(a)



(b)

Figure 6.5 - Spectrum and spectrogram for patient with isoprenaline infusion, (a) before infusion, (b) after infusion

Datas in Table 6.5 show an increase of frequency of post infusion in comparison to pre-infusion. Most of the data (80%) show an increase in DF, in 1 of 5 DF decreased as shown in Figure 6.6. Isoprenaline is a beta-receptor drug [Katzung, 1995, Foster and Boulton, 1991] that will cause a sympathetic response. It has positive chronotropic and inotropic actions because it activates beta receptors. For instance, the frequency is increased (i.e. 5.86 Hz to 6.84 Hz for subject DC).

Table 6.5 - Frequency pre and post isoprenaline infusion

Subject		DC	HL	MW	DK	KS
CS 9-10	pre	5.86	5.37	7.08	6.35	7.57
	post	6.84	5.86	6.84	7.32	8.30

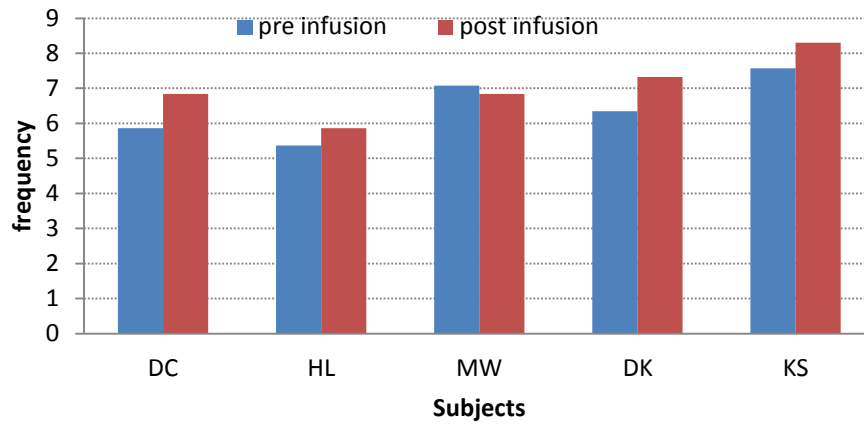
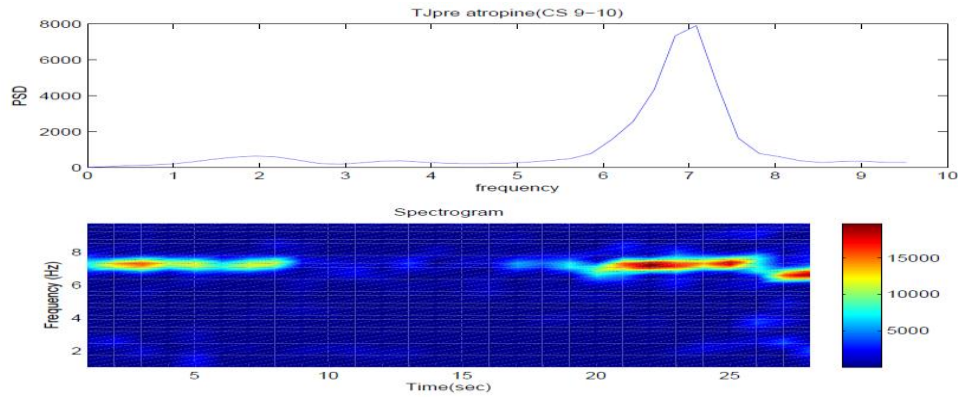
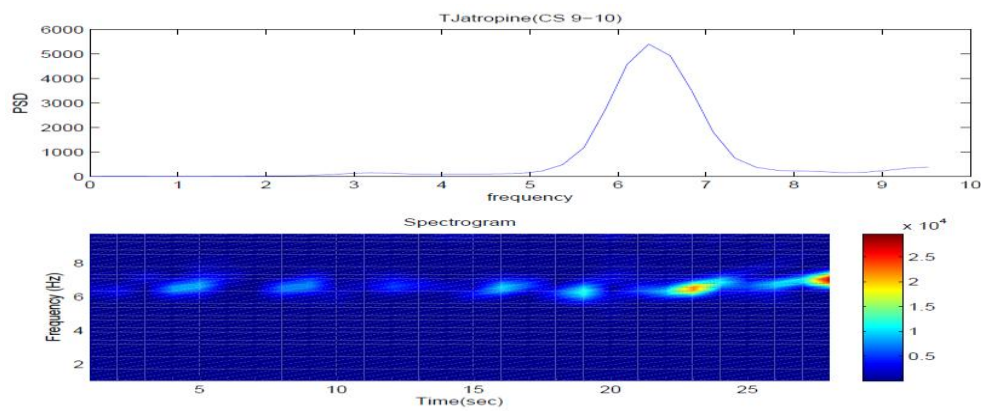


Figure 6.6 - Effect of isoprenaline infusion

Figure 6.7 shows the DF and spectrogram for a patient before and after atropine infusion. The frequencies before and after atropine infusion (subject TJ) are respectively 7.08 Hz and 6.35 Hz. The decrease in frequency after atropine infusion is significant at 5% level ($p=0.025$).



(a)



(b)

Figure 6.7 - Spectrum and spectrogram for patient with atropine infusion, (a) before infusion, (b) after infusion

Datas in Table 6.6 show a decrease in 60% of the cases while for 40% of cases there is no change between pre infusion and post infusion. Theoretically, the frequency should decrease with atropine infusion. In 40% of our results the DF did not change. These might be due to inter individual variability [Hoekema *et al.*, 1999].

Table 6.6 - Frequency pre and post atropine infusion

Subject		CC	DC	HL	MW	VB	CL	DK	KS	WE	TJ
CS 9-10	pre	5.37	7.08	5.62	8.06	5.62	6.59	7.08	7.81	5.86	7.08
	post	5.37	6.84	5.62	8.06	5.13	6.59	6.59	6.59	5.62	6.35

Figure 6.8 represents the results graphically.

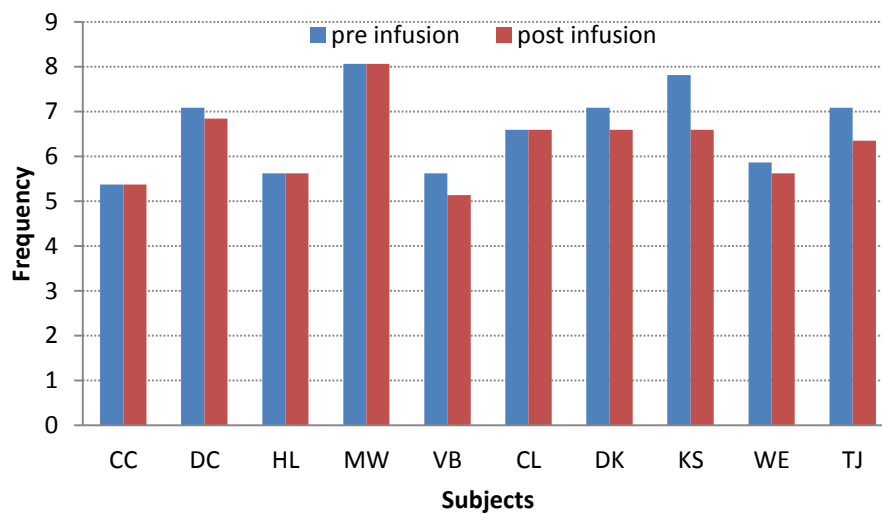


Figure 6.8 - Effect of atropine infusion.

Atropine is an antagonist muscarinic drug [Katzung, 1995, Carlson, 2000]. This drug blocks muscarinic receptors. It block vagal activity, decreases the firing rate in the atrium and, as a result, the dominant frequency decreases (i.e 7.08 Hz to 6.84 Hz for subject DC).

6.3.2 Conclusions

Isoprenaline and atropine are involved in sympathetic and parasympathetic responses respectively. During electrophysiological studies, isoprenaline is used to increase heart rate and to facilitate the induction of AF. Therefore, the atrial activation frequency is increased (for patient DC; pre-stimulation 5.86 Hz and post-stimulation 6.84 Hz). On the other hand, atropine blocks vagal activity and causes atrial activation frequency to decrease (for patient DC; pre-stimulation 7.08 Hz and post-stimulation 6.84 Hz). As a summary, an activation frequency in the atria shows an opposite effect between isoprenaline and atropine. This shows that the DF of AF can be influenced by drug infusion. Hence, this can be supporting evidence for targeting ablation point at the autonomic ganglia area for the treatment of AF.

In the next chapter, we will use non-contact mapping signal of atrial fibrillation. We will deal with the influence of ventricular signals in the analysis. Data other than atrial signal will be removed to minimise their influence to the DF estimation.

7 QRST SUBTRACTION FOR ATRIAL ELECTROGRAMS

7.1 Introduction

During atrial fibrillation (AF), atrial electrical activity is described as chaotic and random [Ng and Goldberger, 2007]. Frequency domain analysis can help to interpret such activity. Ablation at sites with dominant frequency (DF) resulted in a significant prolongation of atrial fibrillation cycle length (AFCL) compared to ablation of sites with non-dominant frequencies [Skanes *et al.*, 1998, Mandapati *et al.*, 2000]. These results justify the use of DF mapping to help identify suitable ablation targets. For higher accuracy of AF data analysis, it is important to minimise the involvement of ventricular activity related data (QRST complex).

A cancellation algorithm was presented by Slocum *et al.* in 1985 [Slocum *et al.*, 1985] who proposed to average QRST complexes and subtraction of this averaged pattern from the electrogram. This worked well, but there were residuals due to minor changes in QRST morphology which were caused by movement of the heart with respiration.

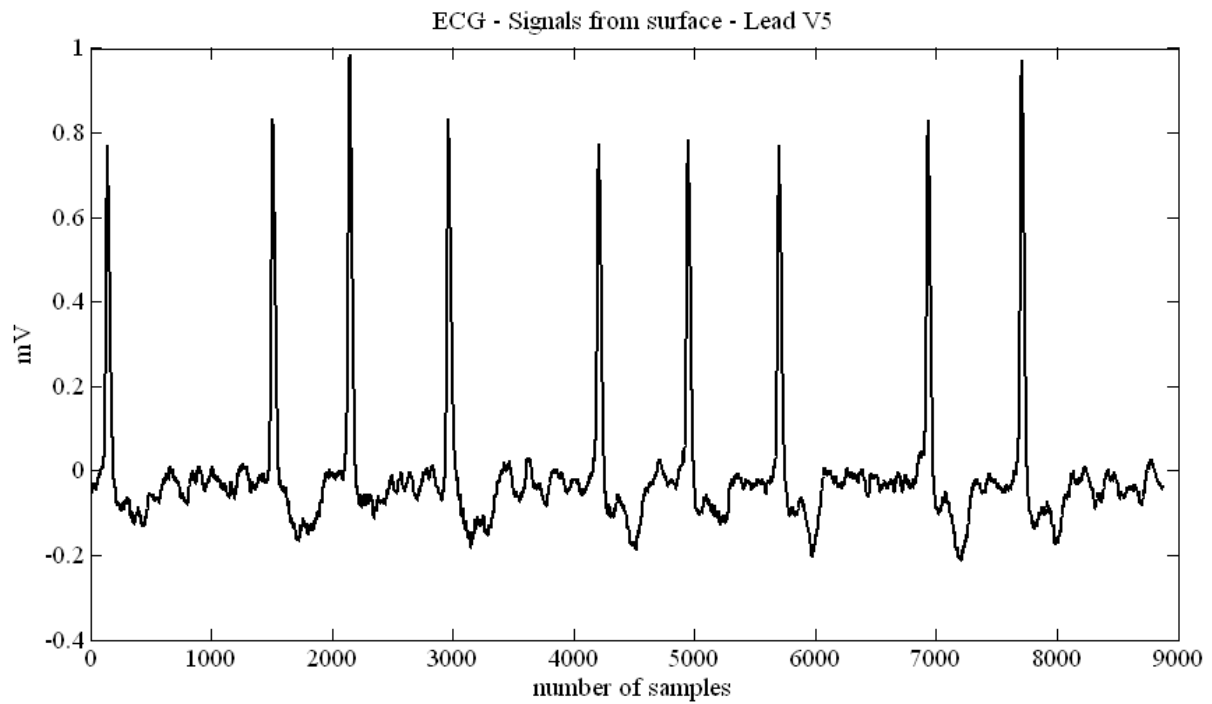
Stridh *et al.* proposed in 2001 a modification of this technique aimed at reducing the effect of respiration and the improvement was most obvious in leads with weak AF (with low amplitude, in their study, leads V2 and V3) [Stridh and Sörnmo, 2001]. Castells *et al.* proposed in 2005 [Castells *et al.*, 2005] a method similar to that by Slocum [Slocum *et al.*, 1985] where mean QRST complex was computed by Principal Component Analysis (PCA) instead of averaging.

We aimed to evaluating the effects of cancellation on unipolar signals with minimal far field ventricular depolarization by removing the electrogram signal at the times when QRS or T waves were present in the ECG and replacing it using three different approaches, flat, linear and spline interpolations.

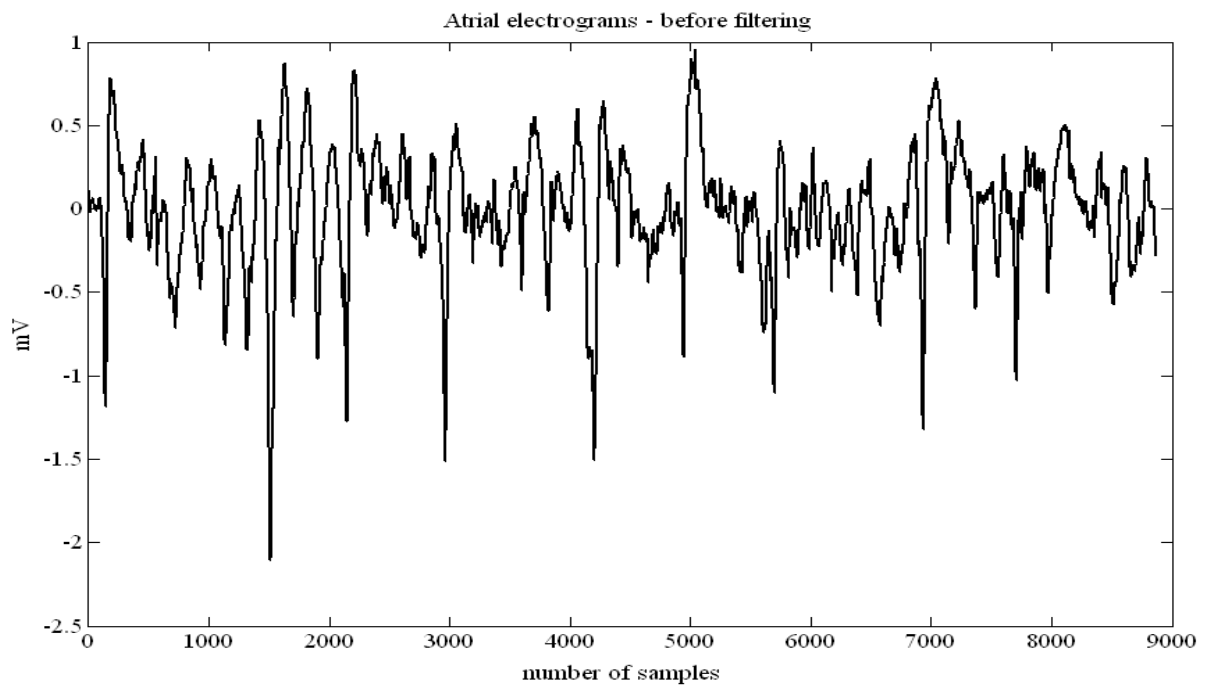
7.2 Methods

In this analysis, the algorithm detected ventricular activations from the QRS complexes of a surface ECG lead. The ECG represents the total of the potentials generated by the heart and contains information on all electrical events occurring in the heart [Shah *et al.*, 2004]. The QRS complex is the dominant characteristic of the ECG signal [Thakor *et al.*, 1984], therefore reliable QRS detection remains an important area of research.

The study was performed in 21-second long continuous segments of each of the 2048 non-contact unipolar electrograms during AF for four different protocols: baseline, after two different drugs infusion (atropine and isoprenaline) and after ablation in five patients with persistent atrial fibrillation. The EnSite System consists of a 9-Fr multielectrode array catheter mounted on a 7.5 ml balloon, amplifiers, and a computer work station [Ahmad *et al.*, 2011]. There are 64 insulated 0.003 inch diameter wires around the circumference of the balloon. Each wire has a 0.0025 inch break in the insulation that serves as the unipolar electrode. The patients underwent catheter ablation guided by contact mapping using Ensite, NavX 6.0, St. Jude Medical, during electro-physiological procedures of AF. The ECG signal from lead V5 for a patient who has AF is shown in Figure 7.1(a).



(a)



(b)

Figure 7.1 - (a) Surface ECG from patient in AF and (b) Intra-cardiac atrial electrogram from the same patient.

Figure 7.1(b) shows unipolar intra-cardiac atrial electrograms measured from inside the atrium. The noncontact mapping system used (EnSite, St. Jude Medical) can export up to 2048 virtual unipolar electrograms from multiple sites simultaneously [Lin *et al.*, 2007] sampled at 1200 Hz over 21 seconds. It consists of atrial signals sometimes contaminated with far field ventricular activity. The patients underwent catheter ablation guided by contact mapping using EnSite, NavX 6.0, St. Jude Medical during electro-physiological procedures to try to cure their AF. It is important to eliminate ventricular signals that contain relatively high frequency components compared with other waves [Okada, 1979]. Therefore, QRST subtraction is the first approach to be implemented for “cleaning” atrial signals before performing spectrum analysis to locate atrial dominant frequencies.

The sweeping of the 3D representation of the atrium of 2048 unipolar electrograms (shown in Figure 7.2) is a spiral along the 32 ‘parallel’ lines from pole to pole stepping down to the next ‘parallel’ after one full turn (and there are 64 ‘meridian’ lines, from pole to pole).

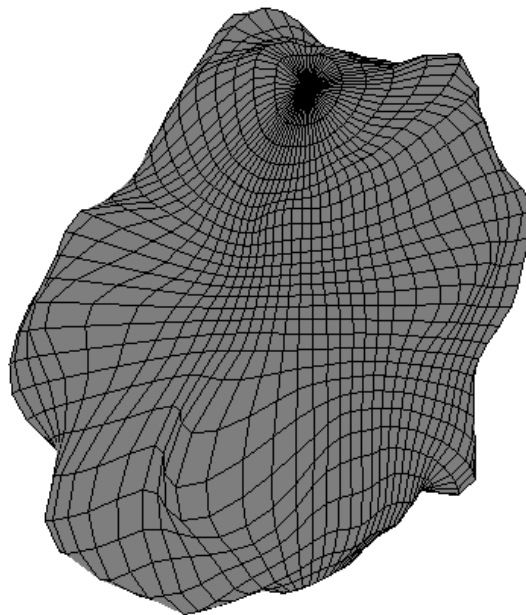


Figure 7.2 - 3D representation of the atrium

7.2.1 QRS Detection

Accurate QRS detection is important to recognize and classify atrial and ventricular signals. Ventricular components, whilst present, could not be accurately identified from the noncontact unipolar atrial electrograms. Therefore, we used signals from the surface ECG as a reference to identify ventricular activity. The data collected from surface ECG and the electrograms are sampled simultaneously. A technique based on that published by Thakor *et al.* [Thakor *et al.*, 1984] was implemented to detect the QRS complexes of the ECG signals. The pass band frequencies, 8 Hz to 20 Hz were determined based on the minimum and maximum duration of the QRS complex (50ms–125ms).

The signal was then rectified and a low pass filter at 6 Hz applied to the rectified signal. The cut-off frequency of this low pass filter is determined by the shortest RR interval of the ECG signals (corresponding to 354 beats per minute). Finite impulse response (FIR) filter design with the window method was used for the low-pass digital filter and MATLAB function ‘filtfilt’ was used to implement the filter while avoiding phase delay.

An adaptive threshold technique was used for QRS detection. The adaptive threshold is adaptive and tends to 75% of the running average of the peak of the magnitude of the QRS complexes [Boardman *et al.*, 2002]. The peaks were detected using this threshold and to avoid detecting the same beat twice, a refractory period (of 280ms) was set, chosen to be a length of time short enough that another beat could not physically occur (214 bpm) [Pan and Willis J. Tompkins, 1985].

Interpolation is the estimation of the unknown samples of a signal using a weighted average of a number of known samples by the neighbourhood [Vaseghi, 2008]. The QRS was replaced by either flat interpolation, linear interpolation or spline interpolation before frequency analysis was performed. The subtracted points (110 ms, with 50 ms before and 60 ms after the detection) are based on the length of typical QRS complex and the ratio 50/60 was selected because the fiducial point of the detector is the first point above the adaptive threshold, which tends to occur before half of the QRS width.

7.2.2 Flat interpolation

In this approach, the subtracted QRS complexes were simply replaced by a baseline value (near to zero).

7.2.3 Linear interpolation

Linear interpolation is often used to fill the gaps in a signal. The interpolation consists of fitting a straight line between two data points and choosing interpolated values at the appropriate positions along that line [William and E.Thomson, 2001]. If we have two known points that have coordinates (x_0, y_0) and (x_1, y_1) , as shown in Figure 7.3, the data series y along the straight line is obtained from the equation

$$\frac{y - y_0}{x - x_0} = \frac{y_1 - y_0}{x_1 - x_0}$$

$$y = \frac{(x_1 - x)y_0 + (x - x_0)y_1}{x_1 - x_0}$$

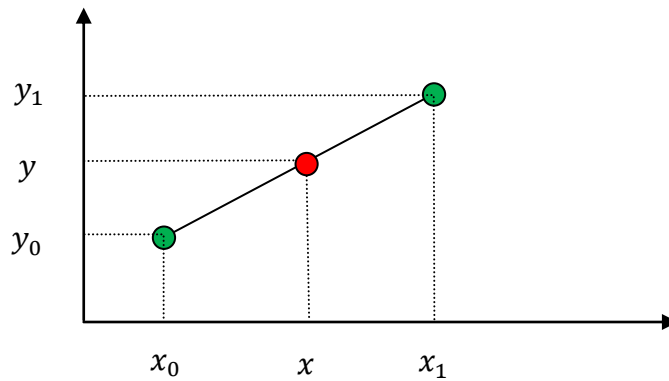


Figure 7.3 - Linear interpolation between the points.

where x_0 and x_1 are the times (positions) of the data collection at the beginning and end of the segment being interpolated and x represents the corresponding time (position) of the desired interpolated value(s) within the interval $[x_0, x_1]$.

7.2.4 Spline interpolation

The term ‘spline’ derives from the flexible drafting tool used by architects to draw piecewise continuous curves [William and E.Thomson, 2001, Greville, 1969, Schumaker, 1993]. Splines have interesting properties such as highly accurate derivative approximation, good convergence and good stability in the presence of round-off errors [William and E.Thomson, 2001]. Splines represent a middle ground between a purely analytical description and numerical finite difference methods which break the domain into the smallest possible intervals. With spline interpolation, we approximate the interpolation function $y(x)$ over the interval $[x_0, x_1]$ by dividing the interval into sub regions with the requirement that there be continuity of the function at the joints. We can define a spline function, $y(x)$, of degree N (with $N=3$ for cubic splines) with values at the joints $x_0 = u_0 \leq u_1 \leq u_2 \dots \dots \leq u_{N-x_1}$ and having the properties:

- (1) In each interval $u_{i-1} \leq x \leq u_i (i = 1, m)$, the function $y(x)$ is a polynomial of degree not greater than N ;
- (2) At each interior point, $y(x)$ and its first $N-1$ derivatives are continuous.

Consider a data series with elements $(x_i, y_i), i = 1, \dots, N$. The first two derivatives $y'(x)$ and $y''(x)$ will be a constant for all x . Here, the prime symbol denotes differentiation with respect to the independent variable x . We write the spline function in the form

$$y(x) = f_i(x); x_i \leq x \leq x_{i+1}, i = 1, \dots, N - 1$$

and specify the following conditions at the junctions of the segments:

- (1) Continuity of the spline function:

$$f_i(x_i) = y(x_i) = y_i, i = 1, 2, \dots, N - 1;$$

$$f_{i-1}(x_i) = y(x_i) = y_i, i = 2, \dots, N;$$

- (2) Continuity of first derivative (slope):

$$f'_{i-1}(x_i) = f'_i(x_i), i = 1, 2, \dots, N - 1;$$

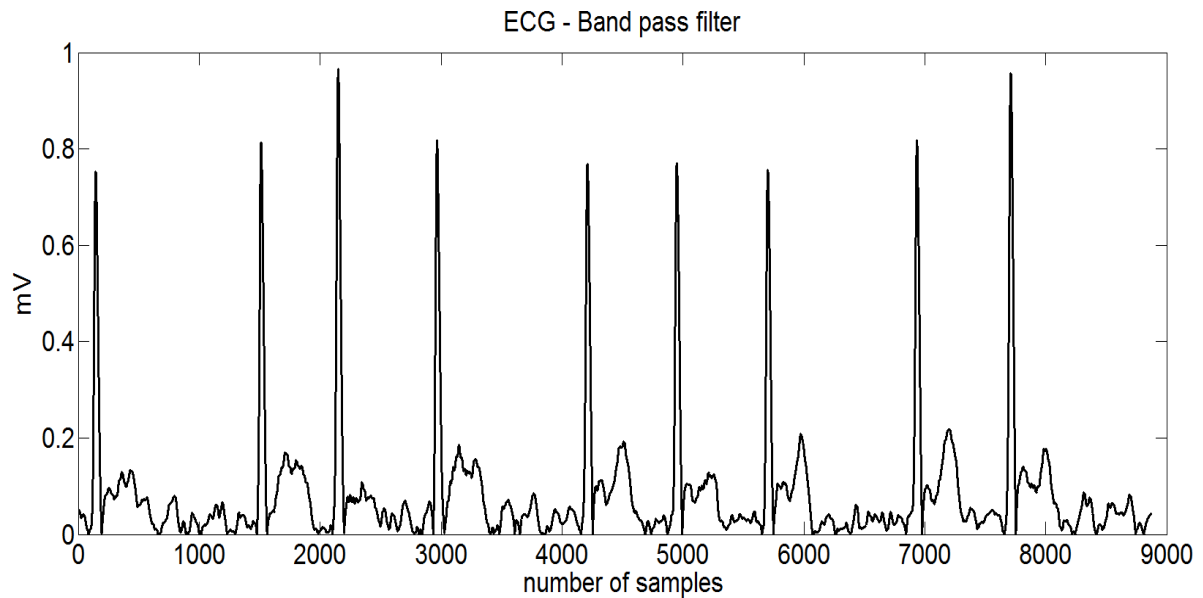
- (3) Continuity of second derivative:

$$f''_{i-1}(x_i) = f''_i(x_i), i = 1, 2, \dots, N - 1;$$

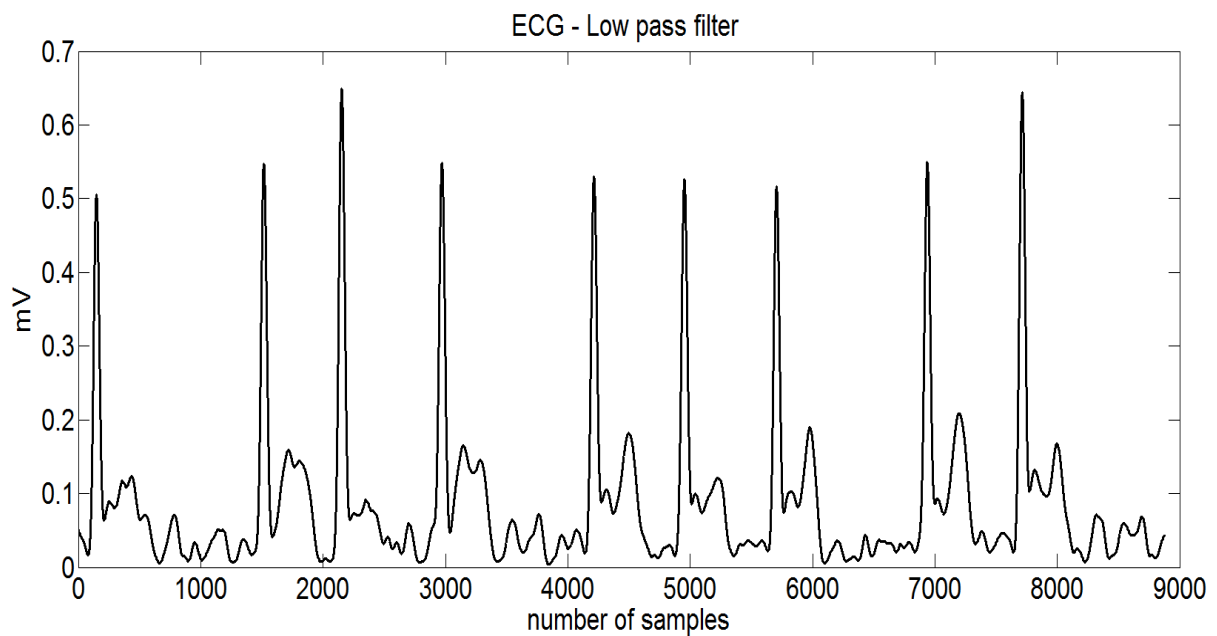
7.3 Results

QRS Detection of intra-cardiac atrial electrograms

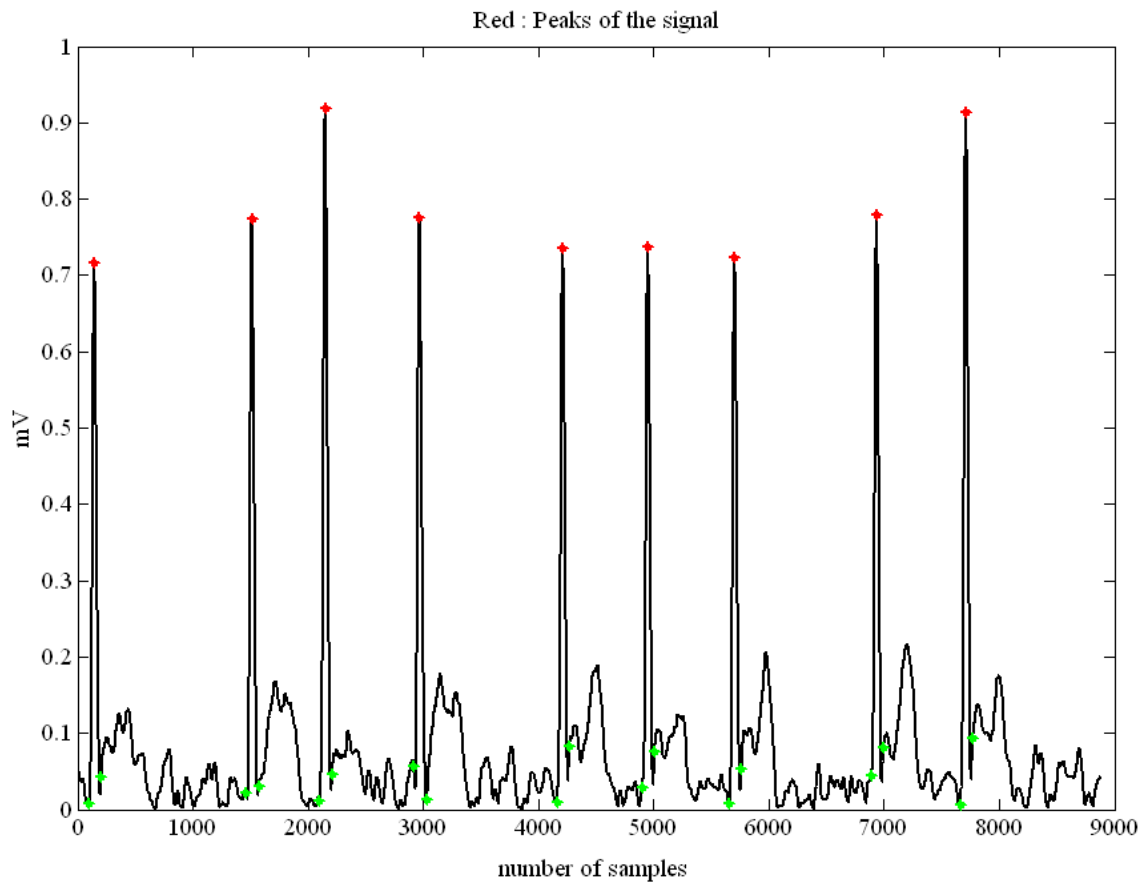
The band pass filter is used to filter the reference signals. This eliminates group delay issues because it uses zero-phase forward and reverse digital filtering. Figure 7.4(a) shows the signal after the band pass filter. The signal after low pass filtering is shown in Figure 7.4(b).



(a)



(b)



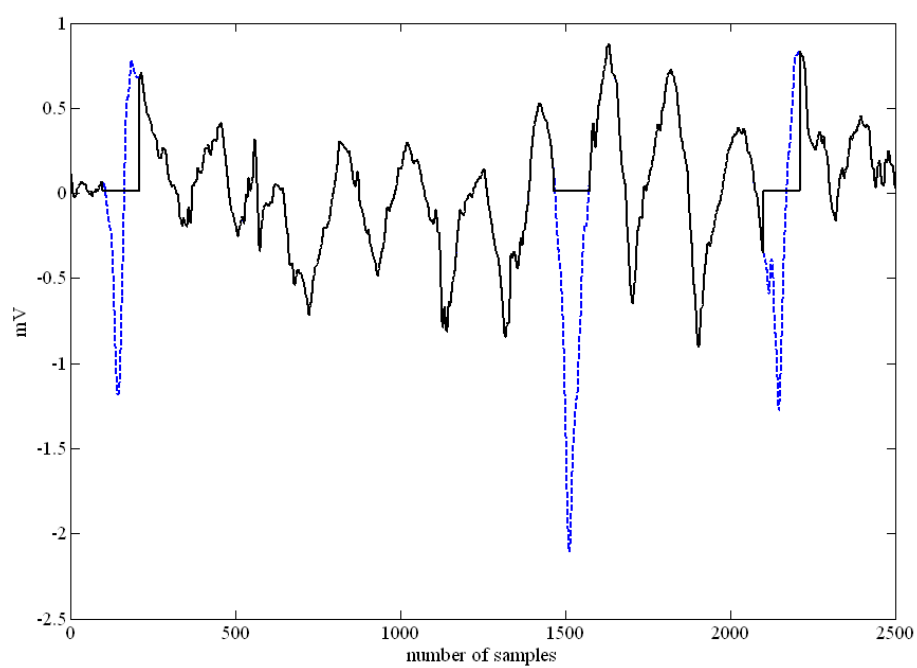
(c)

Figure 7.4 - QRS detection (a) ECG after band pass filter, (b) Low pass filter and (c) Peaks of the signal.

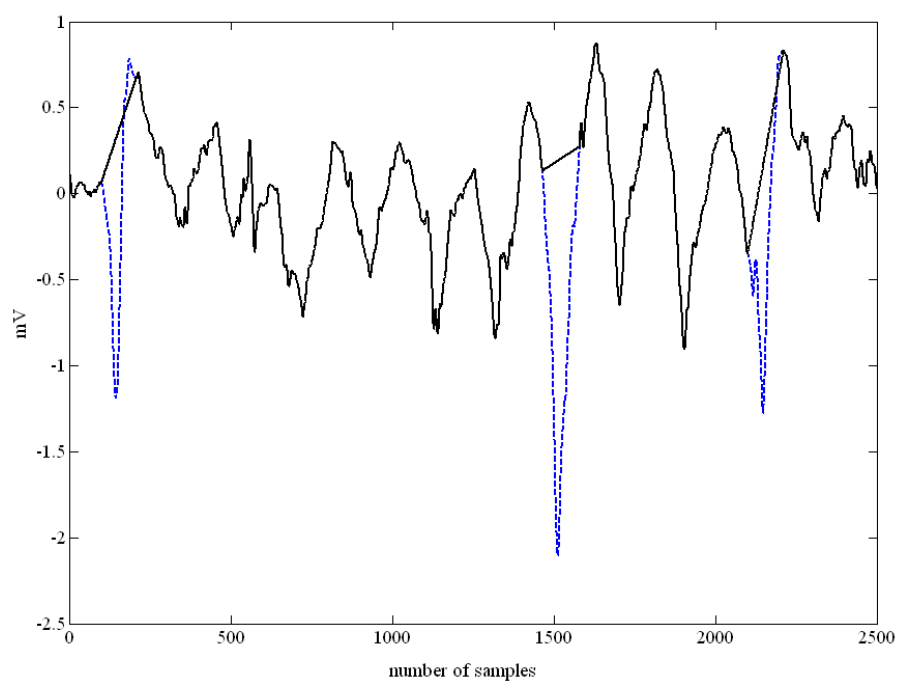
The peaks of the QRS were detected and marked in red. 50 points to the left and 60 points to the right from the peak points are marked in green as shown in Figure 7.4(c).

QRS Subtraction from atrial electrograms

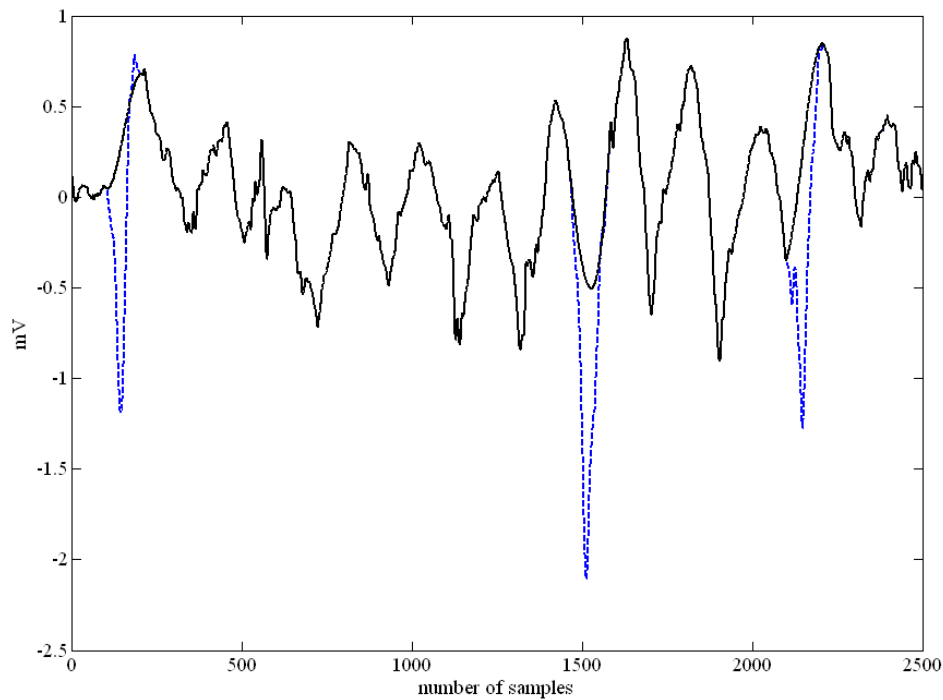
In the 3 different approaches we implemented the 110 subtracted points are replaced by flat interpolation, linear interpolation or cubic spline interpolation as shown in Figure 7.5.



(a)



(b)



(c)

Figure 7.5 - The reference signal with QRS complex (blue dotted line) and atrial electrogram after QRS Subtraction (black line) using (a) flat interpolation (b) linear interpolation and (c) spline interpolation.

The black line represents the atrial electrogram after QRS subtraction (using flat, linear or spline interpolation) while the blue dotted line represents the QRS complex before subtraction was done.

Spectral Analysis

Spectral analysis allows us to investigate the dominant frequencies in a signal, as they are likely to be important to the physical process. Omer [Berenfeld, 2007] and his collaborators investigated the mechanisms that underlie arrhythmias and focussed on the analysis of human AF in the frequency domain. They reviewed the use of the Fourier power spectrum and its DF to study the AF mechanism in patients. In previous papers [Berenfeld *et al.*, 2000,

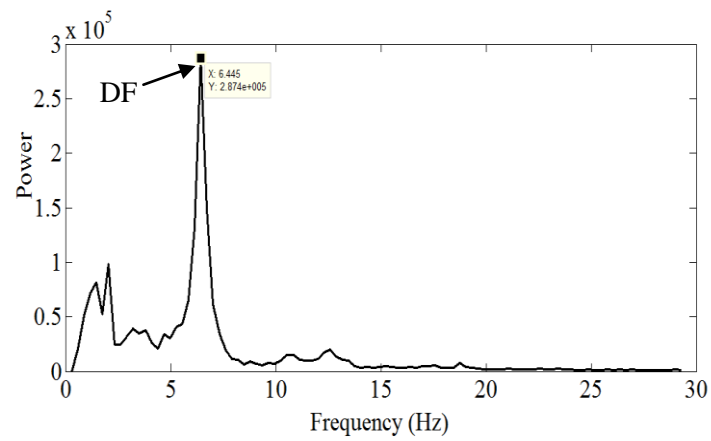
Mandapati *et al.*, 2000], they introduced the method of frequency sampling to identify the spatial distribution of excitation frequencies during AF. Their technique provides accurate localized sites of periodic activity during AF and their results support the hypothesis that stable localized sources are responsible for AF maintenance in the isolated sheep heart.

Dominant Frequency (DF) analysis is a potential tool to analyse atrial rate in AF [Ng and Goldberger, 2007]. The frequency characteristics of different areas of the atria are not the same [Berenfeld *et al.*, 2000], hence DF analysis is used to detect the areas that have rapid activations [Ng and Goldberger, 2007]. DF, defined as the frequency with the highest power between 4 and 10 Hz, was obtained over 7 second-long segments. The DF estimation of atrial electrograms after QRS subtraction was determined after removing the direct current (DC) component to obtain a stationary time series. DC component is the mean value of the signals and it is important to remove it to avoid a strong power at frequency zero in the spectrum. The analysis was performed using FFT with frequency resolution 0.29 Hz and 50% overlap [Steven M.Kay and Marple, 1981, Cooley and Tukey, 1965] . The FFT approach is efficient in terms of computation time [Cooley and Tukey, 1965, Ahmad *et al.*, 2010] and produces reasonable results for a large class of signal processes.

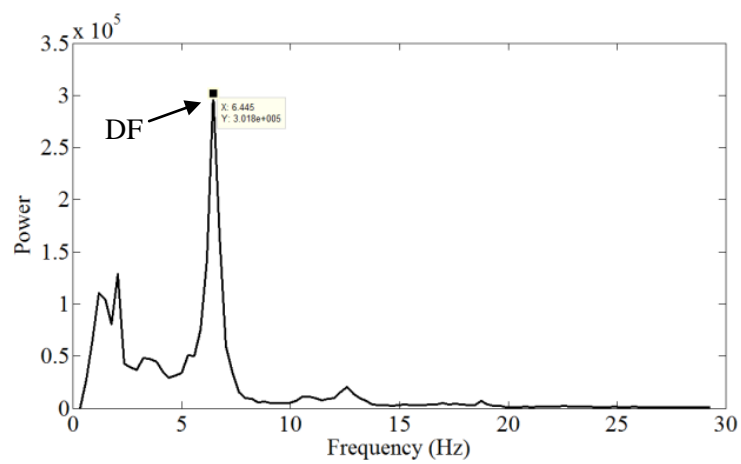
7.4 Discussion

Effect of different QRS Subtraction Approaches on DF

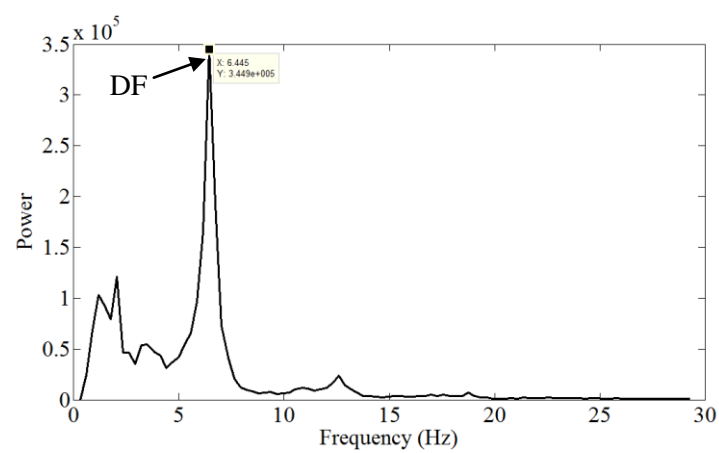
Three different approaches of interpolation were tested to see the effect of the mean spectrum for 2048 electrograms and illustrative results are shown in Figure 7.6 (shown only for the 5th patient here).



(a)



(b)



(c)

Figure 7.6-Mean DF estimation of atrial electrogram using (a) flat interpolation (b) linear interpolation and (c) spline interpolation

In Table 7.1, frequencies were the same value for flat, linear and spline interpolation in each patient except for patient 4. For patient 4, the dominant frequency for flat and linear interpolation is the same but DF for spline is showing a slight reduction. Hence we observed that the method of interpolation made little difference for the determination of the DF of the signals. However, the power amplitude at the DF is different, as shown in Table 7.1.

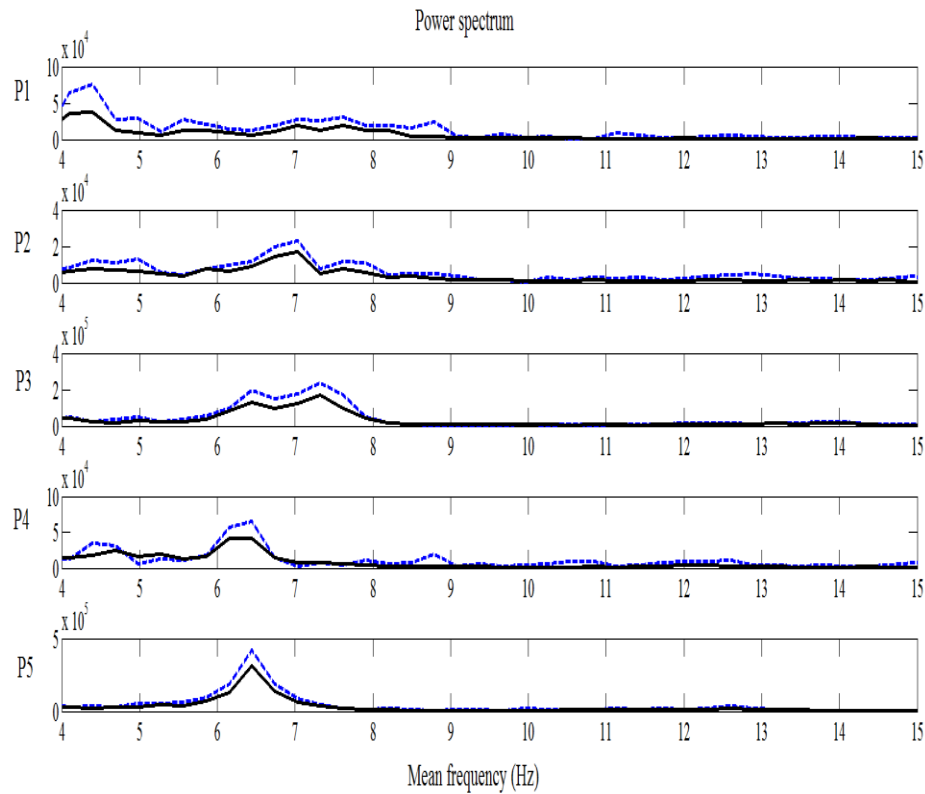
Table 7.1 - DF and power for each interpolation

No	Flat		Linear		Spline	
	Frequency	Power ($\times 10^5$)	Frequency	Power ($\times 10^5$)	Frequency	Power ($\times 10^5$)
1	7.031	16.69	7.031	19.52	7.031	24.12
2	4.395	39.59	4.395	37.49	4.395	52.36
3	7.324	1.639	7.324	1.851	7.324	2.192
4	6.445	44.64	6.445	40.85	6.152	58.56
5	6.445	2.874	6.445	3.018	6.445	4.449

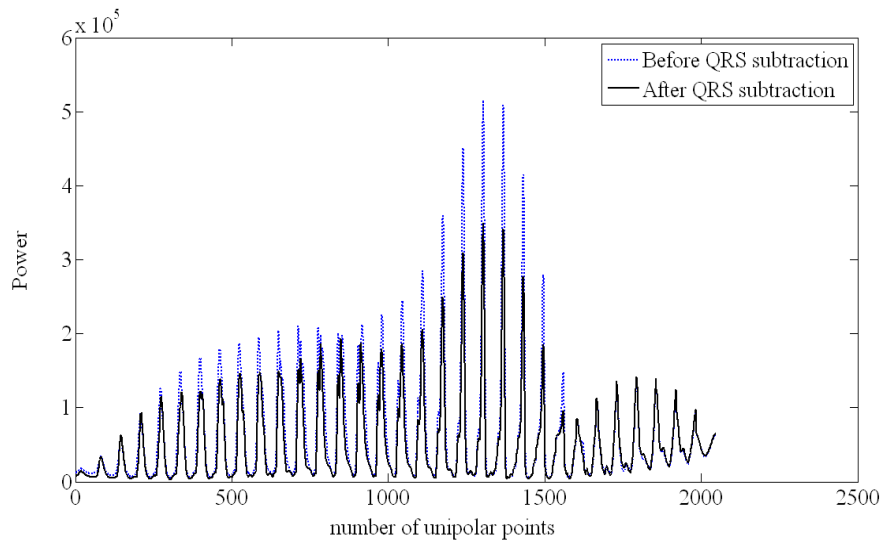
In general, low voltage multiple potential signals between 0.05 mV and 0.25 mV [Wilber, 2008] is the characteristic of CFAEs that will produce low power. This is the reason why low power criteria are considered. The mean power for flat and linear interpolation is lower than for spline interpolation. This is due to the nature of the graph: for flat and linear approaches the end power depends on the slope of the segment of signal to be interpolated. If the signal is on correct a positive slope, the power for linear approach is generally higher than that for flat interpolation while if the signal is on a negative slope the power is lower due to the

reduction of area under the graph. Spline interpolation will normally result in higher power due to the increase of the area under the curve.

Figure 7.7(a) shows the mean frequency for all patients before and after QRS subtraction using flat interpolation. We observed that the power for mean frequency after QRS subtraction is reduced and this is most significant for frequencies above 10 Hz. The reduction of higher frequency power after QRS subtraction shows the effect of cancellation of the QRS influences for the atrial electrograms.



(a)



(b)

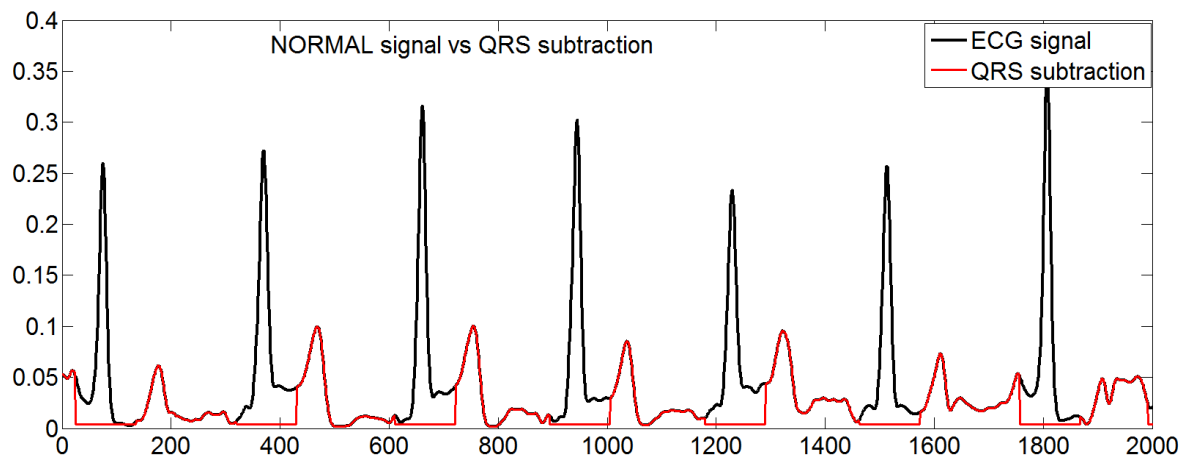
Figure 7.7 - (a) Mean frequency before and after QRS subtraction using flat interpolation (blue dotted line: before subtraction, black line: after subtraction) for patient 1 to patient 5 and (b) Power spectrum, before and after QRS subtraction using flat interpolation.

The analysis for 2048 unipolar atrial electrograms of noncontact mapping shows that the power of the DF s reduced after QRS subtraction. Figure 7.7(b) shows the power spectrum before and after QRS subtraction in one patient. The shape of the figure represents the 3D sweeping of the atrium as explained in the methods section.

In previous studies [Slocum *et al.*, 1985, Stridh and Sörnmo, 2001] , the QRS subtraction was based on the average shape of the QRS signal. In those studies the QRS complex is replaced with some pattern extracted from the signal. In this study we use flat, linear and spline interpolation to replace the QRS complexes. As for QRS detection, the surface ECG is used as a reference while interpolation is done on the atrial electrograms. The advantages of this approach are that i) it is not affected by changes in the shape of the QRS and ii) the dominant frequency values are consistent, irrespective of the choice of the interpolation technique. The disadvantage is that the effect of behaviour of the electrogram during the QRS is lost. The QRS subtraction using three different interpolation techniques only affects the power of the

signals but not the value of DF derived from the electrograms. Finally, mean frequency after QRS subtraction shows low power for frequencies above 10 Hz.

At the beginning of this study, the subtraction includes the QRS complex only (not the T wave). It is argued that T waves might introduce spectral contamination at 3 to 4 Hz and that they should also be removed prior to estimation of DF. To verify this argument, we compared the QRS subtraction with the QRST subtraction approach. We used signals from the surface ECG for normal heart. Using this signal, we can identify the QRS complexes and the T waves clearly. The QRST can be subtracted from the signal accordingly and the comparison of both spectra can be observed. Figure 7.8(a) shows the normal ECG signal versus QRS subtraction while Figure 7.8(b) shows the normal ECG signal versus QRST subtraction using flat interpolation.



(a)

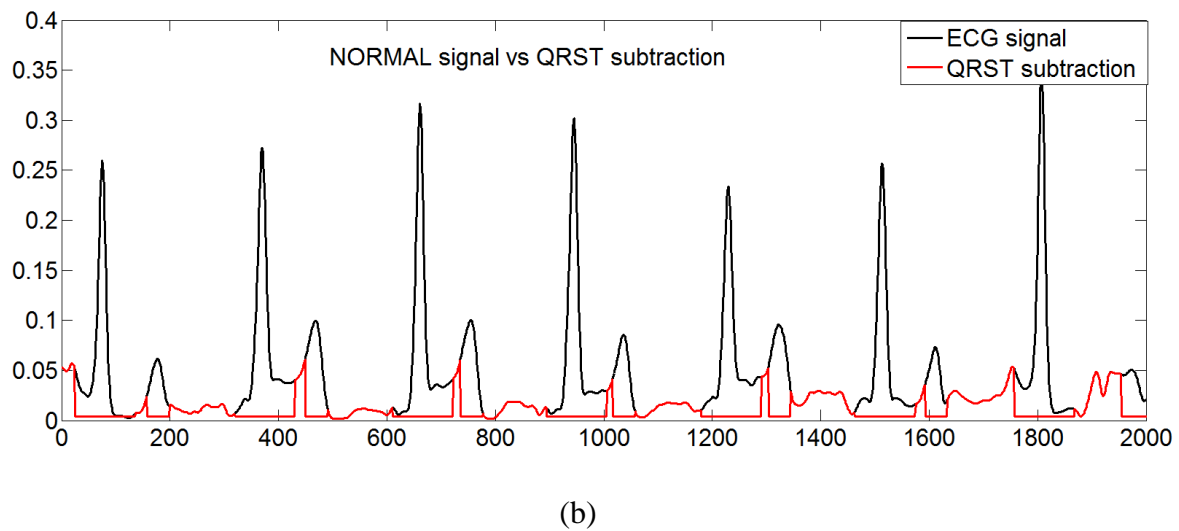


Figure 7.8- (a) Normal ECG versus QRS subtraction signal-(b) Normal ECG versus QRST subtraction signal

The spectrum obtained for QRS and QRST subtraction is shown in Figure 7.9.

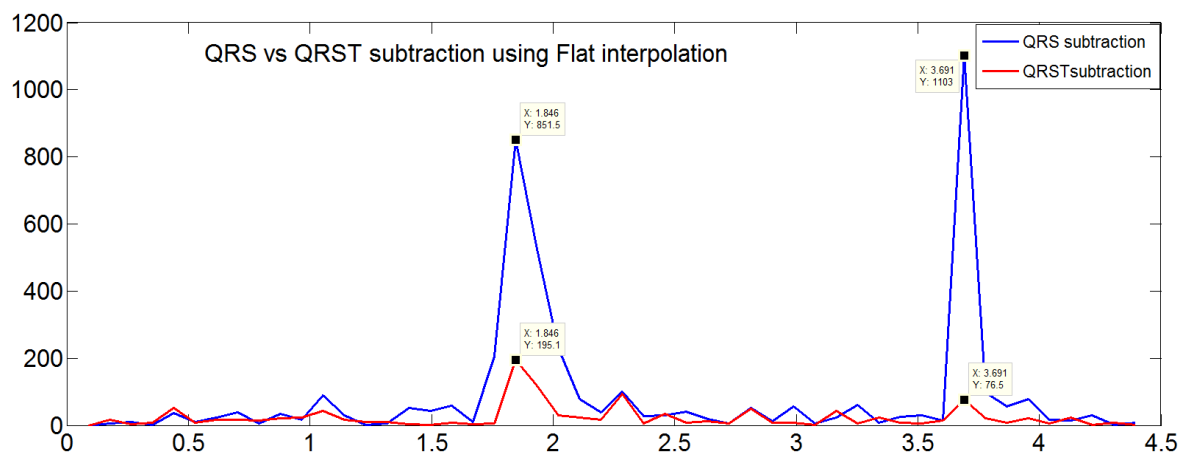
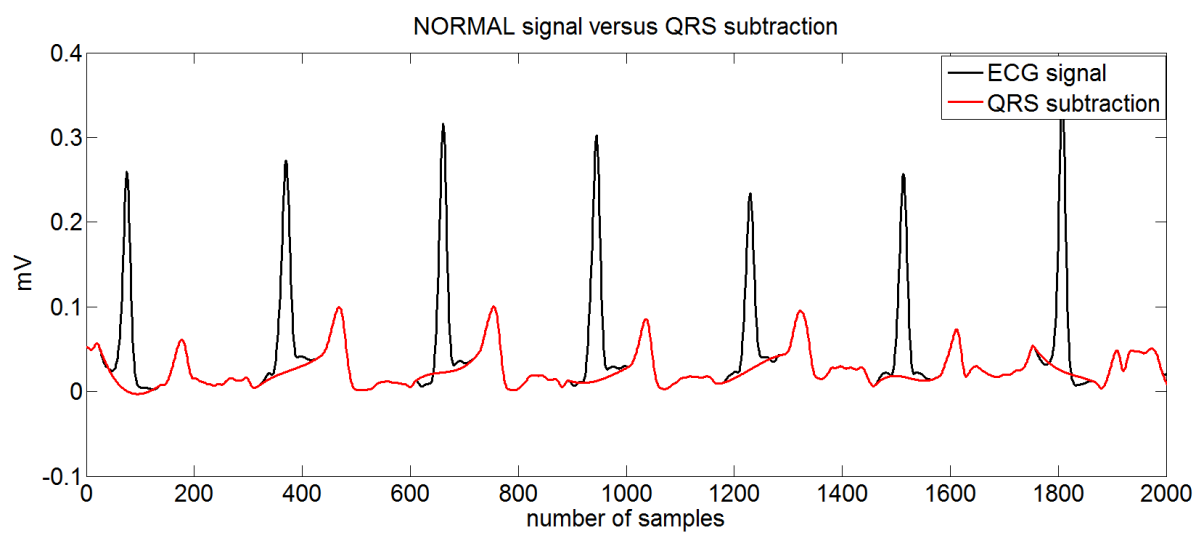


Figure 7.9 – Spectrum : QRS versus QRST subtraction using flat interpolation of surface ECG for normal heart.

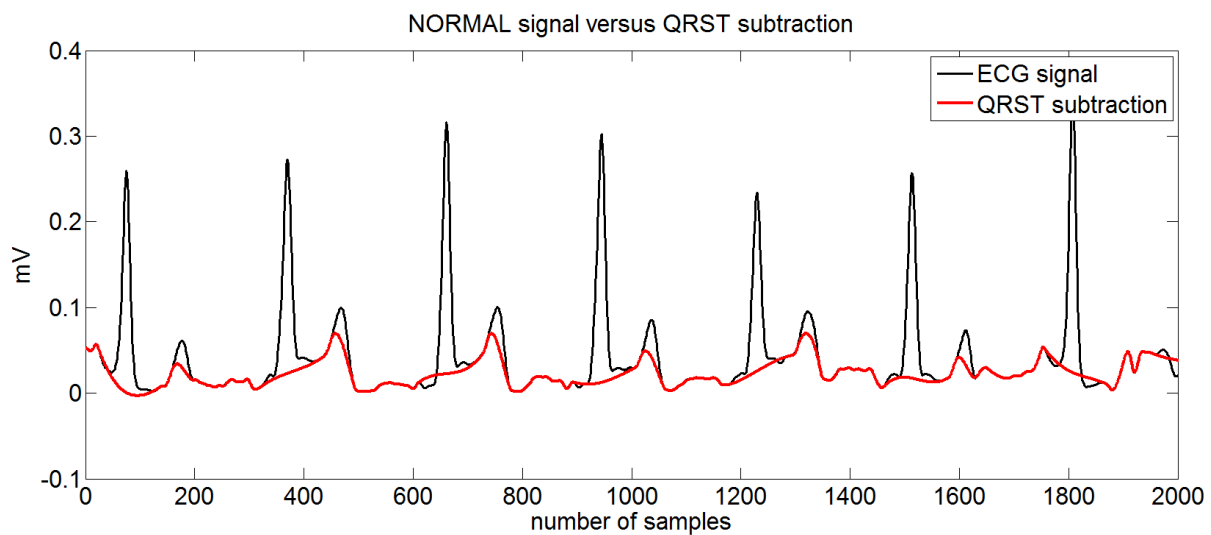
The dominant frequency for normal heart including the QRS and T wave is within 1 to 1.67 Hz (60 to 100 bpm). The dominant frequency shown in Figure 7.9 is the frequency observed after the QRST subtraction (1.8 Hz). Based on this figure the QRS subtraction is pointing at

3.6 Hz instead of 1.8 Hz. On the other hand, the QRST subtraction shows 1.8 Hz as the dominant frequency. The result shows that the T wave is influencing the spectrum.

Spline interpolation is used to compare QRS and QRST subtraction using the surface ECG signal for normal patient. The QRS subtraction is shown in Figure 7.10(a) while the QRST subtraction is shown in Figure 7.10(b).



(a)



(b)

Figure 7.10 – (a) Normal surface ECG signal versus QRS subtraction using spline interpolation and (b) Normal surface ECG signal versus QRST subtraction using spline interpolation

The spectrum for normal surface ECG using spline interpolation is shown in Figure 7.11. Both spectra (QRS and QRST subtraction) have the DF at 3.6 Hz instead of 1.8 Hz. Figure 7.10(b) shows that the T wave is not actually removed when using spline as the tendency of the signal is such that when the spline is introduced it effectively 'reconstructs' the T wave to some extent, hence the frequency band associated to the T wave is not reduced much.

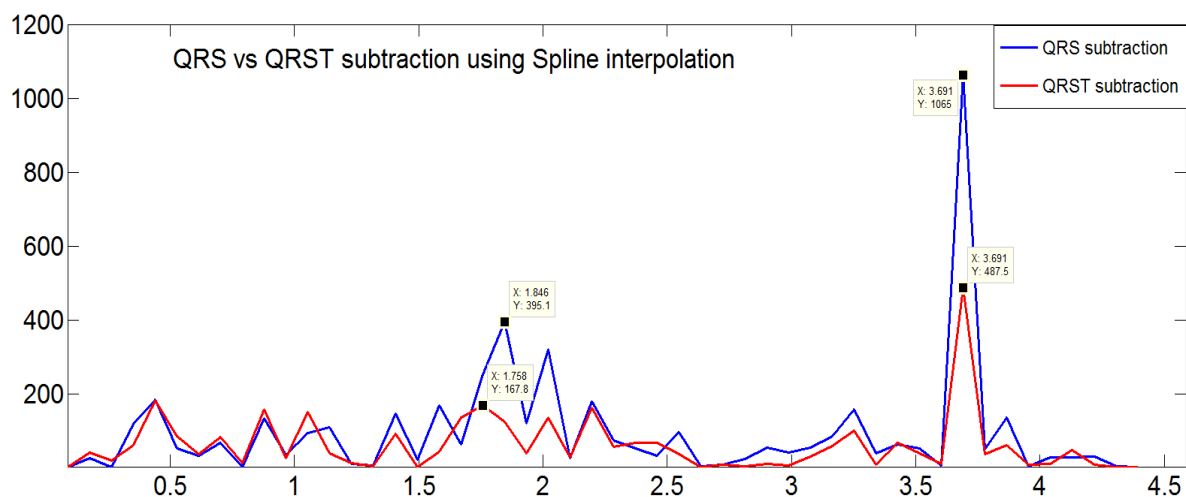


Figure 7.11 - Spectra : QRS versus QRST subtraction using spline interpolation

The QRS and QRST subtraction approach is used to plot the spectrum for surface ECG AF signal using flat interpolation as shown in Figure 7.12. The DF is at 6.15 Hz for both QRS and QRST subtraction. We observed a significant reduction of power at 3 to 4 Hz for the spectrum with QRST subtraction. The results confirmed the argument that T waves might introduce spectral contamination at 3 to 4 Hz.

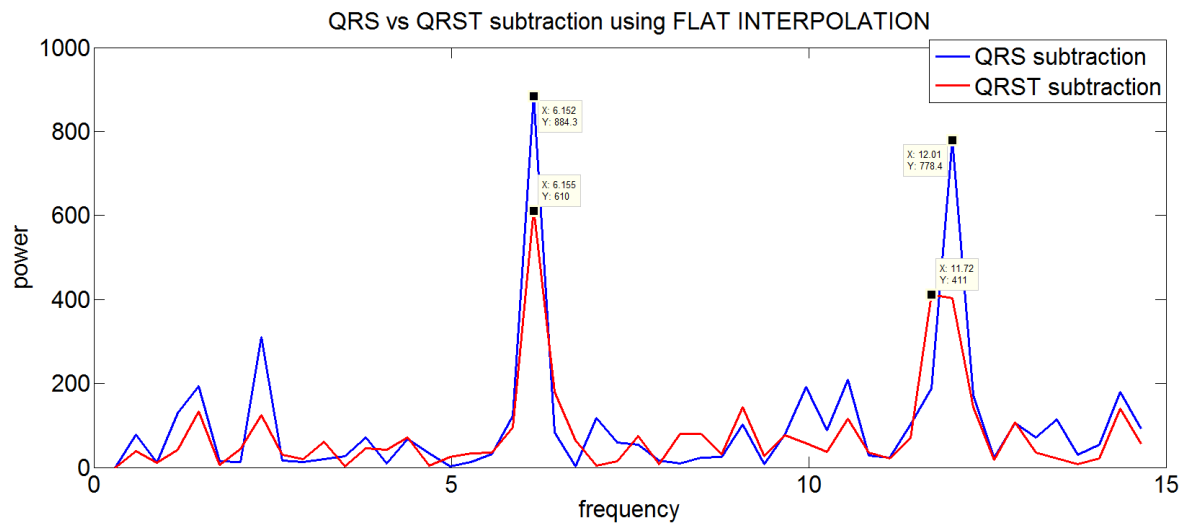


Figure 7.12 - Spectrum from surface ECG of AF signal

Then the QRS and QRST approach are used to plot the spectra for a unipolar atrial electrograms. The spectra are shown in Figure 7.13. The dominant frequency is at 6.58 Hz and no peak at 3 to 4 Hz was observed for both spectra.

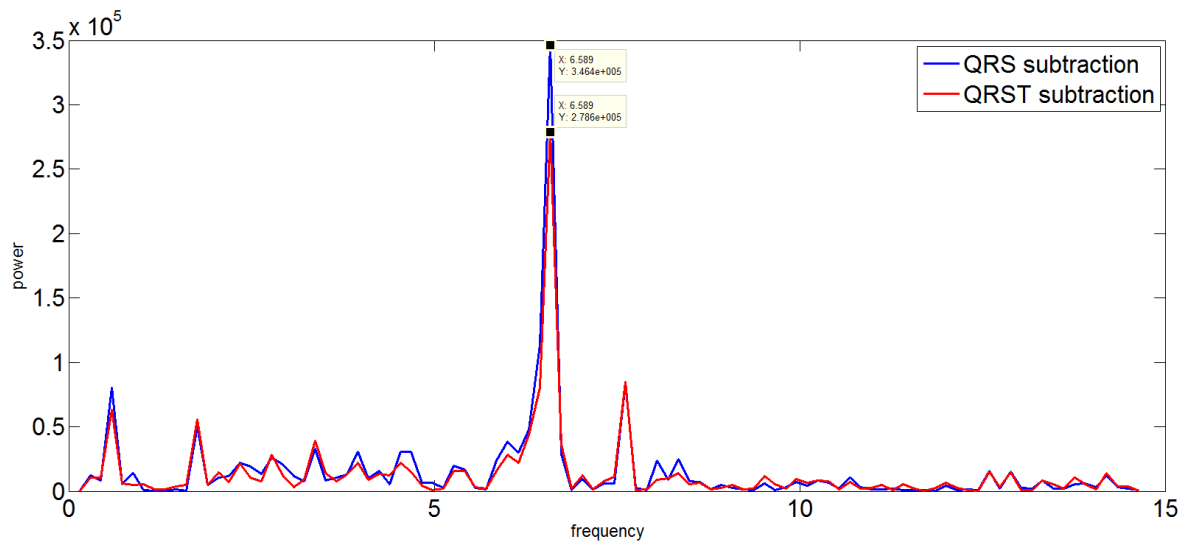


Figure 7.13 – Spectrum for unipolar atrial electrogram

7.5 Conclusions

As a conclusion, QRS subtraction can be used to estimate the dominant frequency. But, there is a residual power at 3 to 4 Hz which is contributed by the T wave, as shown in Figure 7.12. QRST subtraction significantly reduces power at 3 to 4 Hz and works best with flat interpolation compared to spline interpolation. Spline interpolation has, at times, the tendency to reconstitute a wave similar to the T wave when the onset of the T wave is wrongly determined allowing an initial ‘foot’ of the T wave to go through. Figures 7.12 and 7.13 show the spectrum for surface ECG AF signal (DF = 6.15 Hz) and atrial electrogram (DF = 6.58 Hz) respectively. Both frequencies are within AF frequency range.

The results of this chapter will be used in chapter 8.

8 NON CONTACT MAPPING OF ATRIAL FIBRILLATION

8.1 Introduction

Non contact mapping as described in Chapter 3 is an effective method to map and guide radiofrequency catheter ablation. Schilling *et al.* reported for the first human studies using non contact mapping can detect far field endocardial potential from within the cardiac chamber [Schilling *et al.*, 1998]. The accuracy of this technique depends on the distance between the centre of the multi electrode array (MEA) and the endocardium. There is no significant difference in timing between contact catheter and reconstructed electrograms for distance less than 34 mm from the MEA centre but it becomes significant for distances above 34 mm.

8.2 Validation of non contact mapping

In this study, 3 dimensional mapping of 2048 unipolar electrograms were reconstructed using Matlab (MathWorks Inc., USA) [Salinet Jr *et al.*, 2010]. The data files we use have x,y,z coordinates for each 2048 unipolar electrograms (Figure 8.1).

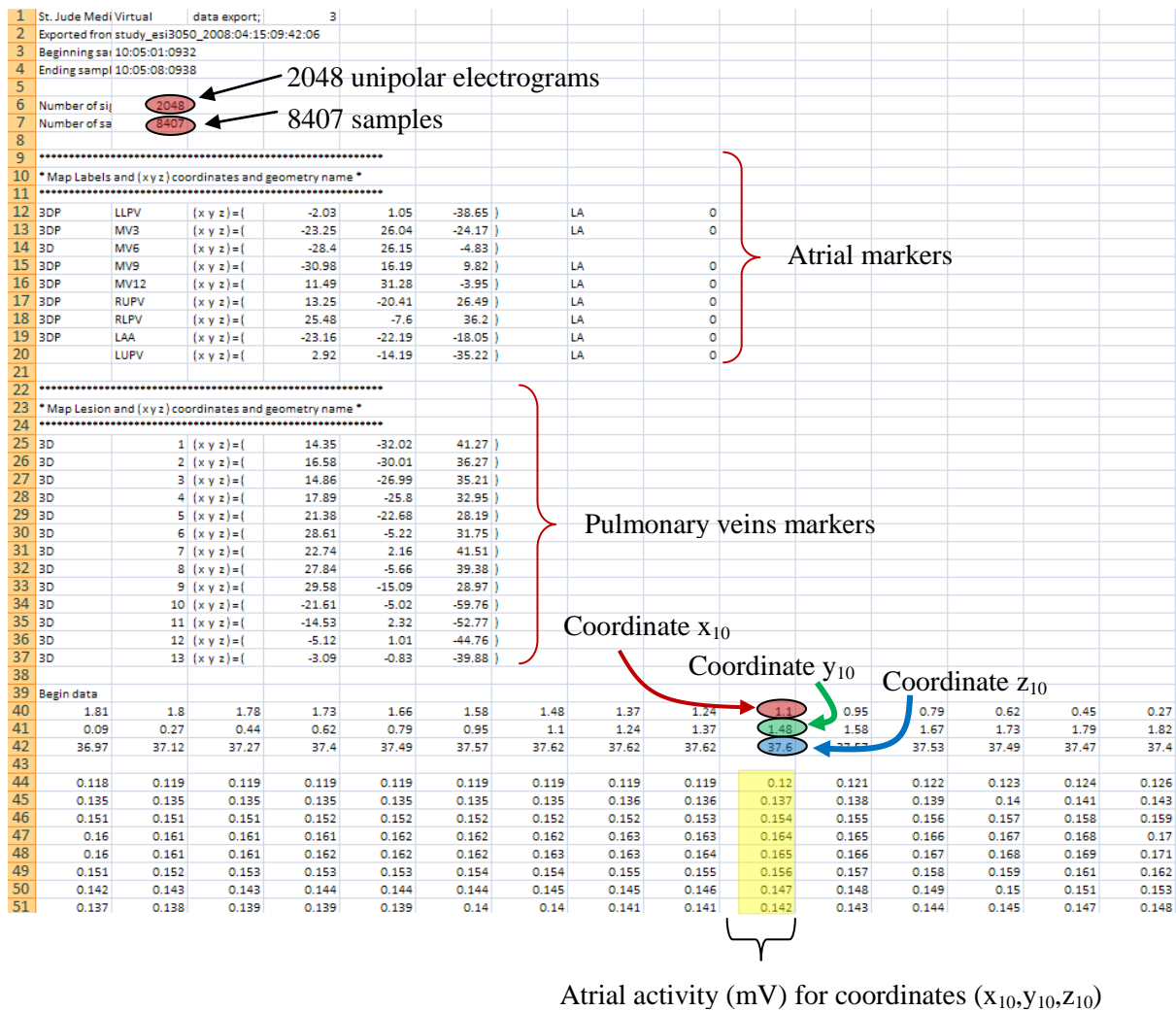


Figure 8.1 - The description of the exported file with the electrograms used in this research.

The 3D geometry was obtained after reshaping the 2048 points to [64 x 32] dimension. As in geography, there are 32 latitudes (parallel lines) and 64 longitudes (meridian lines). In Matlab the function $surface(x,y,z,c)$ is used to paint the surface of the geometry created. The variables x , y and z are the coordinates and the variable c represents a specified colour. The surface colour c can be frequency, power or any other property we are willing to display. The validation of the mapping is similar with reconstructed mapping using EnSite 3000 System. Figure 8.2 shows the comparison of reconstruction for 2048 unipolar electrograms using EnSite 3000 and Matlab.

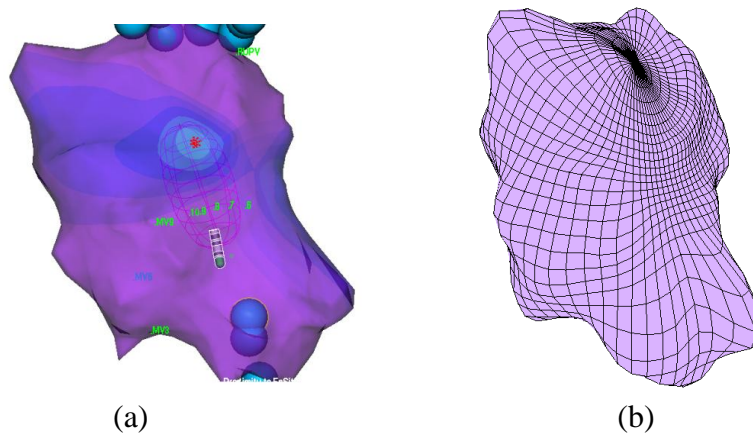


Figure 8.2 - The reconstruction of 3 Dimensional mapping for 2048 points using (a) EnSite 3000 and (b) our representation in MATLAB (the colours have different meanings)

The MATLAB reconstruction of 2048 unipolar electrograms gives a good resolution (Figure 8.2) compared to maps with fewer points such as 256 unipolar electrograms (Figure 8.3).

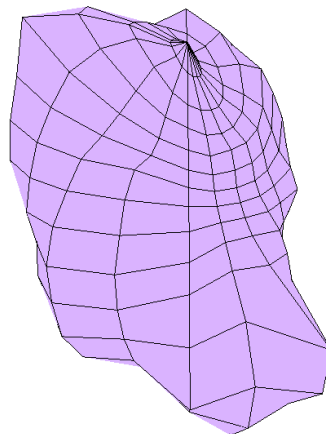


Figure 8.3 - The reconstruction of 3 Dimensional mapping for 256 points using MATLAB.

8.3 Three Dimensional (3D) DF geometry

The signals are obtained from 20-second long segments, sampled at 1200 Hz for 2048 non-contact unipolar electrograms. The determination of DF was calculated using 4-second long

windows (spectral resolution of 0.25 Hz) for each unipolar electrogram. Figure 8.4 represents the 3D map that shows the DF before QRST subtraction within 4 to 12 Hz.

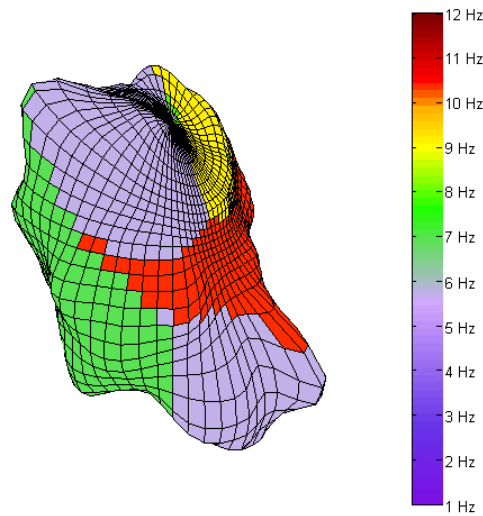


Figure 8.4 - 3D DF mapping.

3D videos of DF maps were produced in AVI format. There are several properties that could be used to perform the movies setting such as quality of the movies, number of frames per second and compression. The 3D DF maps also can be rotated under MATLAB to see the area of interest.

8.4 Adaptive power threshold for dominant frequency estimation in atrial fibrillation

In persistent AF, the current theory is that multiple, random wavelets of activation coexist to create a chaotic cardiac rhythm [Moe *et al.*, 1959] and therapy is challenging [Haissaguerre *et al.*, 2000, Benussi *et al.*, 2000, Oral *et al.*, 2006]. Current guidelines highlight the importance of assessing a number of clinical parameters including patient and arrhythmia characteristics in order to make correct decisions on treatment [Fuster *et al.*, 2006].

Dominant frequency (DF) analysis can be used to identify areas of importance from intracardiac electrograms recorded during AF [Gojraty *et al.*, 2009]. Recent research shows that ablation at sites with DF resulted in a significant prolongation of AF cycle length compared to ablation of sites with non-dominant frequencies [Sanders *et al.*, 2005]. These findings support the use of DF mapping to identify suitable ablation targets to improve outcome, particularly in patients with persistent AF. In this case, it is necessary to perform additional ablation as well as the standard electrical isolation of the pulmonary veins. The main objective in this study is to verify the result of the application of an adaptive power threshold on the estimation of dominant frequency as a means to reduce the number of potential candidates for additional ablation after pulmonary veins isolation (PVI) to those which are more significant in terms of power. The dominant frequency sites can be ‘pruned’ by the use of the regularity index and multiple levels of adaptive power threshold approach. QRS complexes are subtracted from the electrograms (as explained in chapter 7) prior to the determination of DFs to eliminate ventricular interference.

8.4.1 Methods

8.4.1.1 Study design

There was approval from the Local Ethics Committee for mapping and ablation studies for patients undergoing AF ablation which include blood sampling and collection of electrical data during the procedures. Data collected for this study relate to patients who had given written consent. The drugs isoprenaline and atropine were administered to the patients at the discretion of the clinicians during the procedures according to clinical protocol.

Atrial electrograms were recorded in four patients with persistent AF for four different protocols: baseline, after drug infusion (isoprenaline and atropine) and post ablation. The analysis was performed on 2048 non-contact unipolar electrograms sampled at 1200 Hz. The patients underwent catheter ablation guided by contact mapping using EnSite, NavX 6.0 (St. Jude Medical) during electro-physiological procedures of AF. The spectral analysis for these signals is done over 16 s long continuous segments using a 1024-point FFT. We remove the DC component by software before computing the Fourier transform of the signal.

8.4.1.2 Identification of DF

Current studies show that electrical ‘noise’ from ventricular depolarization affects DFs significantly. Ventricular depolarization in non-contact unipolar atrial electrograms was recorded at a number of sites within the atrium including near the annulus, coronary sinus, appendage, and pulmonary veins [Ng and Goldberger, 2007]. We aimed to evaluate the effects of cancellation on unipolar signals with minimal far field ventricular depolarization. In this analysis, the algorithm detected ventricular activations from the QRS complexes of a surface ECG lead. QRS detection was performed using a technique based on that of Thakor [Thakor *et al.*, 1984] with a band pass filter from 8 to 20 Hz, rectification and a 6 Hz low pass filter of the absolute values of the band passed ECG. The QRS complexes were detected and their influence was removed from the atrial electrograms by replacing the segment of signals subtracted using the amplitude of the baseline as described in chapter 7.

The DF was obtained by determining the frequency with the highest spectral power in the physiological frequency range of interest in atrial fibrillation (between 4 and 12 Hz)

[Berenfeld *et al.*, 2000, Skanes *et al.*, 1998]. The dominant frequency and its respective power were obtained for the 16 seconds of electrogram signals of data from all patients.

8.4.2 Pruning DF with Regularity Index (RI)

To ensure reliability in DF detection, we calculated the RI [Skanes *et al.*, 1998, Kalifa *et al.*, 2006] defined as the ratio of the power at the DF and its adjacent frequencies (2-Hz band) in the 1 to 30 Hz band. Only points with RI of more than 0.2 were included in subsequent analysis to control for ambiguity in DF detection related to poor signal-to-noise ratio.

8.4.3 Pruning DF with Adaptive Power Threshold (APT)

In this study, a calculation of adaptive threshold was based on the amplitude of the spectrum (power) of the DFs. The reference power refers to the baseline of power distribution. An adaptive power for the spectrum was calculated by 10 levels of the sorted (min to max) power data population. The power threshold for each spectrum was identified and the multiple thresholds were based on 10%, 20%, 30%, 40%, 50%, 60%, 70%, 80%, 90% and 100% of the maximum data power population. The power threshold set at 20% from maximum data power population is shown in Figure 8.5. The selection of the threshold is dependent on the desired clinical point of view. If the electrophysiologist would like to see the DF with high power, he/she can select a high threshold value but if he/she wants to see the DF with low power, threshold with low value can be selected. The latter have a similar concept to complex fractionated atrial electrograms (CFAEs) that concentrates in low voltage activity [Nademanee *et al.*, 2004]. The DF within physiological range for each threshold was identified for 2048 points over 16 seconds.

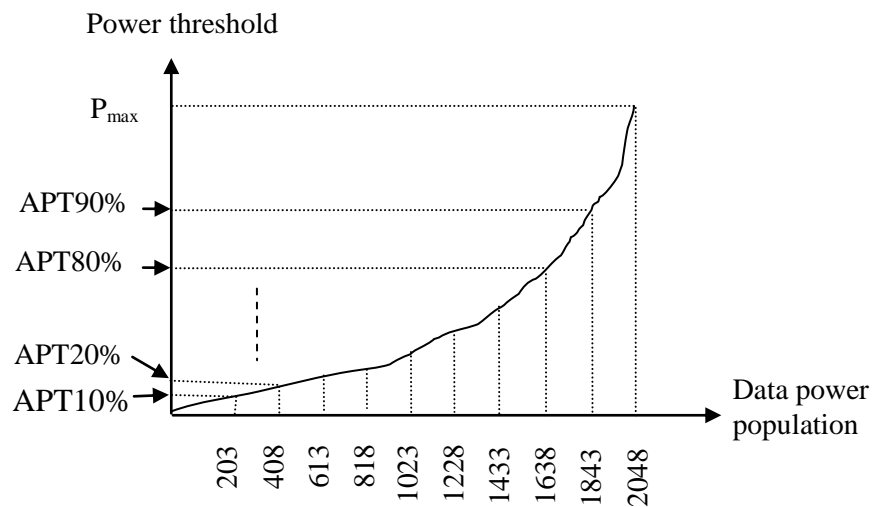


Figure 8.5 - Multiple power thresholds.

8.4.4 Calculating DF Occurrence

In the current study, the calculation of DF occurrence is based on the number of physiological DF occurrence (4 to 12 Hz) counted in 16 seconds recorded data. First, the DF was calculated for one segment consisting of 1024 samples for 2048 unipolar electrograms. The next 1024 samples are used to obtain the second set of DFs and this runs until the end of the data. Thus, in 16 seconds recording, we have 18 spectra (we use 1024 segments sampled at 1200 Hz). Each DF is counted as one occurrence. Then, the total numbers of occurrences for each 2048 unipolar electrograms are obtained over the 18 spectra (Figure 8.6). A 3D map for DF occurrence is plotted.

8.5 Results

The frequencies and power for 2048 points were plotted for each spectrum (using 1024 samples). Figure 8.7 (a) shows the 3D DF maps and Figure 8.7 (b) showing their respective power in 3D for all points for one 16 s long recording.

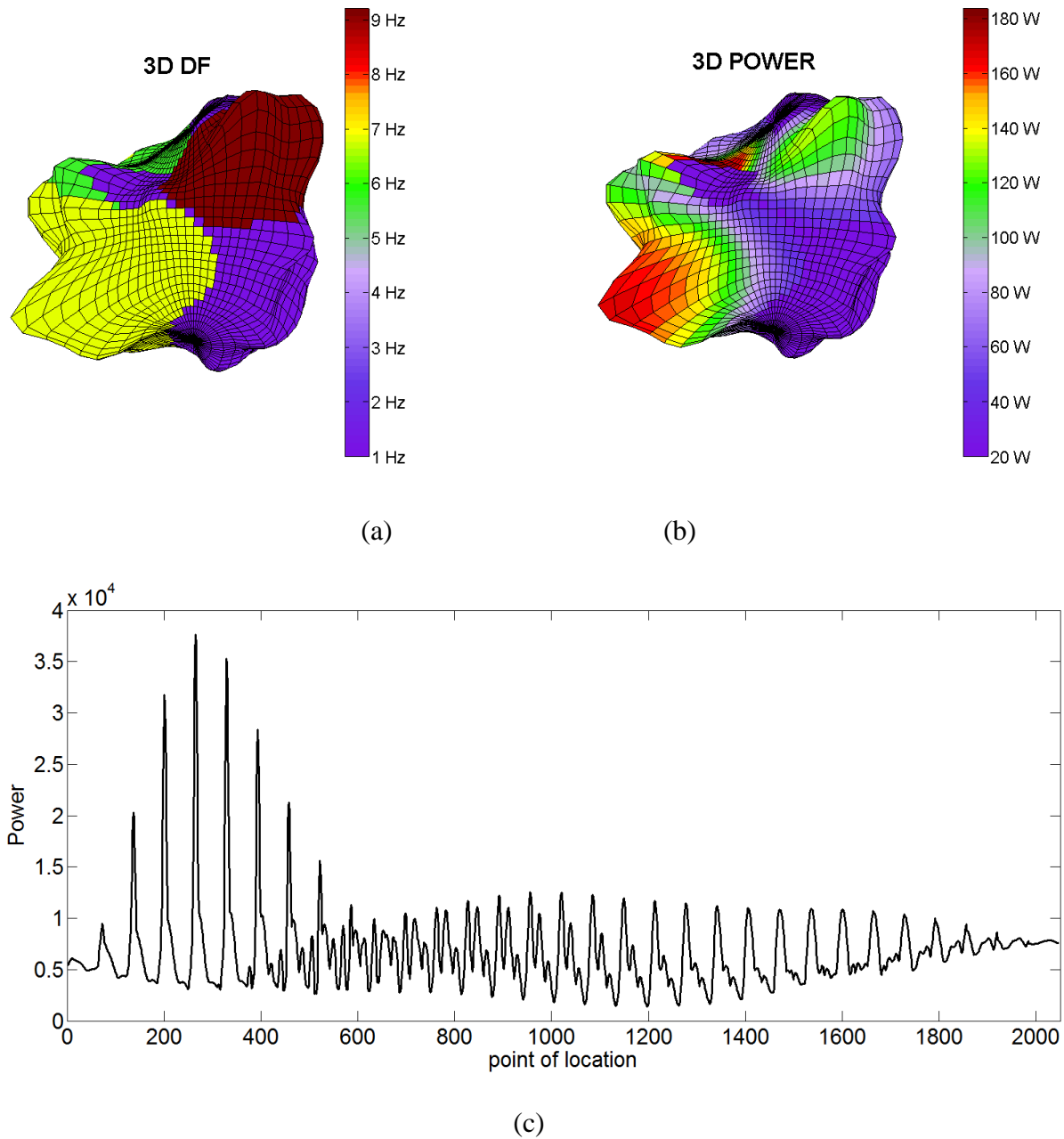
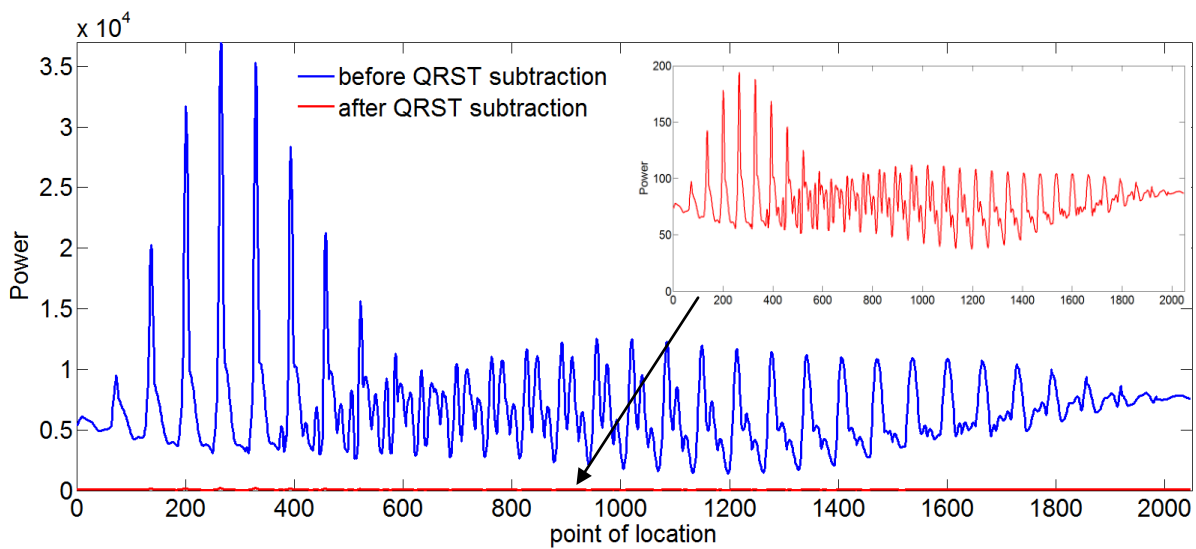


Figure 8.7 - DF and power distribution.

Data in Figure 8.7(c) represents the power distribution for 2048 points (the 3D power maps is shown in Figure 8.7(b)). The shape of the figure representing power can be understood better if we mention that the sweeping of the 3D representation of the atrium is a spiral along the 32 ‘parallels’ from pole to pole stepping down to the next parallel after one full turn across the ‘meridians’ (and there are 64 ‘meridians’).

Spectral analysis and frequency mapping identify localized sites of high-frequency activity and low power during AF in humans with different distributions in persistent AF. DF power is reduced after QRST subtraction as shown in Figure 8.8(a). Figure 8.8(b) and 8.8(c) shows the 3D DF maps before and after QRST subtraction. The DF area after QRST subtraction is significantly smaller than that without QRST subtraction.



(a)

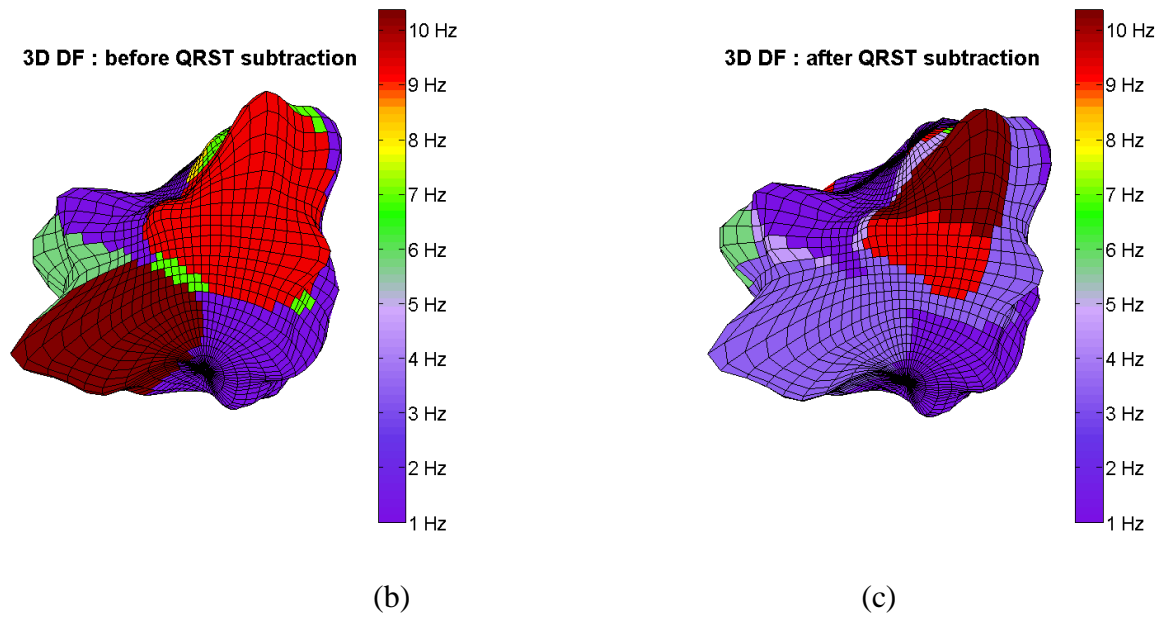


Figure 8.8 - (a) power differences between before (red line) and after (blue line) QRS subtraction, (b) 3D DF before QRST subtraction, and (c) 3D DF after QRST Subtraction with the evident reduction of the area of interest.

Average DF maps before and after QRST subtraction were calculated. A reducing trend of DF power is observed in Figure 8.9, especially at frequencies above around 10 Hz.

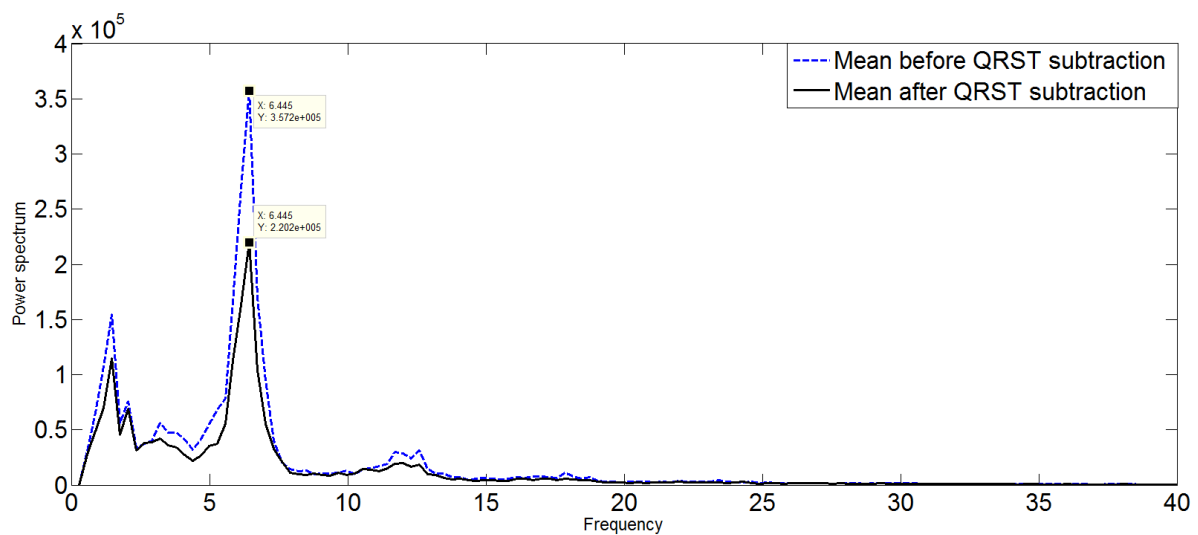


Figure 8.9 - Mean frequency before and after QRST Subtraction

Data in Figure 8.10 show the number of the occurrence DFs cur for baseline in DF-RI and DF-APT with 20% of the maximum data power (DF-APT20%). The average frequency of DF-RI and DF-APT20% are respectively 6.37 Hz and 6.39 Hz. The majority of the maximum power occurs for frequencies that are less than 4 Hz and those are not represented here.

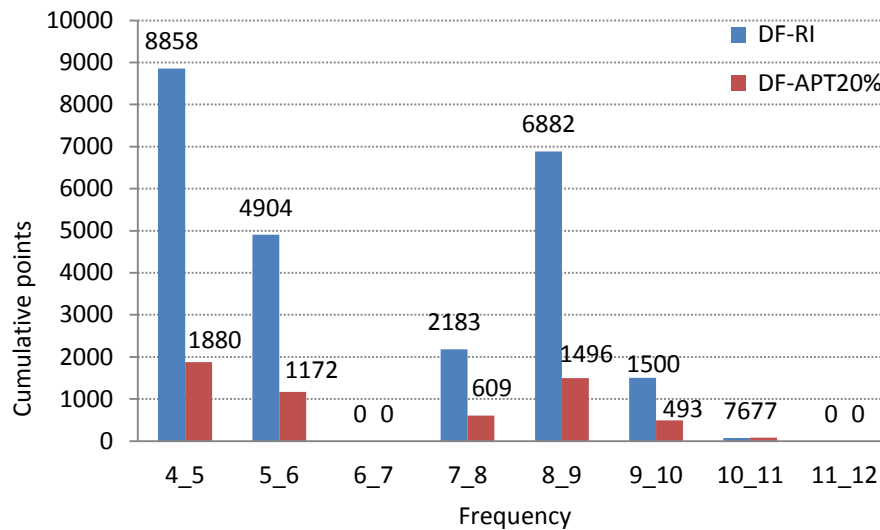


Figure 8.10 - Distribution of DF for Baseline.

Figure 8.11 shows the number of DF for Post ablation in DF-RI and DF-APT20%. The average frequency of DF-RI drifted to 6.01 Hz and 5.86 Hz for DF-APT20%. Again, if the maximum power is for frequencies below 4 Hz, these are not represented here.

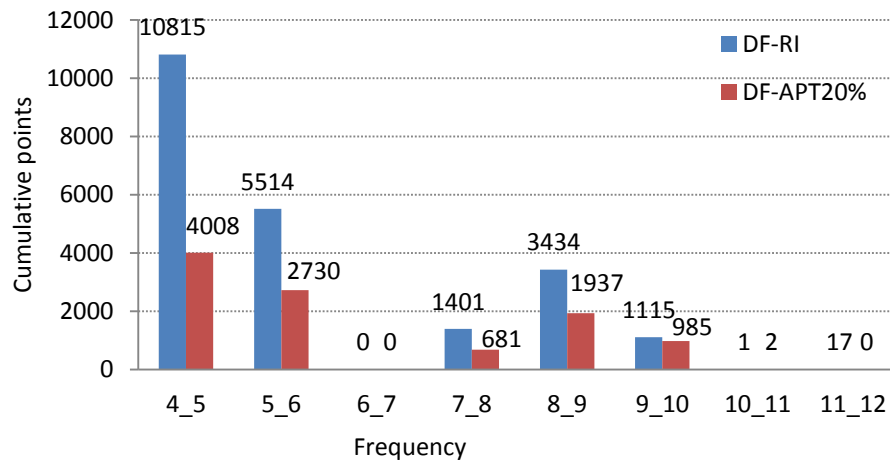


Figure 8.11 - Distribution of DF for Post Ablation with APT20%.

We observe that the average of DF for RI and APT20% at post ablation decreases compared to baseline (as shown in Table 8.1)

Table 8.1 - Average DF for DF-RI and DF-APT20%

Condition	Baseline	Post ablation	Difference
Average DFRI	6.37	6.01	0.36
Average DFAPT20%	6.39	5.86	0.53

Figure 8.12 shows the number of DF points with RI and APT20% for baseline. The number of DF points using APT20% is significantly lower compared to RI.

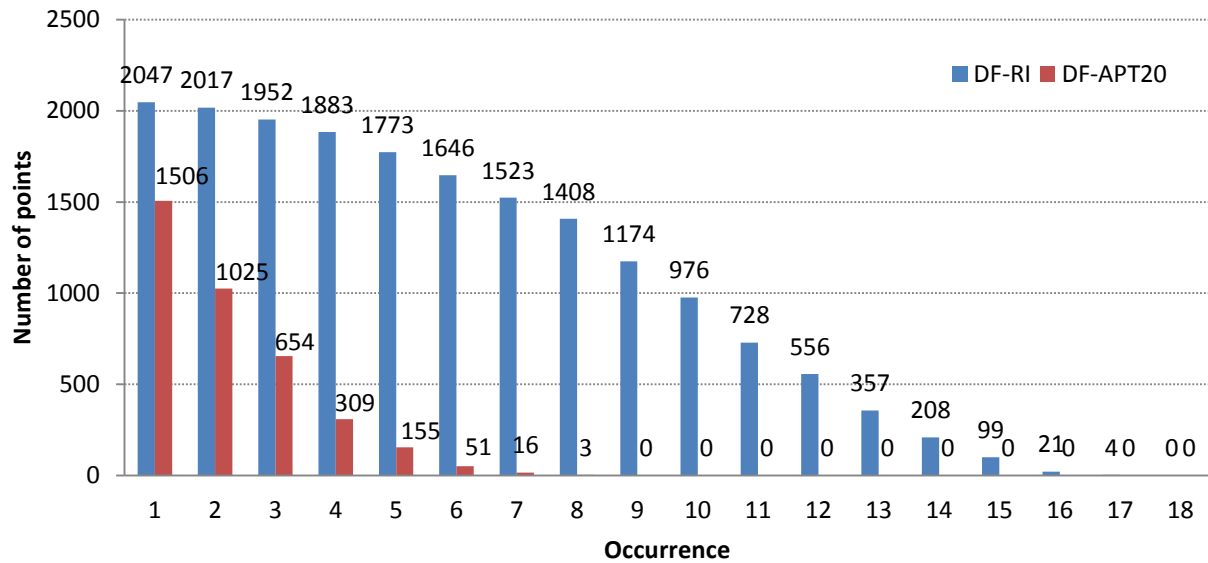


Figure 8.12 - Number of DF points versus occurrence using RI and APT20% for baseline.

8.6 Discussion

The number of DF occurrences using threshold pruning approach decreases if we decrease the threshold from the maximum data power population. Figure 8.14 shows the comparison of 3D DF maps for four patients at baseline which represent the DF occurrences using DFRI, DFAPT10% and DFAPT20% over 16 seconds. The DF maps area varies from patient to patient. It shows that DF mapping with the threshold setting reduces the DF area significantly while still highlighting the centre of the area highlighted by DF-RI analysis.

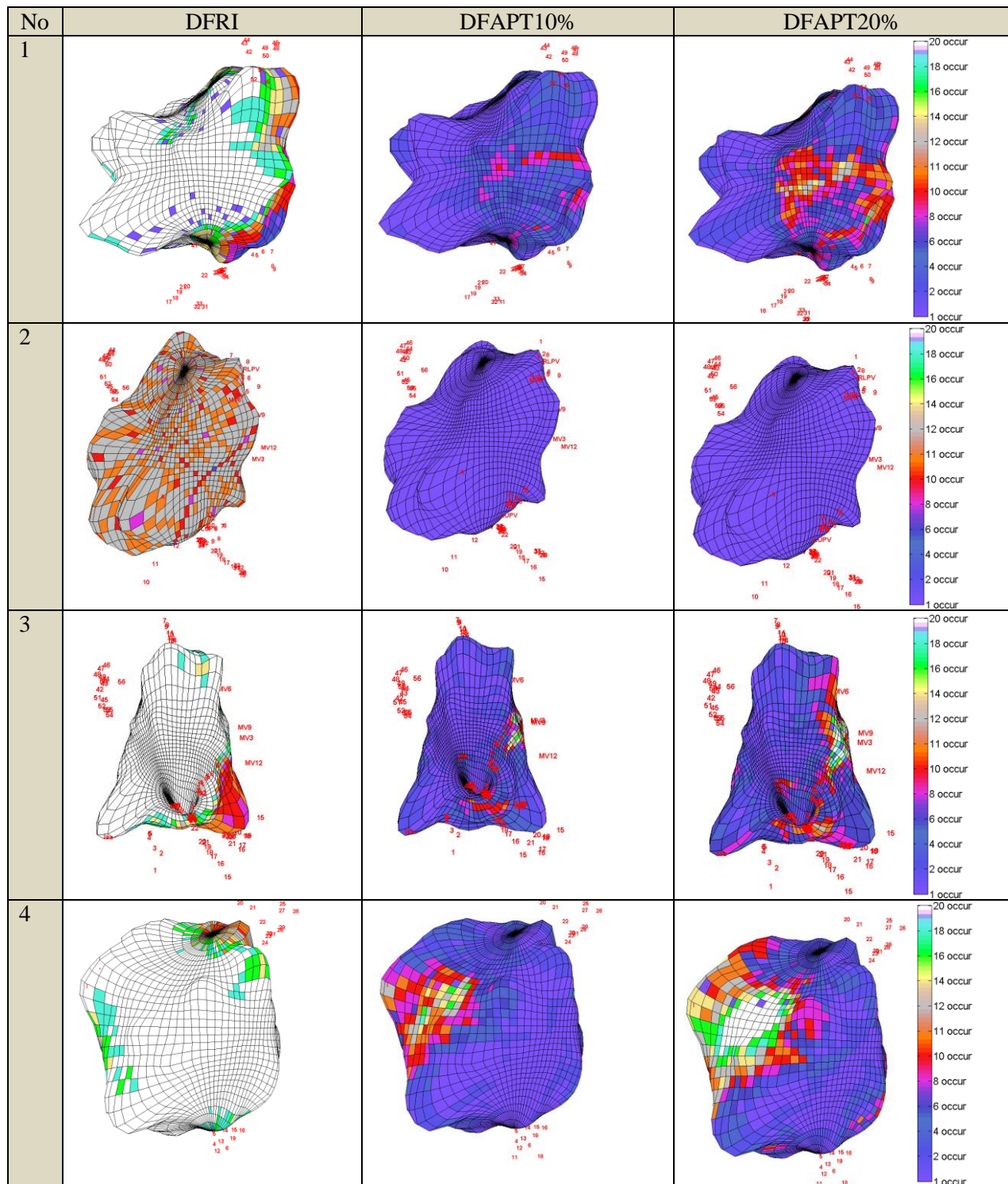


Figure 8.13 - Comparison of DF occurrence over 16 seconds between DFRI, DFAPT10% and DFAPT20%.

Patient 1:

At baseline, DFRI shows scattered distribution of DF occurrence while DFAPT10% shows concentrated occurrence area. DFAPT10% show similar reduction of occurrence area while concentrated DF occurrence area pattern remain. Using DFAPT20%, the area of DF occurrence becomes wider than DFAPT10%.

Patient 2:

At baseline, DFRI shows similar behaviour so that of patient 1. Based on DFAPT10% and DFAPT20%, we could not see a clear DF occurrence area.

Patient 3:

At baseline, DFRI shows scattered distribution of DF occurrence area. DFAPT10% shows concentrated area of occurrence. The behaviour of DFAPT20% is similar with DFAPT10% but the DF area in DFAPT20% is wider.

Patient 4:

At baseline, DFRI shows a widespread of DF occurrence area but DFAPT10% shows lower occurrence of DF. DFAPT10% does not show any significant changes of DF occurrence compare to baseline. We can see the concentrated DF occurrence clearly using APT20%.

Overall, DFRI analysis is observed to produce scattered pattern of DF occurrences while DFAPT10% tends to produce concentrated occurrences. DFAPT20% seems to be a better choice if we want to see more wide spread or clear DF occurrence compared to DFAPT10%. As a summary, DFRI would give an overall idea of the behaviour of DFs which ADAPT20% will help us concentrate attention to DFs with lowest power.

Standard electrical isolation of the pulmonary veins was done for all patients. The DF occurrence observed post ablation suggests that there was no ablation done in the DF area as shown in 3D maps at the baseline.

Different areas of the atrium may intrinsically have different voltages and therefore "artificially" have different power. Areas with low voltages may harbour important rotors which may not be shown if DF is pruned by the (high) power threshold approach. Distance from the balloon also affects voltages and this is compensated by the system (but statistical confidence is reduced for values measured farther than about 4 cm from the data acquisition balloon).

As we mentioned in section 8.4.3, sites with high frequency and low power could be possible drivers of AF (as shown in Figure 8.14). Interestingly, the DF areas with low power showed some concentration around the pulmonary veins (PVs). This result suggests that there might be a correlation with the behaviour of complex fractionated atrial electrograms (CFAEs).

8.7 Conclusions

In this chapter, we successfully provide the facilities to estimate DF with and without QRST influences using 3D mapping. Smaller DF area was observed after QRST subtraction. An average of DF-RI for the baseline (6.37 Hz) is higher than post ablation (6.01 Hz) and this is the same for average of DF APT20% (baseline:6.39 Hz and post ablation: 5.86 Hz). An adaptive threshold tool to monitor the DF sites is provided. With this tool, researcher can choose the threshold level to his/her preference.

Despite Pulmonary Veins isolation being an effective approach for treatment of AF, there are cases when significant DF areas still remain in the atrium after this procedure. This chapter shows how a combination of QRST subtraction and adaptive thresholding technique might help reduce the number of candidate points for further ablation, if needed, after PVI. Further analysis is required to verify the effectiveness of this approach and its contribution to the treatment of AF.

9 CONCLUSIONS AND FUTURE WORK

9.1 Introduction

Atrial arrhythmias contribute to mortality and morbidity and diminish quality of life. The disturbance in the heart rate or heart rhythm may cause discomfort to patients with symptoms such as palpitations, dizziness, chest pains and shortness of breath.

Recent studies have shown that AF signals can be analysed in the frequency domain [Sanders *et al.*, 2005, Takahashi *et al.*, 2006, Sanders *et al.*, 2006, Mandapati *et al.*, 2000, Ng and Goldberger, 2007]. The most common application in AF studies is to determine the dominant frequency for estimating the activation rate of the atria. In this study, there are several approaches that have been taken before and after performing frequency analysis.

9.1.1 Reducing ablation procedure time by choosing a fast computational method

The goal of ablation, to eliminate the trigger that initiates AF, or of the paths that allow it to be sustained, is the most complex interventional electrophysiological procedure [Calkins *et al.*, 2007]. High risk (6%), which grows with procedure time, means one should try to avoid long procedures. In this study we compared several methods to estimate the dominant frequency of the atrial electrograms and measured their computation time. The Fast Fourier Transform method produced an accurate estimation of dominant frequency with the shortest computation time. We suggest that this method would help the electrophysiologist to decrease risk for the patients by obtaining the DF maps while keeping the time of the overall ablation procedure short.

9.1.2 Removing ventricular influences from atrial electrograms

The noncontact mapping system used simultaneously reconstructs 2048 unipolar atrial electrograms of the virtual endocardium. The electrograms occasionally contain ventricular influences that may affect the accuracy of the power spectrum analysis. The implementation of the QRST subtraction minimised the ventricular influences and the QRST subtraction using any of the three different interpolation approaches tested only affects the power of the signals but not the value of DF derived from the ‘filtered’ electrograms.

9.1.3 Observing the behaviour of contact mapping VF signals (from animal studies) and AF signals (from human studies)

The mechanisms of the arrhythmia still remain unclear. Some studies show the mechanism of arrhythmia is re-entrancy [Mines, 1913, Garrey, 1924, Moe *et al.*, 1959] or focal source [Jaïs *et al.*, 1997, Sano and Tohru Sawanobori, 1970, Moe *et al.*, 1959, Haïssaguerre *et al.*, 1998] while other studies show the ANS to be one of the mechanisms that contributes for this arrhythmia [Scherlag *et al.*, 2005, Nakagawa *et al.*, 2008]. However, the mechanism of AF is still debatable. As the signals are irregular, Fourier analysis was implemented to identify the frequency spectrum of the signals and to observe the frequency evolution along time. The changes of the dominant frequency were observed using spectrograms (Figure 9.1).

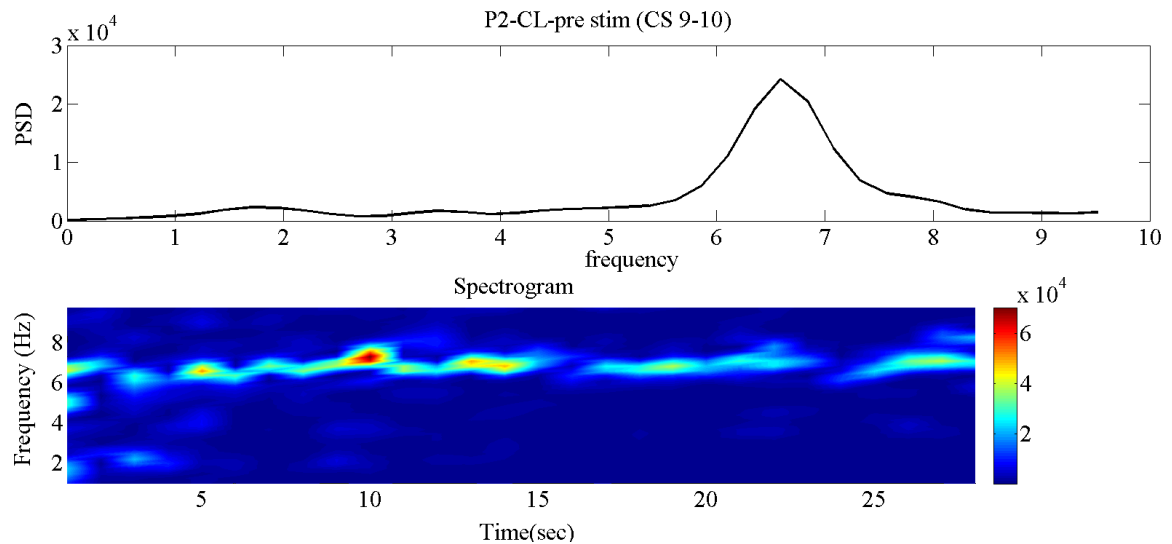


Figure 9.1 - Spectrum and spectrogram.

Spectrograms show that the dominant frequency changes over 30 seconds. During this period, sometimes the frequency power waxes and wanes. As we mentioned in Chapter 6, the red colour indicator represents the frequency with high power while the blue colour represents frequencies with low power. The plotting of such spectrograms allowed us to observe the evolution and the stability of the frequency along time. This method can also be used to identify the frequency and its stability for noncontact mapping signals.

9.1.4 Observing 3D DF maps for noncontact mapping AF signals

The reconstruction of 3D maps using Matlab (MathWorks Inc., USA) allows us to observe the behaviour of DF from a different point of view, relating it to the anatomical site [Salinet Jr *et al.*, 2010]. We used the 3D maps initially to compare the 3D DF maps before and after QRST subtraction. As expected, we found that the overall power is reduced after the QRS subtraction. We also observed that the DF area after QRST subtraction is significantly smaller than before QRST subtraction.

In the study of the focal source as a mechanism of AF, the approach of DF occurrence is used to identify how many DF (within AF physiological range frequency) occurred along time. The total number of DF occurrences was calculated and displayed in 3D maps. In a summary, an area that shows frequent DFs along time is highlighted.

We also developed an adaptive power threshold tool to observe the distribution of the dominant frequencies with an adjustable power threshold setting. This tool allows us to identify the DFs with low power or the DFs with high power. The 3D maps can display the evolution of the DFs within a chosen threshold power bracket. Recent studies show the organization during AF is in a form of periodic activation waves and the period of those waves correlated strongly with DF of the power spectrum [Skanes *et al.*, 1998]. If the electrogram represents the voltage value in every moment of time, its Fourier transform represents the strength of every oscillation in that period of time. In this study, the strong signal oscillations were observed by looking at the DFs with high power (the power of these signals is defined as the squared voltage value of the signal). For this reason, the DFs within a high power bracket are used to observe activation waves of AF. On the other hand, complex fractionated atrial electrograms correspond to signals with low voltage [Nademanee *et al.*, 2004]. The Fourier transform of these signals will correspond to low power DFs. In this situation, the DFs within a low power bracket are chosen for observing the activation waves of AF.

9.2 Future work

9.2.1 Improving the frequency resolution

The fast Fourier transform is the fastest of the techniques we tested for estimating the DF, but it has limitations in frequency resolution. In order to analyse rotors as a possible AF mechanism, a technique able to produce spectra with a better frequency resolution, such as autoregressive (AR) approach, might prove useful. High spatial resolution mapping is needed to observe the propagation of high frequency activity in the atria. The direction of high frequency activity, its velocity and frequency stability are criteria that need to be considered in understanding the mechanisms involved in triggering or sustaining AF.

9.2.2 The optimization of the QRST subtraction method

The implementation of the QRST subtraction and its computation time are important before frequency analysis was performed. In this study, it takes typically 8 to 10 minutes to remove the ventricular influences for 2048 points over 21 seconds. The optimization of the QRST subtraction method with faster computation is important to decrease the ablation procedure time and reducing risk for the patients.

9.2.3 AF signal complexity (Time domain analysis)

Time domain analysis can be used to determine the complexity of intra-cardiac atrial electrograms. Higher complexity is associated with increasing number of interacting wavefronts as well as an increasing fractionation of the atrial activation. Permutation entropy is one of the methods that could be used to estimate the complexity of the signals [Bandt and Pompe, 2002]. Since the complexity is related to fractionation of the signals, it is important to

study the areas where the atrial electrograms are ‘complex’ as these would be possible drivers of AF.

9.2.4 Assessing the efficacy the DF and CFAE sites

The critical areas in the atria are important for targeting the ablation sites. Therefore, other techniques such as complex fractionated atrial electrograms (CFAE) are required to complement the mapping of DF sites and help reveal critical sites for ablation. CFAE is a technique that shows points of slow conduction or pivot points where wavelets turn at the end of the arcs of functional block [Konings *et al.*, 1997]. The efficacy of both techniques (DF and CFAE) could help in identifying the crucial AF sites and lead to AF termination and associated with long term success.

9.2.5 Comparing approaches for estimating DF

Finally, as mentioned in chapter 5, we have consistently estimated DF based on the electrical signal only to find the dominant frequency of the electrical activation. It can be argued that it is valid to search for the dominant frequency of bursts of electrical activity by implementing the rectify-and-low-pass-filtering approach mentioned in chapter 5 as these might correlate better with electrical activation. It would be perhaps interesting comparing the two resulting DF maps.

References

- AHMAD, A., SCHLINDWEIN, F. S. & NG, G. A. (2010) Comparison of Computation Time for Estimation of Dominant Frequency of Atrial Electrograms: Fast Fourier Transform, Blackman Tukey, Autoregressive and Multiple Signal Classification. *Journal of Biomedical Science and Engineering (JBSE)*.
- AHMAD, A. A., J.CALLANS, D., H.HSIA, H. & NATALE, A. (2011) Electroanatomical Mapping: An Atlas for Clinicians. John Wiley & Sons.
- ANDREW, L. & PAUL, F. (1977) Triggered and automatic activity in the canine coronary sinus. *Circ Res.*, 435-445.
- ANURADHA, B., KUMAR, K. S. & REDDY, V. C. V. (2008) Classification of Cardiac Signals using Time Domain Methods. 3, 7-12.
- BAINBRIDGE, F. A. (1915) The influence of venous filling upon the rate of the heart. *J Physiol.* , 50, 65-84.
- BANDT, C. & POMPE, B. (2002) Permutation entropy — a natural complexity measure for time series. *Phys. Rev. Lett.*, 88, 174102.
- BEAUCHAMP, K. G. & YUEN, C. K. (1979) *Digital Methods for Signal Analysis*, London, George Allen & Unwin.
- BENJAMIN, E., WOLF PA, D'AGOSTINO RB, SILBERSHATZ H, KANNEL WB & D., L. (1998) Impact of atrial fibrillation on the risk of death: the Framingham Heart Study. *Circulation*, 946-952.
- BENJAMIN J. SCHERLAG, HIROSHI NAKAGAWA, WARREN M. JACKMAN, WILLIAM S. YAMANASHI, EUGENE PATTERSON, SUNNY PO & LAZZARA, R. (2005) Electrical Stimulation to Identify Neural Elements on the Heart: Their Role in Atrial Fibrillation. *Journal of Interventional Cardiac Electrophysiology* 37-42.
- BENNETT, D. (2002) *Cardiac arrhythmias: practical notes on interpretation and treatment*, New York, NY: , Oxford University Press Inc.
- BENUSSI, S., PAPPONE C, NASCIMBENE S, ORETO G. , CALDAROLA A. , STEFANO P.L., CASATI V. & ALFIERI, O. (2000) A simple way to treat chronic atrial fibrillation during mitral valve surgery: the epicardial radiofrequency approach. *Eur J Cardio_Thoracic Surg*, 17, 524-529
- BERENFELD, O. (2007) Quantifying activation frequency in atrial fibrillation to establish underlying mechanism and ablation guidance. *Heart Rhythm*, 1225-1234.
- BERENFELD, O., MANDAPATI., R., DIXIT., S., ALLAN C. SKANES, JAY CHEN, MOUSSA MANSOUR & JOSE JALIFE (2000) Spatially Distributed Dominant Excitation Frequencies Reveal Hidden Organization in Atrial Fibrillation in the Langendorff-Perfused Sheep Heart. *J Cardiovasc Electrophysiol.*, Vol. II, 869-879.
- BOARDMAN, A., SCHLINDWEIN, F. S., THAKOR, N. V., KIMURA, T. & GEOCADIN, R. G. (2002) Detection of asphyxia using heart rate variability. *Med. Biol. Eng. Comput.*, 618-624.
- BORON, W. R. & BOULPAEP, E. L. (2005) *Medical Physiology*, Elseviers Saunders.
- BRODY, D. A., BRADSHAW, J. C. & EVANS, J. W. (1961) A Theoretical Basis for Determining Heart-Lead Relationships of the Equivalent Cardiac Multipole. *IEEE Transaction on Biomedical Engineering*, 139-143.
- CALKINS, H., BRUGADA J, PACKER DL, CAPPATO R, CHEN SA & HJ, C. (2007) HRS/EHRA/ECAS expert consensus statement on catheter and surgical ablation of atrial fibrillation: recommendations for personnel, policy, procedures and follow-up. *Europace*, 335-379.

- CALKINS, H., JAIS, P. & S.STEINBERG, J. (2008) *A Practical Approach to Catheter Ablation of Atrial Fibrillation*, USA, Lippincott Williams & Wilkins.
- CANNON, W. B. (1920) *Bodily Changes in Pain, Hunger, Fear and Range* D.Appleton and Company.
- CAPPATO, R., CALKINS H., CHEN S.A, DAVIES W., IESAKA Y., KALMAN J., KIM Y.H, KLEIN G., D., P. & A, S. (2005) Worldwide Survey on the Methods, Efficacy, and Safety of Catheter Ablation for Human Atrial Fibrillation. *Circulation*, 1100-1105.
- CARLSON, N. R. (2000) *Physiology of Behavior*, Allyn & Bacon.
- CASTELS, F., C. MORA, J. J. RIETA, D. MORATAL-PEREZ & MILLET, J. (2005) Estimation of atrial fibrillatory wave from single-lead atrial fibrillation electrocardiograms using principal component analysis concepts. *Med. Biol. Eng. Comput*, 557-560.
- CHEN, J., RAVI MANDAPATI, OMER BERENFELD, SKANES, A. C. & JALIFE, J. (2000) High-Frequency Periodic Sources Underlie Ventricular Fibrillation in the Isolated Rabbit Heart. *Circ Res*, 86-93.
- CLIFFORD, G. D., AZUAJE, F. & MCSHARRY, P. E. (2006) *Advanced Methods and Tools for ECG Data Analysis*, Artech House.
- CONOVER, M. B. (1996) *Understanding Electrocardiography*, Mosby.
- COOLEY, J. & TUKEY, O. (1965) An algorithm for the machine calculation of complex Fourier series. *Math Comput*, 297-301.
- COOLEY, J. W., LEWIS, P. A. W. & WELCH, P. D. (1969) The Fast Fourier Transform and Its Applications. *IEEE Transactions on Education*, Vol. 12.
- COOLEY, J. W., PETER A. W. LEWIS & WELCH, P. D. (1967) Historical Notes on the Fast Fourier Transform. *Proceeding of the IEEE*.
- DECAPRIO, V., HURZELER, P. & FURMAN, S. (1977) A comparison of unipolar and bipolar electrograms for cardiac pacemaker sensing. *Circulation*, 750-755.
- DEFATTA & DAVID, J. (1988) *Digital signal processing : a system design approach* Wiley.
- ENGELMANN, T. (1896) Ueber den Einfluss der Systole auf der motorische Leitung in der Herzkammer, mit Bemerkungen zur Theorie allorhythmischer Herzstorungen. *Arch Gesamte Psychol*, 543- 566.
- ERICHSEN, J. (1842) On the influence of the coronary circulation on the action of the heart. *Lond Mag Gazette*, 561-565.
- ERLANGER, J. & BLACKMAN, J. R. (1907) A study of relative rhythmicity and conductivity in various regions of the auricles of the mammalian heart. *Am J Physiol.*, 125-174.
- ERVEN, L. V. & SCHALIJ, M. J. (2010) Amiodarone: an effective antiarrhythmic drug with unusual side effects. *Heart* 1593-1600.
- EVERETT, T. H., KOK, L.-C., VAUGHN, R. H., MOORMAN, J. R. & HAINES, D. E. (2001) Frequency Domain Algorithm for Quantifying Atrial Fibrillation Organization to Increase Defibrillation Efficacy. *IEEE Transactions on Biomedical Engineering*, 48, 969-978.
- FINKEL, R., X.CUBEDDU, L. & A.CLARK, M. (2006) *Pharmacology*, Lippincott William & Wilkins.
- FISH, F. (2004) Ventricular fibrillation: basic concepts. *Pediatr Clin North Am*.
- FORLEO, G. B. & TONDO, C. (2009) Atrial fibrillation :Cure or treat? . *Therapeutic Advances in Cardiovascular Disease* 187-196.

- FOSTER, R. W. & BOULTON, A. J. M. (1991) *Basic Pharmacology*, Butterworth Heinemann.
- FUSTER, V., LARS E. RYDÉN, DAVID S. CANNOM, HARRY J. CRIJNS, ANNE B. CURTIS, KENNETH A. ELLENBOGEN, JONATHAN L. HALPERIN, JEAN-YVES LE HEUZEY, G. NEAL KAY, JAMES E. LOWE, S. BERTIL OLSSON, ERIC N. PRYSTOWSKY, JUAN LUIS TAMARGO, SAMUEL WANN, SIDNEY C. SMITH, JR, A. K. J., CYNTHIA D. ADAMS, JEFFERY L. ANDERSON, ELLIOTT M. ANTMAN, JONATHAN L. HALPERIN, SHARON ANN HUNT, RICK NISHIMURA, JOSEPH P. ORNATO, RICHARD L. PAGE & RIEGEL, B. (2006) ACC/AHA/ESC 2006 Guidelines for the Management of Patients With Atrial Fibrillation—Executive Summary. *J Am Coll Cardiol*, 854–906.
- GALLAGHER, J. J., ROBERT H. SVENSON, JACK H. KASELL, LAWRENCE D. GERMAN, GUST H. BARDY, ARCHER BROUGHTON & GIUSEPPE CRITELLI (1982) Catheter Technique for Closed-Chest Ablation of the Atrioventricular Conduction System *N Engl J Med*, 194-200.
- GARREY, W. E. (1714) The Nature of Fibrillary Contraction of the Heart. -Its Relation to Tissue Mass and form. *American Journal of Physiology*, 397-414.
- GARREY, W. E. (1924) Auricular Fibrillation. *Physiol.Rev*, 215-250.
- GO, A. S., ELAINE M. HYLEK, KATHLEEN A. PHILLIPS, YUCHIAO CHANG, LORI E. HENAULT, JOE V. SELBY & DANIEL E. SINGER (2001) Prevalence of Diagnosed Atrial Fibrillation in Adults National Implications for Rhythm Management and Stroke Prevention: the Anticoagulation and Risk Factors In Atrial Fibrillation (ATRIA) Study. *JAMA*, 2370-2375.
- GOJRATY, S., NIMROD LAVI, ERMENGOL VALLES, STEVEN J. KIM, JOHN MICHELE & EDWARD P. GERSTENFELD (2009) Dominant Frequency Mapping of Atrial Fibrillation: Comparison of Contact and Noncontact Approaches. *J Cardiovasc Electrophysiol*, Vol 20, 997-1004.
- GONSKA, B. D., BAUERLE, H. J. & JAPHA, T. (2009) Atrial fibrillation ablation: Who comes into consideration? . *Herzschrittmachertherapie und Elektrophysiologie* 20, 76-81.
- GREVILLE, T. (1969) *Theory and Applications of Spline Functions*, Academic Press Inc.
- GUYTON, A. C. & HALL, J. E. (1996) *Textbook of Medical Physiology*, W. B. Saunders Company.
- HAÏSSAGUERRE, M., DIPEN C. SHAH, PIERRE JAÏS, MÉLÈZE HOCINI, TEIICHI YAMANE, ISABEL DEISENHOFER, MICHEL CHAUVIN, GARRIGUE, S. & CLÉMENTY, J. (2000) Electrophysiological Breakthroughs From the Left Atrium to the Pulmonary veins. *Circulation* 2463-2465.
- HAISSAGUERRE, M., JAIS P, SHAH DC, ARENTZ, T., KALUSCHE D. , TAKAHASHI A., GARRIGUE S., HOCINI M., PENG J.T. & J., C. (2000) Catheter ablation of chronic atrial fibrillation targeting the reinitiating triggers. *J Cardiovas Electrophysiol* 11, 2-10.
- HAÏSSAGUERRE, M., MELEZE HOCINI, PRASHANTHAN SANDERS, FREDERIC SACHER, MARTIN ROTTER, YOSHIHIDE TAKAHASHI, THOMAS ROSTOCK, LI-FERN HSU, PIERRE BORDACHAR, SYLVAIN REUTER, RAYMOND ROUDAUT, JACQUES CLEMENTY & PIERRE JAIS (2005) Catheter Ablation of Long-Lasting Persistent Atrial Fibrillation:Clinical Outcome and Mechanisms of Subsequent Arrhythmias. *J Cardiovasc Electrophysiol*, , 16, 1138-1147.
- HAÏSSAGUERRE, M., PIERRE JAÏS, DIPEN C. SHAH, ATSUSHI TAKAHASHI, MÉLÈZE HOCINI, GILLES QUINIOU, STÉPHANE GARRIGUE, ALAIN LE

- MOUROUX, PHILIPPE LE MÉTAYER & CLÉMENTY, J. (1998) Spontaneous Initiation of Atrial Fibrillation by Ectopic Beats Originating in the Pulmonary Veins. *N Engl J Med*, 659-66.
- HAÏSSAGUERRE, M., PRASHANTHAN SANDERS, MÉLÈZE HOCINI, LI-FERN HSU, DIPEN C. SHAH, CHRISTOPHE SCAVÉE, YOSHIHIDE TAKAHASHI, MARTIN ROTTER, JEAN-LUC PASQUIÉ, STÉPHANE, G., JACQUES CLÉMENTY & PIERRE JAÏS (2004) Changes in Atrial Fibrillation Cycle Length and Inducibility During Catheter Ablation and Their Relation to Outcome. *Circulation*, 3007-3013.
- HAÏSSAGUERRE, M., SHAH, D. C., PIERRE JAÏS, MORIO SHODA, JOSEF KAUTZNER, THOMAS ARENTZ, DIETRICH KALUSHE, ALAN KADISH, MIKE GRIFFITH, FIORENZO GAÏTA, TEIICHI YAMANE, STEPHANE GARRIGUE, MELEZE HOCINI & CLÉMENTY, J. (2002) Role of Purkinje Vonducting System in Triggering of Idiopathic Ventricular Fibrillation. *The Lancet*.
- HAMPTON, J. R. (2008) *The ECG made easy*, Churchill Livingstone Elsevier.
- HAN, J. & MOE, G. K. (1964) Nonuniform Recovery of Excitability in Ventricular Muscle. *Circ. Res.*, 44-60.
- HAYES, M. H. (1996) *Statistical Digital Signal Processing and Modelling*, John Wiley & Son.
- HOCINI, M., PIERRE JAÏS, PRASHANTHAN SANDERS, YOSHIHIDE TAKAHASHI, MARTIN ROTTER, THOMAS ROSTOCK, LI-FERN HSU, FRÉDÉRIC SACHER, SYLVAIN REUTER, CLÉMENTY, J. & HAÏSSAGUERRE, M. (2005) Techniques, Evaluation, and Consequences of Linear Block at the Left Atrial Roof in Paroxysmal Atrial Fibrillation: A Prospective Randomized Study. *Circulation*, 3688-3696.
- HOEKEMA, R., UIJEN G.J.H., ERNING L.V & A.V, O. (1999) Interindividual Variability of Multilead Electrocardiographic Recordings. *Journal of Electrocardiology*, 32.
- HOFFMAN, B. & CRANFIELD, P. (1960) *Electrophysiology of the Heart*, New York, McGraw-Hill.
- HORDOF, A., EDIE, R., MALM, J., HOFFMAN, B. & ROSEN, M. (1976) Electrophysiologic properties and response to pharmacologic agents of fibers from diseased human atria. *Circulation*, 774-779.
- HUANG, J., TAI CT, LIN YJ, TING CT, CHEN YT, CHANG MS, LIN FY, LAI WT & SA, C. (2006) The mechanisms of an increased dominant frequency in the left atrial posterior wall during atrial fibrillation in acute atrial dilatation. *J Cardiovasc Electrophysiol.* , 17, 178-188.
- HUANG, S. K., BHARATI, S., GRAHAM, A. R., LEV, M., MARCUS, F. I. & ODELL, R. C. (1987) Closed chest catheter desiccation of the atrioventricular junction using radiofrequency energy—A new method of catheter ablation *Journal of the American College of Cardiology*, 9, 349-358
- HUSSER, D., MARTIN STRIDH, LEIF SORNMO, S. BERTIL OLSSON & ANDREAS BOLLMANN (2004) Frequency Analysis of Atrial Fibrillation From the Surface Electrocardiogram. *Indian Pacing and Electrophysiology Journal* Vol 4, 122-136.
- IFEACHOR, E. C. & JERVIS, B. W. (2002) *Digital Signal Processing: A Practical Approach*, Prentice Hall.
- ISSA, Z. F., MILLER, J. M. & ZIPES, D. P. (2009) Clinical arrhythmology and electrophysiology: a companion to Braunwald's heart disease. Saunders Elsevier.
- JACQUEMET, V., LUKAS KAPPENBERGER & HENRIQUEZ, C. S. (2008) Modeling Atrial Arrhythmias: Impact on Clinical Diagnosis and Therapies. *IEEE Reviews in Biomedical Engineering*, 1, 94-114.

- JAÏS, P., HAÏSSAGUERRE, M., SHAH, D. C., CHOUAIRI, S., GENCEL, L., HOCINI, M. & CLEMENTY, J. (1997) A Focal Source of Atrial Fibrillation Treated by Discrete Radiofrequency Ablation *Circulation*, 572-576.
- JAÏS, P., MÉLÈZE HOCINI, LI-FERN HSU, PRASHANTHAN SANDERS, CHRISTOPHE SCAVEE, RUKSHEN WEERASOORIYA, LAURENT MACLE, FLORENCE RAYBAUD, STÉPHANE GARRIGUE, DIPEN C. SHAH, PHILIPPE LE METAYER, JACQUES CLÉMENTY & HAÏSSAGUERRE, M. (2004) Technique and Results of Linear Ablation at the Mitral Isthmus. *Circulation*, 2996-3002.
- JAÏS, P., SHAH, D. C., HAÏSSAGUERRE, M., TAKAHASHI, A., LAVERGNE, T., HOCINI, M., GARRIGUE, S., BAROLD, S. S., MÉTAYER, P. L. & CLÉMENTY, J. (1999) Efficacy and Safety of Septal and Left-Atrial Linear Ablation for Atrial Fibrillation. *Am J Cardiol* 139R-146R.
- JALIFE, J. (2000) Ventricular Fibrillation: Mechanisms of Initiation and Maintenance. *Annu. Rev. Physiol.*, 25-50.
- JALIFE J, BERENFELD O, SKANES A & R., M. (1998) Mechanisms of Atrial Fibrillation: Mother Rotors or Multiple Daughter Wavelets, or both. *J. Cardiovasc. Electrophysiol*, S2-12.
- JOSEPH, T. C. (2002) *Guide to ECG analysis*, Lippincott.
- JOSEPHSON, M. E. (2008) Clinical cardiac electrophysiology: Techniques and interpretations. 4 ed., Wolters Kluwer/ Lippincott William and Wilkins.
- KALIFA, J., KAZUHIKO TANAKA, ALEXEY V. ZAITSEV, MARK WARREN, RAVI VAIDYANATHAN, DAVID AUERBACH, SANDEEP PANDIT, KAREN L. VIKSTROM, ROBERT PLOUTZ-SNYDER, ARKADZI TALKACHOU, FELIPE ATIENZA, GÉRARD GUIRAUDON, JOSÉ JALIFE & OMER BERENFELD (2006) Mechanisms of Wave Fractionation at Boundaries of High-Frequency Excitation in the Posterior Left Atrium of the Isolated Sheep Heart During Atrial Fibrillation. *Circulation*, 626-633.
- KANNEL, W., WOLF, P., EJ, B. & D, L. (1998) Prevalence, incidence, prognosis, and predisposing conditions for atrial fibrillation: Population-based estimates. *Am J Cardiol* 2N-9N.
- KARCH, M. R., BERNHARD ZRENNER, ISABEL DEISENHOFER, JÜRGEN SCHREIECK, GJIN NDREPEPA, JUN DONG, KATRIN LAMPRECHT, PETRA BARTHEL, ETIENNE LUCIANI, ALBERT SCHÖMIG & CLAUS SCHMITT (2005) Freedom From Atrial Tachyarrhythmias After Catheter Ablation of Atrial Fibrillation A Randomized Comparison Between 2 Current Ablation Strategies. *Circulation* 2875-2880.
- KATZUNG, B. G. (1995) *Basic and Clinical Pharmacology*, Prentice Hall.
- KAY, S. M. (1988) *Modern Spectral Estimation Theory & Application*, Prentice Hall.
- KLABUNDE, R. E. (2005) *Cardiovascular physiology concepts*, Lippincott Williams & Wilkins. .
- KLOECK, W., CUMMINS, R. O., CHAMBERLAIN, D., BOSSAERT, L., CALLANAN, V., CARLI, P., CHRISTENSON, J., CONNOLLY, B., ORNATO, J. P., SANDERS, A. & STEEN, P. (1997) The Universal Advanced Life Support Algorithm *Circulation*, 2180-2182.
- KNECHT, S., MÉLÈZE HOCINI, WRIGHT, M., LELLOUCHE, N., O'NEILL, M. D., MATSUO, S., NAULT, I., CHAUHAN, V. S., MAKATI, K. J., BEVILACQUA, M., LIM, K.-T., SACHER, F., DEPLAGNE, A., DERVAL, N., BORDACHAR, P., JAÏS, P., CLÉMENTY, J. & HAÏSSAGUERRE, M. (2008) Left atrial linear lesions are

- required for successful treatment of persistent atrial fibrillation. *European Heart Journal*, 2359-2366.
- KONINGS, K. T. S., JOEP L.R.M. SMEETS, OLAF C. PENN, HEIN J.J. WELLENS & MAURITS A. ALLESSIE (1997) Configuration of Unipolar Atrial Electrograms During Electrically Induced Atrial Fibrillation in Humans *Circulation*, 1231-1241.
- LAMB, J. F., INGRAM, C. G., JOHNSTON, I. A. & PITMAN, R. M. (1991) *Essentials of Physiology*, Blackwell Scientific Publications.
- LAZAR, S., SANJAY DIXIT, FRANCIS E. MARCHLINSKI, DAVID J. CALLANS & P.GERSTENFELD, E. (2004) Presence of Left-to-Right Atrial Frequency Gradient in Paroxysmal but Not Persistent Atrial Fibrillation in Humans. *Circulation*, 3181-3186.
- LEMAY, M., VESIN, J.-M., IHARA, Z. & KAPPENBERGER, L. (2004) Suppression of Ventricular activity in the Surface Electrocardiogram of Atrial Fibrillation. Springer.
- LEVY, M. N. & PAPPANO, A. J. (2007) *Cardiovascular Physiology*, Mosby Elsevier.
- LEVY, M. N., STANTON, B. A. & KOEPPEN, B. M. (2006) *Principles of Physiology*, Elsevier Mosby.
- LEVY, M. N. & ZIESKE, H. (1969) Autonomic control of cardiac pacemaker activity and atrioventricular transmission. *Journal of Applied Physiology*, Vol. 27, 465-470.
- LÉVY, S. (2009) Current atrial fibrillation guidelines and therapy algorithms: Are they adequate? *J Interv Card Electrophysiol* 111-116.
- LIN, W.-S., CHING-TAI TAI, MING-HSIUNG HSIEH, CHIN-FENG TSAI, YUNG-KUO LIN, HSUAN-MING TSAO, JIN-LONG HUANG, WEN-CHUNG YU, SHIH-PING YANG, YU-AN DING, CHANG, M.-S. & CHEN, S.-A. (2003) Catheter Ablation of Paroxysmal Atrial Fibrillation Initiated by Non-Pulmonary Vein Ectopy. *Circulation* 3176-3183.
- LIN, Y.-J., CHING-TAI TAI, JIN-LONG HUANG, KUN-TAI LEE, PI-CHANG LEE, MING-HSIUNG HSIEH, SHIH-HUANG LEE, SATOSHI HIGA, YOGA YUNIADI, TU-YING LIU & SHIH-ANN CHEN (2005) Characterization of Right Atrial Substrate in Patients with Supraventricular Tachyarrhythmias. *J Cardiovasc Electrophysiol*, 16, 173-180.
- LIN, Y.-J., SATOSHI HIGA, TSAIR KAO, HAN-WEN TSO, CHING-TAI TAI, SHIH-LIN CHANG, LI-WEI LO, WANWARANG WONGCHAROEN & SHIH-ANN CHEN (2007) Validation of the Frequency Spectra Obtained from the Noncontact Unipolar Electrograms During Atrial Fibrillation. *J. Cardiovasc Electrophysiol*, Vol. 18, 1147-1153.
- LOGAN, K., WJ MCILWAINE, AA ADGEY & PANTRIDGE, J. (1981) Recurrence of ventricular fibrillation in acute ischemic heart disease. *Circulation*, 1163-1167.
- LURIA, D. M., NEMEC, J., ETHERIDGE, S. P., COMPTON, S. J., KLEIN, R. C., CHUGH, S. S., MUNGER, T. M., SHEN, W. K., PACKER, D. L., JAHANGIR, A., REA, R. F., HAMMILL, S. C. & FRIEDMAN, P. A. (2001) Intra-Atrial Conduction Block Along the Mitral Valve Annulus During Accessory Pathway Ablation: Evidence for a Left Atrial "Isthmus. *Journal of Cardiovascular Electrophysiology*, 12, 744-749.
- LYNN, P. A. & FUERST, W. (2000) *Introductory Digital Signal Processing with computer applications*, John Wiley & sons.
- MANDAPATI, R., ALLAN SKANES, JAY CHEN, BERENFELD, O. & JALIFE, J. (2000) Stable Microreentrant Sources as a Mechanism of Atrial Fibrillation in the Isolated Sheep Heart. *Circulation*, 194-199.
- MANSOUR, M., RAVI MANDAPATI, OMER BERENFELD, JAY CHEN, FARAMARZ H. SAMIE & JALIFE, J. (2001) Left-to-Right Gradient of Atrial Frequencies During Acute Atrial Fibrillation in the Isolated Sheep Heart. *Circulation*, 2631-2636.

- MARIEB, E. N. & HOEHN, K. (2007) *Human Anatomy & Physiology*, Pearson Benjamin Cummings.
- MARK, S. K., WILLIAM, H. B. & PETER, J. W. (1989) Sudden Cardiac Death: Etiologies, Pathogenesis, and Management. *Disease-a-Month*, 35, 385-445
- MARKIDES, V. & SCHILLING, R. J. (2003) Atrial Fibrillation: Classification, Pathophysiology, Mechanisms and Drug Treatment. *Heart*, 939-943.
- MARPLE, L. (1980) A New Autoregressive Spectrum Analysis Algorithm. *IEEE Transactions on Acoustics, Speech, and Signal Processing*, Vol. ASSP-28, 441-454.
- MARPLE, S. L. (1987) *Digital Spectral Analysis with Applications*. Prentice Hall.
- MAYER, A. G. (1908) Rhythmical pulsation in Scyphomedusae *Carnegie Inst. Wash. Publ*, 113-131.
- MCWILLIAM, J. A. (1889) Cardiac Failure and sudden death. *BMJ*, 6-8.
- MICKEY, S. E., HALLSTROM, A. P., COPASS, M. K., BERGNER, L., SHORT, F. & PIERCE, J. (1984) Treatment of Ventricular Fibrillation: Emergency Medical Technician Defibrillation and Paramedic Services. *JAMA*, 251, 1723-1726.
- MINES, G. R. (1913) On Dynamic Equilibrium in the Heart. *The Journal of Physiology*, XLVI, 349-383.
- MOE, G. K., J. A. ABILDSKOV & SYRACUSE, N. Y. (1959) Experimental and Laboratory Reports: Atrial Fibrillation as a Self-Sustaining Arrhythmia Independent of Focal Discharge. *Am. Heart J.*
- NACCARELLI, G. V., WOLBRETTE, D. L., KHAN, M., BHATTA, L., HYNES, J., SAMII, S. & LUCK, J. (2003) Old and New Antiarrhythmic Drugs for Converting and Maintaining Sinus Rhythm in Atrial Fibrillation: Comparative Efficacy and Results of Trials. *The American Journal of Cardiology*, 91, 15-26.
- NADEMANEE, K., JOHN MCKENZIE, EROL KOSAR, MARK SCHWAB, BUNCHA SUNSANEWITAYAKUL, THAVEEKIAT VASAVAKUL, CHOTIKORN KHUNNAWAT & NGARMUKOS, T. (2004) A New Approach for Catheter Ablation of Atrial Fibrillation: Mapping of the Electrophysiologic Substrate. *Journal of the American College of Cardiology*, Vol 43, 2044-2053.
- NAIR GM, NERY PB, DIWAKARAMENON S, HEALEY JS, CONNOLLY SJ & CA., M. (2009) A systematic review of randomized trials comparing radiofrequency ablation with antiarrhythmic medications in patients with atrial fibrillation. *J Cardiovasc Electrophysiol.* , 20, 138-144.
- NAKAGAWA, H. & JACKMAN, W. M. (1998) Use of a Three-Dimensional, Nonfluoroscopic mapping system for catheter ablation of typical atrial flutter. *PACE*, 1279-1286.
- NAKAGAWA, H., YOKOYAMA, K., SCHERLAG, B., KATARI, V., AOYAMA, H., FORESTI, S. & JACKMAN, W. (2008) Ablation of Autonomic Ganglia. IN CALKINS, H., JAIS, P. & S. STEINBERG, J. (Eds.) *A Practical Approach to Catheter Ablation Atrial Fibrillation*. Lippincott William & Wilkins.
- NATH, S., C LYNCH, 3D, WHAYNE, J. & HAINES, D. (1993) Cellular electrophysiological effects of hyperthermia on isolated guinea pig papillary muscle. Implications for catheter ablation. *Circulation* 1826-1831.
- NATHAN, H. & ELIAKIM, M. (1966) The Junction Between the Left Atrium and the Pulmonary Veins: An Anatomic Study of Human Hearts. *Circulation*, 412-422.
- NATTEL, S. (2003) Basic Electrophysiology of the Pulmonary Veins and Their Role in Atrial Fibrillation: Precipitators, Perpetuators and Perplexers. *J cardiovasc Electrophysiol*, Vol 14, 1372-1375.

- NATTEL, S., AKIKO SHIROSHITA-TAKESHITA, BIANCA J.J.M. BRUNDEL & RIVARD, L. N. (2005) Mechanisms of Atrial Fibrillation: Lessons From Animal Models. *Cardiovascular Diseases*, Vol. 48, 9-28.
- NATTEL, S., ANGE MAGUY, SABRINA LE BOUTER & YEH, Y.-H. (2007) Arrhythmogenic Ion-Channel Remodeling in the Heart: Heart Failure, Myocardial Infarction, and Atrial Fibrillation. *Physiol Rev*, 425-456.
- NAVIA, J. L., GILLINOV, A. M. & MCCARTHY, P. M. (2009) Curative surgery for atrial fibrillation: Current status and minimally invasive approaches *Minerva Cardioangiologica* 52, 155-168.
- NG, G. A., KIERAN E. BRACK & COOTE, J. H. (2001) Effects of direct sympathetic and vagus nerve stimulation on the physiology of the whole heart – a novel model of isolated Langendorff perfused rabbit heart with intact dual autonomic innervation. *Experimental Physiology* Vol. 86, 319-329.
- NG, J. & GOLDBERGER, J. J. (2007) Understanding and Interpreting Dominant Frequency Analysis of AF Electrograms. *J Cardiovasc Electrophysiol*, Vol. 18, 680-685.
- NIEMANN, J., CB CAIRNS, SHARMA, J. & LEWIS, R. (1992) Treatment of prolonged ventricular fibrillation. Immediate countershock versus high-dose epinephrine and CPR preceding countershock. *Circulation*, 281-287.
- O'DONNELL, D., FURNISS, S. S. & BOURKE, J. P. (2002) Paroxysmal Cycle Length Shortening in the Pulmonary Veins During Atrial Fibrillation Correlates with Arrhythmogenic Triggering Foci in Sinus Rhythm. *Journal of Cardiovascular Electrophysiology*, 13, 124-128.
- OKADA, M. (1979) A Digital Filter for the QRS Complex Detection. *IEEE Transactions on Biomedical Engineering*, BME 26.
- OLAF, J. E. (2002) Temperature Controlled Radiofrequency Ablation. *Indian Pacing and Electrophysiology Journal*, 2, 66-73.
- ORAL, H., CHRISTOPH SCHARF, AMAN CHUGH, BURR HALL, PETER CHEUNG, ERIC GOOD, SRIKAR VEERAREDDY, FRANK PELOSI, J. & MORADY, F. (2003) Catheter Ablation for Paroxysmal Atrial Fibrillation: Segmental Pulmonary Vein Ostial Ablation Versus Left Atrial Ablation. *Circulation* 2355-2360.
- ORAL, H., KNIGHT, B. P., TADA, H., ÖZAYDIN, M., CHUGH, A., HASSAN, S., SCHARF, C., LAI, S. W. K., GREENSTEIN, R., JR, F. P., STRICKBERGER, S. A. & MORADY, F. (2002) Pulmonary Vein Isolation for Paroxysmal and Persistent Atrial Fibrillation. *Circulation*, 1077-1081.
- ORAL, H., PAPPONE C, CHUGH A, GOOD E, BOGUN F, PELOSI F, BATES E.R, LEHMANN M.H, VICEDOMINI G, AUGELLO G, AGRICOLA E, SALA S, SANTINELLI V & MORADY F (2006) Circumferential pulmonary-vein ablation for chronic atrial fibrillation. *Engl J Med*, 354, 934-941.
- PACHON, J. C. M., PACHON, E. I. M., PACHON, J. C. M., LOBO, T. J., PACHON, M. Z., REMY N.A. VARGAS, PACHON, D. Q. V., M, F. J. L. & JATENE, A. D. (2004) A new treatment for atrial fibrillation based on spectral analysis to guide the catheter RF-ablation. *Europace* 590-601.
- PAK, H., YS, O., LIU YB, WU TJ, KARAGUEUZIAN HS, LIN SF & PS., C. (2003) Catheter ablation of ventricular fibrillation in rabbit ventricles treated with beta-blockers. *Circulation*, 108, 3149-3156.
- PAN, J. & WILLIS J. TOMPKINS (1985) A Real-Time QRS Detection Algorithm *IEEE Transactions on Biomedical Engineering*, Vol. BME-32, 230-236.
- PAPPONE, C., GIUSEPPE ORETO, SALVATORE ROSANIO, GABRIELE VICEDOMINI, MONICA TOCCHI, FILIPPO GUGLIOTTA, ADRIANO

- SALVATI, COSIMO DICANDIA, MARIA PIA CALABRÒ, PATRIZIO MAZZONE, ELEONORA FICARRA, CLAUDIO DI GIOIA, SIMONE GULLETTA, STEFANO NARDI, VINCENZO SANTINELLI, BENUSSI, S. & ALFIERI, O. (2001) Atrial Electroanatomic Remodeling After Circumferential Radiofrequency Pulmonary Vein Ablation: Efficacy of an Anatomic Approach in a Large Cohort of Patients With Atrial Fibrillation. *Circulation* 2539-2544.
- PAPPONE, C., ROSANIO S, AUGELLO G, GALLUS G, VICEDOMINI G, MAZZONE P, GULLETTA S, GUGLIOTTA F, PAPPONE A & V, S. (2003) Mortality, morbidity, and quality of life after circumferential pulmonary vein ablation for atrial fibrillation: Outcomes from a controlled nonrandomized long-term study. *J Am Coll Cardiol* 185-197.
- PAPPONE, C. & SANTINELLI, V. (2005) Atrial Fibrillation Ablation: State of the Art. *The American Journal of Cardiology*, 96.
- PAPPONE, C. & SANTINELLI, V. (2008) Ablation of Atrial Fibrillation. *Arrhythmia Management*.
- PHILIP, J. P. & PETER, R. K. (2001) *Cardiac Arrhythmia: Mechanisms, Diagnosis & Management*, Lippincott Williams & Wilkins, .
- PISARENKO, V. F. (1973) The retrieval of Harmonics from a Covariance Function. *Geophys. J.R.astr.Soc*, 347-366.
- PROAKIS, J. G. & DIMITRIS, G. M. (1996) *Digital signal processing*, Prentice Hall International.
- PRUDENTE, L. A., MOORMAN, J. R., LAKE, D., XIAO, Y., GREEBAUM, H., MANGRUM, J. M., DIMARCO, J. P. & FERGUSON, J. D. (2009) Femoral vascular complications following catheter ablation of atrial fibrillation *Journal of Interventional Cardiac Electrophysiology* Vol 26, 59-64.
- QIN, H., JIAN HUANG, JACK M. ROGERS, GREGORY P. WALCOTT, DENNIS L. ROLLINS, WILLIAM M. SMITH & RAYMOND E. IDEKER (2005) Mechanisms for the Maintenance of Ventricular Fibrillation: The Nonuniform Dispersion of Refractoriness, Restitution Properties, or Anatomic Heterogeneities? *J Cardiovasc Electrophysiol*, Vol. 16, 888-897.
- ROBLES, D. M., E.O., B., R., C., P., & AL, E. (1978) Definition of terms related to cardiac rhythm. *American Heart Journal*, 95, 796-806.
- ROPELLA, K., AV SAHAKIAN, JM BAERMAN & SWIRYN, S. (1988) Effects of procainamide on intra-atrial [corrected] electrograms during atrial fibrillation: implications [corrected] for detection algorithms. *Circulation*, 1047-1054.
- ROSTOCK, T., LUTOMSKY, B., STEVEN, D. & WILLEMS, S. (2007) The Coronary Sinus as a Focal Source of Paroxysmal Atrial Fibrillation: More Evidence for the 'Fifth Pulmonary Vein'? *PACE* 1027-1031.
- ROTHBERGER, C. & WINTERBERG, H. (1915) ber Vorhofflimmern und Vorhofflattern. *Pflugers Arch Gesamte Physiol Menschen Tiere*, 42- 90.
- SAHADEVAN, J., KYUNGMOO RYU, LEORA PELTZ, CELEEN M. KHRESTIAN, ROBERT W. STEWART, ALAN H. MARKOWITZ & ALBERT L. WALDO (2004) Epicardial Mapping of Chronic Atrial Fibrillation in Patients Preliminary Observations. *Circulation*, 3293-3299.
- SALINET JR, J., AHMAD, A., BROWN, P., STAFFORD, P., NG, G. A. & SCHLINDWEIN, F. (2010) Three-dimensional Frequency Mapping from the Noncontact Unipolar Electrograms in Atrial Fibrillation. *Computing in Cardiology* Belfast, UK.

- SANDERS, P., NALLIAH, C., DUBOIS, R., TAKAHASHI, Y., HOCINI, M., ROTTER, M., ROSTOCK, T., SACHER, F., HSU, L., JÖNSSON, A., O'NEILL, M., JAÏS, P. & HAÏSSAGUERRE, M. (2006) Frequency Mapping of the Pulmonary Veins in Paroxysmal Versus Permanent Atrial Fibrillation. *J Cardiovasc Electrophysiol.* , 17, 965-972.
- SANDERS, P., OMER BERENFELD, MÉLÈZE HOCINI, PIERRE JAÏS, RAVI VAIDYANATHAN, LI-FERN HSU, STÉPHANE GARRIGUE, YOSHIHIDE TAKAHASHI, MARTIN ROTTER, FRÉDÉRIC SACHER, CHRISTOPHE SCAVÉE, ROBERT PLOUTZ-SNYDER, JOSÉ JALIFE & MICHEL HAÏSSAGUERRE (2005) Spectral Analysis Identifies Sites of High-Frequency Activity Maintaining Atrial Fibrillation in Humans. *Circulation*, 789-797.
- SANO, T. & TOHRU SAWANOBORI (1970) Mechanism Initiating Ventricular Fibrillation Demonstrated in Cultured Ventricular Muscle Tissue. *Circ. Res.*, 201-210.
- SCANAVACCA, M., F.PISANI, C., HACHUL, D., LARA, S., HARDY, C., DARRIEUX, F., TROMBETTA, I., NEGRAO, C. E. & SOSA, E. (2006) Selective Atrial Vagal Denervation Guided by Evoked Vagal Reflex to Treat Patients With Paroxysmal Atrial Fibrillation. *Circulation*, 114, 876-885.
- SCHARF, C., ORAL, H., CHUGH, A., HALL, B., GOOD, E., CHEUNG, P., PELOSI JR., F. & MORADY, F. (2004) Acute effects of left atrial radiofrequency ablation on atrial fibrillation. *Journal of Cardiovascular Electrophysiology* 15, 515-521.
- SCHERLAG, B. J., HIROSHI NAKAGAWA, WARREN M. JACKMAN, WILLIAM S. YAMANASHI, EUGENE PATTERSON, SUNNY PO & LAZZARA, R. (2005) Electrical Stimulation to Identify Neural Elements on the Heart: Their Role in Atrial Fibrillation. *Journal of Interventional Cardiac Electrophysiology* 37-42.
- SCHILLING, R. J., KADISH, A. H., PETERS, N. S., GOLDBERGER, J. & DAVIES, D. W. (2000) Endocardial mapping of atrial fibrillation in the human right atrium using a non-contact catheter. *European Heart Journal* 550-564.
- SCHILLING, R. J., PETERS, N. S. & DAVIES, D. W. (1998) Simultaneous Endocardial Mapping in the Human Left Ventricle Using a Noncontact Catheter Comparison of Contact and Reconstructed Electrograms During Sinus Rhythm *Circulation*, 887-898.
- SCHMIDT, R. (1979) Multiple emitter location and signal parameter estimation. *Proc. RADC Spectrum Estimation Workshop*.
- SCHUMAKER, L. (1993) *Spline Function: Basic Theory*, Malabar Florida, Krieger Publishing Company.
- SHAH, D., YAMANE, T., CHOI, K.-J. & HAÏSSAGUERRE, M. (2004) QRS Subtraction and the ECG Analysis of Atrial Ectopics. *A.N.E.* , Vol.9, 389-398.
- SHIMIZU, A., UEYAMA, T., YOSHIGA, M., SAWA, A., SUZUKI, S., SUGI, N. & MATSUZAKI, M. (2007) Spectral Analysis of Atrial Fibrillation Cycle Lengths Comparison Between Fast Fourier Transform Analysis and Autocorrelation Function Analysis Using Multipurpose Physio-Informatic Analysis Software. *Circ J*, 71, 242 - 251.
- SKANES, A. C., MANDAPATI, R., BERENFELD, O., DAVIDENKO, J. M. & JALIFE, J. (1998) Spatiotemporal Periodicity During Atrial Fibrillation in the Isolated Sheep Heart. *Circulation*, 1236-1248.
- SLOCUM, J., E BYROM, L MCCARTHY, A SAHAKIAN & SWIRYN, S. (1985) Computer detection of atrioventricular dissociation from surface electrocardiograms during wide QRS complex tachycardias. *Circulation* 1028-1036.
- SPACH, M. & DOLBER, P. (1986) Relating extracellular potentials and their derivatives to anisotropic propagation at a microscopic level in human cardiac muscle. Evidence for

- electrical uncoupling of side-to-side fiber connections with increasing age. *Circ. Res.*, 356-371.
- STEVEN M.KAY & MARPLE, S. L. (1981) Spectrum Analysis-A Modern Perspective. *Proceedings of the IEEE* 69.
- STEVENSON, W. G. & SOEJIMA, K. (2005) Recording Techniques for Clinical Electrophysiology. *J Cardiovasc Electrophysiol*, 16, 1017-1022.
- STRIDH, M. & SÖRNMO, L. (2001) Spatiotemporal QRST Cancellation Techniques for Analysis of Atrial Fibrillation. *IEEE Transactions on Biomedical Engineering*, Vol. 48.
- TADA, H., ORAL, H., WASMER, K., GREENSTEIN, R., FRANK PELOSI, J., KNIGHT, B. P., STRICKBERGER, S. A. & MORADY, F. (2002) Pulmonary Vein Isolation: Comparison of Bipolar and Unipolar Electrograms at Successful and Unsuccessful Ostial Ablation Sites. *Journal of Cardiovascular Electrophysiology*, 13, 13-19.
- TAKAHASHI, N., SEKI, A., IMATAKA, K. & FUJII, J. (1983) Fibrillatory wave size in paroxysmal atrial fibrillation. *Jpn Heart J.*, 24, 309-314.
- TAKAHASHI, Y., SANDERS, P., JAÏS, P., HOCINI, M., RÉMI DUBOIS, ROTTER, M., ROSTOCK, T., NALLIAH, C. J., SACHER, F., CLÉMENTY, J. & HAÏSSAGUERRE, M. (2006) Organization of Frequency Spectra of Atrial Fibrillation: Relevance to Radiofrequency Catheter Ablation. *J Cardiovasc Electrophysiol*, 17, 382-388.
- THAKOR, N. V., JOHN G. WEBSTER & TOMPKINS, W. J. (1984) Estimation of QRS Complex Power Spectra for Design of a QRS Filter. *IEEE Transaction on Biomedical Engineering*, BME-31, 702-706.
- TORTORA, G. J. & DERRICKSON, B. H. (2009) *Principles of Anatomy and Physiology*, John Wiley & Sons, Inc.
- VALENZUELA, T. D., ROE, D. J., CRETIN, S., SPAITE, D. W. & LARSEN, M. P. (1997) Estimating Effectiveness of Cardiac Arrest Interventions : A Logistic Regression Survival Model *Circulation*, 3308-3313.
- VANWORMER, A. M., RUTH LINDQUIST & SUSAN E. SENDELBACH (2008) The effects of acupuncture on cardiac arrhythmias: A literature review. *Heart Lung* 425-431.
- VASEGHI, S. V. (2008) *Advanced Digital Signal Processing and Noise Reduction*, Wiley.
- VAYA, C. & RIETA, J. (2007) ECG Signal Quantization Effects in the Analysis of Atrial Fibrillation. *Computers in Cardiology*. Durham, NC.
- VREEDE-SWAGEMAKERS, J. D., GORGELS, A., DUBOIS-ARBOUW, W., REE, J. V., DAEMEN, M., HOUBEN, L. & WELLENS, H. (1997) Out-of-hospital cardiac arrest in the 1990's: a population-based study in the Maastricht area on incidence, characteristics and survival *J Am Coll Cardiol*, 30, 1500-1505.
- WEAVER, W. D., COBB, L. A., COPASS, M. K. & HALLSTROM, A. P. (1982) Ventricular Defibrillation - A Comparative Trial Using 175-J and 320-J Shocks. *N Engl J Med* 307, 1101-1106.
- WEAVER, W. D., COBB, L. A., HALLSTROM, A. P., FAHRENBRUCH, C., COPASS, M. K. & RAY, R. (1986) Factors Influencing Survival After Out-of-Hospital Cardiac Arrest. *Journal of the American College of Cardiology*, 7, 752-757.
- WEISS, J. N., ZHILIN QU, PENG-SHENG CHEN, SHIEN-FONG LIN, HRAYR S. KARAGUEUZIAN, HIDEKI HAYASHI, ALAN GARFINKEL & ALAIN KARMA (2005) The Dynamics of Cardiac Fibrillation. *Circulation*, 1232-1240.

- WELCH, P. D. (1967) The use of Fast Fourier Transform for the Estimation of Power Spectra: A Method Based on Time Averaging Over Short, Modified Periodograms. *IEEE Transactions on Audio and Electroacoustics*, AU-15.
- WIENER, N. & ROSENBLUETH, A. (1946) The mathematical formulation of the problem of conduction of impulses in a network of connected excitable elements, specifically in cardiac muscle. *Arch Inst Cardiol Mex.* , 16, 205-265.
- WIGGERS, C. J. (1940) The Mechanism and Nature of Ventricular Fibrillation. *American Heart Journal*, 20, 399-412.
- WIGGERS, C. J. & WEGRIA, R. (1940) Ventricular fibrillation due to single, localized Induction and condenser shocks applied during The vulnerable phase of ventricular systole. *American Journal Physiology*, 128, 500-505.
- WILBER, D. J. (2008) Catheter ablation of cardiac arrhythmias: Basic concepts abd clinical applications. John Wiley & Sons.
- WILLIAM, J. E. & E.THOMSON, R. (2001) *Data Analysis methods in Physical Oceanoghaphy*, Gulf Professional Publishing.
- WINTERBERG, H. (1906) Ueber Herzflimmern und seine Beeinflussung durch Kampher. *Z Exp Pathol Ther*, 182-208.
- WOLF, P., ABBOTT, R. & KANNEL, W. (1991) Atrial fibrillation as an independent risk factor for stroke: the Framingham Study. *Stroke*, 983-988.
- YOUNGSON, R. M. (1992) Dictionary of Medicine. HarperCollins Publisher.
- ZHANG, M., LI, Z.-Z., LIU, X.-P., DONG, J.-Z. & MA, C.-S. (2009) Coronary sinus: an important target of catheter ablation of atrial fibrillation. *Chin Med J* 122, 2912-2913.
- ZIPES, D. & KNOPE, R. (1972) Electrical properties of the thoracic veins. *Am J Cardiol*, 29, 372-376.

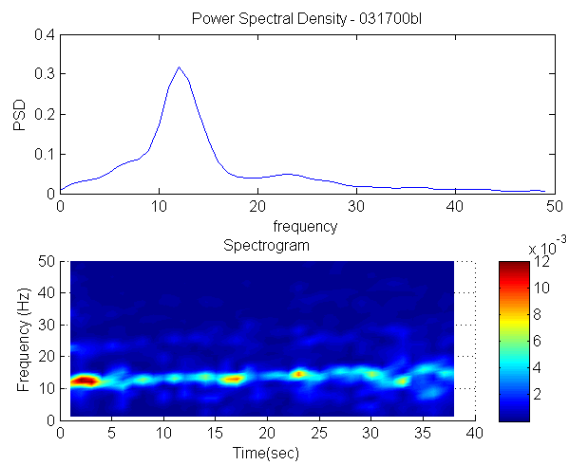
Appendix 1 - Monophasic action potential signals

-0.365	-0.09	-0.3375	-0.4975
-0.375	-0.095	-0.345	-0.4975
-0.3875	-0.0975	-0.3525	-0.495
-0.3975	-0.1	-0.36	-0.495
-0.4075	-0.1025	-0.3675	-0.4925
-0.4175	-0.1075	-0.375	-0.49
-0.42	-0.1075	-0.3775	-0.4925
-0.42	-0.1125	-0.38	-0.5
-0.4225	-0.115	-0.38	-0.5075
-0.4325	-0.1175	-0.385	-0.5175
-0.47	-0.1225	-0.3975	-0.525
-0.515	-0.125	-0.4125	-0.535
-0.5625	-0.1275	-0.43	-0.545
-0.61	-0.1325	-0.445	-0.5475
-0.6375	-0.1375	-0.465	-0.545
-0.6675	-0.1425	-0.4775	-0.5375
-0.6775	-0.15	-0.49	-0.5225
-0.6575	-0.1575	-0.495	-0.495
-0.6325	-0.1625	-0.4975	-0.4525
-0.6125	-0.17	-0.51	-0.405
-0.55	-0.175	-0.5125	-0.35
-0.42	-0.1825	-0.54	-0.2875
-0.28	-0.19	-0.575	-0.22
-0.14	-0.1925	-0.5725	-0.1675
-0.0025	-0.1975	-0.525	-0.1425
0.06	-0.205	-0.4075	-0.1225
0.0725	-0.205	-0.23	-0.1
0.0725	-0.21	-0.1025	-0.08
0.07	-0.215	-0.0775	-0.0575
0.0625	-0.22	-0.0875	-0.025
0.055	-0.225	-0.105	0.02
0.0475	-0.2275	-0.115	0.06
0.035	-0.2275	-0.12	0.07
0.025	-0.2325	-0.1275	0.075
0.01	-0.2325	-0.13	0.07
0	-0.24	-0.135	0.0575
-0.0075	-0.25	-0.1375	0.045
-0.0175	-0.255	-0.1375	0.035
-0.0275	-0.26	-0.14	0.0325
-0.0375	-0.2675	-0.14	0.0275
-0.045	-0.27	-0.1425	0.0225
-0.05	-0.275	-0.1425	0.02
-0.055	-0.2825	-0.1425	0.02
-0.065	-0.295	-0.145	-0.005
.0775	-0.31	-0.1475	-0.0275
-0.085	-0.3225	-0.1575	-0.07

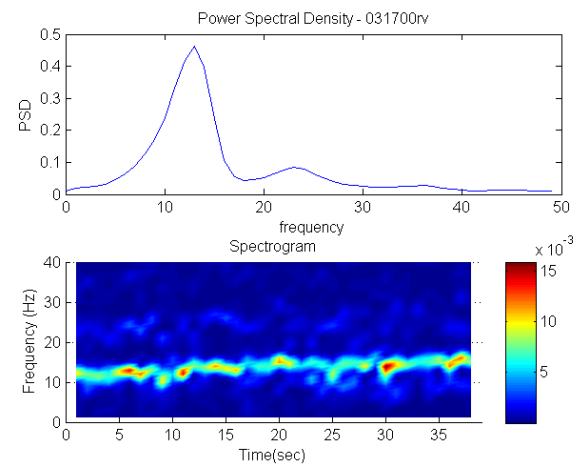
20001 data (031700bl)

Appendix 2 - Spectrum and spectrogram for VF studies

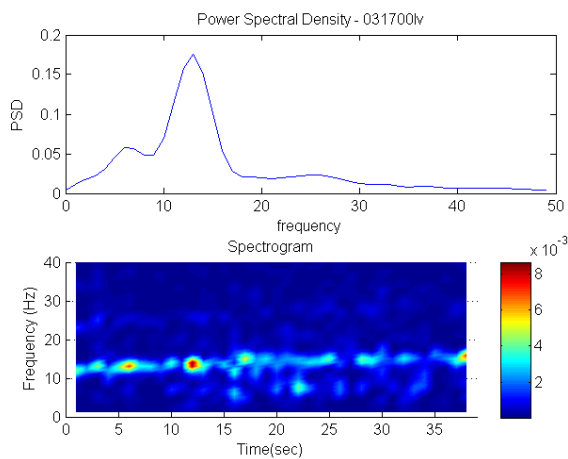
The figures below show the frequency spectrum (top diagram of each figure) and spectrograms (bottom diagram of each figure) for ventricular fibrillation (from animal studies). The spectrograms represent the frequency evolution along time. The Fourier transform was calculated separately for each segment, each with 1000 points sampled at 1000 Hz, frequency resolution 1 Hz and an overlap of 50% with a Hamming window.



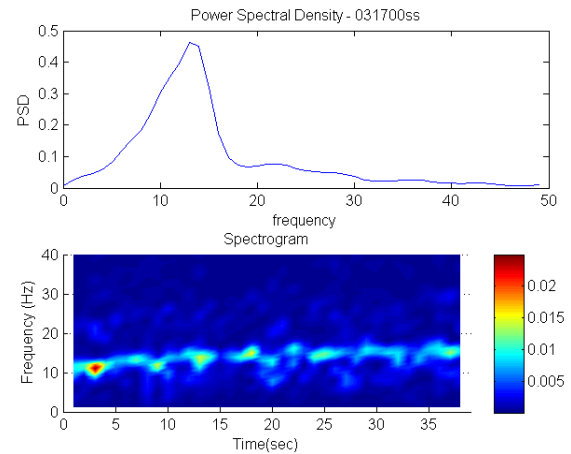
(a)



(b)

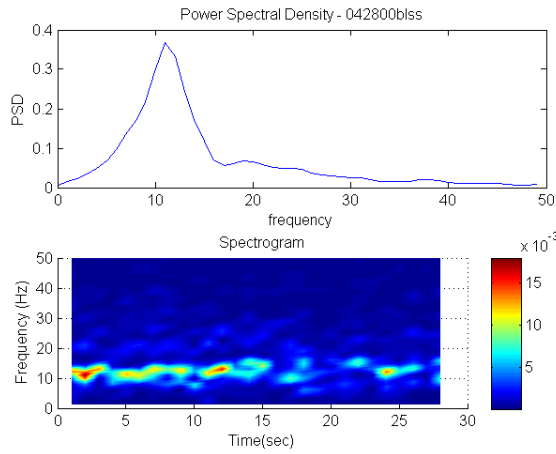


(c)

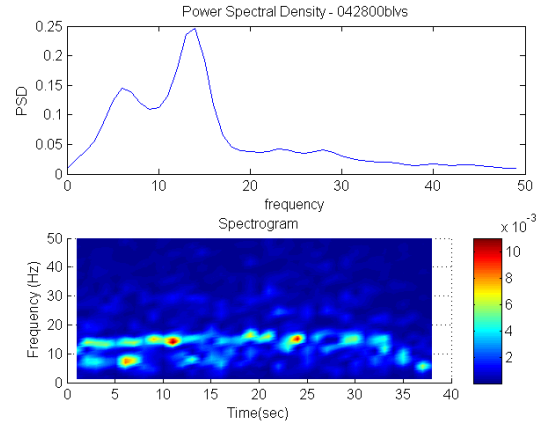


(d)

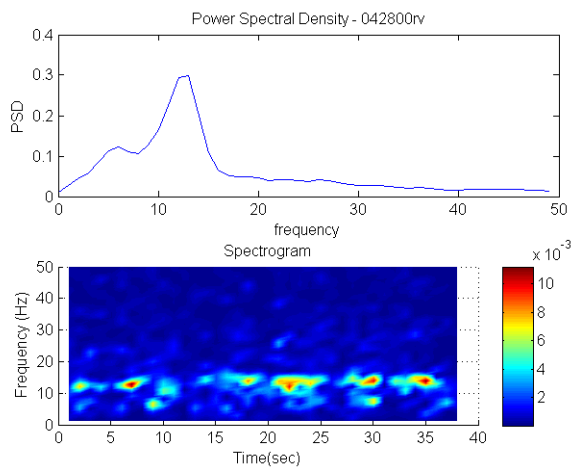
Appendix 2 a– Sample 031700 (a) baseline (b) right vagus nerve stimulation (c) left vagus nerve stimulation (d) sympathetic nerve stimulation



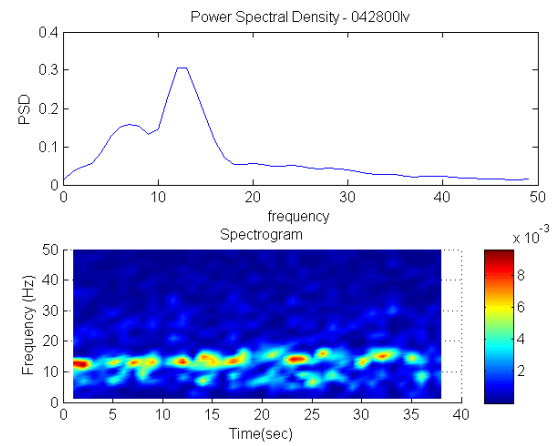
(a)



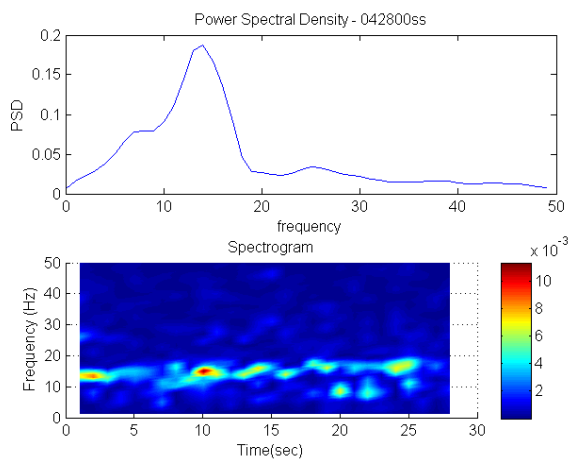
(b)



(c)

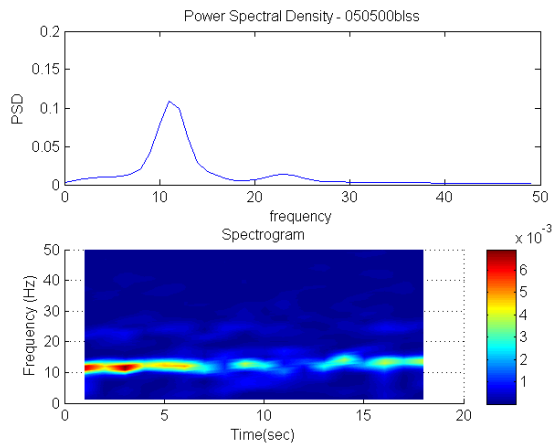


(d)

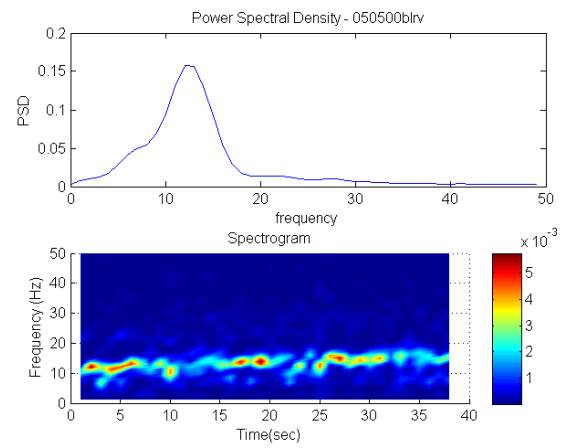


(e)

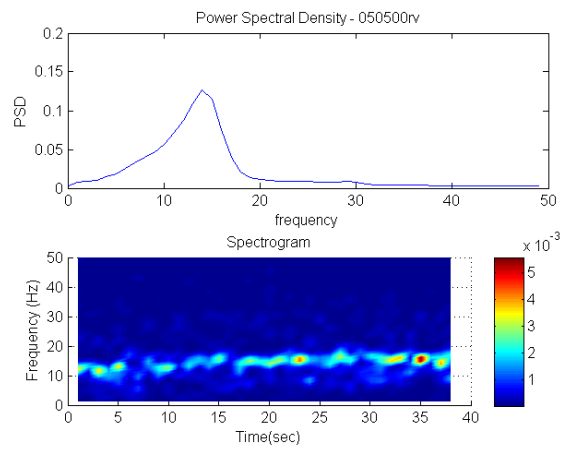
Appendix 2 b– Sample 042800 (a) baseline before sympathetic stimulation (b) baseline before vagus stimulation (c) left vagus nerve stimulation (d) right vagus nerve stimulation (e) sympathetic nerve stimulation



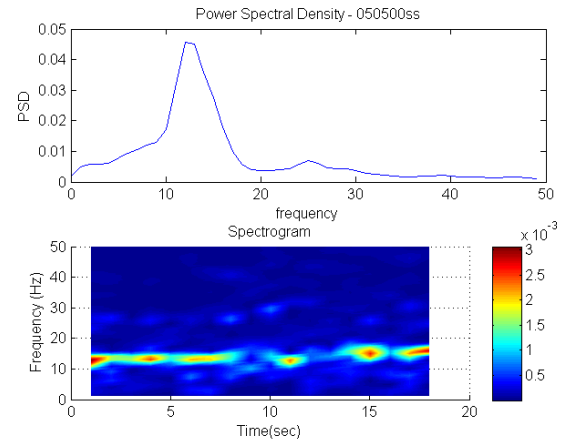
(a)



(b)

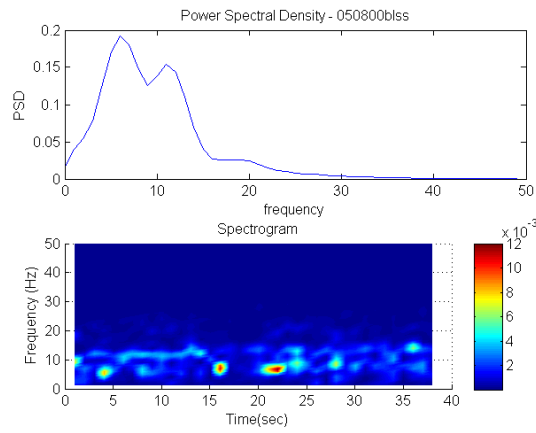


(c)

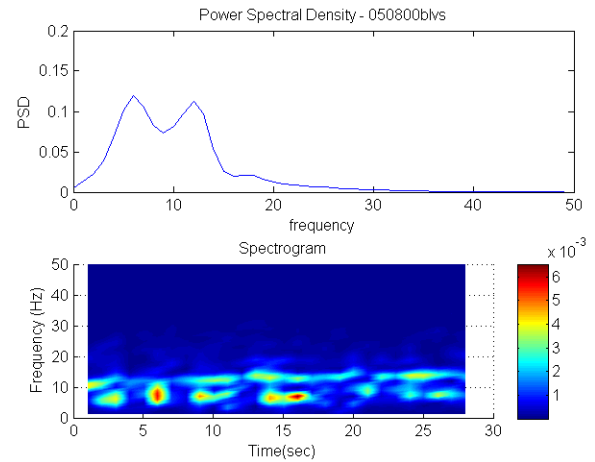


(d)

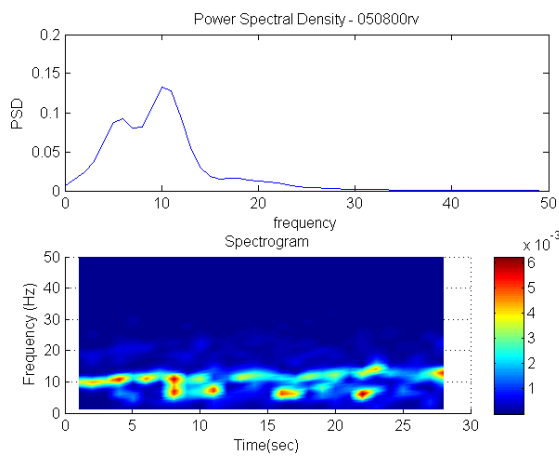
Appendix 2 c – Sample 050500 (a) baseline before sympathetic stimulation (b) baseline before vagus stimulation (c) right vagus nerve stimulation (d) sympathetic nerve stimulation



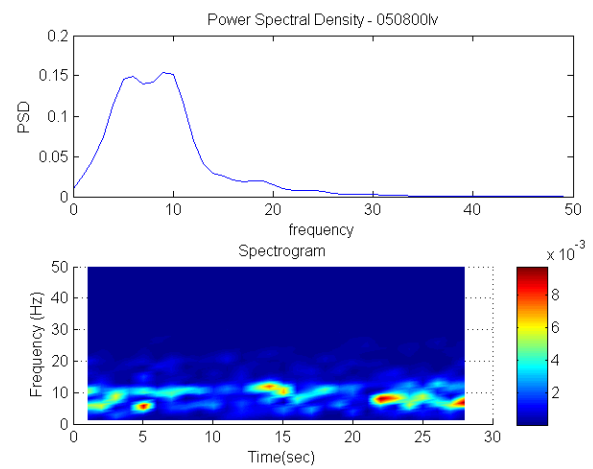
(a)



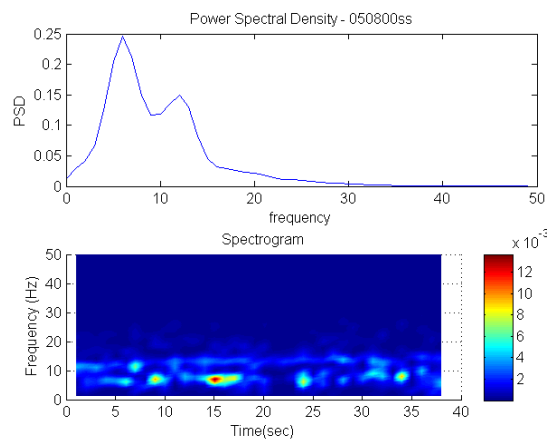
(b)



(c)

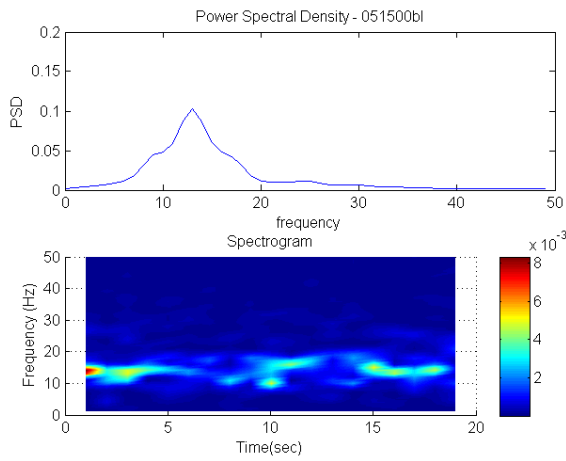


(d)

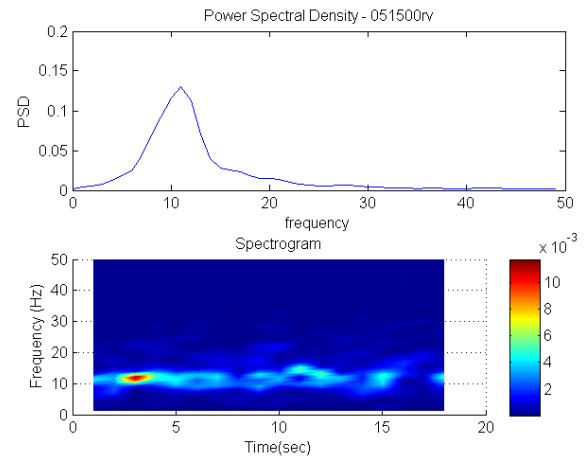


(e)

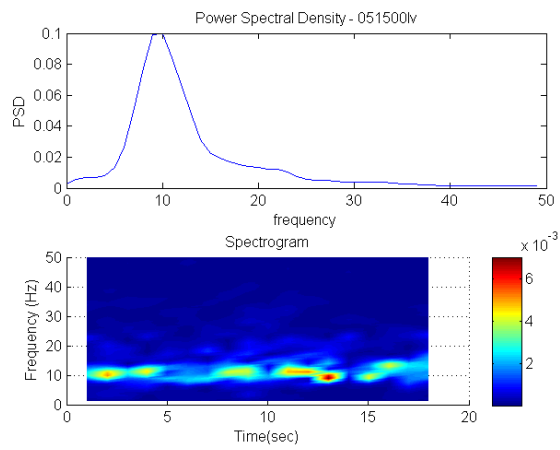
Appendix 2 d – Sample 050800 (a) baseline before sympathetic stimulation (b) baseline before vagus stimulation (b) right vagus nerve stimulation (c) left vagus nerve stimulation (d) sympathetic nerve stimulation



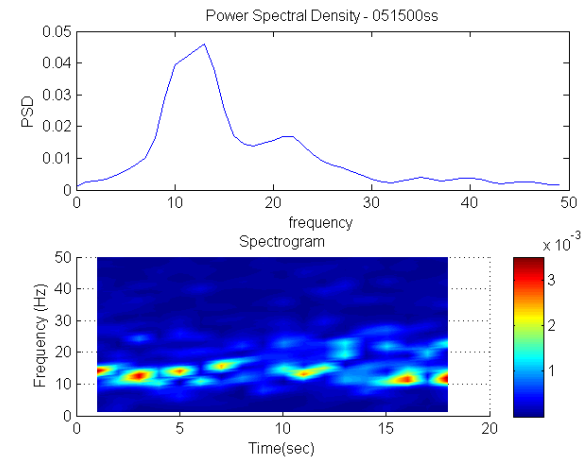
(a)



(b)

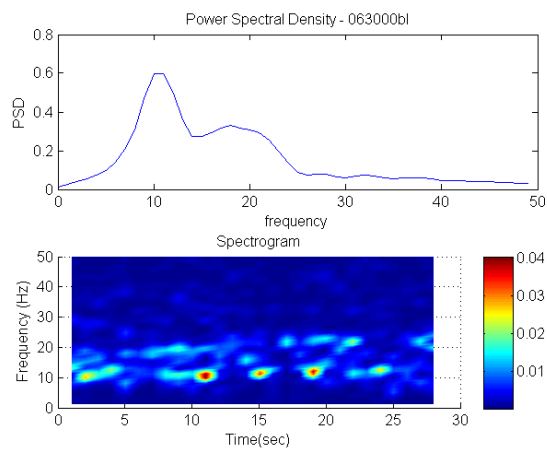


(c)

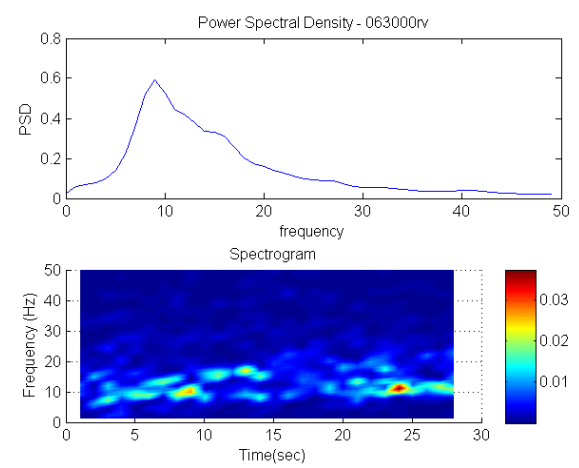


(d)

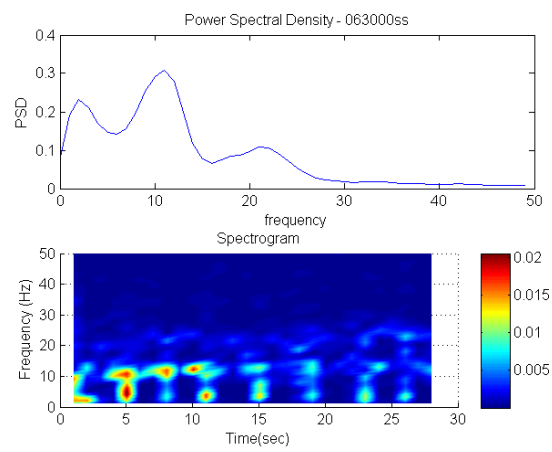
Appendix 2 e – Sample 051500 (a) baseline (b) right vagus nerve stimulation (c) left vagus nerve stimulation (d) sympathetic nerve stimulation.



(a)



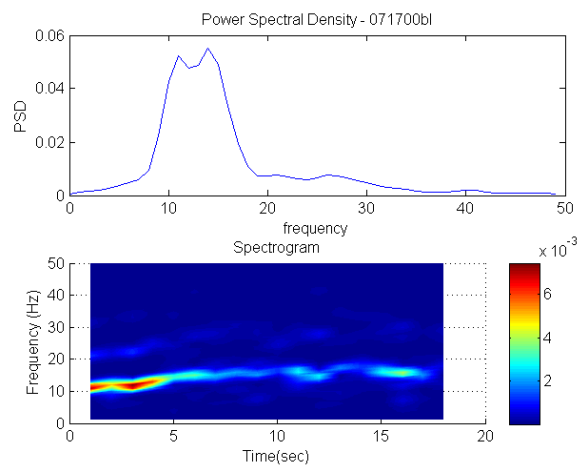
(b)



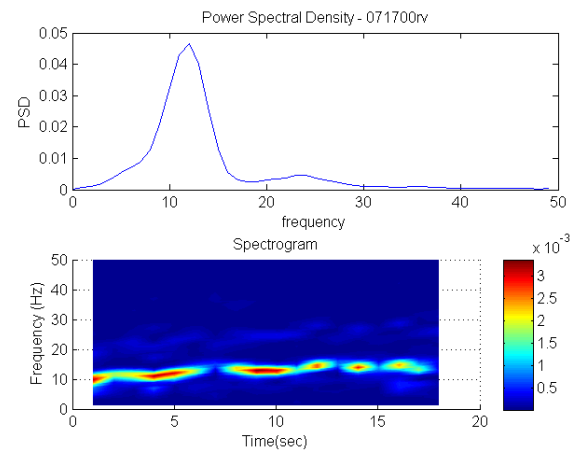
(c)

Appendix 2 f – Sample 063000 (a) baseline (b) right vagus nerve stimulation

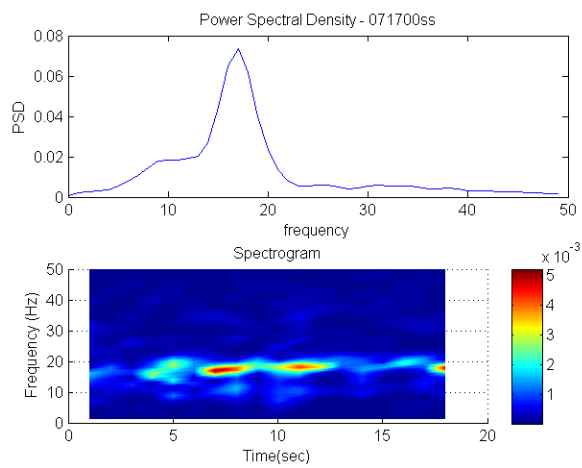
(c) Sympathetic nerve stimulation



(a)



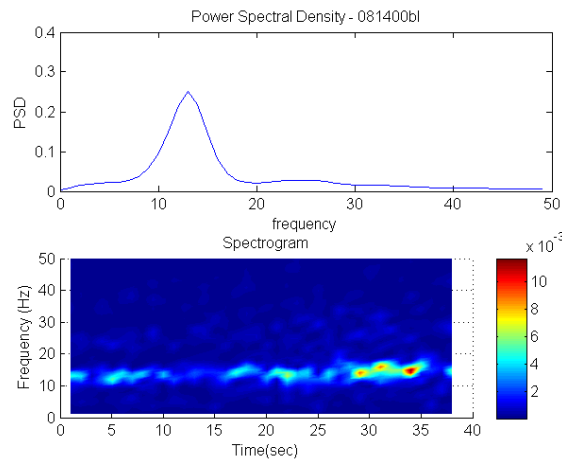
(b)



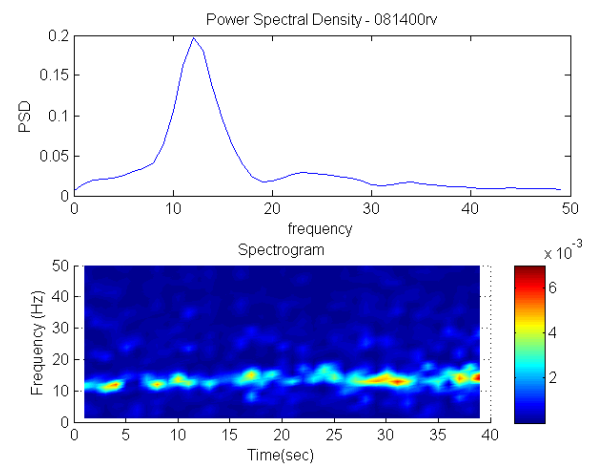
(c)

Appendix 2 g – Sample 071700 (a) baseline (b) right vagus nerve stimulation

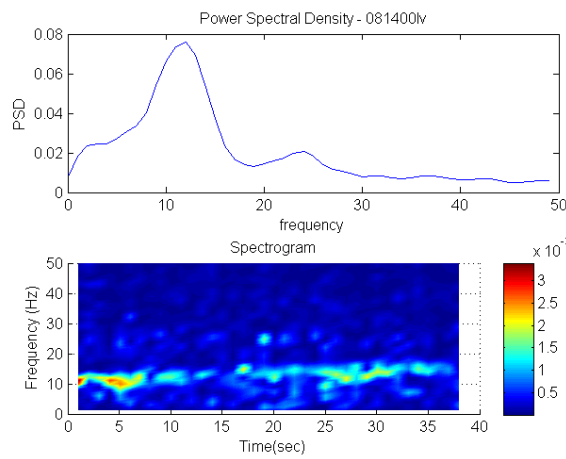
(c) Sympathetic nerve stimulation



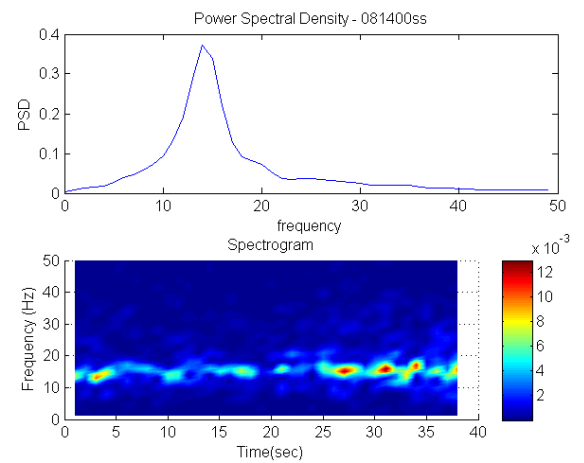
(a)



(b)



(c)



(d)

Appendix 2 h – Sample 081400 (a) baseline (b) right vagus nerve stimulation (c) left vagus nerve stimulation (d) sympathetic nerve stimulation

List of published work

Papers in proceedings of refereed conferences

1. **Ahmad A.**, Schlindwein, F.S., Tuan J.H., Ng G.A., “Frequency Domain Analysis for the Study of Atrial Arrhythmias”, IEEE EMBSS UKRI Postgraduate Conference on Biomedical Engineering and Medical Physics, July 12-14, 2009.
2. **Ahmad A.**, Schlindwein, F.S., Tuan J.H., Ng G.A., “Digital Processing for the Study of Atrial Arrhythmias”, World Congress on Medical Physics and Biomedical Engineering, September 7-12, 2009,
3. **Ahmad A.**, Schlindwein, F.S., Tuan J.H., Ng G.A., “Isoprenaline and atropine effect on atrial arrhythmias study”, ASME2010 10th Biennial Conference on Engineering Systems Design and Analysis, Istanbul, Turkey, July 12-14, 2010.
4. JL Salinet Jr, **A Ahmad**, P Stafford, G Andre Ng, FS Schlindwein, “Three-dimensional Frequency Mapping from the Noncontact Unipolar Electrograms in Atrial Fibrillation”, Computing in Cardiology 2010, September 26-29, 2010.
5. JL Salinet Jr, **A Ahmad**, P Brown, JH Tuan, P Stafford, G Andre Ng, FS Schlindwein, “High Density Noncontact Frequency Mapping Reveals Distinct Dominant Frequency Behavior In Persistent Atrial Fibrillation”, The Heart Rhythm Society’s 32nd Annual Scientific Sessions, Moscone Center, San Francisco, USA, May 4-7, 2011.

Journal papers (Published)

6. **Ahmad A.**, Schlindwein, F.S., Ng G.A., “Comparison of computation time for estimation of dominant frequency of atrial electrograms: Fast Fourier Transform, Blackman Tukey, Autoregressive and Multiple Signal Classification”, J. Biomedical Science and Engineering, doi:10.4236/jbise.2010.39114, Published Online September 2010. N. 3, pp.843-847, 2010.
7. **Ahmad A.**, Salinet Jr JL, Brown P, Tuan JH, Stafford P, Ng G Andre, Schlindwein FS, “QRS Subtraction for Atrial Electrograms: Flat, Linear and Spline Interpolation.” Submitted to: Medical & Biological Engineering & Computing, vol. 49. N. 11, pp. 1321-1328, November 2011.

Journal paper (to be submitted)

8. **Ahmad A.**, Salinet Jr JL, Brown P, Tuan JH, Stafford P, Ng G Andre, Schlindwein FS, “Adaptive power threshold for dominant frequency estimation in atrial fibrillation.”

To be submitted to: IEEE Transaction on Biomedical Engineering or Physiological Measurement.